Development and Deployment of an Airborne Gas Chromatography/Mass Spectrometer to Measure Tropospheric Volatile Organic Compounds

Jamie Minaeian

PhD

University of York

Chemistry

September 2016

Abstract

Airborne Volatile Organic Compounds are present throughout the atmosphere in a wide variety of species. An airborne Gas Chromatography/Mass Spectrometer was developed to measure these compounds in places otherwise inaccessible for ground- or ship-based instruments. The instrument was fitted to the UK FAAM BAe-146 Atmospheric Research Aircraft, and deployed on a number of campaigns. By the end of the project, the instrument was capable of making measurements that compared extremely well to other systems, meaning the proof of concept was successful. During the SAMBBA campaign, vertical profiles of biogenic and anthropogenic species were determined from the ground, up to 8000 m. These showed the extent to which different compounds (for example CO, benzene) were able to escape the planetary boundary layer and enter the free troposphere. Isoprene, however, with a much shorter lifetime of 0.5 hours, was primarily constrained to the boundary layer. Additionally, an analysis of biomass burning emissions was compared to those in literature. In particular the CO:VOC ratio was compared, with some species exhibiting very close comparisons, and others showing very different ratios leading to the conclusion that the CO:VOC ratio for some compounds is highly dependent on the species of trees. Measurements from the CAST campaign determined the extent to which naturally occurring halogenated species can travel from their source at the ocean surface, up to the lower stratosphere, affecting ozone levels. A comparison was also conducted with 3 other aircraft systems, for which the GC/MS was in good agreement. Finally, flights were conducted around the North Sea Oil and gas fields to determine background levels of compounds, in case of further leaks from natural gas extraction. Whilst the GC/MS could not identify specific plumes, calculations were performed to enhance the readings, showing very different levels of benzene emitted, which was dependent on the rig type.

Contents

List of Figures

List of Tables

Acknowledgements

Firstly, I would like to acknowledge my supervisor, Professor Ally Lewis, for his support, encouragement and explanations. In addition, the following members of WACL both past and present need a special mention: Steve Andrews for being patient and assisting with electronics and practical GC, Jim Hopkins for assistance with diagnosing GC issues, Ruth Purvis and Sarah Moller for explaining things over and over to me, and to Ruth for always keeping an eye open for jobs! Thanks to Marvin, who moaned when he originally wasn't mentioned, and Rachel with Lyx/Latex help.

The rest of WACL have also helped hugely with a variety of different issues, and for keeping me entertained throughout the past 5 years.

Thanks to NCAS for funding this PhD.

Thanks too to my friends both nationally and internationally for keeping my mind off my PhD, especially Simon for frequently descending on my house armed with Xbox and beer..

Many thanks to my Mum, Dad and brother for supporting me emotionally and financially-good luck in Australia Peter!

Finally, thanks to my wife, Jessica. Without you this thesis would simply not have happend. Thanks for always being there for me and listen to me moan when things went wrong.

Declaration

I declare that this thesis is a prensentation of original work and I am the sole author. This work has not previously been presented for an award a this, or any other, University. Figures 4.5, 4.6, 4.7 and 4.9 in Chapter four have been included as part of a paper by Andrews et al (2016), submitted to the journal Atmospheric Measurements and Techniques. All sources are acknowledged as References

Chapter 1

Introduction

1.1 Introduction

1.1.1 Structure and Composition

The atmosphere of our planet is divided into distinct layers, separated from each other by a temperature inversion. These temperature inversions form a distinct barrier between two layers, restricting transport between the layers above and below the centre of inversion. These layers are shown in Figure 1.1. As altitude increases, pressure decreases on a logarithmic scale. In addition, each layer displays different physical characteristics.

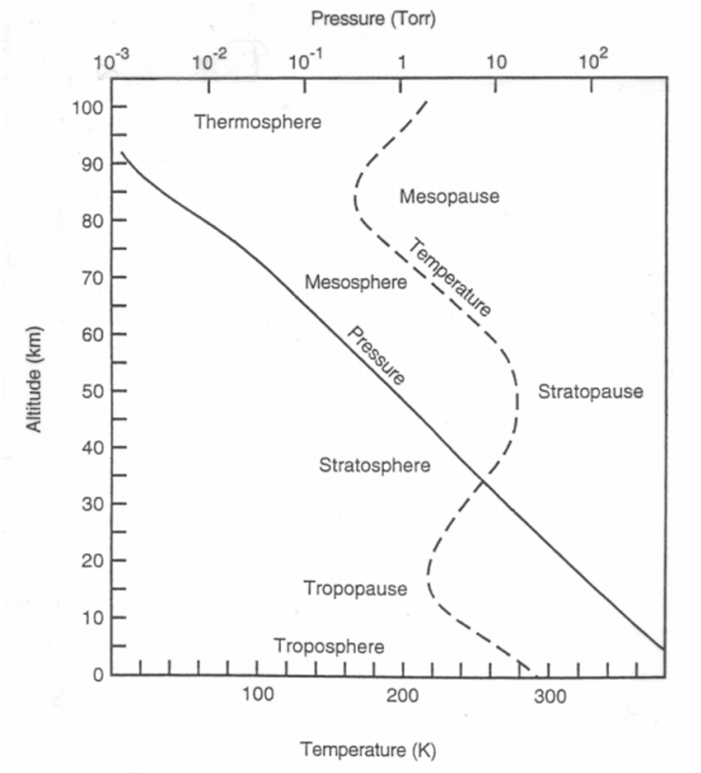

Figure 1.1: Average temperature and pressure variation with altitude at mid-latitudes, showing distinct layers of the atmosphere

All human activity takes place in the troposphere (with the exception of high-flying aircraft). The troposphere contains approximately four fifths of the total atmosphere by mass and 99 % of all water vapour and aerosols. This is despite the fact that it has an average depth of $\sim$ 17 km, making it the shallowest layer. The Earths gravity pulls air towards the surface, keeping the troposphere the shallowest, as well as the densest layer.

The troposphere can, in turn, be separated again into two distinct layers: the planetary boundary layer (PBL), and the free troposphere (FT). Separating these two layers is an entrainment zone, where compounds can cross from one to the other, albeit at a slower

rate than mixing/transporting through a single layer. The PBL is characterised by large amounts of vertical mixing due to vigorous convective currents. The Earths surface absorbs the suns energy, heating up the air at the bottom of the troposphere. This causes warm, less dense air to rise, whilst cold, dense air sinks. This leads to the vigorous vertical mixing, characteristic of the PBL. The PBL typically consists of the first 500 - 2000 m of the atmosphere. The free troposphere allows horizontal and vertical mixing, transporting airborne pollution around the planet in weather systems.

Understanding the composition of the troposphere is vital in order to assess the impact that humans are having on the planet. Different regions of the troposphere vary hugely in their composition, as a result of localised emissions, and global atmospheric processes. Volatile organic compounds (VOCs) are the name given to a subset of compounds in the atmosphere that exhibit specific properties that are relevant to both air pollution and climate processes. They are organic compounds that have a high vapour pressure at ambient temperatures. These compounds exist in thousands of different chemical forms, and display a wide variety of chemical functionalities, and physical properties. They are present at a wide range of mixing ratios (Atkinson, 2000; Barletta et al., 2002; Seco et al., 2011) and have different atmospheric reactivities (Darnall and Lloyd, 1976). Methane is the most abundant organic molecule in the atmosphere and is treated separately in atmospheric science, compared to other organic compounds (Wuebbles and Hayhoe, 2002). It has a much longer lifetime - around 10 years, and behaves as a greenhouse gas. All other organic compounds are much less abundant than methane; those organic compounds containing only carbon and hydrogen are generally referred to as Non-methane hydrocarbons (NMHCs). Other compounds with other functional groups are present including alcohols, aldehydes, ketones and nitrates, with all of them falling within the definition of VOC.

Sources and sinks of VOCs are as varied as their possible chemical structures. Generally, sources can be grouped into two broad categories: natural/biogenic (for example, bacterial activity) and anthropogenic (e.g. emissions from cars, power stations). Numerous subclassifications in each category can be created. Natural sources include emissions from plants, trees, the ocean etc., (termed biogenic) and can also include chemicals that also have anthropogenic sources. For instance, SO_2 is from both coal cumbustion and volcanic activity, benzene is from fuels, solvents, but also naturally occurring forest fires. Conversely, anthropogenic processes can lead to changes in natural composition, as a result of human activity (for instance, emissions from palm oil plantations). Sinks of organic

compounds can be physical, such as wet or dry deposition, or chemical, usually via oxidation. The lifetime of VOCs is generally somewhere between a few hours and a few weeks, meaning they can also undergo short- and long-ranged transport in air. This thesis will be primarily be concerned with chemical sources and sinks in the PBL and free troposphere.

1.1.1.1 Hydroxyl Radical, OH

Due to the large amount of water in the troposphere, the hydroxyl radical governs the daytime chemistry. Most trace gases can be oxidised by OH, eventually forming CO_2, given enough time, and suitable atmospheric conditions. All species that react with the hydroxyl radical can be said to have an OH lifetime, which varies from the order of a few minutes (eg isoprene), to years (eg methane) depending on the species.

The hydroxl radical, OH, provides the troposphere with most of it's oxidative capacity. It is able to oxidise most VOCs, causing them to become less volatile and more prone to removal via wet deposition, as their solubility in water increases. This means that OH is essentially a detergent for the atmosphere, converting pollutants into a form that is more easily removed. The hydroxyl radical is formed from another oxidising species: ozone (O_3). The formation of OH from ozone and water is shown in Equations 1.1 - 1.3, with hv indicating UV light.

$$O_3 + hv \rightarrow O(^1D) + O_2 \tag{1.1}$$

$$O(^1D) + O_2 + M \rightarrow O_3 + M \tag{1.2}$$

$$O(^1D) + H_2O \rightarrow \mathbf{2OH} \tag{1.3}$$

Light with wavelengths shorter than 310 nm is sufficient to split ozone into diatomic oxygen and an oxygen atom in a singlet excited state. The majority of O does not form OH from the triplet excited state. Most of these oxygen atoms react with diatomic oxygen, reforming ozone. However approximately 3% react with water vapour, forming the hydroxyl radical (Wine and Ravishankara, 1981; Monks, 2005). Note that the 'M' is any non reactive species, which removes excess reaction energy. This role is usually nitrogen, N_2, as it is highest in abundance. Due to it's high reactivity, OH has an extremely short atmospheric lifetime and at sea level, mixing ratios are in the region of 0.1 ppt, which is approximately 2 x 10^6 molecules cm^{-3}.

Compounds that do not react with OH as readily usually have a long atmospheric lifetime. These compounds include nitrous oxide (N_2O), carbon dioxide (CO_2), and many

halogenated species. As the rate of removal from the atmosphere is slow, compounds such as these can exist for long enough to undergo transport to the stratosphere. This is particularly important for halogenated species, which can catalytically destroy ozone (see chapter 4).

1.1.1.2 Stratospheric Ozone

The next species to be considered is ozone. Ozone is an extremely important gas in our atmosphere for several reasons. Firstly, it removes almost all UV radiation between 240 nm and 290 nm (termed UV-C) from light entering the Earths atmosphere. These wavelengths are lethal to a wide variety of cell types, from unicellular bacteria, to cells in plants and animals. The process by which ozone is formed occurs in the stratosphere, which in turn, is made stable by the ozone absorbing the light of the high energy UV radiation, generating heat. In the middle of the troposphere, some of the UV light has been filtered out by air above it, meaning it is cooler, than the top of the stratosphere. Because of this, temperature increases in altitude, setting up a temperature inversion. This gives the stratosphere a stable structure. The process of generating and removing ozone in the stratosphere is shown in Equations 1.4 - 1.7.

$$O_2 + hv \rightarrow 2O \tag{1.4}$$

$$O + O_2 + M \rightarrow O_3 + M \tag{1.5}$$

$$O_3 + hv \rightarrow O + O_2 \tag{1.6}$$

$$O + O_3 \rightarrow 2O_2 \tag{1.7}$$

These equations show the Chapman cycle of ozone in the stratosphere (Chapman, 1930). It shows how ozone mixing ratios can be maintained, by implementing a steady-state model. However, with the introduction of pollutants and other trace gases, this cycle can be perturbed, usually leading to a loss of ozone. This is shown in Equations 1.8 -1.10, where X is nitrogen oxide (NO) or a halogen atom.

$$X + O_3 \rightarrow XO + O_2 \tag{1.8}$$

$$XO + O \rightarrow X + O_2 \tag{1.9}$$

$$Net : O + O_3 \rightarrow 2O_2 \tag{1.10}$$

It is important to note that X is recycled at the end of the reaction, causing the cycle to continue catalytically. The effect of halogenated compounds (specifically those termed chloro- fluoro- carbons (CFCs)) on stratospheric ozone was realised in 1985 with the discovery of the Antarctic ozone hole (Farman et al., 1985). As a consequence, the Montreal protocol was enacted in 1989 which aimed at reducing the anthropogenic release of CFCs from refrigerators and industrial processes. Twenty years later, it has been reported that the Antarctic ozone hole has started to heal (Solomon et al., 2016). This also shows the long-term problems compounds such as CFCs can cause, given that it has taken 20 years to begin reversing the damage done to the ozone layer.

1.1.1.3 Tropospheric Ozone

Whilst most atmospheric ozone is located in the stratosphere (90 %) (Lelieveld and Dentener, 2000), the remaining 10 % exists as tropospheric ozone. This remaining 10 % is critical in determining oxidation processes in the troposphere, primarily of VOCs. It is also considered a major pollutant at ground level. For example, the US Environmental Protection Agency (EPA) has published guidelines regarding ozone exposure in built up areas and over ecosystems. The guidelines state that the 8-hour average mixing ratio for ozone should not exceed 80 parts per billion (ppb) (EPA, 1998).

Ozone in the troposphere is a major component of photochemical smog, along with particulate matter and other oxidant products such as peroxyacetyl nitrate (PAN). Photochemical smog is prevalent in many major cities, such as Los Angeles, London, Tokyo and Beijing. This is caused by a build up of NO from vehicles over night, and pre-dawn. Once the sun rises, NO is oxidised to NO_2, colouring the atmosphere brown. NO_x is also considered to be a pollutant in itself, defined as the total of NO and NO_2. However, NO_2 can also be photolysed back to NO, yielding a oxygen atom, which then reacts with diatomic oxygen to form ozone (reaction 5). The build up of ozone can go on to react with VOCs, causing them to oxidise to more harmful compounds, such as aldehydes. Additionally, as compounds become more oxidised, they become increasingly less volatile, and can partition into the aerosol phase, causing a build up of particulate matter, causing a haze in the lower atmosphere. Finally, the oxidation of VOCs yields the RO_2 radical, which then reacts with NO, forming NO_2. This then forms further ozone, as in reaction 1.12 . The reactions of NO_x, O_3 and a NMHC, RH, are shown in reactions 1.11 - 1.16 (Crutzen, 1970).

$$NO + O_3 \rightarrow NO_2 + O_2 \tag{1.11}$$

$$NO_2 + h\nu \rightarrow NO + O(^3P) \tag{1.12}$$

$$NO_2 + O(^3P) \rightarrow NO + O_2 \tag{1.13}$$

$$RH + OH \rightarrow R\cdot + H_2O \tag{1.14}$$

$$R\cdot + O_2 + M \rightarrow RO_2 + M \tag{1.15}$$

$$RO_2 + NO \rightarrow RO + NO_2 \tag{1.16}$$

This is summed up in Figure 1.2. RH and CO are released from many sources, along with NO, which builds up. On reaction with OH and then oxygen, RH becomes RO_2, which in turn reacts with NO to form NO_2. This can then go on to react with more O_2 to form ozone.

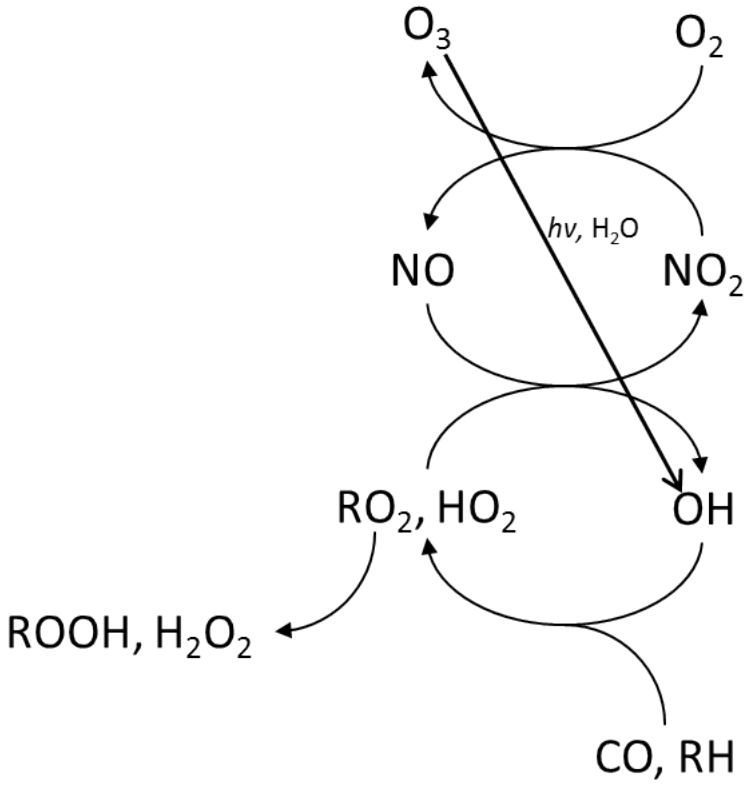

Figure 1.2: Ozone, NO_x and RH cycling in the troposphere. Note that sunlight must be present for these reactions to occur

1.1.2 Emissions of NMHCs

Global estimates of NMHCs and other species are continually being published and vary between studies using different model parameters (Guenther et al., 1995; West et al., 2013; Sindelarova et al., 2014). For instance, modelled emissions of isoprene vary, with estimates in the region of 550 Tg/year, mainly from vegetation. Additionally the oceans form a source of biogenic NMHCs to the atmosphere (Jones et al., 2010). For some compounds, particularly halogenated VOCs, the ocean is an extremely important source, whilst for NMHCs, it has been reported that the oceans contribute very little compared to anthropogenic activities (**?**). Biogenic emissions make up the vast majority of NMHCs released to the atmosphere, by almost an order of magnitude (Guenther et al., 1993, 1995). However, anthropogenic emissions are given off by cars, industrial processes and a wide range of human activities. As a consequence, they are released in large concentrations in areas with high population density and importantly they are co-emitted near to NO_x sources which provides the right chemical environment to generate ozone. The impact of anthropogenic VOCs is therefore large, because of the co-location with other pollutants. The emissions of VOCs are therefore central to air pollution control and they are restricted by numerous international agreements, such as the Gothenburg protocol, which was established to reduce emissions of SO_2, NO_x, VOCs and ammonia in developed, Northern Hemispheric countries. Estimates of emissions of VOCs are reported in inventories; the UK emissions are reported in the National Atmospheric Emissions Inventory (NAEI), with London emissions also being reported by the London Atmospheric Emissions Inventory (LAEI). The national emissions map for NMHCs is shown in Figure 1.3. As discussed, the principle issue with NMHCs is their reactions with oxidising compounds, either the hydroxyl radical or NO_x. Coupled with sunlight, high levels of NMHCs can be oxidised, becoming a source of photochemical smog.

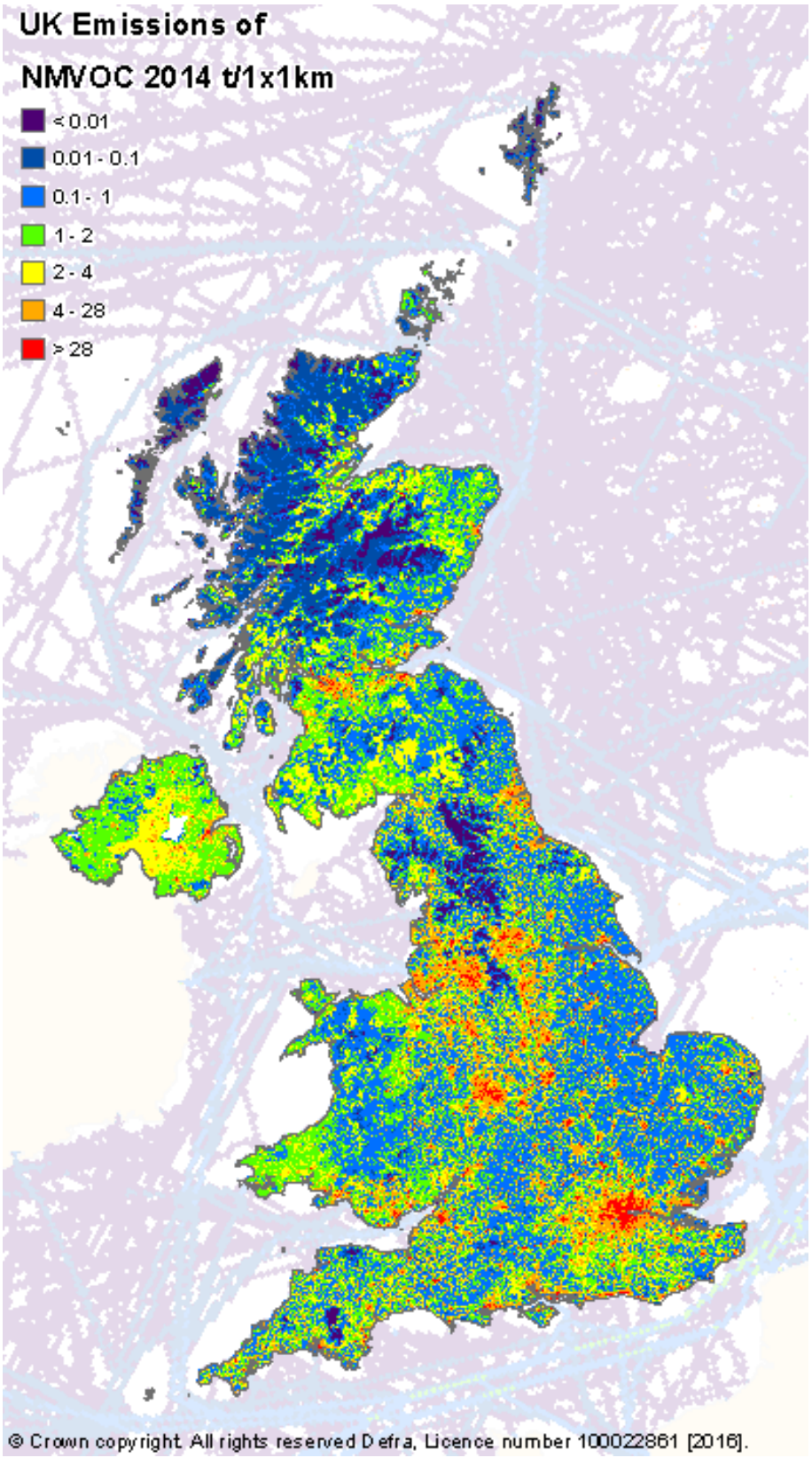

Figure 1.3: NAEI emissions map for the UK for 2014. The map is coloured by total Non methane VOCs, with a resolution of 1 km grid boxes. *Image courtesy of DEFRA*

1.1.3 Removal Processes

1.1.3.1 Wet and Dry Deposition

Depending on the solubility of a given compound, it can be removed from the atmosphere through uptake to a water droplet, or by irreversibly adsorbing to a solid surface, such as the ground, or a building. If a compound is suitably water soluble, it can be dissolved in rain water, or sea spray and undergo further reactions in solution, removing it from the atmosphere. Dry deposition accounts for a very small proportion of NMHC removal, as compounds must be close to the surface and be able to undergo specific interactions.

1.1.3.2 Chemical Removal Processes

As previously stated, NMHCs can be removed from the atmosphere by reaction with the OH radical. Alkanes react with OH to produce an alkyl radical, which in turn, react with O_2 to produce peroxy radicals. At each stage, the original alkane becomes more water soluble, and therefore easier to remove from the atmosphere by wet deposition. The series of reactions are shown in equations 1.14 - 1.17. Equation 1.17 shows a hydrogen abstraction from RH, forming an alkyl radical.

$$OH + RH \rightarrow R + H_2O \tag{1.17}$$

$$R + O_2 + M \rightarrow RO_2 + M \tag{1.18}$$

$$RO_2 + NO \rightarrow RO + NO_2 \tag{1.19}$$

$$RO + O_2 \rightarrow R = O + HO_2 \tag{1.20}$$

Alkene reactions follow a similar path insofar as every step increases the polarity and generally the solubility of the resulting secondary product. However, alkene reactions with ozone can occur across the unsaturated bond. All these reactions have the potential to then produce products that can interact with the reaction cycles of NO_x, with ozone as the product. This is a cyclic reaction, with the RO_2 and NO being reformed. Once the alkyl radical has been formed, it reacts with O_2, forming NO_2, which then photodissociates, yielding an excited oxygen atom. This goes on to react with diatomic oxygen, forming ozone. This is shown in reactions 1.18 - 1.20.

$$RO_2 + NO \rightarrow RO + NO_2 \tag{1.21}$$

$$NO_2 + hv \rightarrow NO + O(^3P) \tag{1.22}$$

$$O(^3P) + O_2 \rightarrow O_3 \tag{1.23}$$

1.1.4 Transport

Atmospheric transport plays a critical role in the distributions of NMHCs around the globe. The PBL is the key area involved in the initial vertical transportation of emissions, due to it's proximity to the surface, and strong surface heating which generates convection. As the sun heats up the surface, air is heated from the bottom, causing convective currents to transport compounds in the vertical direction. As the intensity of sunlight is at a maximum at the equator and a minimum at the poles, the convective currents vary over the globe. As the warm air at the equator rises, it cools and moves poleward towards the mid latitudes and then a return flow passes underneath at low levels. As the air cools, it then sinks around the mid latitudes, and moves back towards the equator, filling the void left by the warm air rising. On a stationary planet, this circulation could extend all the way from equator to pole, however the Earth's rotation generates a Coriolis displacement, this generates three distinct circulations, or Hadley cells, in which air is continually recycled between the equator and approximately 30 °N and °S. A diagram of this process is shown in Figure 1.4.

Two other cells exist that follow the same pattern- the mid latitude (or Ferrel) cells (30° to 60°), and the polar cells (60° to 90°). All of these cells are involved with prevailing trade winds, and can carry pollution huge distances. As well as these cells circulating air, there are many more influences on global atmospheric circulation, surface roughness and changing regional weather systems. These processes make the atmosphere a highly complex, dynamic system and if it is to be understood, both the composition and the meteorology must be determined.

Additionally, exchanges can take place between both the boundary layer and free troposphere and the stratosphere and Troposphere. The areas separating these layers can be penetrated by longer lived species, and additionally, the separating layers can undergo a range of folding events and intrusions.

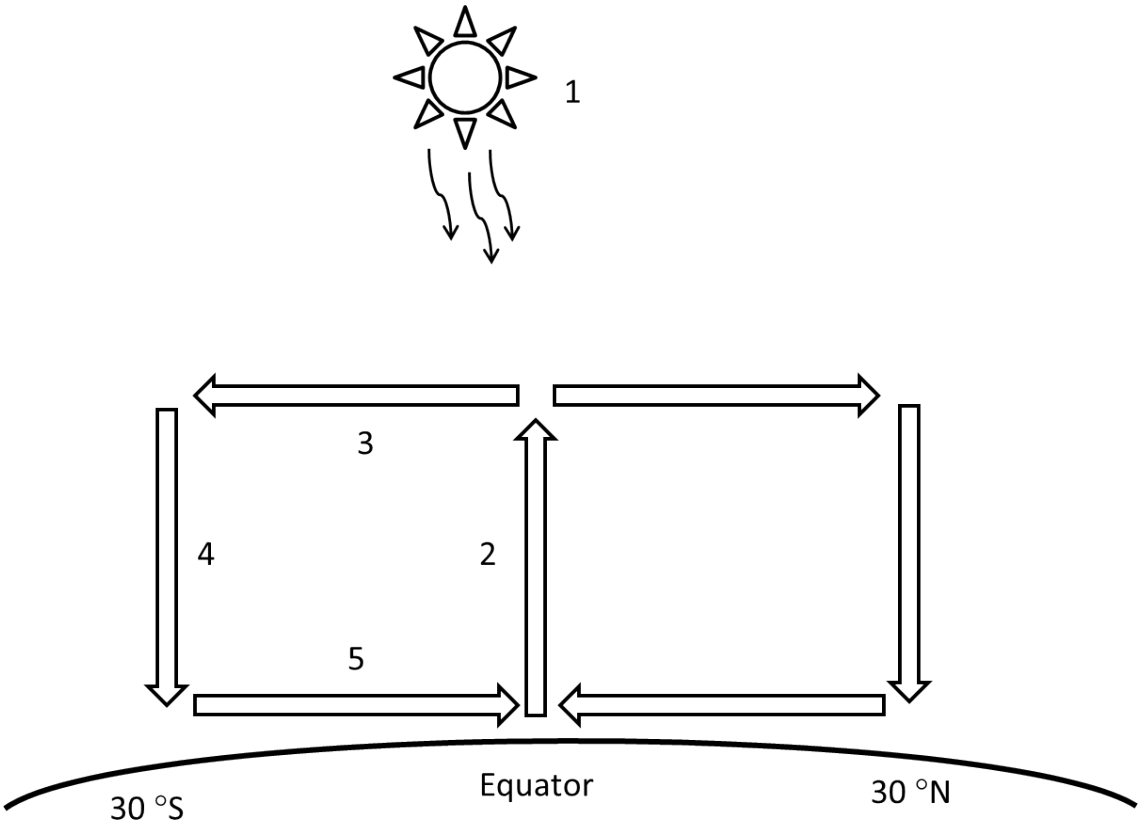

Figure 1.4: A representation of the Hadley cell, indicating air flows that create the cell. 1) Sunlight heats up the surface at the equator, which in turn heats up the air parcel above. 2) This air parcel rises rapidly as it's hotter and less dense than the air around it. 3) The air parcel ceases to rise, and is moved latitudinally by air rising beneath it. 4) The air parcel cools and sinks as it becomes more dense. 5) The air moves back towards the equator to fill the void by air rising, and heats up again, completing the cycle.

1.1.5 Measurement Platforms and Technique

1.1.5.1 Ground Based Sampling

There exist a series of 31 ground based constant monitoring stations certified by the World Meteorological Organization (WMO) Global Atmospheric Watch program (GAW) that provide the main evidence for background concentrations of air pollutants including VOCs. The basis behind this is that every station under their jurisdiction is calibrated to the same degree of scrutiny, making measurements more accurate and reliable. GAW stations fit can fit into a number of categories, depending on the location of the site, the placement of inlets and how rigorous the calibration procedure. Stations that fit all criterea with regards to these factors are termed 'Global' Stations', with other stations fullfilling the requirements for either Regional, or Local stations. The sites shown in 1.5 are the locations of the gloal stations only. One such site is the Cape Verde Atmospheric

Observatory (CVAO). The site is situated on the Cape Verdean island of Sao Vincente and, due to prevailing trade winds coming over the Atlantic, provides data from an open marine environment. A number of measurements are taken there including O_3, CO, NO, NO_2, NO_y, VOCs and halocarbons. The locations of all 31 GAW sites are shown in Figure 1.5. Different instruments measuring the same species can also be deployed to sites such as this, allowing direct intercomparisons to take place. Sites such as these produce long term datasets. This allows for the monitoring of differences in seasonal and annual profiles to be quantified, leading to deductions on natural and anthropogenic climate change.

Figure 1.5: Locations of global GAW stations across the planet.

Urban monitoring is more extensive than background monitoring due to high population densities, and the close proximity of several types of emission sources. Additionally, ground based monitoring stations exist in many different cities around the world to monitor urban pollution. London employs the use of $\approx$ 120 monitoring stations, known as the London Air Quality Network (LAQN). They measure pollutants such as CO, O_3, NO_2, PM 2.5, PM 10 and sulphur dioxide. The data from these sites are used to produce air quality forecasts and current levels of pollution for the public. The network is shown in Figure 1.6. However, VOC monitoring is done by a much more sparse set of stations. Only 4 automated stations exist, for the measuring of benzene and 1, 3 butadiene, as these two compounds are the only two that are monitored and regulated. These regulations state that concnetrations of these compounds should not exceed 5 and 2.25 μ m$^{-}3$ respectively. The non-automatic stations are slightly more numerous with 35 stations around the UK.

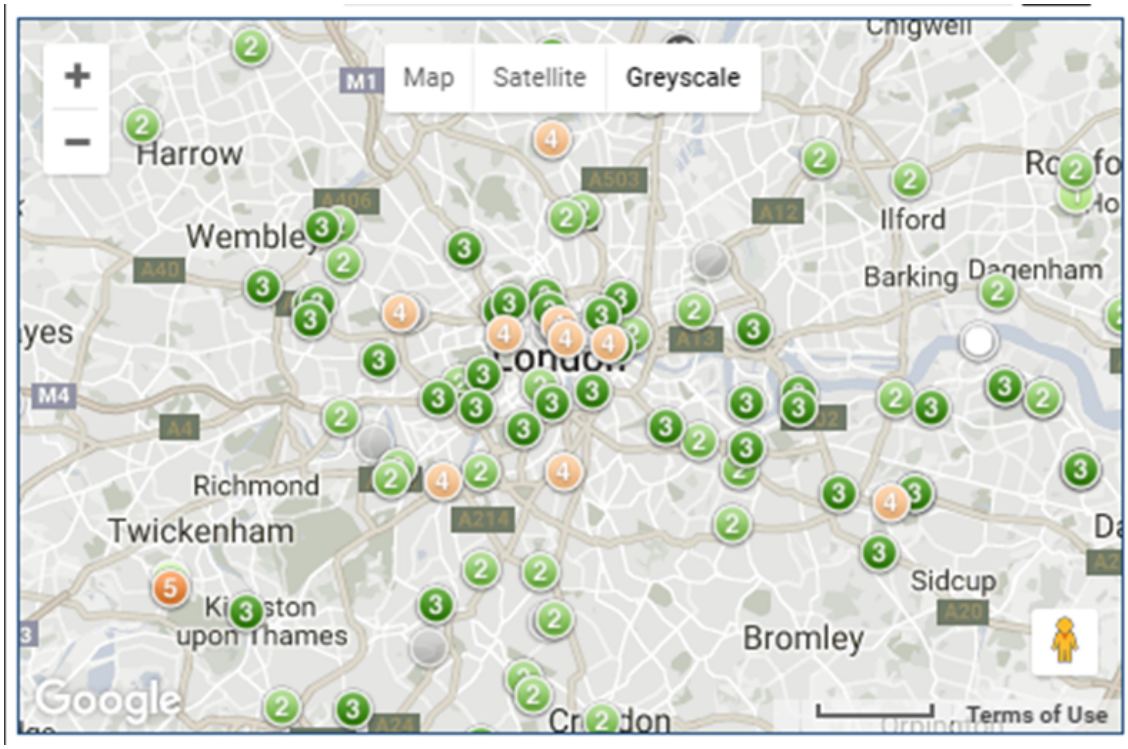

Figure 1.6: Location of the LAQN sites, displaying the level of air quality on a scale of 1-10. *Image courtesy of Kings College London*

The disadvantages of ground based stations is that they are usually fixed in position, meaning spatial variability is compromised. It is often not practical to set up ground based stations in all regions, due to issues such as politics or remoteness of location. Additionally, vertical profiles cannot be established, as measurements are taken at fixed altitudes, usually from a tower, which does not extend above the boundary layer. Finally, ground based stations are limited to the 1/3rd of the planet not covered by water.

1.1.5.2 VOC Trends

Over the past 15 years, measurements taken at urban background and kerbside sites have shown a decrease in the concentration of benzene and 1, 3 butadiene. This has largely been driven by improved vehicle emissions, and efforts to phase out the use of benzene as a solvent in industrial proccess and in gasoline. The decline in 1, 3 butadiene is attributed to the introduction of the three-way catalytic converter, now commonly fitted to gasoline engines. These trends are shown in Figures 1.7 and 1.8,

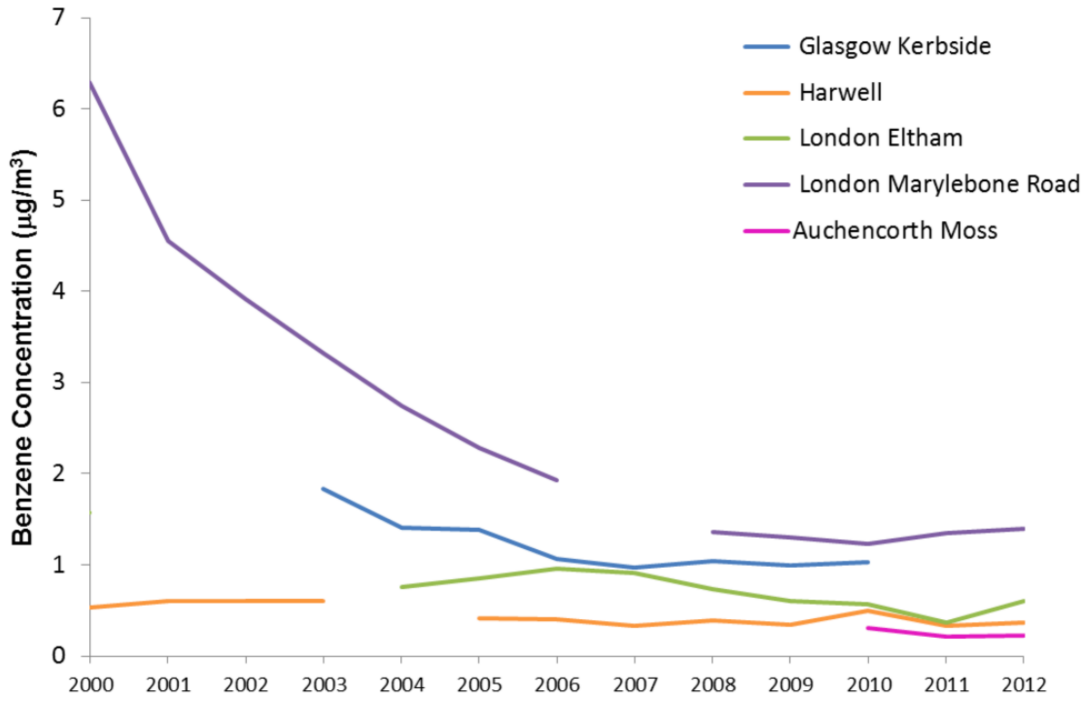

Figure 1.7: Trends in benzene as measured by the DEFRA Automatic hydrocarbon network. Data displayed is annual average data for benzene from the site *Image Courtesy of Defra*

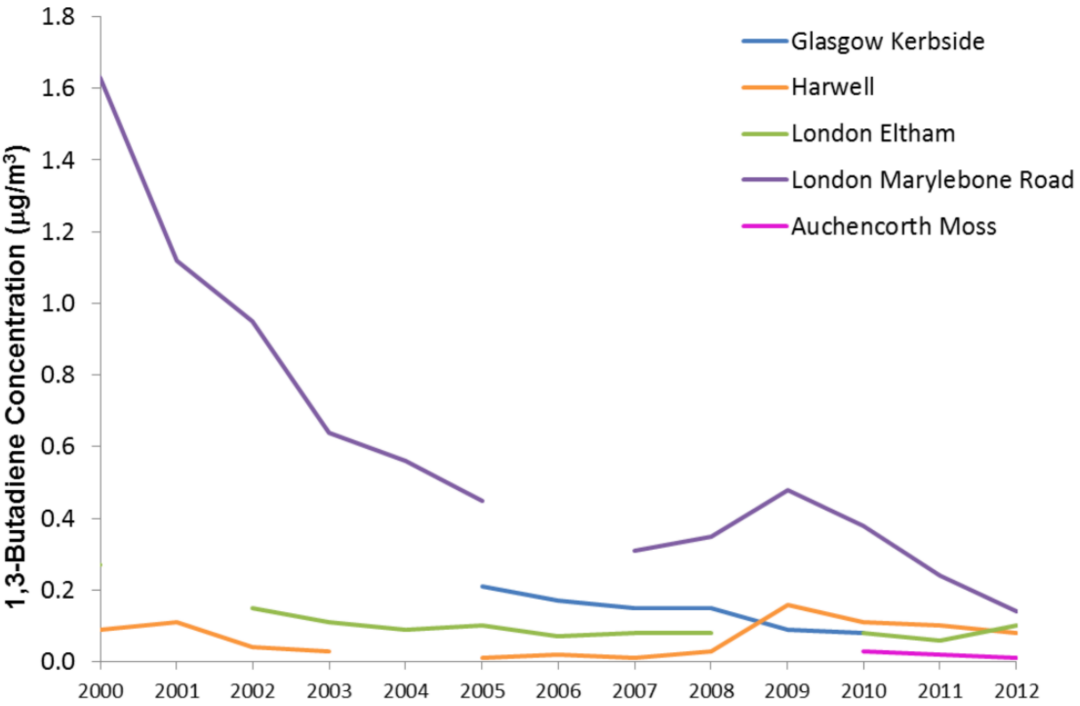

Figure 1.8: Trends in butadiene as measured by the DEFRA Automatic hydrocarbon network. Data displayed is annual average data for butadiene from the site *Image Courtesy of Defra*

1.1.5.3 Ship Based Sampling

UK has a fleet of research ships, run by the Natural Environment Research Council (NERC) and the British Antarctic Survey (BAS). Instuments placed on ships can sample air far away from land masses, and therefore far away from any local anthropogenic sources. Additionally, ship based sampling also includes the analysis of trace gases and biological components in the ocean. Trace gases in seawater can be analysed using Automated Purge and Trap with subsequent separation and detection by GC/MS. Full details can be found in Andrews et al. (2015). However, there are a series of problems associated with ship based sampling. Firstly, it is very time consuming and costly to operate instruments on ships. Wind direction can also play a part, as data must be discarded if the wind carries the ships emissions towards instrument sample inlets. As with ground based stations, ship based sampling is limited to the 2/3rds of the Earths surface covered by water.

1.1.5.4 Aircraft Based Sampling

Aircraft have the capacity to sample regions inaccesible by any other means. They allow spatial coverage of pollutants to be determined over a large area, in a brief period of time, meaning that emissions can be traced from the source for many miles to determine their transformation and dilution in air (for example Hewitt et al. (2003); Allan et al. (2014); Lewis et al. (2013) etc.). Additionally, they are capable of sampling at a large number of altitudes, from the surface up to a given aircrafts ceiling altitude. There are some drawbacks to airborne sampling platforms. Typically, the speed at which aircraft moves is on a timescale significant to the timescale some measurements can be made. This means that rather than a measurement being taken at a specific location, it is the average over the distance moved during the sampling time. Additionally, using aircraft places an upper limit on the amount of equipment that can be carried, and flights must be completed within the limitations of the aircrafts range. Finally, instruments placed on board must be able to withstand a large range of temperatures, pressures and humidities, both inside the aircraft and in the sample stream.

However, aircraft measurements have the advantage of being able to sample in a wide variety of locations, both over land and ocean. There still remain some restrictions due to political and safety reasons (for example, the FAAM aircraft must always nominate a redirect airport, in case of emergency, and therefore must carry enough fuel to reach the

redirect airport, shortening the flight time).

There have been many instances of the use of instuments mounted on aircraft for the use of measuring atmospheric composition. Measurement techniques include both online and offline air analysis, with instruments such as Proton Transfer Reaction mass spectrometry (PTR-MS), Chemical Ionisation Mass Spectrometer (CIMS) and Broadband cavity enhanced absorption spectroscopy (BBCEAS) (for example (Le Breton et al., 2013; Aruffo et al., 2016; Hewitt et al., 2003; Heald et al., 2008; Pan et al., 2016; **?**). These instruments and studies have been extremely successful in determining concentrations of a wide variety of species. However, these methods can have certain drawbacks, mainly in that for compounds that produce the same mass ions upon ionisation (see section 1.1.7.2) the instruments are unable to speciate compounds. In order to solve this, the separation of compounds based on volatilities is neccessary for the speciation of certain compounds. Therefore the use of a gas chromatograph can be employed.

1.1.6 Overview of Gas Chromatography

Chromatography is the science of separating a mix of compounds. Therefore Gas Chromatography (GC) involves the separation of a mix of chemicals into their constituent parts. In order to perform a GC analysis of a mix of gases, each chemical must be able to exist in the vapour phase at the operating temperatures applied to the separation medium.

The mix is passed through a column using a carrier gas (mobile phase). The column is internally coated with a stationary phase that interacts with analytes. Compounds go through a series of partitions between the stationary phase and mobile phase. Different compounds undergo different interactions with the stationary phase. At the end of the column, specific compounds elute in a discrete band. The time taken for compounds to elute from the column is known as the retention time and differences in retention time are the means by which components can be distinguished for one another. Modern standard GCs consist of an oven, the column and an electronic pressure controller (EPC) to regulate conditions inside the column. In most separations, the oven slowly heats the column, and each compound transitions into the vapour (mobile) phase, and elutes from the column. Many parameters can be changed to tailor a separation to a particular mixture.

Following separation, the eluent is passed into a detector, to determine the amount of material present. The result is usually displayed in the form of a chromatogram, with time along the x-axis, and an abundance-related parameter on the y-axis. These chromatograms give a baseline, due to noise on the detector and any trace compounds in the carrier gas, and peaks, which indicate the presence of a separated compound. Detectors used in conjunction with gas chromatography are many and various. The choice of detector depends on the amount of information needed, and the chemical structure of analytes.

1.1.6.1 Theoretical Plates and Chomatographic Resolution

Gas chromatography can be compared to the process of fractional distillation in two distinct ways. Firstly, both processes separate mixes based on a compounds boiling points (or vapour pressures). A GC program is usually run with a temperature gradient, heating up as the analysis continues. A fractional distillation column has a temperature gradient applied to it. The mixture enters at the bottom of the column, where it is heated. As compounds travel up the column, they cool, until the temperature matches their boiling point. Throughout the column at specific temperatures, plates are fitted to collect the fraction condensing. In GC, a separation can also be said to have plates, but these are

purely theoretical. The number of theoretical plates, N, describes the number of active sites in the stationary phase an analyte can bind to. It is important to note that this number is a purely theoretical measure of peak width for a peak at a specific retention time. It can also be referred to as column efficiency. The number of theoretical plates is determined by Equation 1.24. A column with a higher number of theoretical plates will yield narrower peaks than one with a low number. L is the length of a given column, and HETP is the height equivalent for theoretical plates.

$$N = \frac{L}{HETP} \tag{1.24}$$

N can also be calculated from a peak, using the retention time and peak width of a particular analyte. This is given in Equation 1.25.

$$N = 5.54 \left(\frac{t_r}{w_{\frac{1}{2}}} \right)^2 \tag{1.25}$$

The HETP can be calculated using the Van Deemter equation shown in Equation 1.23, where A is the Eddy-diffusion parameter, B is the difffusion coefficient, C is the resistance to mass transfer coefficient and u is the linear velocity. In capillary columns, A is equal to 0, as this refers to the convoluted path taken by molecules travelling down a packed column.

$$HETP = A + \frac{B}{u} + C.u \tag{1.26}$$

An alternative way of calculating HETPfor capillary columns is to use the Golay equation:

$$H = \frac{B}{\mu} + C.u \tag{1.27}$$

The Van Deemter equation gives a different curve for each carrier gas. In general, lighter gases have a higher optimum velocity. Whilst nitrogen has the lowest height of theoretical plates, it can only operate at very slow velocities ($\approx$ 10 cm/sec). Hydrogen and helium have a slightly higher value for HETP, but are more consistent over a practical range. This is shown in Figure 1.9.

In practice, these theoretical values are rarely calculated, due to uncertainties in the parameters. It is more common to calculate the resolution of he peak, R_s. This is given in Equation 1.24.

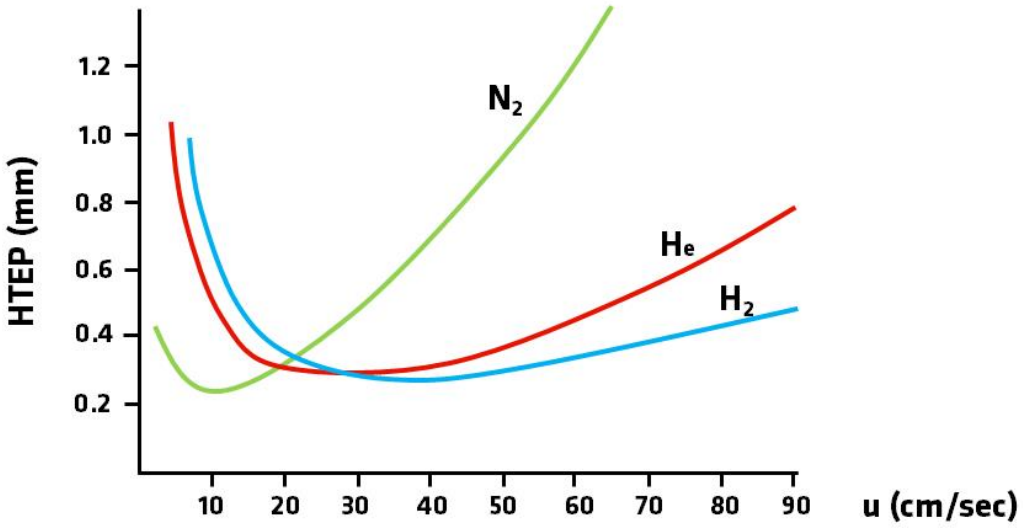

Figure 1.9: Van Deemter plot of theoretical plate height against gas velocity for N_2, He and H_2

$$R_s = \frac{\sqrt{N}}{4}\left(\frac{\alpha - 1}{\alpha}\right)\left(\frac{k'}{1+k'}\right)^2 \tag{1.28}$$

Where α is the selectivity factor and k is the capacity factor. Based on the Van Deemter graph, the best carrier gas to use for fast separation is H_2. However, as it is highly explosive, in practice the most commonly used carrier gas is He.

1.1.6.2 Applications of GC in Atmospheric Measurements

GC is a highly versatile technique, as there are many parameters that can be altered and tailored to meet a specific separation need. Therefore, it makes GC ideal for atmospheric mixtures. Depending on the target analyte, column parameters (length, id and stationary phase) and temperature can be varied, to analyse a wide range of compounds- from C_1 to $> C_{20}$. Additionally, GC systems have decreased significantly in cost over the last few decades, and have become easier to transport. GC has been widely used for analysing atmospheric composition, usually from ground-based constant monitoring stations, but also from a variety of different platforms (for example Montzka et al. (1996); Ribes et al. (2007); Wang et al. (1995); Graham (2002) and many more). Samples can be collected and analysed either *in situ*, or from canisters, bags, cylinders or adsorption tubes filled in the field and brought back to the laboratory for analysis. Platforms for *in situ* measurements include tower masts and road side inlets, as well as road vehicles, ships and aircraft.

1.1.7 Thermal Desorption

Atmospheric samples are too dilute to directy measure VOCs by GC analysis. A simple injection of a dried gas would not contain enough analyte in order to produce a recognisable signal on resulting chromatograms. Additionally, the presence of oxygen in the sample would interfer oth with the adsorbing/desorbing processes, and with subsequent separation. Therefore some method of preconcentration is neccessary. One such widely used method of preconcentration is thermal desorption. In principle, thermal desorption is a simple method of taking large samples of air ($\approx$ 1 L), and analysing it for organic compounds. An air sample is passed over a sorbent, held at a low temperature whilst all organic compounds adsorb to the sorbent. The trap is then flushed with an inert gas to remove oxygen. Prior to separation, the sorbent is flash heated and all desorbed compounds are passed down the column. In this way, compounds in extremely low concentrations can be detected by GC/MS. More information on the specific technique used here is given in Chapter 2.

1.1.8 Mass Spectrometer Theory and Applications

1.1.8.1 Mass Spectrometer Theory

Detector selection is an important consideration in gas chromatography. The choice of detector will depend on the type of analyte, with specific detectors being highly specialised. For example, a Nitrogen Chemiluminescence Detector (NCD) is used exclusively for detection of nitrogen containing compounds. Additionally, the amount of information required about analytes is also important. For the characterisation of unknowns and the identification of compounds, a mass spectrometer is required. The mass spectrometer can give chemical structures based on characterisitic fragmentation patterns. These can then be compared to a library to give a probable structure.

When coupled to GC, mass spectrometry is among the most sensitive of detectors, with the most sensitive being able to detect compounds in mixing ratios as low as a few parts per quadrillion (ppq). Additionally, by changing the ion source, or mode in which the mass spectrometer operates, it is possible to tailor the sensitivity of the spectrometer to specific families of compounds.

The principle on which mass spectrometry works is as follows: after elution from the column, analytes pass into the ion source. Here, using a range of different methods, or

combination of methods, analytes are ionised, and accelerated towards a mass analyser. This filters the ions, leaving ions with a single mass/charge (m/z) ratio to pass through to the detector. The mass analyser cycles through the range of mass ions programmed extremely quickly (a rate of $>$ 100 Hz). A high cycle rate means a large range of mass ions can be scanned. The cycle rate requires a balance between scanning all mass ions and a higher ion dwell time, which leads to improved sensitivity.

1.1.8.2 Ionisation

Analytes can be ionised in a number of different ways. These can broadly be separated in to two categories: hard and soft ionisation. Hard ionisation imparts a large amount of energy onto analytes causing them to fragment in a specific pattern. One such example is electron ionisation. Analytes are directed past a heated filament, which, when a voltage is applied across it, releases electrons with 70 eV of energy. Upon collision with an eluting analyte, the energy imparted is sufficient to cause an electron to be 'knocked off'. This process imparts a large amount of energy onto the target ion, causing the ion to fragment, assuming that the imparted energy is greater than the bond dissociation energy. The interaction is shown in Equation 1.25, with M being an analyte.

$$M + e^- \rightarrow M^{+\bullet} + 2e^- \tag{1.29}$$

Soft ionisation techniques essentially follow the same pattern, but without imparting excess energy onto the analyte, causing it to fragment. One such example of this is chemical ionisation which is used in Proton transfer reaction mass spectrometry (PTR-MS). PTR-MS makes use of protonated water (H_3O^+) in a reaction with analytes. A proton is transferred from the protonated water to the target analytes, causing them to be positively charged. A condition for this is that analytes must have a greater proton affinity than water, and as such, some compounds cannot be ionised in this way. However, less energy is transferred in the process, meaning compounds retain their structure, with the addition of a proton. Many other compounds can be used in chemical ionisation, such as methane, ammonia and isobutane. This makes it a highly versatile technique.

1.1.8.3 Mass Analysis

Once analytes are ionised, they are accelerated into the mass analyser. Mass analysers can be very diverse, but usually involve an electromagnetic field. Quadrupole MS is possibly

the most common of mass analysers. It employs four charged rods held parallel to each other, so as to create a hyberbolic field when a voltage is applied across them. The voltage is alternated between the pairs of rods. Rods adjacent to each other carry an equal, but opposite charge, which sets up the hyberbole. As ions enter the mass analyser,they begin to oscillate. Based on the frequency of the oscillation of the charges applied to the rods, all but ions with a single m/z ratio will develop an unstable oscillation, causing them to either be removed from the system, or collide with one of the rods, neutralizing them. However, the target ion will maintain a stable oscillation along the path length and emerge at the detector.

Quadrupoles can be used independently, or as a front end for another mass analyser. They are commonly coupled to Time Of Flight (TOF) mass analysers. After emerging from the quadrupole, ions are directed into the flight tube. At the end of the flight tube is a reflectron, kept at an electric field of known strength. The amount of time taken for ions to move towards the reflectron and back towards the detector is dependent on its m/z ratio. Heavier, weakly charged ions will take a longer path than smaller, highly charged ions. Even though the change in distance, and therefore time, is small, the TOF can give a highly accurate mass accuracy. TOFs can also be used independently of quadrupoles.

1.1.8.4 Detection

Detection of ions is usually carried out by an Electron Multiplier (EM). Ions emerging from the mass analyser are directed towards the EM, where they are acclerated towards an electron rich plate which forms one side of a cone-like chamber. Upon striking the plate, the ions themselves are neutralised, however, the energy released from striking the plate is sufficient to release additional electrons from the plate. These collide with the other side of the cone, and another set of electrons is released. A cascade of electrons moves down the cone, causing a change in voltage, which can be detected and amplified. The size of the change in voltage is proportional to the number of ions striking the plate. A schematic of an EM is shown in Figure 1.10.

There have been many instances of mass spectrometry used to measure atmospheric composition (for example Yuan et al. (2014); Yassaa and Williams (2005); Ribes et al. (2007); Andrews et al. (2016)). One of the main challenges of using mass spectrometry in field work is their large power consumption. In order to achieve optimum results, the mass spectrometer should be kept on, and under vacuum for as long as possible (or is practical).

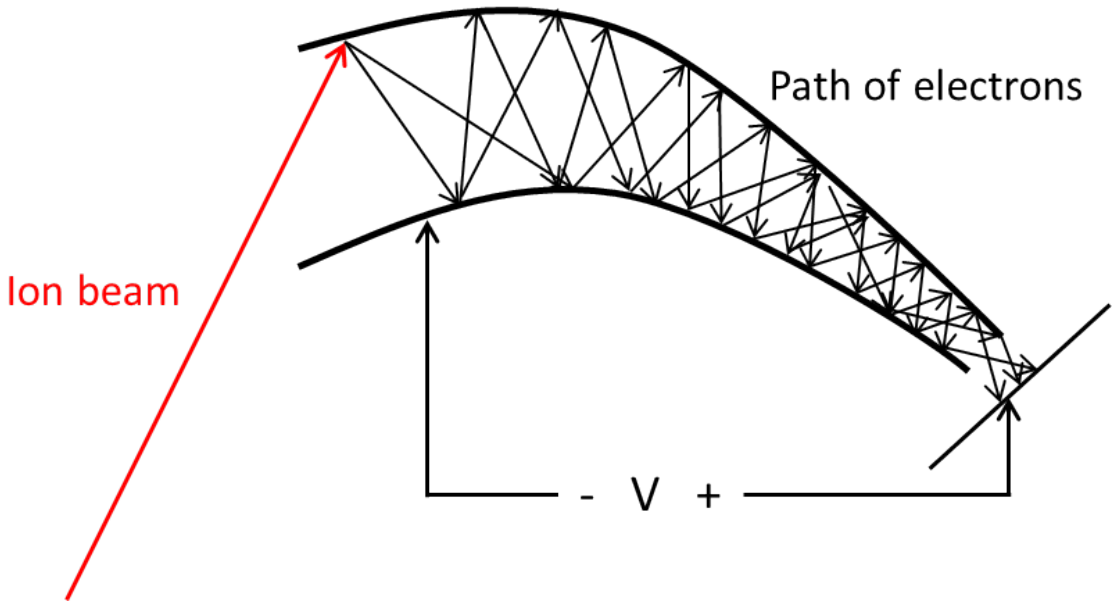

Figure 1.10: Schematic of an Electron Multiplier detector. Ions strike the electron rich plate, initiating a cascade of electrons, which can be detected by a voltmeter.

Typically, mass spectrometers also require a roughing pump to ensure the chamber is kept under vacuum, as air and water can interfere with the transmission of ions. Additionally, mass spectrometers are fairly large pieces of equipment, so during fieldwork, this must be taken into consideration.

1.1.9 Overview

This thesis will focus on work done on, and data gathered by the University of York airborne GC/MS system. To date, the instrument has been fitted on the FAAM aircraft, a modified BAe-146, for five campaigns in total; four overseas, and one UK based campaign. The aircraft in flight is shown in Figure 1.11.

Figure 1.11: The FAAM BAe-146-301 ARA in flight. The probes and inlets can be seen mounted to the body, nose and under the wings, giving the aircraft the capacity to make a large range of different measurements- from meteorology and cloud microphysics to atmospheric composition of a wide range of species. *Image Courtesy of FAAM*

1.1.9.1 FAAM BAe-146

UK airborne studies typically use a variety of aircraft, with the largest being the Facility for Airborne Atmospheric Measurements (FAAM) BAe-146-301 large Atmospheric Research Aircraft (ARA). Modifications to the aircraft include extending the cabin, removal of most seats, extension of the fuel tanks and, crucially, the fitting of a series of sampling pipes and probes to the nose, body and wings. All instruments on board are fitted into racks, which take the place of most of the seats. Around 20 seats are kept on board for the instrument operators.

The aircraft typically has a flying range of four to five hours, travelling at $\approx$ 100 m/s, or 200 knots. Whilst measuring, the aircraft travels at this speed consistently, to ensure

Figure 1.12: View from the rear of the aircraft during a flight, showing the lines of racks housing the scientific instrumenation. *Image Courtesy of Jim Hopkins*

a steady air flow down the sample pipe. The flight duration is dependent on the science payload. Whilst the aircraft allows measurements to be made in otherwise inaccesible locations, the speed at which it travels can have a detrimental effect on the scientific measurements. For instance, all samples cannot be described as being made in a fixed location, but instead are an average over the distance moved during the sample time.

The aircraft has a ceiling altitude of 32,000 ft ($\approx$ 10 km), however, as the majority of instruments are calibrated to measure in the boundary layer and lower troposphere, compositional science is rarely conducted at this height. Additionally, The aircraft has a lower altitude limit of 100 ft. It can also perform drops to 50 ft above the ocean for short periods of time. This is critical for measuring within the boundary layer, as well as determining sources of emissions. Aircraft flight plans can be continually altered, depending on incoming science data. This is usually done at the request of the mission scientist, who is stationed on the flight deck, monitoring the data stream from the aircraft internal intranet (HORACE prior to 2014, DECADES post-2014). All instrument operators can monitor the core data, and act on it *in situ* for instance, by filling a Whole Air Sampling (WAS)

Config 14a Var ACCACIA 1d Diagram 1 of 2.png

Config 14a Var ACCACIA 1d Diagram 1 of 2.png

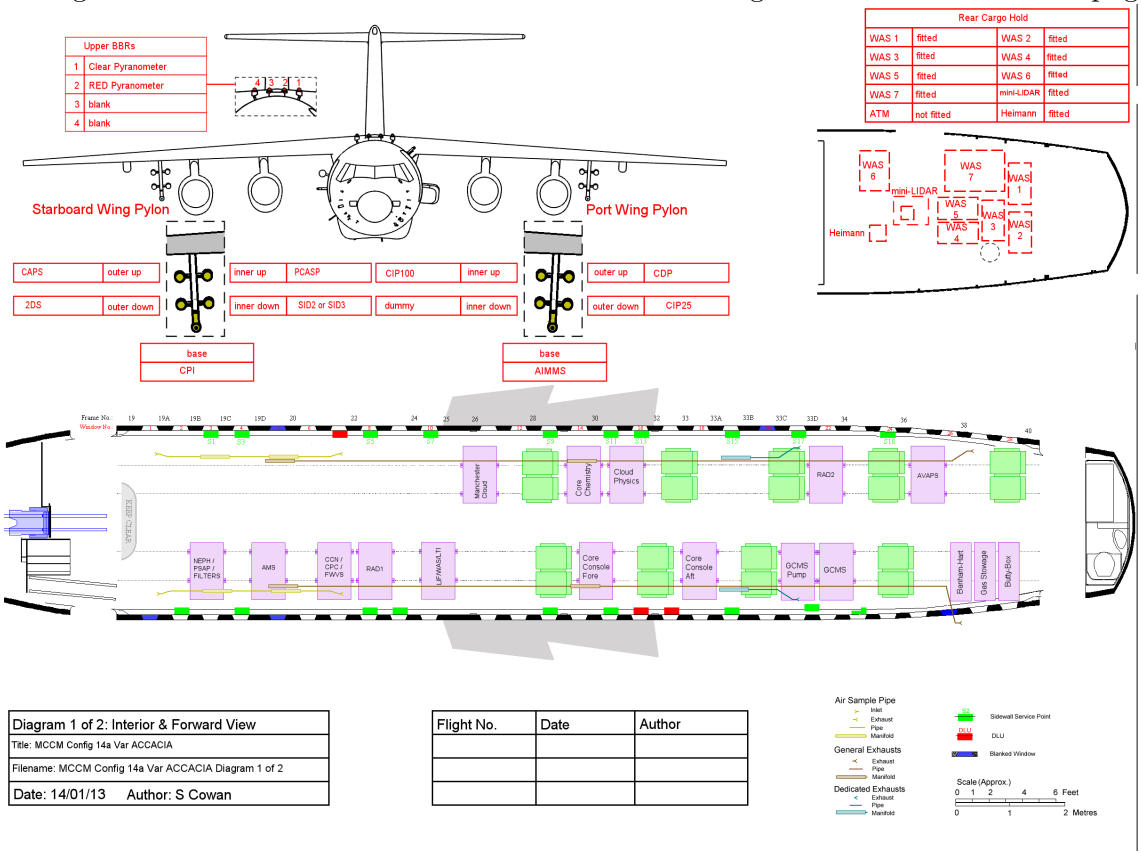

Figure 1.13: Example of a configuration of instruments onboard the aircraft.

cannister. WAS cannisters are internally coated with an inert substance (SILCO)S, and filled to ≈ 2 bar with an air sample. This is then analysed offline by numerous different methods, usually GC with either Flame Ionisation Detection (FID) or MS.

1.1.10 Thesis Overview

This thesis will primarily discuss development, modifications and deployment of the University of York airborne GC/MS. As stated, the instrument has been fitted to the FAAM ARA for 5 different flying campaigns.

Chapter 2 details the modifications made to the instrument during the course of this project. Previous work was conducted to streamline the sample and analysis time of the instrument and, using this, additional work was carried out on the instrument, specifically the sample introduction element of the instrument.

Chapter 3 analyses the data collected during the South American Biomass Burning Analysis (SAMBBA) campaign. A number of flights were conducted over the Amazon rainforest during the forest fire season, to investigate the impact of forest fires both regionally and globally. Vertical profiles of biogenic and anthropogenic tracers were plotted to determine the vertical extent of these emissions. Additionally, further work was conducted to determine VOC:CO ratios in order to validate global model studies.

Chapter 4 discusses results from the Coordinated Airborne Studies in the Tropics (CAST) campaign. Vertical profiles of halogenated organic compounds were produced from the ocean surface to the lower straosphere. This was done in conjunction with measurements taken aboard two other aircraft flying above, to give a full vertical profile of these halogenated compounds. Extensive cross calibrations were conducted to verify the data from all platforms. Additionally, back trajectories were computed along with calculations to determine the age of air masses, depending on high and low ozone mixing ratios.

Chapter 5 investigates fugitive emissions from the North Sea Oil and Gas rigs. The *in situ* GC/MS was once more deployed to investigate the emissions, if any, of larger NMHCs. Flights were conducted to survey background emissions, and the direct emissions from a group of rigs collectively termed 'Forties'. The methane trace was used to determine whether measurements were in or out of the plume. However, the plume length averaged at ≈ 20 seconds, meaning that the GC/MS was unable to directly measure mixing ratios of NMHCs within the plume. Therefore, calculations were performed to estimate emissions in a number of plumes. This was done for ≈ 20 plumes, with calculated emissions varying largely. It was concluded that this was due to the wide variety of actitvities taking place on each rig. Overall, the instrument was generally unsuitable for this kind of anaylsis, as the sample time was too long. However, the conclusion that can be drawn is that in

plumes, concentrtions of larger NMHCs arelow, but potentially extremely significant for species emitted directly such as CH_4 and NO_x, as these were found to be higher than those reported in inventories.

Chapter 2

Experimental and Instrument Development

2.1 Experimental and Instrument Development

Deploying an instrument on an aircraft generates a separate set of practical issues when compared to a ground based instrument. These can include health and safety regulations, restrictions on size and weight, or restrictions on operation. Whilst the GC/MS instrument here was being designed, the individual sub-components were chosen for specific reasons, with size, performance and reliability in mind.

Conditions for operating on the aircraft are very different from operating ground based instruments. Power requirements are carefully monitored to ensure the aircraft generators are capable of delivering power to all instruments. Additionally, issues of size and mass are important. Instruments are typically required to fit into specially made racks with all instruments, wiring and tubing to be contained within the rack. This is to ensure that all components of the instrument are secured and no overhanging parts and reduce the risk of snagging wires etc. A further consideration for aircraft measurements is time resolution. For a moving platform, the faster a measurement can be made, the greater the spatial resolution of the observation. Finally, the speed at which the instrument can be taken from a cold 'off' state to a fully operational state is of critical importance. As no tools are allowed on the aircraft during taxi, take-off and in flight, all mechanical work, as well as calibrations, must be carried out within a pre-flight period, typically a few hours. During this chapter, the modifications described were undertaken with the limitations imposed by aircraft capabilities and protocols in mind.

This chapter will focus on developments made to the University of York aircraft gas chromatography/mass spectrometer (GC/MS) system between 2012 and 2015. In this section, the optimization of the individual components of the instrument will be discussed in detail, with modifications highlighted and explained. The instrument used throughout this project was a rack mounted, airborne dual-channel thermal desorption GC/MS. The instrument configuration is shown in Figure 2.1

The instrument in its initial state will be described first, followed by the modifications made prior to each campaign. The period between 2012 and 2015 will be covered.

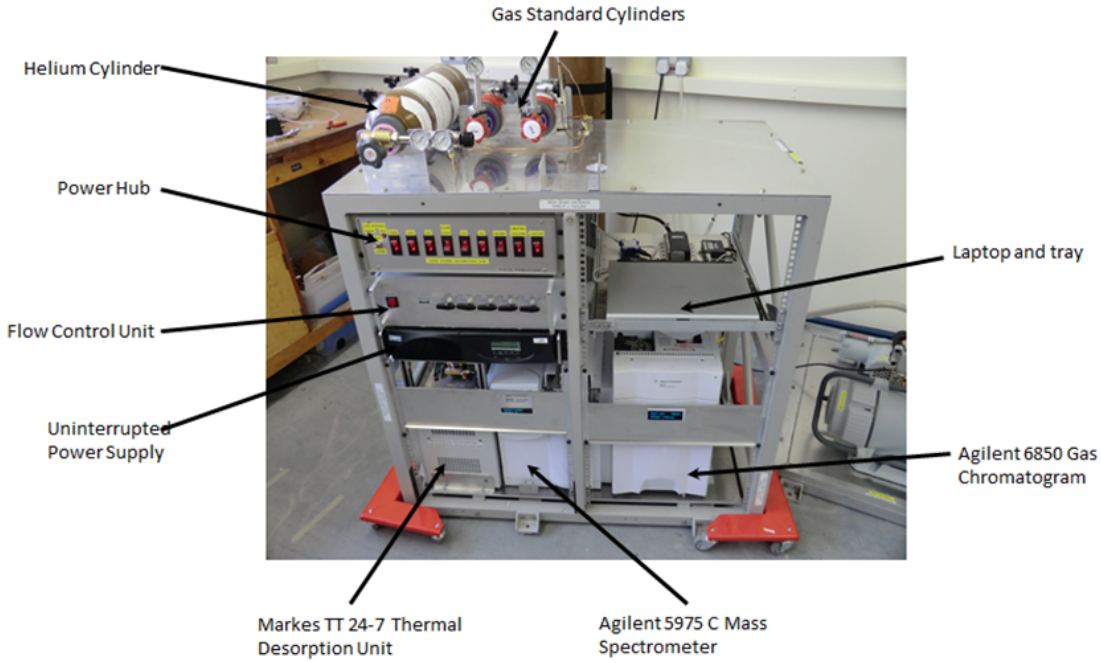

Figure 2.1: The University of York aircraft GC/MS rack, with key components indicated

2.1.1 Instrument in its Initial State

2.1.1.1 Cylinders and Calibrations

The carrier gas used was helium, a compromise giving a reduced number and height of theoretical plates, but without the issues associated with an explosive environment created with using H_2 as a carrier gas (see chapter 1). The cylinder was mounted on top of the rack using two AEROX cylinder brackets (AEROX, USA). The carrier gas used was of chromatography grade (< 0.0001 % impurity) and was passed through a hydrocarbon and moisture trap prior to use. The carrier gas pressure was set by the regulator to 40 psi. This was sufficient to supply the electronic pressure controlled GC with enough pressure at maximum temperatures and supply the thermal desorption unit with a purge gas. Two calibration cylinders were also mounted on top of the rack. These were both 1.2 L NPL cylinders (NPL, UK), with one containing a 15 component VOC standard in nitrogen and the other containing 5 ppb of deuterated toluene in nitrogen.

2.1.1.2 Sample Pressurisation/Pump Tray

In flight, the instrument drew sample air in from outside the aircraft through a piece of 3/8' stainless steel tubing using a double- headed, 400Hz metal bellows pump (Senior Aerospace) located on the pump tray powered by 115 V. It was then passed through a

mechanical pressure relief valve, which was adjusted to flow at 5 bar. The sample was then pushed through the subsequent instruments with a postive pressure on the outlet side. Also located on the pump tray was the mass spectrometer Edwards XDS scroll pump (Edwards, UK), powered by 230 V.

2.1.1.3 Power Distribution Box (PDB)

Power was fed to the instrument from a side service port on board the aircraft. This provides 230 V to each of the instruments. The power distribution box then sent power to the separate instruments. Table 2.1 shows the power consumption of each item, along with the total.

Table 2.1: Table showing the Power consumption of the various components of the aircraft GC/MS

Item #	Designation	Voltage	Circuit Breaker (A)	Current 230V	Current 115V	Max Power
S02	UPS Power	230V	10	0.7		161
S03	MS	230V	5	4.5		1035
S04	UPS Supply	230V	5	N/A		
S05	Flow control	230V	5	1.35		310.5
S06	TD	230V	5	1.7		391
S07	GC	230V	10	3.9		897
S08	Fan Rack	230V	5	1		230
S09	Heated column (not used)	230V	5	N/A		
S10	Laptop	230V	1	0.1		23
S12	Sample pump	Three phase	7.5		5.2	1196
S13	Vaccuum pump	230V	5	4.1		943
					Max power draw	5186.5

The power consumption calculated here is for the maximum power used by each instrument, usually at power start-up, known as transient power. As the instruments are powered up separately (see appendix 1), in practice, the instrument never draws the 5.2 kW shown in the table. The gas chromatograph and mass spectrometer are powered via the Uninterrupted Power Supply (UPS), in order to protect them from potential power outages on the aircraft.

2.1.1.4 Flow Control Box (FCB)

The flow control box was designed and built in-house. The main function of the FCB was to manipulate air samples and prepare them for analysis. Air samples must be dry before analysis (Fehsenfeld et al. (1992)). Water vapour within the column can interact with both the column itself and with analytes passing through the column causing unfavourable interactions with the stationary phase. This can lead to a distortion of peak shapes.

Additionally, water also plays a negative role within the mass spectrometer, shortening the life of the ion source, and interfering with the ion beam. In the initial configuration of the GC/MS, water was removed using a Nafion membrane prior to preconcentration. Nafion is a highly polar polymer made up of heavily fluorinated monomers, causing water molecules to pass through, which are then absorbed by a molecular sieve, whilst blocking any other compounds.

The sample was passed through a 50 cm long Nafion membrane tube (manufactured in-house), surrounded by desiccator beads and water-sensitive indicator. A humidity sensor was also present in the system to alert the operator if the humidity increased. Following water removal, the sample was directed into a four position, and then a two position valve (both VICI, USA). The purpose of the four position valve was to enable the operator to switch between an air sample, a zero gas sample and a standard whilst in flight. Figure 2.2 shows a schematic of the valve.

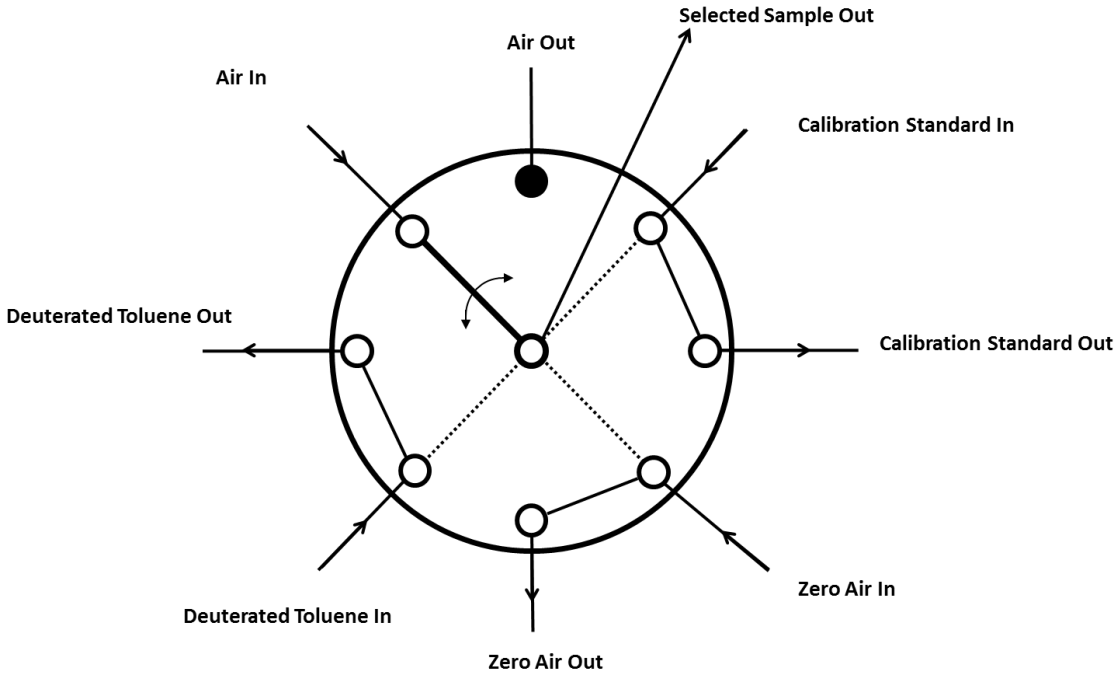

Figure 2.2: A schematic of the four-position valve used to change between different sample types

Deuterated toluene (D-toluene) was used as an internal standard, in order to track changes in MS sensitivity. D-toluene was used as it is not present in detectable quantities in the atmosphere, and produces a strong signal at retention times similar to other analytes. The two position valve was used to add a 5 μL aliquot of deuterated toluene to each sample by filling a 5 μL loop with a 5 ppb standard of deuterated toluene in nitrogen. The valve

then actuates to flush the contents on the loop into the sample stream. The schematic is shown in Figure 2.3.

The two valves were powered by a 24V, 2.2A power supply (RS Components, UK). To control the valve, a National Instruments controller was fitted, and controlled by a 12V power supply. The controller received a trigger from the thermal desorption unit (see section 2.1.1.5), which in turn, actuated the valve.

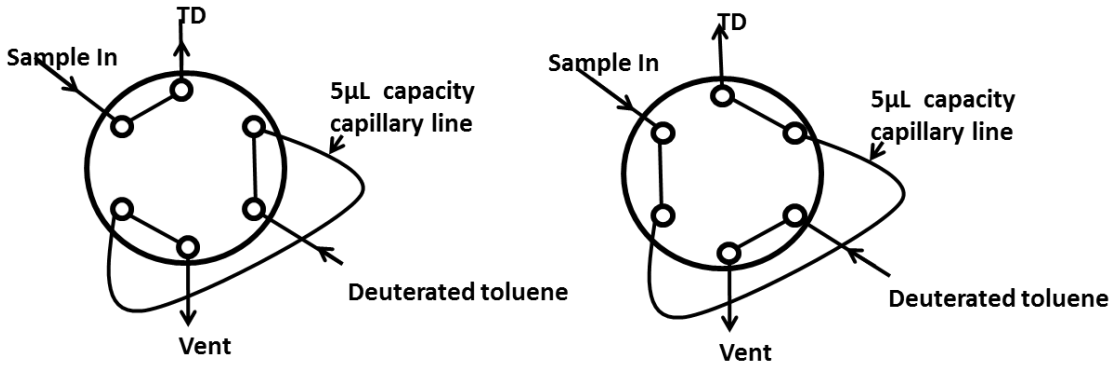

Figure 2.3: A schematic of the two position valve used to track mass spectrometer sensitivity shown in both positions with the sampling position on the left and the injecting position on the right

2.1.1.5 Thermal Desorption Unit (TDU)

The thermal desorption unit is a Markes TT-24/7 (Markes, UK). The system employs two glass traps, containing sorbents, and cooled to low temperatures. The sample gas is then passed through them, with volatile organics preconcentrated. The traps are then flash heated, the organics desorbed and the sample passed onto the GC column via a capillary transfer line. The sample from the FCB was directed to the thermal desorption unit via a piece of 1/8 stainless steel tubing. The sample was directed over either one of the traps via a series of patented heated valve assemblies from Markes International.

The instrument contains two alternating traps to allow constant uninterrupted sampling. Whilst one trap is collecting and concentrating a sample on the adsorbent, the other is desorbing previously collected organics onto the GC column, followed by a cooling down stage. The traps were filled with Tenax TA, chosen as it has a documented affinity with intermediate volatile organic compounds (VOCs), is suitable for monoterpenes, and does not trap CO_2 (Andrews et al. (2015); Brown and Purnell (1979); MacLeod and Ames (1986)). The traps were cooled to -10 ° C whilst the air sample was passed over them and out through the instrument exhaust. Samples were collected over 5 minutes at a flow rate

of 200 mL/min, therefore sampling 1 L of air. This flow rate and sample volume was chosen after confirming breakthrough tests on isoprene, one of the more volatile compounds to be measured by this system. Figure 2.4 shows the results from a breakthrough test on isoprene.

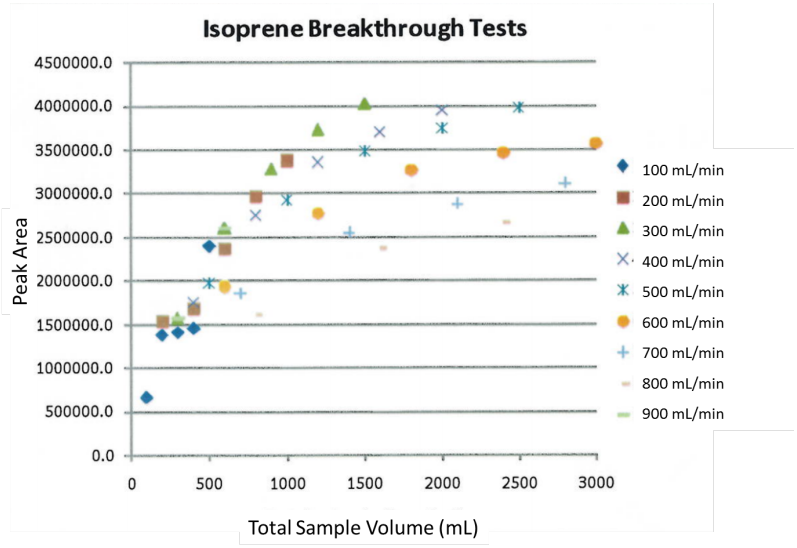

Figure 2.4: Isoprene breakthrough tests. A total sample volume of 1 L with a flow rate of 200 mL/min was chosen, as this was a compromise between compounds breaking through, a large enough sample volume for less abundant compounds, and a fast overall rate of sample collection.

The isoprene breakthrough tests were performed at these volumes and flow rates. The tests at 100 mL/min were discontinued as repeated tests were unreliable. Runs at 50 mL/min were not conducted, as this would have taken too long to acquire enough sample for analysis. Post sampling, the traps were purged for 6 seconds with helium, removing any water vapour and oxygen from the trap. The purge flow rate was set to 150 mL/min. The trap was then heated rapidly to 230 °C for desorption with a flow of helium. These were directed onto the transfer line by the heated valves, and then on to the GC column. The flow rate over the trap was held at 1.6 mL/min, and was controlled by the GC electronic pressure controller (EPC, also referred to as the pneumatics module). In order to calculate the flow rate through the column, the EPC reads the pressure leaving from, and returning to the TD. A split was also applied to the injection, to avoid overloading the column, which causes irregular peak shapes. The split flow was controlled using a needle valve to ˜16 mL/min leading to a 10/1 split. A full flow diagram of the instrument is shown in Figure 2.5.

The diagram also shows two additional tubes- desorption and split tubes. These in-

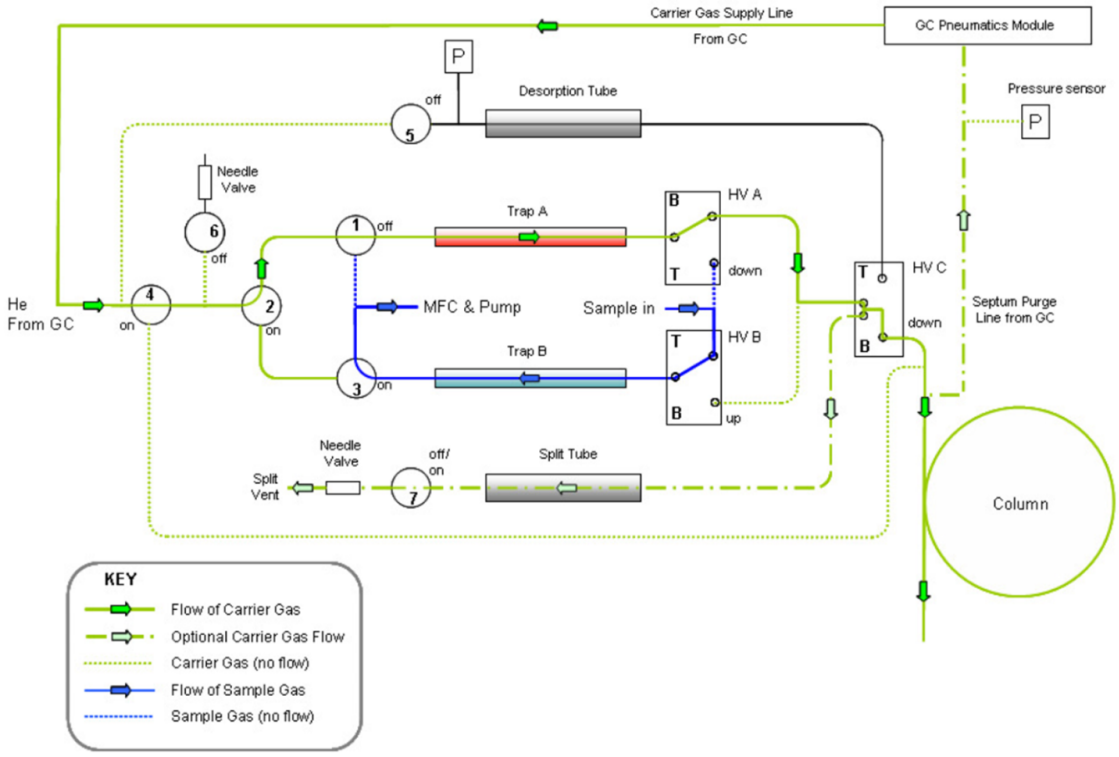

Figure 2.5: A flow diagram of the Thermal Desorption Unit showing all potential flow paths. (Markes (2006)).

crease the functionality of the instrument. The desorption tube slot can be used to conduct offline analyses of samples collected in the field. The split tube can be used to recollect any analyte in the split flow. However, neither of these functions were used during this project.

2.1.1.6 Gas Chromatograph (GC)

The aircraft instrument employs the use of a 6850 Agilent gas chromatograph. This specific instrument was chosen due to its smaller footprint when compared to other GC ovens. As a top loading GC, the column can be changed and fitted without removing the GC from the rack. This was preferable for an aircraft instrument, as it meant that columns could easily be changed during campaigns. After preconcentration on the TD, the sample was passed down a heated transfer line, internally coated with deactivated silica. The stationary phase used depends upon the target analytes (see chapter 1). However, in order for fast analysis times, all columns used were 10m in length, and with a carrier flow of 1.6 mL/min. The GC was set to splitless injection mode as the split is controlled by the TD unit. Previous optimization work was performed for the GC and a temperature

program of 50 ° C to 150 ° C with a ramp rate of 40 ° C/min was found to be the best compromise between analysis time, and resolution.

2.1.1.7 Mass Spectrometer (MS)

Mass spectrometric detection was carried out using a 5975C Agilent MS. Again, this was chosen due to its smaller footprint, when compared to other bench top mass spectrometers, which is key for an aircraft instrument due to limits on space. Ionisation of analytes was carried out using electron ionisation at 70 eV. Following ionisation, a quadrupole is used to select ions based on their m/z ratio (see chapter 1), and passed through a triple axis to the detector. Essentially, the ion beam is directed along 3 different paths, according to the m/z ratio of ions. This narrows the ion beam, improving sensitivity. Detection is carried out by an electron multiplier. The mass range is set to 44 amu to 250 amu, in order to quantify large organic species. The transfer line between the GC and the ion source was set to 250 ° C, with the ion source at 250 ° C, and the mass analyser set to 200 ° C. These temperatures were selected in order to reduce the amount of water inside the mass spectrometer, by keeping all sections of the instrument hot, so that water vapour passed through the instrument, leaving the ion beam unaffected, leading to greater ion transmission. The mass spectrometer can be set to operate in selected ion monitoring (SIM), full scan mode, or a combination of the two. When operating in SIM, the user enters a series of ions to monitor, and the quadrupole exclusively selects these ions. The principle advantage of this is a higher dwell time on these particular ions, increasing the number of ions impacting on the detector, leading to a larger peaks and a higher signal to noise. In SIM the analyser is only monitoring particular ions, resulting in a greater number of points per peak and leading to a more resolved peak shape and greater reliability when integrating. The main disadvantage is that other ions go undetected. Therefore unknowns and potentially important compounds are missed. Whilst SIM yields more accurate data for known analytes, it is not able to determine unknowns, or monitor impurities and baseline drift. The detector employed by the mass spectrometer was an Electron Multiplier, as described in Chapter 1.

2.1.2 Modifications

This section discusses the modifications made to the instrument prior to each campaign.

2.1.2.1 Cold-finger water removal

Due to time constraints, the Nafion drying method was not fully tested prior to the instrument's first deployment (Quantifying the impact of BOReal forest fires on Tropospheric oxidants using Aircraft and Satellites (BORTAS) field campaign in Canada). Therefore, prior to the South American Biomass Burning Analysis (SAMBBA) campaign, the effect of Nafion on specific analytes was tested. This campaign investigated the effects of boreal forest fires on the regional, and global climate. As such, the measurement focus was primarily on isoprene and monoterpenes, as well as biomass burning compounds such as benzene. Because of the relatively high polarity of some analytes (MVK, MACR, furan), the use of Nafion as a water removal device was deemed unsuitable. On analysis of the data, several unknown ghost peaks were present in the chromatograms. A series of tests carried out during the campaign indicated that the source of these peaks was indeed the Nafion dryer and, in addition, the drier was adversely affecting OVOCs present in the sample. The use of the Nafion was therefore discontinued for the rest of the BORTAS campaign and no drier was used. However, this was a major compromise, and with water present in the system, the baseline of the chromatograms rose significantly; peak shapes were poor and the detection limit was high, particularly for boundary layer measurements.

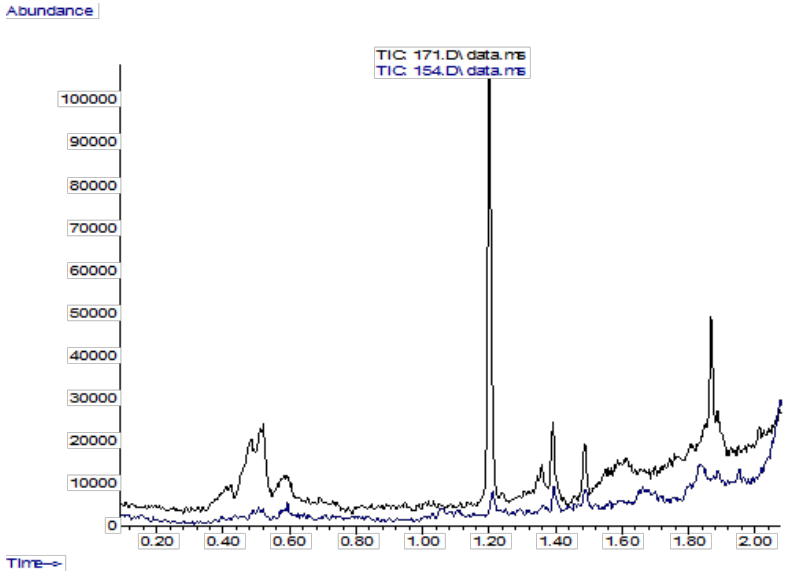

Figure 2.6: Chromatograms of two high purity nitrogen samples showing two different drying methods. The samples were passed through either a length of Nafion tubing (black) or a glass cold finger (blue)

An alternative method of removing water vapour from a sample is to chill the gas stream down to below 0 ° C with water freezing out as ice. However, due to costs and aircraft regulations, cryogenic cooling processes, for example,the use of liquid nitrogen, were unfeasible. A cold-finger device using the Peltier effect was designed instead. Two Peltier plates were used to cool a piece of glassware down to sub-zero temperatures. The Peltier effect is a manifestation of the thermoelectric effect, passing a current across a semiconductor invokes a change in temperature across the device. Heat is directed towards one plate, whilst the other plate experiences a cooling effect. These plates were arranged in between a heat sink and the glass cold finger. Two fans were positioned at one end of the heat sink to dissipate the heat produced by the Peltier plates. A copper sheath was designed to evenly conduct the cooling around the cold finger and placed on the cool side of the Peltier plates. The design of the device is shown in Figure 2.7.

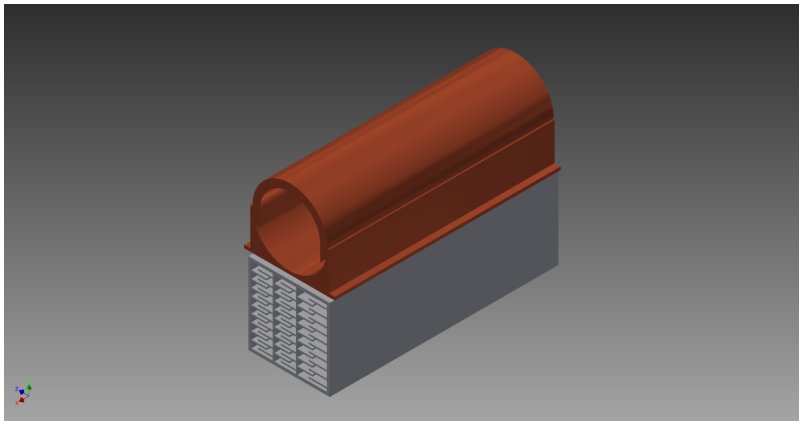

Figure 2.7: CAD image of the Peltier Water trap, showing the heat sink in grey, and the copper sheath in orange

Initially, this setup produced temperatures of ∼ -15 ° C both whilst in the laboratory and in the aircraft rack. The instrument was then deployed to Sweden as part of the Aerosol-Cloud Coupling and Climate Interactions in the Arctic (ACCACIA) campaign. Once in the field the cold finger was capable of reaching temperatures of ∼-10 ° C. This temperature discrepancy was due to the different ambient temperatures in the laboratory (typically 20 ° C) and the aircraft when fully loaded with operating instruments (up to 30 ° C).

2.1.2.2 On-column refocusing

In order to improve chromatographic peak shapes, a cold on column refocusing system was developed. Chromatographic peak width in GC is fundamentally limited by the

injection peak width, which in this case, is determined by the TDU heating ramp rate, trap volume and carrier flow. The timetaken for the trap to heat from trapping temperature (approximately 0 °C to desorption temperature (230 °C) was determined as being $\sim$ 5 seconds and had a volume of around 5 mL, giving a basic injection width of around 3 seconds. In order to reduce this and produce sharper peaks, liquid CO_2 was sprayed onto the head of the column, re-focusing analytes before a fast relaunch onto the main GC column. This created considerably sharper peaks in the chromatograms, improving resolution and increasing signal to noise. The knock on effect of having greater peak shape was that the injection could be run in 'splitless' mode. Prior to this modification, the split was set at 10:1, so by removing this, the sensitivity of the instrument was increased by a factor of 10. The system used liquid withdrawl CO_2 from a cylinder, mounted horizontally on the top of the rack. A pneumatically actuated valve controlled by a microcontroller determined when the CO_2 was directed onto the column, where expansion of the liquified CO_2 created a cold spot on column, which reached temperatures of around -78 °C. All compounds entering the column were adsorbed onto the stationary phase, until the CO_2 stream was turned off. The CO_2 T-piece was then heated by the turbulent oven air and all compounds then very rapidly desorbed and passed through the column. The result of this was that species eluted from the column in a much narrower band, improving peak shape. Figure 2.8 shows two overlaid chromatograms with ion 117 (carbon tetrachloride) extracted. The image shows runs with, and without, a liquid CO_2 injection.

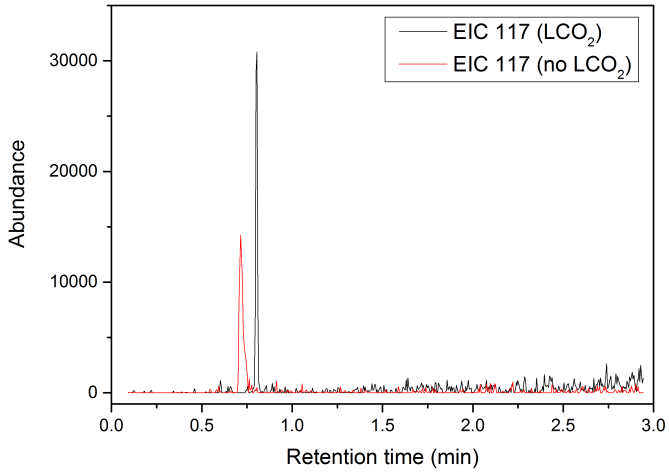

Figure 2.8: Chromatogram showing the improvement in carbon tetrachloride peak shape with addition of liquid CO2 (in black) refocussing, compared to without liquid CO2 (in red)

The two peaks have similar areas and are for the same mixing ratio. The area with and without the CO_2 is 212921 and 212130 respectively. The run in black shows the carbon tetrachloride peak with the injection of liquid CO_2. As can be seen, the peak is significantly narrower, and therefore easier to integrate and with higher signal to noise.

2.1.2.3 Nafion bundle drier

The Coordinated Airborne Studies in the Tropics (CAST) was a campaign that took place in the Western Tropical Pacific. The compounds to be analysed were halocarbons. These are unaffected by Nafion, so it was suitable to use (**?**).

Due to high temperatures and levels of humidity in the region, the Peltier device was deemed to be an unsuitable method of water removal for this campaign. Temperatures on board were too high to allow sufficient heat removal from the warm side of the Peltier plates. A different water removal system was implemented. As the campaign was focussed primarily on halocarbon compounds, a counter current Nafion membrane was used, with no effect on the compounds analysed. A bundle of Nafion tubes were placed in the sample stream, whilst a small pump directed a flow of gas round a loop and across the Nafion membranes in the opposite direction to the sample flow. In addition, the loop contained a tube of drying material, to remove water from the loop, and so the sample stream. A schematic of the setup is shown in Figure 2.9. Note the directions of sample and drying gas flow are opposite.

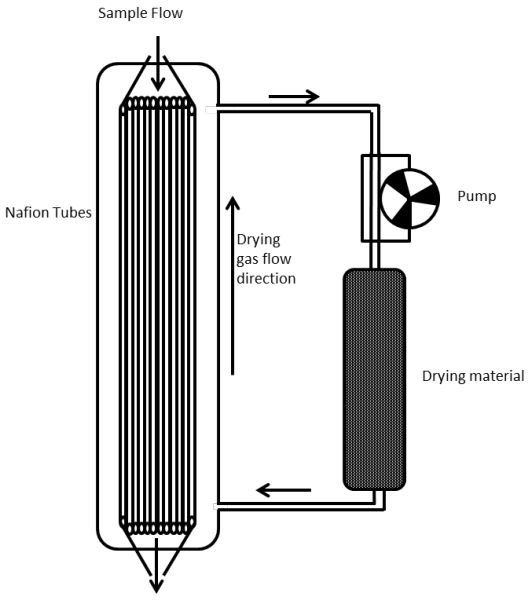

Figure 2.9: Schematic of the Nafion membrane water removal system used during the CAST campaign

As the sample flowed through the Nafion tubes, the dry air flowed in the opposite direction, whilst water vapour moved across the membrane along a concentration gradient. The water was removed from the loop by the drying material to complete the process.

The Nafion drying technique was deemed to be acceptable for this campaign for several reasons. Firstly, the focus of the campaign was to measure halogenated compounds, which are largely unaffected by Nafion. Secondly, the MS was run in SIM mode in order to produce a larger signal to noise ratio as mixing ratios for these compounds are significantly lower than many hydrocarbons. Therefore, no ghost peaks were observed in the chromatograms.

A second modification was made to the CO_2 system. Rather than locate a single 2L cylinder on top of the rack, a stand containing two 5L liquid CO_2 cylinders (with dip tubes) was built on the pump tray. This was to minimise CO_2 wastage, and ensure that it never ran out inflight. The two cylinders were connected by a T-piece, so when 1 cylinder was emptied, the other could be opened, ensuring a constant flow.

2.1.2.4 Stirling cooler water removal and CO_2 heater

Before the instrument was deployed on the Oil and Gas campaign (see chapter 5), the flow control box was redesigned due to the addition of several modifications. The sample dryer was changed again, this time for a Free Piston Stirling Engine (FPSC) (Twin Bird, Japan). The Stirling engine operates by expansion and compression of a small Helium reservoir using a free mounted piston. A piston head is moved in and out of the Helium reservoir, moving heat from the head of the device to the heat exchanger. Thermodynamically, the expansion of a gas leads to a decrease in temperature, whilst the compression of a gas leads to an increase in temperature. Therefore, as the piston moves, heat is moved from one region to another. The Stirling cooler was powered by a 24 V, 8 A power supply, although the device only requires 100 W to run at maximum power. A 24 V fan was used to draw heat away from the heat exchanger. The cold head is capable of reaching temperatures lower than -80 ° C within a fairly short amount of time (˜1 hour). The advantage of this is that it can reach an operational temperature within the aircraft pre-flight period of 4 hours. A schematic of a Stirling cooler is shown in Figure 2.10. The piston and displacer work to remove heat from the cold expansion space, towards the ambient compression space.

In order to remove water from a gas sample, a glass cold finger was encased in an

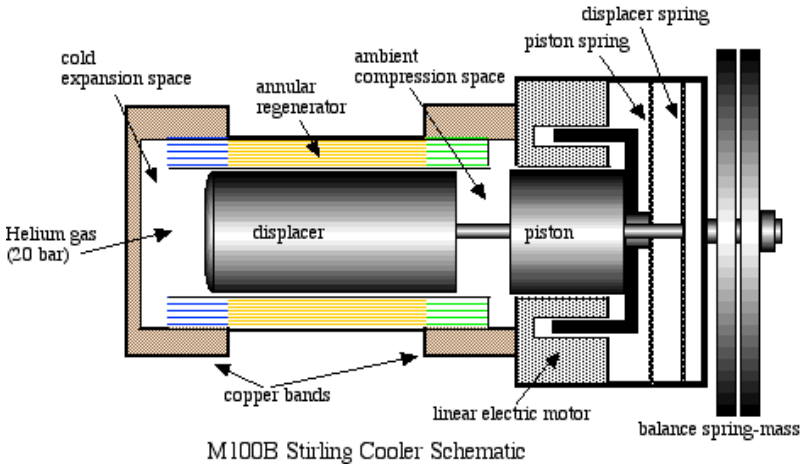

Figure 2.10: Schematic diagram of a Stirling Cooler, with key components labelled (Global Cooling Inc.).

aluminium sheath, into which the cold head was fitted. The aluminium sheath conducted heat away from the entire cold finger. The entire assembly was surrounded by a piece of insulation. A K-type thermocouple was inserted into the aluminium sheath to read the temperature into a proportional integral derivative (PID) loop. This kept the temperature of the cold sheath at a constant -30 ° C. The Stirling cooler was only provided with 50% of its maximum power (100 W), but was still able to achieve required temperatures in < 30 minutes. This temperature was sufficient to freeze water out of the sample passing through, leaving no liquid water for organic compounds to adsorb onto. In order to accommodate the Stirling cooler, other components in the flow control box needed to be redesigned. The 4-position valve, in practice, was rarely used in flight. All calibrations were carried out on the ground either pre- or post-flight. Therefore, it was removed to allow room for the Stirling cooler. In addition, control of the 2-position valve was moved to the Arduino Leonardo already mounted to control the CO2.

Several additional modifications were made to improve instrument sensitivity and reliability. An addition was also made to the CO2 trap. A series of tests showed that the CO2 trap was taking ˜ 1 minute to heat up to oven temperature (Figure 2.11). This was having a detrimental effect on the chromatography. In order to address this issue, the T-piece was wrapped in a length of PTFE coated nichrome wire. This wire has a large resistance, and heats up to high temperatures when a voltage is applied to it. Therefore, rather than taking 1.2 minutes, the T-piece was instead heated rapidly to > 150 ° C. Figure 2.12 shows the improvement in peak width with the introduction of the heater.

A Back Pressure Controller was also included in the recertification. This was due to a sample pressure issue found during the CAST campaign. A change in cabin pressure

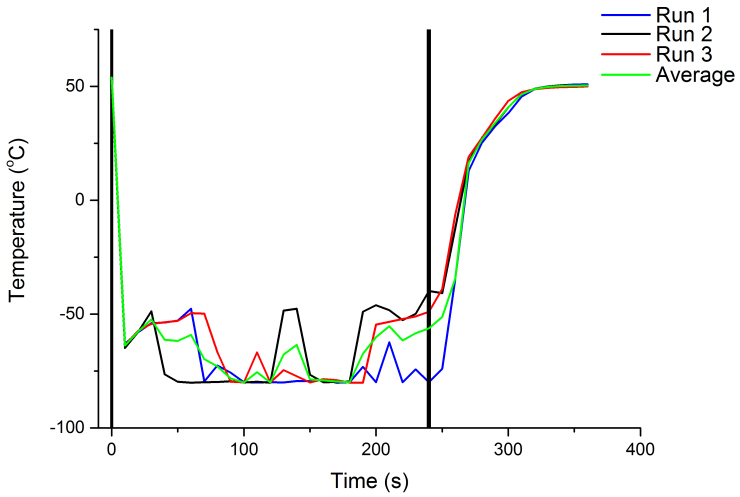

Figure 2.11: Time profile of the CO_2 T piece. The black lines indicate when the CO_2 was turned on, and off. Temperature fluctuations are due to ice crystals forming and blocking the holes where the CO_2 is released. It is also important to note the time taken for the T-piece to warm up again after the CO_2 is turned off.

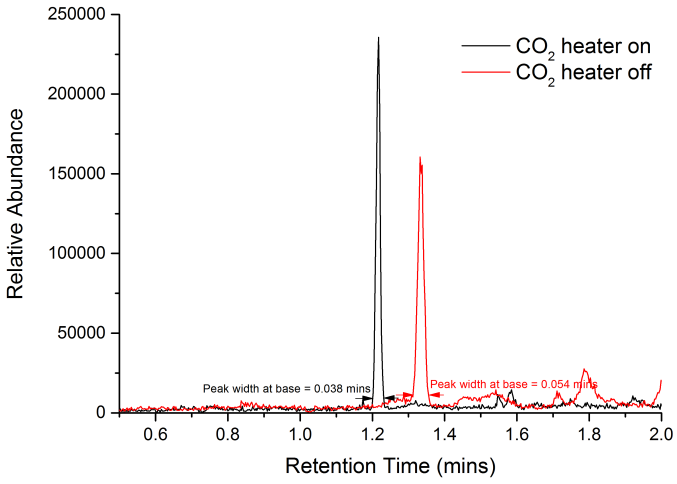

Figure 2.12: Extracted ion chromatogram of ion 117 (carbon tetrachloride) of two GC analyses showing the further improvement in peak width, one in which the CO_2 heater was turned on for 30 seconds at the start of the run (black) and one in which the CO_2 heater was turned off during the entire run (red). The peak widths are shown for comparison.

led to a change in the peak area of carbon tetrachloride (used as an internal standard). Carbon tetrachloride can be used as an internal standard, as it is present in consistent mixing ratios throughout the troposphere. This placed a limit on the ability to track mass spectrometer sensitivity. However, the cabin pressure did not decrease linearly with altitude. This further increased the uncertainty of sensitivity tracking. Therefore a back

pressure controller was fitted (Alicat, UK), and calibrated to absolute pressure, in order to overcome the changing cabin pressure. Figures 2.13 and 2.14 show carbon tetrachloride peak area for a flight during the CAST campaign. Figure 2.13 shows a time series of carbon tetrachloride and altitude. A clear relationship between the two can be seen. At low altitudes (below 3000 m) the carbon tetrachloride is level at ˜230000 counts. However, as the altitude increases, the carbon tetrachloride falls. The relationship between the two is shown in Figure 2.14. This includes 3 flights from the campaign. It shows a large distribution in the carbon tetrachloride peak area, which is due to the changing altitude.

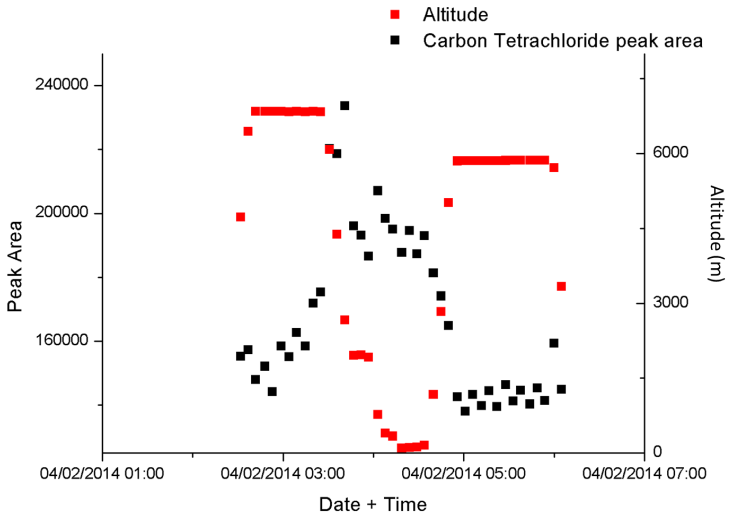

Figure 2.13: A time series showing carbon tetrachloride and GC/MS averaged altitude over the course of a single flight during CAST. As altitude increases, carbon tetrachloride decreases.

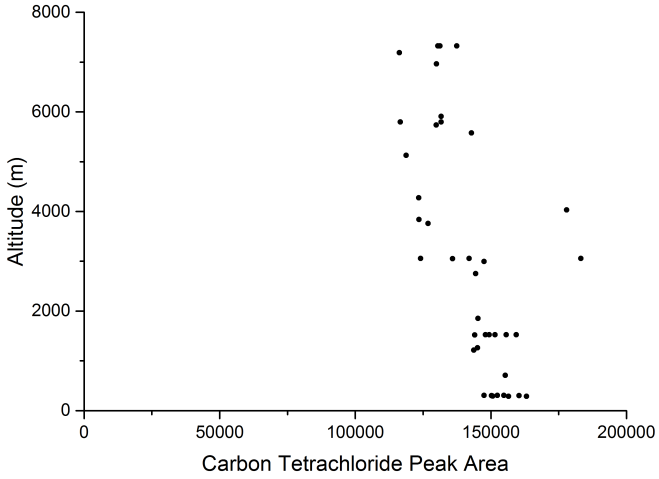

Figure 2.14: A vertical profile of carbon tetrachloride during CAST, showing a large distribution

Figure 2.15 shows a vertical profile of carbon tetrachloride during a single Oil and Gas campaign flight. This was done after the back pressure controller was fitted. The scale of the x-axis has been corrected to account for different integrator parameters, and thus the two can be compared. The data from the Oil and Gas flights show a markedly reduced spread over the range of altitudes, indicating the success of the modifications.

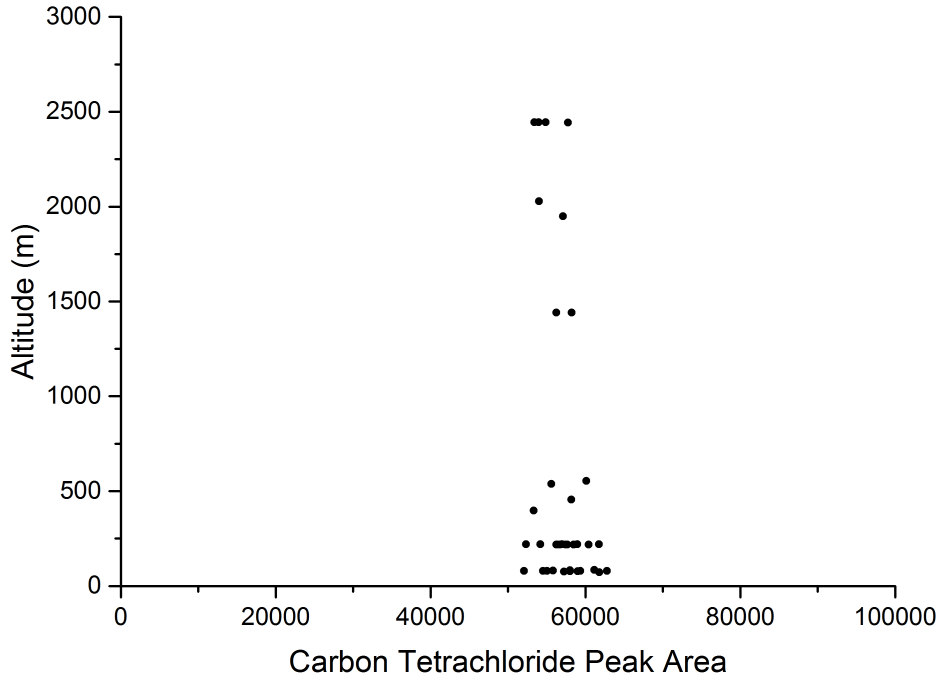

Figure 2.15: A vertical profile of carbon tetrachloride during Oil and Gas, showing a reduced distribution in peak areas.

Figure 2.16 shows the two plots on the same axis, with the Oil and Gas data in red and the CAST data in black. Despite the lack of measurements at high altitudes in the Oil and Gas campaign, the reduced spread in the Oil and gas data can be seen.

In order to more accurately demonstrate the decrease in spread between the two campaigns, the percentage standard deviation of a series of flights were calculated. The results of these are shown in Table 2.2. The mean standard deviation from CAST is calculated as 13.5 %. This drops to 6.5 % during the Oil and Gas campaign, showing the success of the addition of the back pressure controller.

The flow control box was completely redesigned to accommodate the stirling engine and the other modifications. The entire box was re-wired and the path of the gas flow was redesigned. The introduction of the Stirling cooler required addition of a 24 V, 8

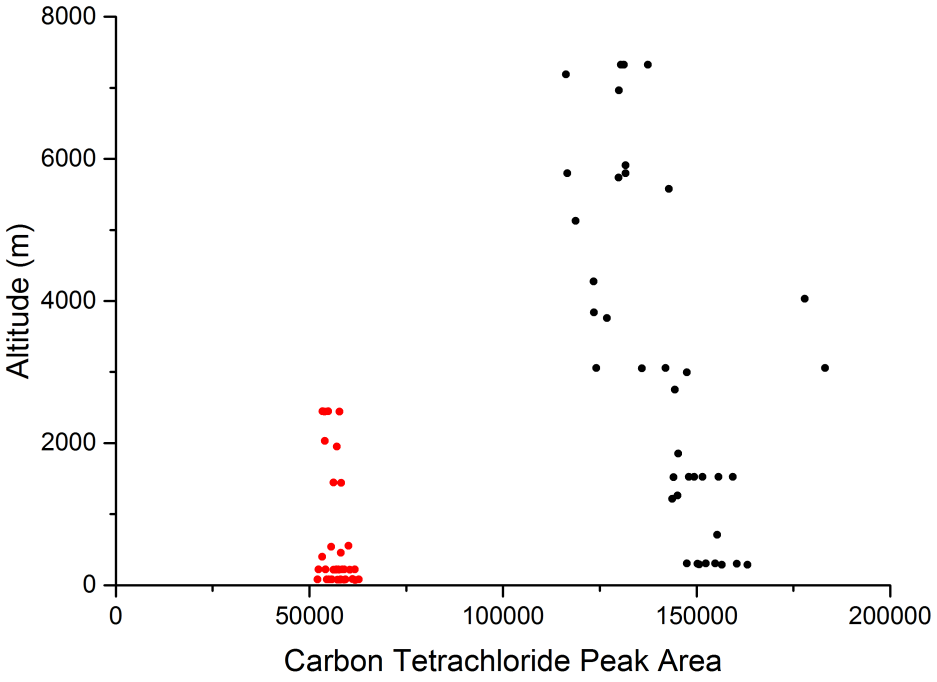

Figure 2.16: The vertical profiles of the two flights plotted onto the same axis. The reduction in the spread of the carbon tetrachloride data can be seen in the Oil and Gas data (red) when compared to the CAST data (black).

A power supply, as on start up, the Stirling cooler could draw as much as 100 W. A Proportional-Integral-Derivative (PID) controller was used to regulate the temperature at the cold head. The PID took the temperature from a thermocouple, inserted into the aluminium cold sheath. Based on this temperature, the PID controller would then give a signal to the Stirling cooler to either use more, or less power. The PID controller took power straight from the 230 V AC supply. A fan and the Valco valve, used to add an aliquot of deuterated toluene to the sample were also run off the 24 V 8 A supply. The 24 V 2 A supply provides power to the CO_2 actuator, the back pressure controller and the relays for the line, and trap heaters. The Arduino microcontroler is powered by either the USB connection from the PC, or from the 12 V supply. These electrical modifications are shown in Figure 2.17.

The sample flow paths were also modified to accommodate the additional components. Several different gases were fed into the box: air sample, gas standard, deuterated toluene and helium, which acted as an actuator gas for the CO_2 system. The air sample was fed in straight from the double headed metal bellows pump, at high pressure. The back pressure controller was positioned parallel to the main sample line and restricted the

Table 2.2: The standard deviation of carbon tetrachloride from 6 Oil and Gas flights, and 6 randomly chosen CAST flights. The mean standard deviation drops from 13.5 % to 6.7 % when the back pressure controller was integrated into the system.

	CAST	**Oil and Gas**
% Standard Deviation		
Flight 1	15.9	5.6
Flight 2	10.9	10.7
Flight 3	10.1	4.8
Flight 4	22.4	5.5
Flight 5	4.6	7.9
Flight 6	17.2	6.0
Average	**13.5**	**6.7**

pressure to 2.5 bar (absolute pressure). Excess air was vented into the cabin. Following this, the air sample was directed into the two position valve, in which the deuterated toluene was introduced. Following this, a series of valves could be opened to pass either the air sample, or the gas standard through. Which ever sample was selected was passed through the coldfinger to remove water vapour, and directed out to the thermal desorption unit for preconcentration. Visual representation of these can be seen in Figure 2.18.

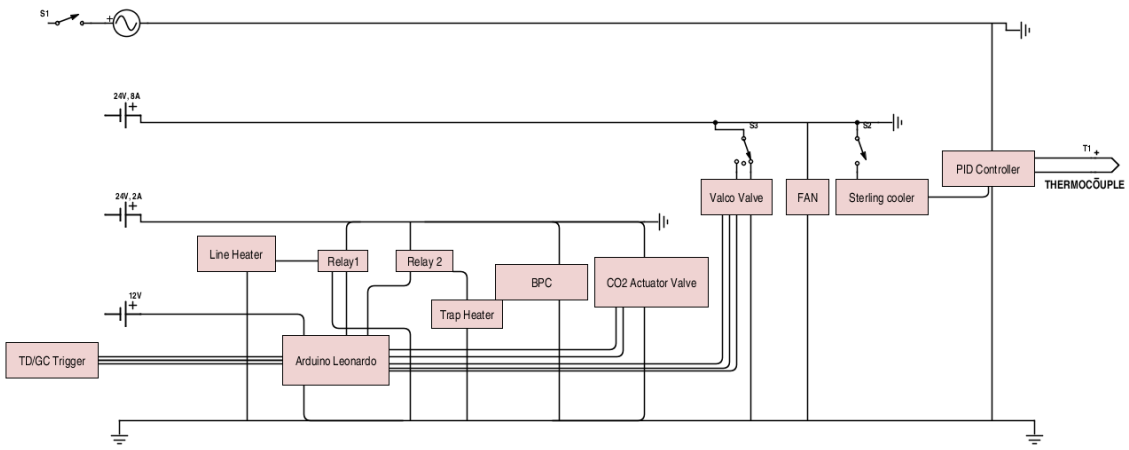

Figure 2.17: Schematic showing the internal electronics of the flow control box used during the Oil and Gas campaign

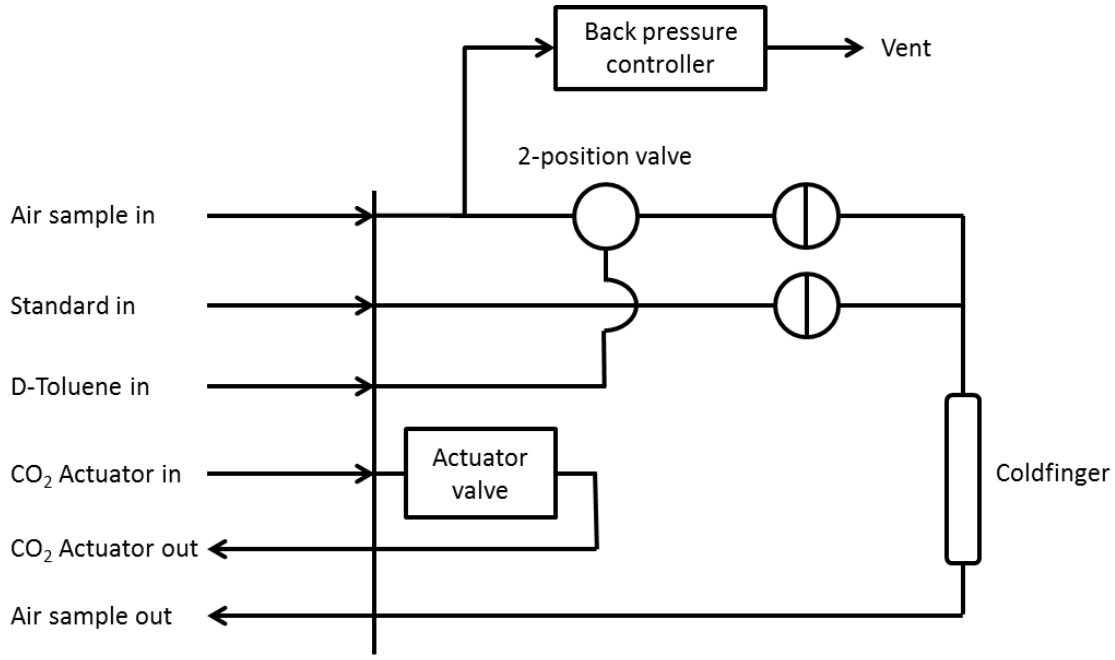

Figure 2.18: Schematic showing all flow paths in the flow control box used during the Oil and Gas campaign

2.1.2.5 Arduino Microcontroller

The microcontroller used to monitor processes in the flow control box was an Arduino Leonardo (RS, UK). The board was given a series of inputs. Firstly, two triggers were taken from the Thermal Desorption unit, one from each trap. These triggers took the form of a closed contact, taken from the trap solenoid valves. Three additional inputs were taken from several switches on the front of the box, allowing the user to test the system for faults prior to takeoff. Two of these switches were used to test the CO_2 system. One acted as a manual on/off switch, which was also used to purge the CO_2 line prior to each flight, and whenever the cylinder was changed. The other put the system in 'automatic mode,' causing the microcontroller to only take a signal from the Thermal Desorption unit traps. The final input was a closed contact from the gas chromatograph. The GC was programmed to trigger this 10 seconds into each run, ensuring the CO_2 was turned off at the same time for each run, reducing the shift in retention time.

The board was also given a list of outputs. These included an activation signal for the deuterated toluene and CO_2 systems, the signal for the CO_2 system to fire the cold trap, and an output for heating the lines within the box. No input was required for this as lab tests confirmed that a constant 12 V across the heater wire was sufficient to heat the lines to 60 ° C.

2.1.3 Instrument Performance and Reproducibility

In order to produce consistent data, on flying days, the instrument is operated in the same way, based on a Standard Operating Procedure (SOP). The order in which calibrations, blanks and samples are run is critical to producing viable data. The order is briefly described below.

2.1.3.1 Standard Operation Procedure

Access to the aircraft is usually 4 hours prior to takeoff. Upon access, the GC and MS are turned on, allowing the MS to pump down to a workable vacuum. The helium is turned on in order to clean the GC column. After the MS vacuum reads $\sim$ 2 x 10^{-5} Torr, the TDU is turned on and allowed to heat up. The traps were then set to cycle and inject into the GC, which was held at 200 C, in order to remove any impurities from the traps, the transfer line and the column. At this stage the Flow Control Box was turned on, and the Stirling cooler set to - 30 $^{\circ}$ C. At TO - 1.5 hr, the calibration cylinder was connected to the inlet, and a minimum of 6 calibration runs were carried out. Time permitting, the sample lines were then connected up to a pure nitrogen cylinder to purge the lines. Before the cabin doors were closed, the nitrogen was disconnected, and the instrument was left running trap blanks. Sampling began once the aircraft reached 5000 ft and the seatbelt signs were turned off. For full SOP see Appendix 1.

2.1.3.2 Calibrations

Throughout this chapter, the various stages of the instrument have been described. The practical upshot of these modifications was to improve the peak shape, sensitivity, and reliability of the data gathered in flight. To this end, a flight day was simulated in the laboratory. The instrument was started up from cold following the above procedure. However, instead of sampling air, a calibration cylinder containing real air was connected to the instrument inlet, and sampled for 7 hours, in order to simulate a two sector flight but with the same sample on every GC run. In total, 78 samples were taken, including 8 blank runs (four prior to, and four after the calibration samples). Figure 2.19 shows a time series of benzene and carbon tetrachloride during the calibration period.

This calibration was run three times, on three consecutive days, to simulate the kind

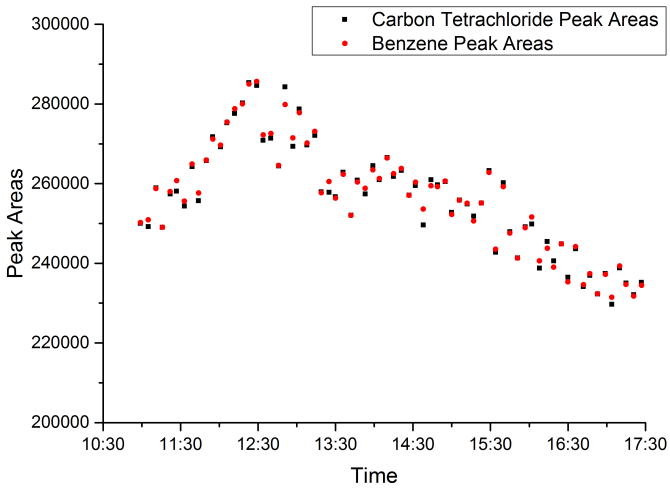

Figure 2.19: Time series of carbon tetrachloride and benzene peak areas measured during a 7 hour long flight simulation / calibration.

of intensive flying of a typical campaign. The plots of carbon tetrachloride over the whole three days are shown in 2.20.

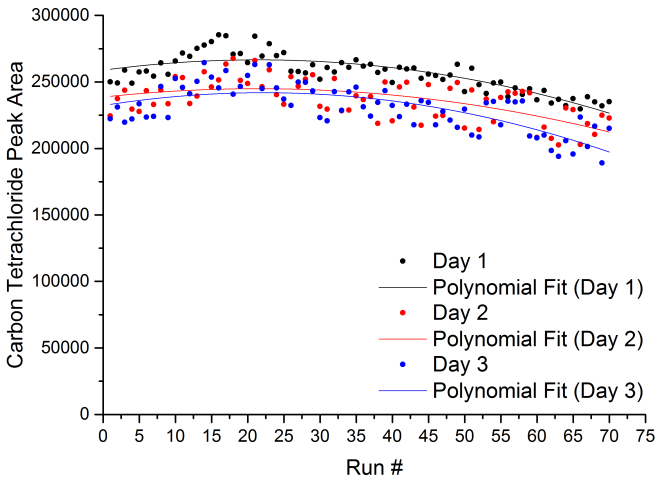

Figure 2.20: Overlaid plot of the three days of calibrations run on the GC/MS, showing how the sensitivity changes both over a flight time, and between different days. A polynomial best fit line (2nd order) was fitted to each data series. The statistics are shown in the table below.

The slight trend observed in Figure 2.19 is due to changes in Mass Spectrometer sensitivity. Initially, for the first 2 hours, the peak areas of benzene and carbon tetrachloride

Table 2.3: Scatter, mean and standard deviations of the plots shown in Figure 2.20. Whilst there is some variation in the scatter, the % Standard Deviations are consistently low (¡10 %)

Day	**1**	**2**	**3**
Polynomial Order	2	2	2
Scatter (R-Square)	0.7	0.36	0.54
Mean	256330.1	236573.8	230506.3
Standard Deviation	13694.77	15250.53	17211.61
% SD	5.342632	6.446416	7.466872

increase, as the mass spectrometer turbopump removes more contaminants from the system (particularly air and water). The removal of contaminants improves the transmission of analytes from the ionisation source to the detector (as discussed in chapter 1). Therefore peak areas of analytes increases. However, after an 'optimum' vacuum has been reached, and transmission of analytes from ionisation source to detector reaches a maximum, key surfaces within the mass spectrometer become contaminated by small amounts of air and water within the sample itself. For instance, the repeller, used to accelerate ions from the source to the mass analyser, suffers from ion burn, reducing in its efficiency. Therefore a negative trend in analyte peak areas is observed.

The purpose of this experiment was to establish the 'raw' reproducibility of the instrument over a period equivalent to that of a dual sector flight. As carbon tetrachloride is used to track mass spectrometer sensitivity, it would be expected that some correlation will be seen between analytes, and carbon tetrachloride. Figure 2.21 shows the relationship between them.

Figure 2.21 shows plots of benzene and toluene, as these are two of the most commonly used analytes for the instrument. Both show a very strong correlation, with benzene and toluene having an R^2 value of 0.99 and 0.90 respectively (where 1 is a perfect correlation). With other analytes, particularly acetone and *m/p* xylene, R^2 value is lower, as shown in Figure

In general, all compounds show a good correlation with CCl_4. All have an R^2 value of ≥ 0.5. Specific compounds show different R^2 values, due to different reasons. Acetone, for example, when plotted against CCl_4, is highly scattered. However, when the data is split into GC runs that came from Trap A and Trap B, an improved correlation is seen. This is due to non-uniform packing within the traps themselves. The traps have to be filled

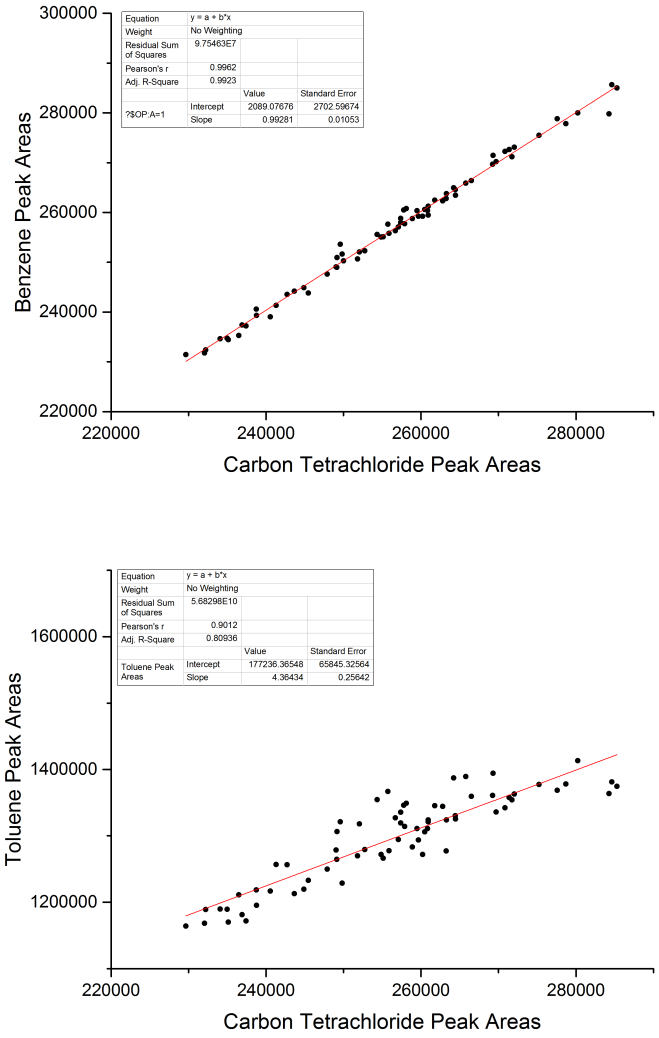

Figure 2.21: Correlation between carbon tetrachloride and benzene (top), and carbon tetrachloride and benzene (bottom), observed during the 7 hour calibration

with sorbent by hand, so some discrepancies are to be expected. This phenomenon affects acetone more than other compounds due to its high volatility (vapour pressure: 30.6 kPa @ 25 ° C) when compared to benzene or toluene (vapour pressure: 12.7 kPa, 2.79 kPa @ 25 ° C respectively.

The *m/p* xylenes suffer from a poorer correlation than benzene or toluene. This is largely due to their abundance and retention time. Throughout the GC run, the background increases when operating the mass spectrometer in scan mode. Therefore, as the *m/p* xylenes elute later on in the chromatogram, and are of lower abundance, a lower signal to noise ratio is observed, causing higher scatter in the data.

For benzene, prior to correcting for carbon tetrachloride, the scatter in the data was

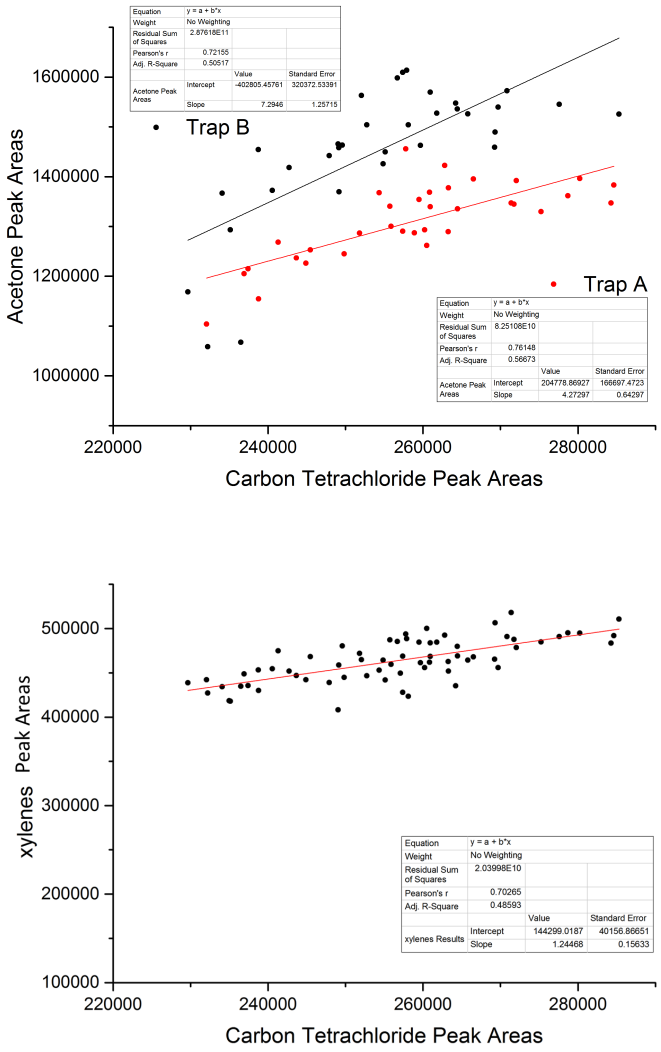

Figure 2.22: Correlations between carbon tetrachloride and acetone (top), and *m/p* xylenes (bottom). The acetone plot is separated based on the trap used to preconcentrate the sample, as non-uniform packing of the sorbent between traps has a large effect on highly volatile species.

calculated to be ∼5 %. However, once the correction factor was applied, the scatter, or standard deviation of the data was calculated as 0.45 %. The corrected benzene is shown in Figure 2.23. Note that the scale is the same as in Figure 2.19 so a direct comparison can be seen.

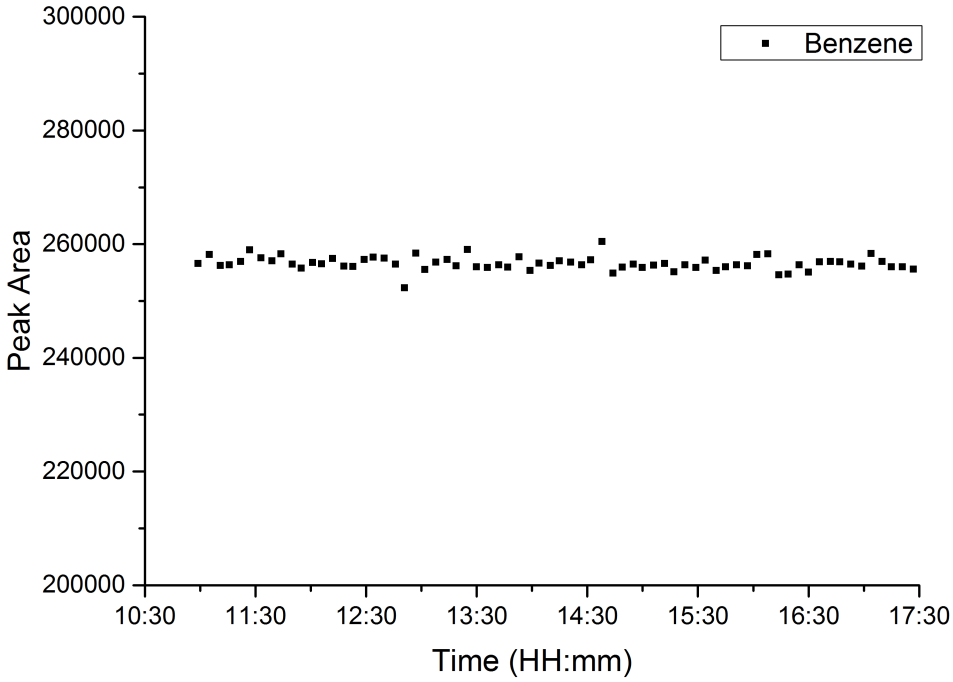

Figure 2.23: Time series of benzene peak area after the 7 hour calibration, following applying a correction factor based on carbon tetrachloride peak area. The scatter is significantly lower.

It is important to note, however, that it is impossible to truly recreate the conditions on the aircraft under lab conditions. The experiment conducted here represents a 'best case' scenario, where incoming sample pressure, temperature, humidity, and oxidative capacity are kept constant. However, this experiment does show how, given ideal conditions, the instrument performs.

2.1.4 Instrumental Errors

There are also the instrumental errors to consider.Some of these errors stem from the instrument itself, while others relate to the data processing involved. Instrument errors affect either the precision or the accuracy. This is usually rectified using a known standard, however there also are inherrent errors in processing a standard. This can include, for instance, the standard not being the same as the sample being measured. In this case, all standards used with this instrument were VOCs in nitrogen, whereas the sample being measured was air, a nitrogen/oxygen mix. The way these two samples are processed may differ within the instrument. Additionally the instrument was not calibrated at all ranges of the sample, sometimes due to time constraints, other times due to the practical

limitations of diluting, or concentrating, a gas standard sample. Therefore, it was assumed that the response of the instrument was liinear across the range of mixing ratios measured. Additionally, all mass flow controllers, pressure sensors and controllers, and temperature sensors have their own associated errors, which, whilst documented, can all add to the total instrument error.

Further sources of instrumental error stem from certain specific areas of the instrument itself. The VOC cold traps are filled with the sorbent by hand, and as such would not be packed identically. The two traps will therefore differ in the amount of sorbent added, and the available surface area. Once the traps desorb, the amount of time taken and the amount of adsorbed VOCs will differ. The best way to charactise this was to run a number of standard samples on each trap, and observe the differences in retention times. As previously stated, due to the instrument not having a dedicated operator during the SAMBBA campaign, this was not implemented. However, for the following campaigns, attempts were made to ensure that it was, with an acceptable RSD being ¡10% for carbon tetrachloride for the gas standard used. This was a limit imposed as it was a balance between reducing the error, and have the instrument reliably collect data for a flight.

The drift in Mass Spectrometer sensitivity is also a source of error. As the MS had to be turned off and restarted before each flight, the pressure within the vacuum changed with each flight. However, as long as the instrument was properly characterised prior and after each flight, this could be compensated for.

As far as errors introduced during the data processing stage is concerned, potentially the biggest source was the integration of peaks. Ideally, all GC peaks would be a pencil-thin Gaussion distribution, making integration of peaks easier. However, and particularly with the SAMBBA data set (see section 3.1.2), this was not the case. Of the few compounds that were able to be extracted, the peak shape was less than ideal. This made manual and automatic integration much harder, and introduced a significant source of error. One way to reduce this error was to have the same operator integrate the peaks, meaning the same method of integration was used. However, this is asubjective approach to peak integration.

Finally, and perhaps most significantly, due to the nature of the measurements being taken, repeat measurements are impossible. The dynamic nature of the atmosphere, coupled with the limits of an aircraft means that the only way to make repeat measurements of an air sample would be to isolate it. This is could be achieved using a WAS cannister, which is of course done, but removes the ability to make *in situ* measurements.

The best way to limit errors in this case is to report all numbers en masse, and conduct more statistical analyses on them, including taking the standard deviation and relative standard deviation (RSD), as well as plotting figures, as above and in other chapters, with box and whisker plots, so to instead show the range of data, rather giving than individual points with an associated estimated error.

2.1.5 Conclusions

This chapter describes the various modifications and changes made to the University of York airborne GC/MS from September 2012 - present. Water removal is vital for accurate, repeatable GC analyses, but with water vapour vastly differing in different regions of the atmosphere, the instrument has had to employ a wide variety of different removal mechanisms. Initially, a box Nafion dryer was used which was successful in removing water vapour, but also introduced impurities to the sample. Secondly, a cold finger was used which employed the Peltier effect to freeze water out of samples. This was successful in the laboratory, and in Arctic conditions which contain very little water vapour, but was not suitable for tropical environments. For the analysis of halocarbon species in the tropics, a counter-current Nafion dryer was used. As the MS was run in SIM only mode, ghost peaks were not apparent, meaning that this use was successful. Finally, a Stirling engine cooled cold finger was designed and implemented, which was installed on the instrument for flying around the UK. In the future, the Stirling cooler will be deployed in other, more humid conditions to determine it's suitability.

The addition of the cold on column liquid CO_2 system enabled the removal of a split flow on the TDU, as peaks were much narrower, leading to less co-elution. This meant the sensitivity of the instrument was increased by 10. The introduction of the heating tape around the CO_2 T-piece led to even narrower peaks.

Finally, the introduction of the back pressure controller stabilised the sample flow, meaning that the instrument was able to operate at all altitudes, without being affected by changing external, and internal, pressures. Whilst many additional modifications could be made (ie. the use of cryogenics to cool the GC oven and traps faster; the use of a resistively heated column for faster GC analysis) given the scope of the project, along with aircraft regulations, the instrument is now more sensitive and produces more reproducible data.

For reference, a timeline of modifications is shown in Figure 2.24, and a summary of drying methods and GCMS parameters is given in Table 2.4.

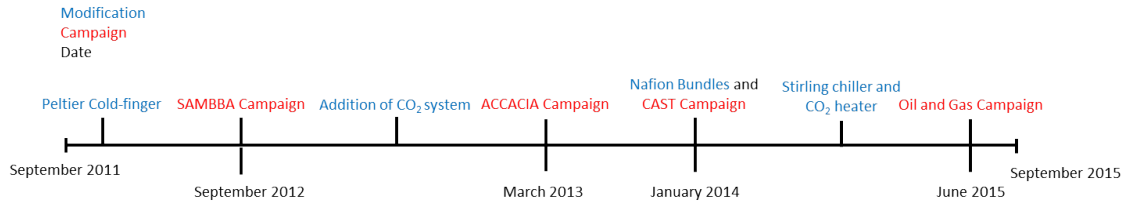

Figure 2.24: Timeline of campaigns and instrument modifications during the period September 2011 to September 2015.

Table 2.4: Table outlining the drying methods and GCMS parameters on different campaigns throughout this project

	SAMBBA	**ACCACIA**	**CAST**	**Oil and Gas**
Drying Method	Peltier Trap	Peltier Trap	Countercurrent Nafion	Stirling Chiller
Sample Flow (mL/min)	450	200	200	200
Sample Volume (mL)	1350	1000	1000	1000
GC Start Temperature (C)	50	50	50	50
Ramp Rate (C/min)	40	40	40	40
GC End Temperature (C)	170	180	180	180
Stationary Phase	5% Diphenyl, 5% dimethylpolysiloxane	5% Diphenyl, 5% dimethylpolysiloxane	RTX-502.2	5% Diphenyl, 5% dimethylpolysiloxane
Column Length (m)	10	10	10	10
ID (m)	0.18	0.18	0.15	0.18
Film Thickness (m)	0.4	0.4	0.2	0.4
SIM/SCAN	SCAN	SCAN	SIM	SCAN
Ion Range	40 - 180	40 - 180	Specific to each ion window	40 - 180
Compounds Measured	Isoprene, BTEX, terpenes, MACR, MVK	Isoprene, BTEX, terpenes, DMS	Chloro- and bromocarbons	Isoprene, BTEX, terpenes, DMS

Chapter 3

The Vertical and Spatial Distribution of Isoprene over Amazonia

3.1 The vertical and Spatial distribution of Isoprene over Amazonia

This chapter will discuss data gathered, and issues that arose, during the South American Biomass Burning Analysis (SAMBBA) Campaign, based in Porto Velho, Brazil, in September and October 2012.

3.1.1 Introduction

Volatile organic compounds (VOCs) are found throughout the atmosphere varying widely in concentrations, reactivity, functionality and volatility. They can have a large impact on local and regional air pollution and, on global scales, influence oxidative capacity of the atmosphere, and the lifetime and abundance of the greenhouse gases methane and ozone.

Biogenic emissions of volatile organic compounds (VOCs) are thought to be significantly greater than anthropogenic emissions globally (up to 90% of global total mass emission with isoprene compromising ˜44%) (Guenther et al., 1995). In turn, biogenic emissions are dominated by emissions from tropical forested regions. These regions receive high levels of radiation and experience warm temperatures, which are key drivers for vegetation emissions (Guenther et al., 1993). Of the many different types of biogenic VOC, isoprene is well established as the largest single source strength of non-methane hydrocarbons (NMHCs).

Whilst the rate of atmospheric emissions of VOCs, and isoprene in particular, is high in the tropics, so is the rate of destruction. High UV radiation, coupled with elevated temperatures and humidity within the boundary layer, result in high turnovers via hydroxyl, OH. There remain however some considerable uncertainties in isoprene chemistry, not least that, based on current mechanistic understanding, it is difficult to reconcile simultaneous observations of high levels of both isoprene and OH in the tropical forest boundary layer (Taraborrelli et al., 2012). Various recent papers have proposed mechanisms by which OH may be recycled, rather than lost, on isoprene reaction (da Silva et al., 2010). Given the scale of tropical forests (occupying ˜17.5% of the Earths land area) and the pivotal role of these regions in atmospheric oxidation, testing and refining descriptions of these processes is a key area for research.

The hydroxyl radical (OH) is the main driving force for oxidation of VOCs. Reactions between OH and an organic compound, RH (where R is any hydrocarbon), yield the

peroxy radical, RO_2, which then affect the NO_x cycle, yielding ozone. In addition, continued oxidation of RO_2 eventually yields CO_2, also contributing to the greenhouse effect (Crutzen and Delany, 1985). CO generated in reactions between RO_2 and OH has been estimated to contribute 39% of the global CO budget arising from biogenic isoprene and terpene oxidation alone. Less volatile compounds, once oxidised, can also condense into the aerosol phase, creating secondary organic aerosol (SOA) or adding mass to existing aerosols (Andreae, 1997).

Atmospheric oxidation of isoprene (via the OH radical) yields several different peroxy radicals (Atkinson, 2000). These in turn are followed by production of alkoxy radicals (in the presence of NO_x), and finally carbonyl compounds. Methyl vinyl ketone (MVK) and methacrolein (MACR) are the two initial stable products of isoprene oxidation with the highest yield. Measurements of MVK and MACR allow a test of performance of chemical mechanisms, and many surface field measurements of MVK and MACR have been published (eg (Kesselmeier et al., 2000)). A study by Warneke et al. (2001), investigating isoprene and its oxidation products in a tropical forest region using PTR-MS from an aircraft, showed isoprene concentrations of between ˜1 and 5 ppbv at low altitudes (below 2 km), and the sum of MVK and MACR as between ˜0.5 and 2.5 ppbv at low altitudes. This is in agreement with a study by Crutzen et al. (2000) who found an average concentration of 2.6 ppbv for isoprene and 1.2 ppbv for the sum of MVK and MACR within the boundary layer.

Whilst measurements of isoprene, MVK and MACR at the surface provide some insight into the oxidative process, there have been far fewer attempts to validate the mechanism through the boundary layer and free troposphere. The limited number of measurements of MVK and MACR exist as a combined measurement, determined using the PTR-MS methodology which is unable to separate these isobaric compounds easily. Speciated measurements are required however if the relative branching ratios in the degradation scheme are to the assessed. This chapter reports, for the first time, vertical profiles of MVK and MACR as separate species in the boundary layer and free troposphere above the Amazon rain forest.

Globally, it has been estimated that forest fire emissions can contribute ˜8.4x10 g CO yr^{-1} to atmospheric CO concentrations, calculated to 12-20 % (Crutzen et al., 1979). Andreae and Merlet (2001) determined over 70 other organic compounds in biomass burning plumes, combining data from several different reports. Additionally, benzene emissions

from forest fires have been shown to travel long distances, and affect benzene mixing ratios far away from the source Lewis et al. (2013).

This chapter reports data from the South American Biomass Burning Analysis (SAMBBA) field campaign, using the FAAM BAe-146 atmospheric research aircraft. The campaign took place over the Amazon rain forest in September/October 2012 (during the Amazonian dry season). Observations were made of speciated VOCs, including isoprene and benzene, over a range of altitudes from 100 m up to 8000 m. Air samples were collected and analysed using an aircraft mounted in situ GC/MS system, capable of measuring ˜20 non-methane organic compounds (NMOCs) simultaneously. Since observations were made during the Amazon dry season, biomass burning adds a further significant source of chemicals to the local atmosphere. Biomass burning yields high concentrations of trace gases such as CO, N_2O, NO, CH_4 and many other hydrocarbons, notably aromatics such as benzene and nitrogen containing compounds such as acetonitrile.

3.1.2 Experimental and Flight Planning

Airborne GC/MS measurements were performed on board the UK FAAM BAe-146 as part of the SAMBBA campaign in September/October 2012 over the Brazilian Amazon. The aircraft was based at Porto Velho International airport (coordinates: -8.7148077 N, -63.9011504 E, altitude: 88 m) and 20 science flights were executed with the aim of characterising biomass burning over forested areas and biogenic emissions from pristine forests. It is important to note that I was not able to be in attendence for the field measurements and was therefore prevented from taking a pro-active part in this campaign. I was therefore unable to influence measurements, and those who took the measurements, whilst trained in preparing the instrument for flight, were not specialists in operating the instrument at its peak. Additionally, this campaign took place less than a month after this project began, and hence, no work with regards to the chromatography was completed. Finally, there were several issues with regards to the chromatography during the campaign, which due to not having a dedicated operator, were not addressed during the campaign. Therefore, there were only a few compounds that could be reliably integrated, such as isoprene, benzene and toluene. The xylenes and terpenes could not be reliably analysed due to a scattered and noisy baseline.

The instruments deployed to on the aircraft are shown in table **??**.

This chapter reports measurements of isoprene and benzene for the entire campaign. Measurements were taken using an online Gas Chromatography/Mass Spectrometer (GC/MS) system coupled to a thermal desorption unit for analysing samples (see chapter 2). Measurements were taken approximately every 5 minutes. Air was drawn in through a 3/8 stainless steel rear facing inlet via a window blank in the skin of the aircraft. A 400 Hz double headed all-metal bellows pump was used to draw air in and pressurize air to the thermal desorption unit upstream of the GC/MS, with a pressure relief valve in line to prevent over pressuring.

Aircraft measurements are particularly challenging to make using GC/MS since the instrument is typically only switched on around three hours prior to making first measurement. This is a safety measure imposed on the aircraft and ensures personnel are present whenever power is provided to the aircraft or scientific equipment. The manufacturer recommends leaving 24 hours after powering up the mass spectrometer in order to achieve a stable vacuum. Instead, the instrument relies on maintaining a part of its vacuum from the previous day/flight. Additionally, the instrument is subject to severe changes in am-

bient temperature and humidity in the cabin and samples air with very different humidity characteristics. Potential changes or drift in instrument sensitivity over the course of a flight were tracked using two methods. The air sample was directed through a stainless steel two-position sampling valve (VICI, USA) which was used to introduce 5 L aliquot of 5 ppm fully deuterated D8-toluene standard gas into the sample line. In addition to this, the instrument was set to detect carbon tetrachloride, a very long-lived atmospheric pollutant that exists in approximately the same mixing ratios throughout the troposphere. The use of both these compounds helped to correct for run-to-run changes in mass spectrometer sensitivity.

Further checks on the instrument sensitivity were carried out using comparisons to the aircraft Whole Air Sampling (WAS) system. The WAS system fills evacuated silco-treated canisters with an air sample in flight to then be analysed by GC/FID on the ground. An agreement between the two methods added confidence to the measurements made by GC/MS.

The GC/MS instrument and GC/FID instrument were calibrated using WMO-GAW traceable standards from the National Physical Laboratory (Teddington, UK). Water was removed from the air sample gas using a glass cold trap held at -10 °C.

A pair of Tenax TA traps positioned in parallel were used to pre- concentrate air samples using a two channel thermal desorption system (TT24-7, Markes, UK). For each measurement, 1 L of air was sampled over five minutes (200 mL/min flow rate). The traps were held at 10 °C during sampling but were used in sequential manner (i.e. one trap was sampling, the other was desorbing/being prepared for the next sample), giving a very high sampling duty cycle of the order 90 %. To rephrase, the instrument was almost continually sampling, resulting in no gaps in atmospheric data. The traps were purged with helium after sampling, to remove interferences, chiefly oxygen and water, then desorbed using rapid trap heating (>100 C/min) to 230 °C and the sample transferred onto the GC column. The GC (6850, Agilent Technologies, Wilmington USA) was fitted with an RTX-5 column (with dimensions length: 10m, ID: 0.18 m, d.f. 0.2 m) and detection was by a 5975C mass spectrometer (Agilent Technologies). The mass spectrometer was set up to perform a full scan from 44-250 amu, with a rate of 10 scans second^{-1}. The mass spectrometer has the capability to analyse only pre-selected ions (selected ion mode), which can lead to increased dwell time on those ions and increased overall sensitivity. However, in order to determine the complete composition of forest emissions, this was not used. A

more detailed explanation of the instrument and parameters can be found in chapter 2.

External calibrations were performed using a 17 component standard containing basic hydrocarbons, BTEX, and monoterpenes. These were performed to provide a reference by which sample concentrations were calculated. Figure 3.1 shows an extracted ion chromatogram of an external standard used to calibrate the instrument.

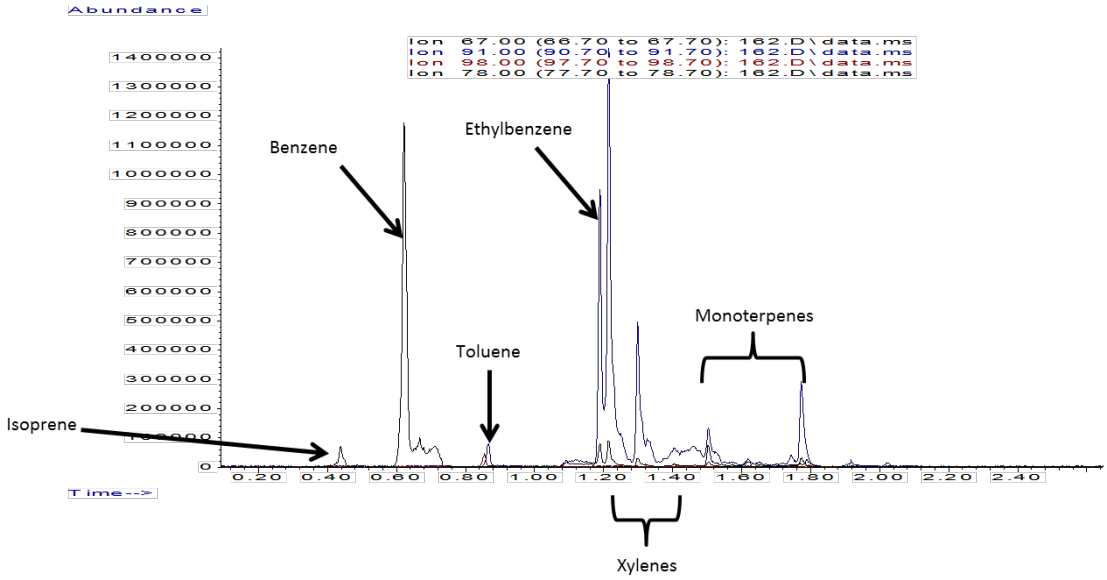

Figure 3.1: Extracted ion chromatogram of a calibration standard used during the SAMBBA campaign. Ions 67, 91, 98 and 78 are extracted showing isoprene, benzene, toluene, ethyl benzene (with xylenes) and monoterpenes (e.g., α -pinene).

To raise confidence in the measurements, a comparison between the GC/MS and WAS systems and the GC/MS and PTR-MS systems were performed. The isoprene data from the WAS system was matched temporally to the nearest GC/MS data point, for data over the whole campaign. The PTR-MS reported isoprene data at a rate of 1 Hz. Therefore, the PTR-MS data was averaged over the GC/MS sample times. Figure 3.2 shows the comparison between the GC/MS and WAS systems. It is important to note that due to isoprene and furan having the same mass ions, the PTR-MS is unable to distinguish between them. Therefore, data given by the PTR-MS is a combined isoprene and furan measurement.

The comparison between the GC/MS and WAS systems shows a slight correlation, with an R^2 value of 0.55. The scatter, and the offset can be accounted for due to differences in sampling methods. It is also important to note that the figures reported by the GC/MS are a five minute average, whereas the WAS data is averaged over 10 - 20 seconds. These samples were collected both over pristine forest, and biomass burning regions. Figure 3.3

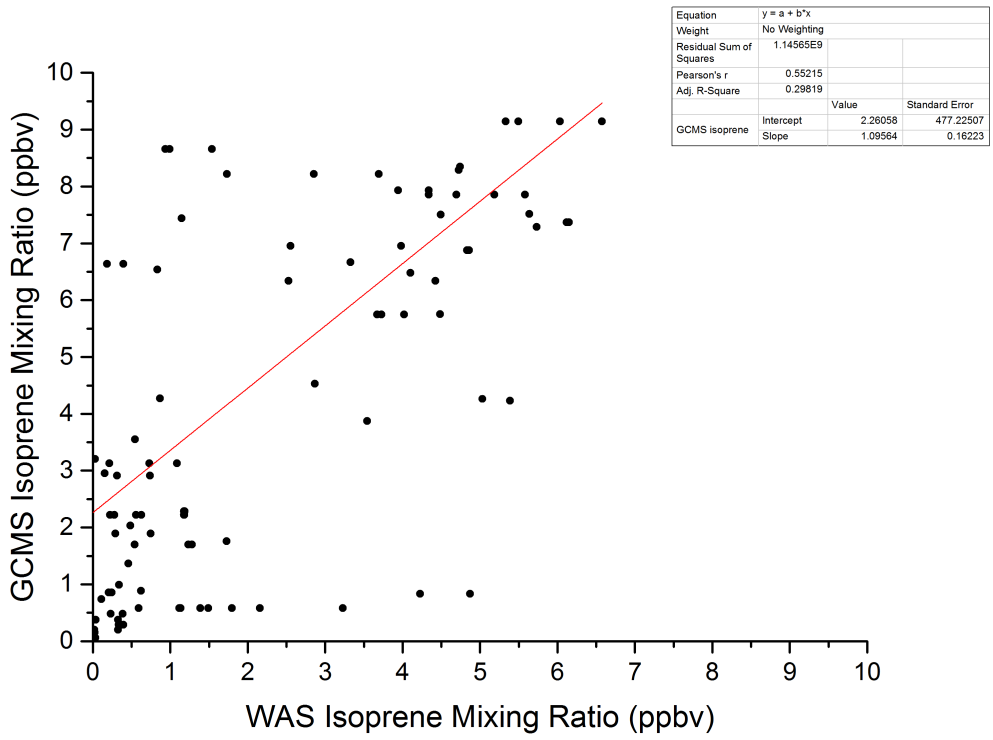

Figure 3.2: A comparison between isoprene as measured by the WAS system and the *in situ* GC/MS system. The graph shows a highly scattered correlation, as demonstrated by an R^2 value of 0.55.

shows the comparison between the GC/MS and PTR-MS analysed isoprene.

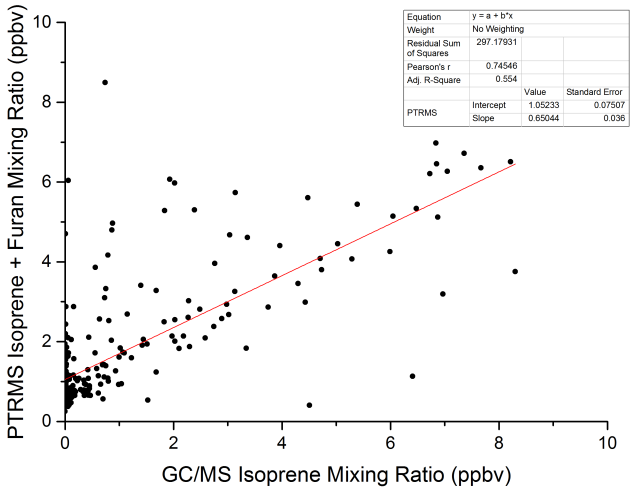

Figure 3.3: A comparison between isoprene as measured by the PTR-MS and the *in situ* GC/MS. The figure shows the PTR-MS data as averaged over the GC/MS sample times, over the entire campaign. The two data sets show good agreement with an R^2 value of 0.75. The offset in the data can be attributed to differences in sampling methods, as well as furan mixing ratios.

When compared with the PTR-MS, the GC/MS data agrees favourably, and has an R^2 value of 0.75. The slope for the best fit line is calculated as 0.65, which accounts for the PTR-MS measuring both isoprene and furan. Disprepancies, particularly in the upper left quadrant, are attributed to high furan levels from biomass burning rather than isoprene. The highest point has a corresponding CO mixing ratio of 450 ppbv, which corresponds to a 200 ppbv enhancement over the background. This lends confidence to the measurements made by the GC/MS, despite a direct intercalibration not having been conducted.

In addition to the GC/MS, WAS and PTR-MS for VOC and OVOC analysis, the aircraft was also fitted with an in situ ozone, CO and NO_x analyser. Ozone measurements were obtained using a Thermo Scientific TE49C commercial gas analyser. The instrument can measure the amount of ozone in an air sample between 0.05-500 ppbv, giving a large detection range. The instrument uncertainty is estimated at ± 3 % for values above 100 ppbv and 3 ppbv for measurements below 100 ppbv. CO measurements were obtained using a rack-mounted Aerolaser AL 5002 analyser (O'Shea et al., 2013). This instrument employs the use of UV light (wavelength 150 nm) to stimulate CO fluorescence, which is detected via an optical filter and photomultiplier. The Aerolaser is calibrated between 0-500 ppbv, with an estimated uncertainty of 1.5 ppbv at 100 ppbv. More details are given in Gerbig et al. (1999). Finally, NO_x measurements were given using an Air Quality Design Chemiluminescence gas analyser (with a photolytic converter for NO_2). The instrument is calibrated between 0-50 ppbv, with an uncertainty of ± (6 % + 2) ppbv.

3.1.3 Results

This section will discuss the data gathered from the *in situ* GC/MS during the SAMBBA campaign, and a comparison with the WAS system. Initially, positional and chemistry data (ozone, CO etc) were extracted and averaged over the five minute thermal desorption sampling times. Figures 3.4 and 3.5 show the track of the aircraft made during the campaign, with Figure 3.4 showing the average locations of the GC/MS samples, and Figure 3.5 showing the track plot coloured by CO. Flights to the East and South were generally conducted over sparse forest, or Cerrado-type vegetation, whilst flights to the North and West were conducted over dense pristine forest. Forest fires were frequent in both conditions, due to anthropogenic clearing of these areas. Figure 3.5 clearly shows the locations of forest fires. Concentration data were binned into 500 m vertical bins from the surface, to 8500 m in order to produce averaged profiles for analysis.

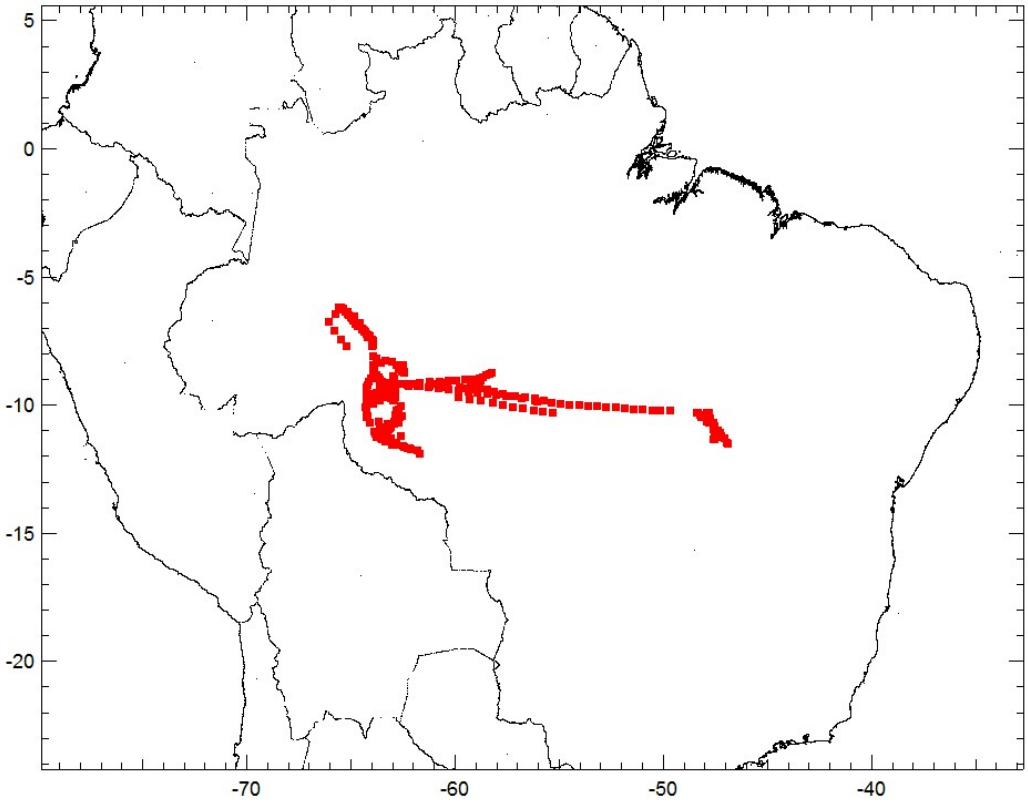

Figure 3.4: Aircraft position over the entire SAMBBA campaign averaged over the GC/MS sample times. The points show the mid-sample time for each chromatogram.

During the campaign, ozone mixing ratios varied between < 1 and > 90 ppb, as shown in Figure 3.6. Absolute mixing ratios depend heavily upon proximities to forest fires, which

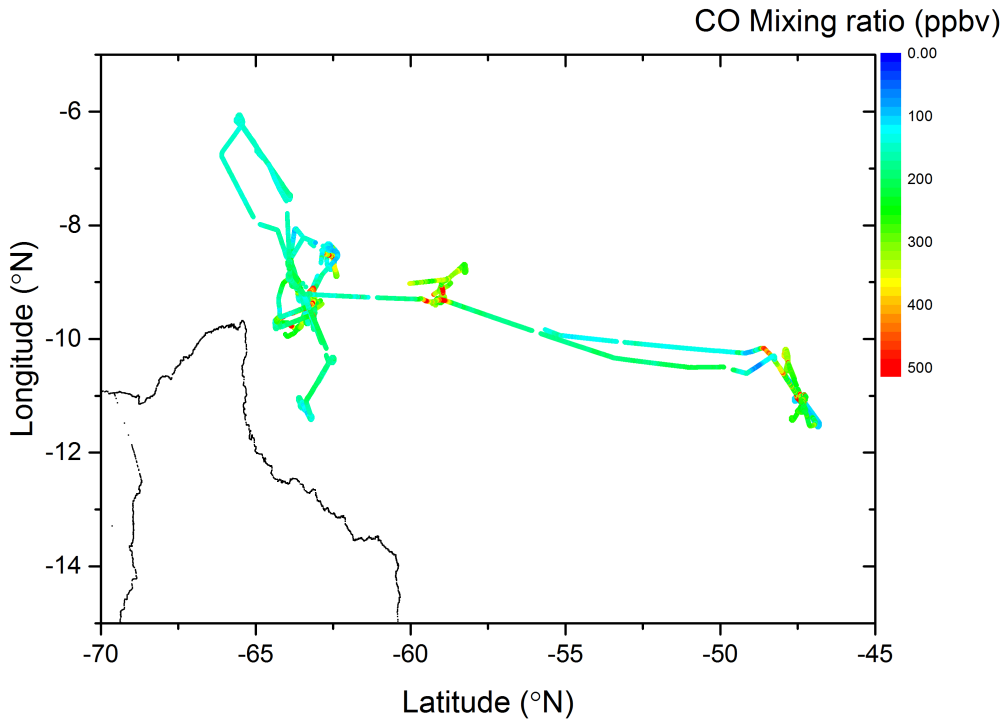

Figure 3.5: Track plot of aircraft position over the entire SAMBBA campaign, coloured by CO.

also accounts for the large spread of the data. The general shape of the profile shows an increase in ozone mixing ratio with an increase of altitude, which is to be expected as higher up, the troposphere has more stratospheric influence, with airmasses slowly detraining across the tropopause from the stratosphere, as well as events such tropopause folding. In an area such as the Amazon, where high total VOC mixing ratios combine with high humidities and high levels of UV light, the absolute mixing ratios are higher when compared to oceanic ozone measurements (Browell et al., 1988; Gregory et al., 1988).

In order to determine the amount of VOCs entering the free troposphere, the height of the boundary layer needed to be determined. The boundary layer height is affected by surface temperatures and solar intensity, and therefore cycles both diurnally, and annually.The average height of the boundary layer can be determined over the period of the campaign. During flights, the aircraft performed a series of altitude profiles from the surface, up to 8000 m. These profiles can be used to find the height of the temperature inversion, taken as a measure of boundary layer height. A representative selection of 10 profiles is presented here, from different days of the campaign, and at different times of the day. An analysis of these profiles gave an average boundary layer height of 2300 m ±

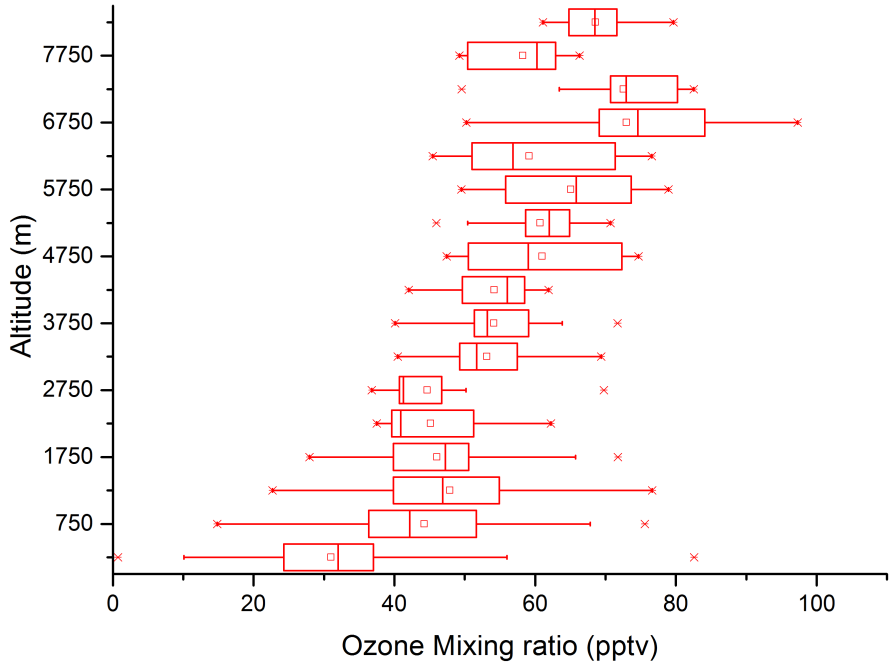

Figure 3.6: Vertical profile of ozone collected during the SAMBBA campaign. The 1 Hz data provided by the aircraft has been averaged over the GC/MS sample times (5 mins) and binned to 500 m to produce the distributions. The box and whisker plots represent the mean, median, interquartile range, bottom 5 %, top 95 % and outliers.

50 above the surface. This is in agreement with previous studies conducted in the region. Figure 3.7 shows an example of the type of plot used to determine the boundary layer height.

Once the boundary layer height was determined, the vertical profiles of VOCs could be compared against this. For short-lived compounds, the expectation would be that these would be confined to the boundary layer, and a sharp decrease in mixing ratio would be expected at between 2000 and 2500 m (taking into account fluctuations in the boundary layer height). Biomass burning releases CO into the atmosphere and, coupled with a long OH dependent lifetime of ˜2 months, can undergo detrainment out of the boundary layer to the free troposphere (Petrenko et al., 2013). A less distinct reduction at the BL would be expected for longer lived VOCs, also from biomass burning. Once in the free troposphere, compounds can undergo significant long range transport. Figure 3.8 shows the vertical profile of CO, which includes data taken across the whole campaign, and then averaged between the GC/MS sampling times.

The profile shows some modest decrease around the region of 2400 m but it is clear

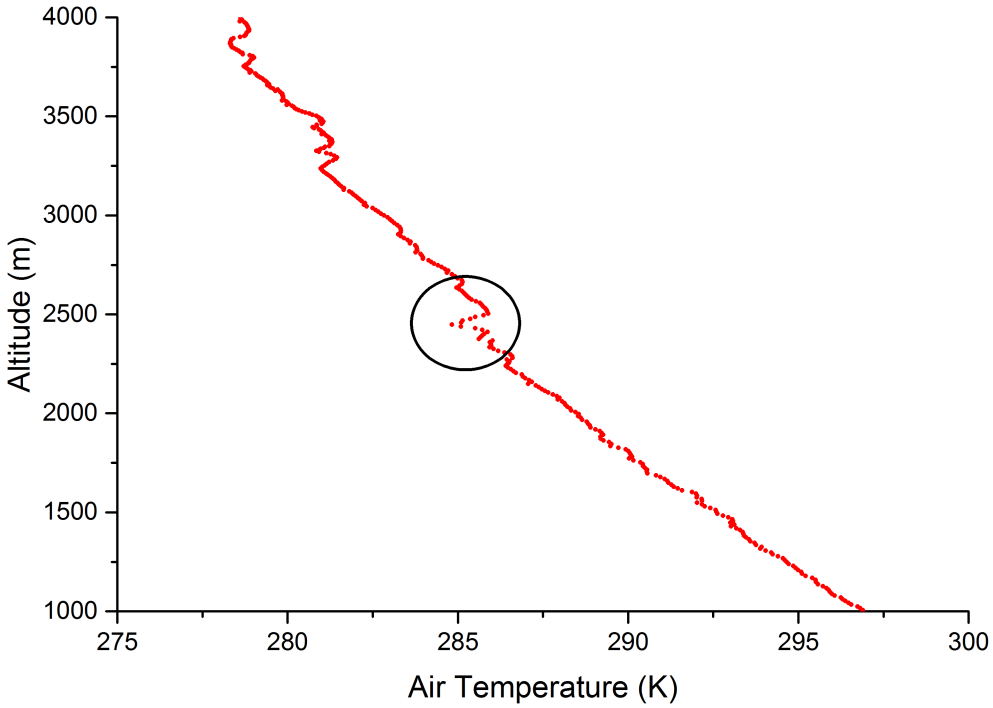

Figure 3.7: A plot of one of the altitude profiles made by the aircraft during the SAMBBA campaign. This shows air temperature against altitude and was used to determine the height of the planetary boundary layer. The temperature inversion which occurs at the top of the boundary layer is indicated by the circle at approximately 2450 m.

that CO is not wholly constrained to the boundary layer, and the temperature inversion at the top of it does not represent a significant barrier. This is due to the long OH dependent atmospheric lifetime being longer than the rate of detrainment from the boundary layer to the free troposphere as determined by the vertical wind speed.

By contrast, the same vertical profile for benzene is shown in Figure 3.9. The profile shows a gradual decrease in benzene mixing ratio with an increase in height. As the source of benzene is in forest fires, the heat from the surrounding air increases the rate of vertical transport. Therefore, initially, the air parcel is rapidly lifted. As the surrounding air cools, the parcel rises, until it reaches the same temperature as the surrounding air. Given an OH dependent lifetime of ˜10 days in the tropics, the rate of vertical mixing from the surface to the free troposphere is greater than the VOC lifetime (Rasmussen and Khalil, 1983; Atkinson, 2000). Lifetimes are calculated from the reaction rate constant, assuming a set OH mixing ratio, as shown in Equations 3.1 and 3.2.

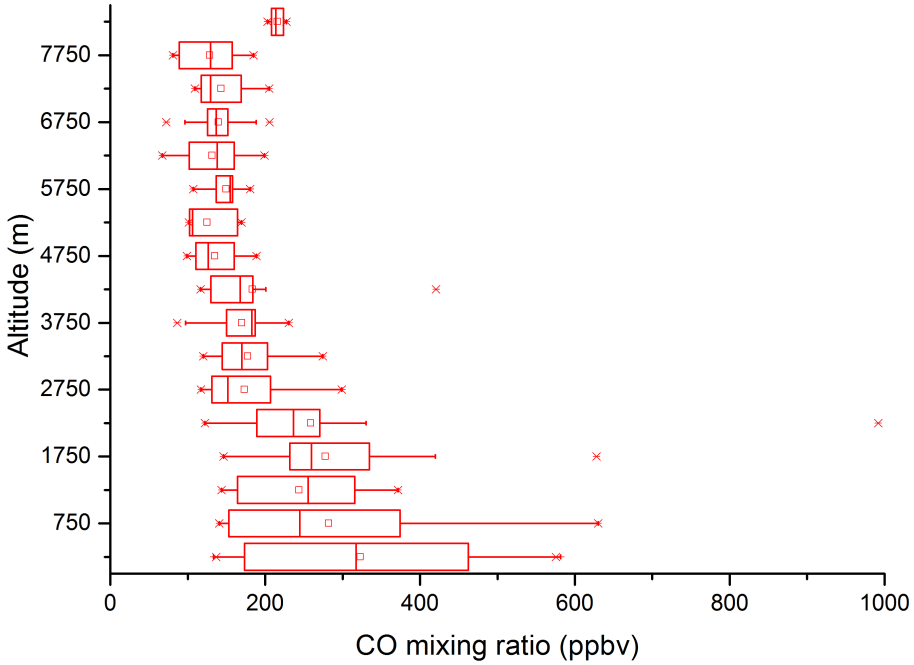

Figure 3.8: A vertical profile of CO as measured over the Amazon rainforest during the SAMBBA campaign. The data has been averaged over the GC/MS sampling times and split into 500 m bins.

$$k = k_{OH}\,[OH]\,[benzene] \tag{3.1}$$

$$\frac{1}{\tau} = k\,[OH] \tag{3.2}$$

Benzene can enter the free troposphere due to this vertical transport. Based on the average values on the vertical profile, it can be estimated that 20 - 30 % of benzene emitted from the surface is able to escape into the free troposphere, to undergo long range horizontal transport. The remaining 70 - 80 % was either oxidised in the boundary layer, re-deposited to the surface, or carried to other locations. Lewis et al. (2013) describes how emissions from forest fires can impact benzene mixing ratios in remote locations, far away from the sources.

Figure 3.9 shows a gradual decrease in mixing ratio in the region of 2400 m, the average top of the boundary layer. This is consistent with the atmospheric lifetime of benzene being shorter than that of CO, but longer than the rate of vertical transport within the boundary layer. Finally, the vertical profile for isoprene was produced. The

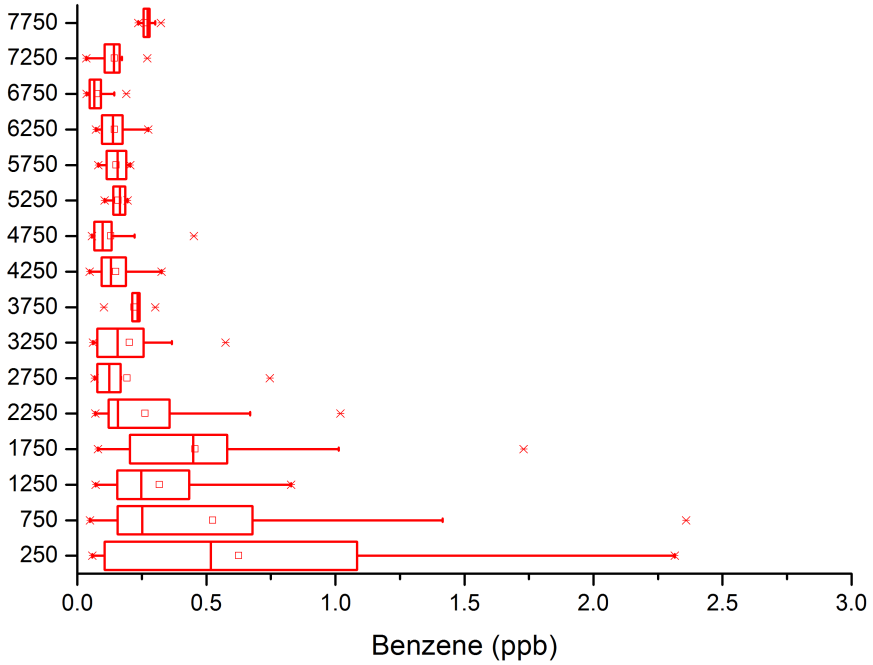

Figure 3.9: Vertical profile of benzene mixing ratio measured during the SAMBBA campaign by the *in situ* GC/MS. The steady decline in mixing ratio shows that benzene is less confined to the boundary layer than other more reactive species such as isoprene.

primary source of isoprene in this environment is biogenic, from green plants and trees on the surface. Isoprene has a very short OH dependent lifetime of ≈30 mins (Atkinson, 2000). Therefore, it would be expected that almost no isoprene is able to escape from the boundary layer. Figure 3.10 shows the vertical profile of isoprene over the entire campaign.

The drop in the isoprene mixing ratio can be seen at the top of the boundary layer. Mixing ratios average at ˜ 1-2 ppbv in the boundary layer, dropping to below detection limit (approximately 0.4 ppbv, as calculated by 3x signal:noise ratio) in the free troposphere. This shows that isoprene is almost entirely constrained to the boundary layer. Therefore isoprene cannot directly undergo longer range transport. However, the isoprene reacts with OH in the boundary layer, to form other products. These include methyl vinyl ketone, methacrolein, and formaldehyde. It is therefore important to understand the chemistry and transport of these compounds, in order to determine the total effect of isoprene in the Amazon. If these compounds also undergo vertical transport into the free troposphere, the area of influence of isoprene is much larger than the Amazonian boundary layer.

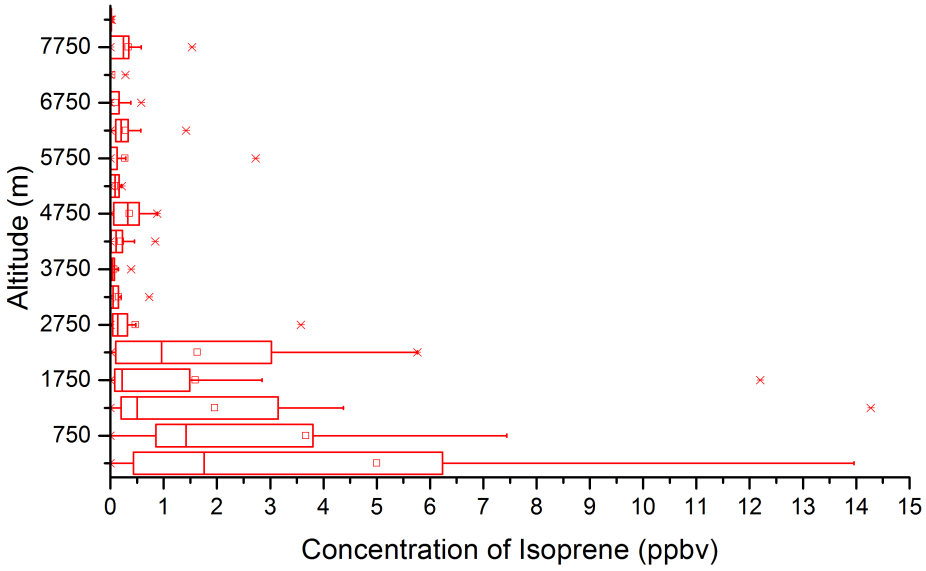

Figure 3.10: Vertical profile of isoprene as measured during the SAMBBA campaign by the *in situ* GC/MS. The drop in mixing ratio at 2500 m shows that isoprene is almost entirely constrained to the boundary layer.

Attempts were also made to separate the data into the two regions analysed during the course of the campaign- biomass burning regions, and pristine forest. These two areas can be assumed to be chemically different, due to the differing processes. For the purposes of this, NO was chosen as a tracer for biomass burning, as this was by far its strongest source in the region. Upon analysis of the data, a limit of 100 ppb of NO was used, with mixing ratios below that deemed as 'background' over the forest, and mixing ratios above indicative of close proximity to biomass burning regions.

The NO mixing ratios were then averaged over the GC/MS sampling times, and the GC/MS data was then filtered for NO mixing ratios either exceeding or falling below this 100 ppb limit. The data for isoprene and benzene was then plotted for each of these conditions as shown in Figures **??** and **??**.

Benzene and isoprene were plotted as an example of tracers from each condition. However, as can be seen from Figures **??** and **??**, there is little to no dependence on forest type for either tracer. Many possibilities exist that could explain this, for example, a well mixed boundary layer, but what is more likely is the long sample time for the instrument when compared to the forest fire plumes. Therefore the instrument was not

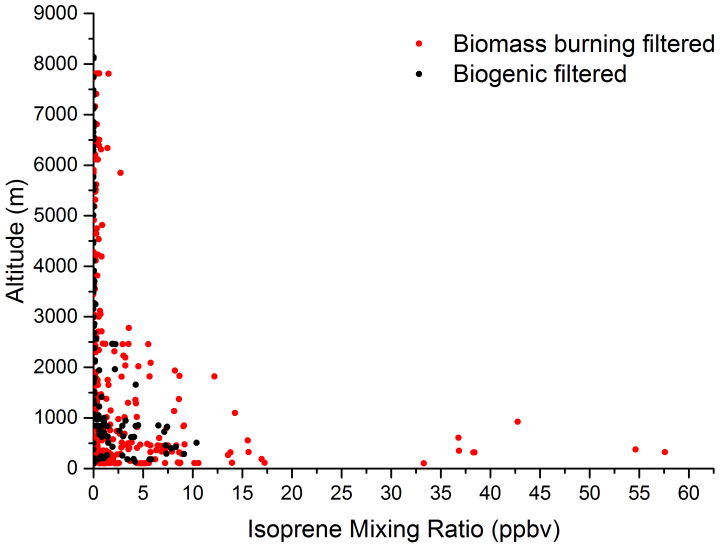

Figure 3.11: Isoprene vertical profile coloured by forest type.

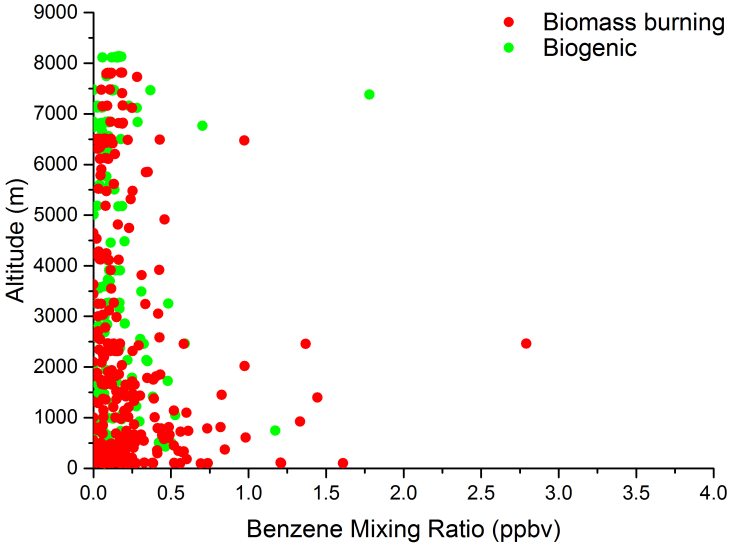

Figure 3.12: Benzene vertical profile coloured by forest type.

necessarily capable of distinguishing between regions of biomass burning, and regions of pristine forest.

3.1.4 Methyl Vinyl Ketone and Methacrolein Analysis

The secondary remit of this project was to determine speciated vertical profiles of the principle oxidation products of isoprene. The major products of isoprene oxidation are methyl vinyl ketone (MVK) and methacrolein (MACR) and are formed from the reaction of isoprene with the OH radical. The products formed then undergo photodissociation to MVK and MACR (Atkinson and Arey, 2003). The reaction pathways are shown in Figure 3.13.

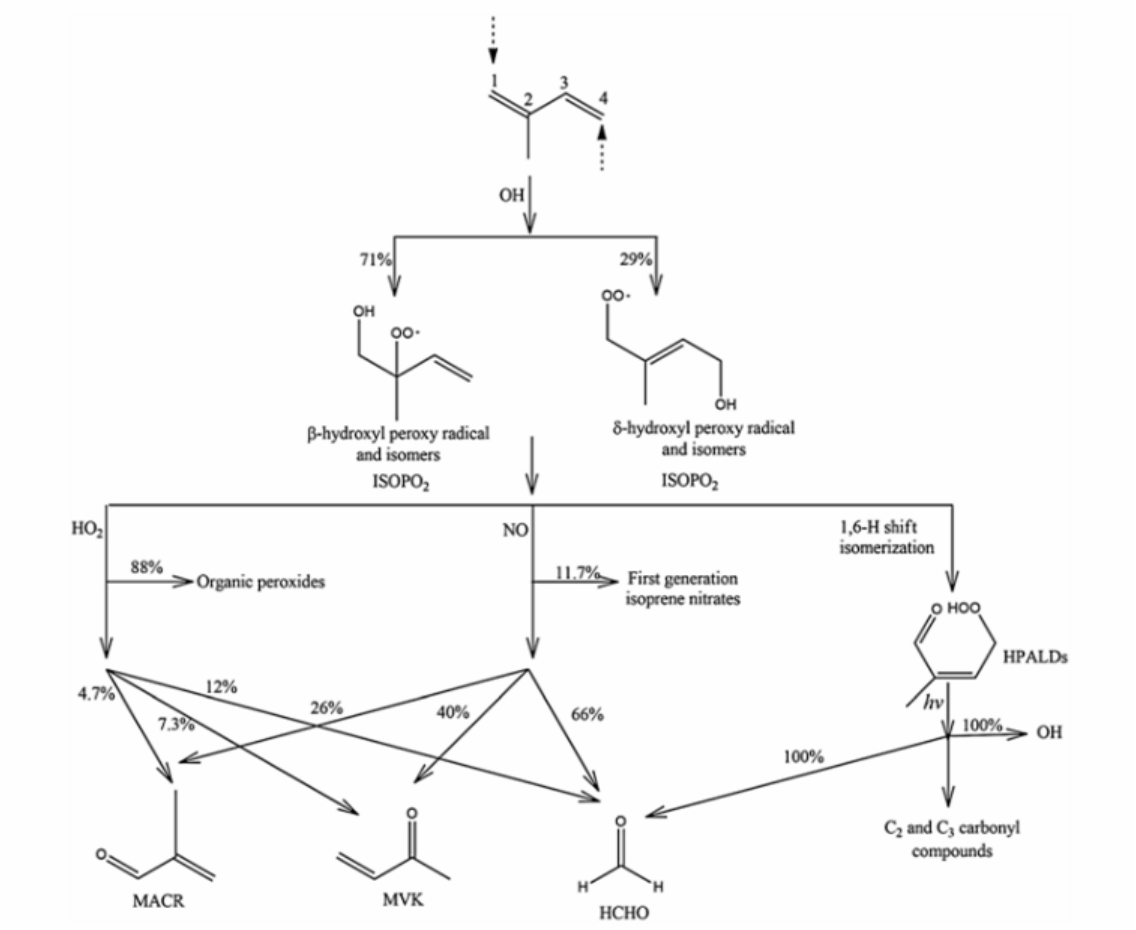

Figure 3.13: Schematic of the first stage of the isoprene oxidation mechanism initiated by OH (Figure and caption reference: Mao et al., 2013)

The reaction scheme shows the three main oxidation products of isoprene. Formaldehyde is another major product, but its formation from isoprene is more comprehensively understood (for example: Luecken et al., 2012; Jones et al., 2009; Zhu et al., 2016, etc.). However, the chemistry and transport of MVK and MACR are less well covered. Full vertical, speciated profiles of the two compounds have not been measured before above the Amazon, one of the largest isoprene emitting regions on the planet. Attempts were

made here to try and attempt this.

These two compounds are notoriously difficult to separate, as they have extremely similar volatilities and form ions with the same m/z. Therefore, speciation by PTR-MS is impossible, with analysis by GC/MS also presenting challenges. However, efforts were made using the aircraft GC/MS to determine mixing ratios of MVK and MACR, initially by attempting to separate by chromatography, and secondly by using minor ions. The results from the attempts at separating the compounds are shown here. Figure 3.14 shows the mass spectra of MVK and MACR, whilst Figure 3.15 shows an EIC of ions 55 and 70, representing major ions of MVK and MACR (note that the GC/MS scans from 44 amu, in order to reduce interference from other contaminant ions). The mass spectra show strong signals at m/z 70 for both compounds, whilst the spectrum for MVK shows a signal at m/z 55.

Table 3.1: Details of instruments fitted to the FAAM BAe-146 during the SAMBBA campaign in September/October 2012. See references for more details.

Species / parameter	**Method / Instrument details**	**Averaging time**	**Precision/ accuracy**	**Affiliation, Reference**
Physics / Positional				
Position, wind (U,V,W)	INS, GPS, Turbulence Probe , RadAlt	1s	0.01 P/Ps	FAAM, Petersen and Renfrew (2009)
Humidity (Dew Point, Temperature)	General Eastern Hygrometer	1s	0.5 - 3 K (pressure dependent)	FAAM, Ström et al. (1994)
Temperature	Rosemount Sensor, Aerospace Ltd	1s	0.3K	FAAM
Cloud Microphysics	CDP	1s		FAAM, Rosenberg et al. (2012)
Chemistry				
CO	UV resonance fluorescence, Aerolaser 5002	1s	1 ppbv	FAAM, Gerbig et al. (1999)
O_3	UV absorption, TECO 49C	1s	1 ppbv	FAAM, Wilson and Birks (2006)
CO_2, CH_4	CEAS, Los Gatos, USA	1s	0.5 ppmv and 2.5 ppbv respectively	FAAM, UoM, O'Shea et al. (2013)
NO, NO_2	Chemiluminescence with photolytic conversion for NO2, Air Quality Design Inc	10s	5 pptv and 15 pptv respectively	FAAM, UoY, Pike et al. (2010)
NMHCs (C_1-C_7)	Whole Air Sampling with analysis by GC/FID	30s (Fill time)	Species Dependent	UoY, Hopkins et al. (2003)
PAN	PAN-GC, Ai Qualitek	90s	5pptv	UoY, UoL, FAAM, Whalley et al. (2004)
NMHCs	PTRMS	1s	Species Dependent	UEA, Murphy et al. (2010)
NMHCs	GC/MS	5 min	Species Dependent	UoY, Andrews et al. (2016)
Aerosol				
Particle Size	APS, TSI	0.1s	0.1 microns	UoM
Water Content	CCN, CPC	1s	0.2 microns	UoM, Roberts and Nenes (2005)
Aerosol Chemistry	TOF-AMS	1s	Species Dependent	UoM, Jayne et al. (2000)

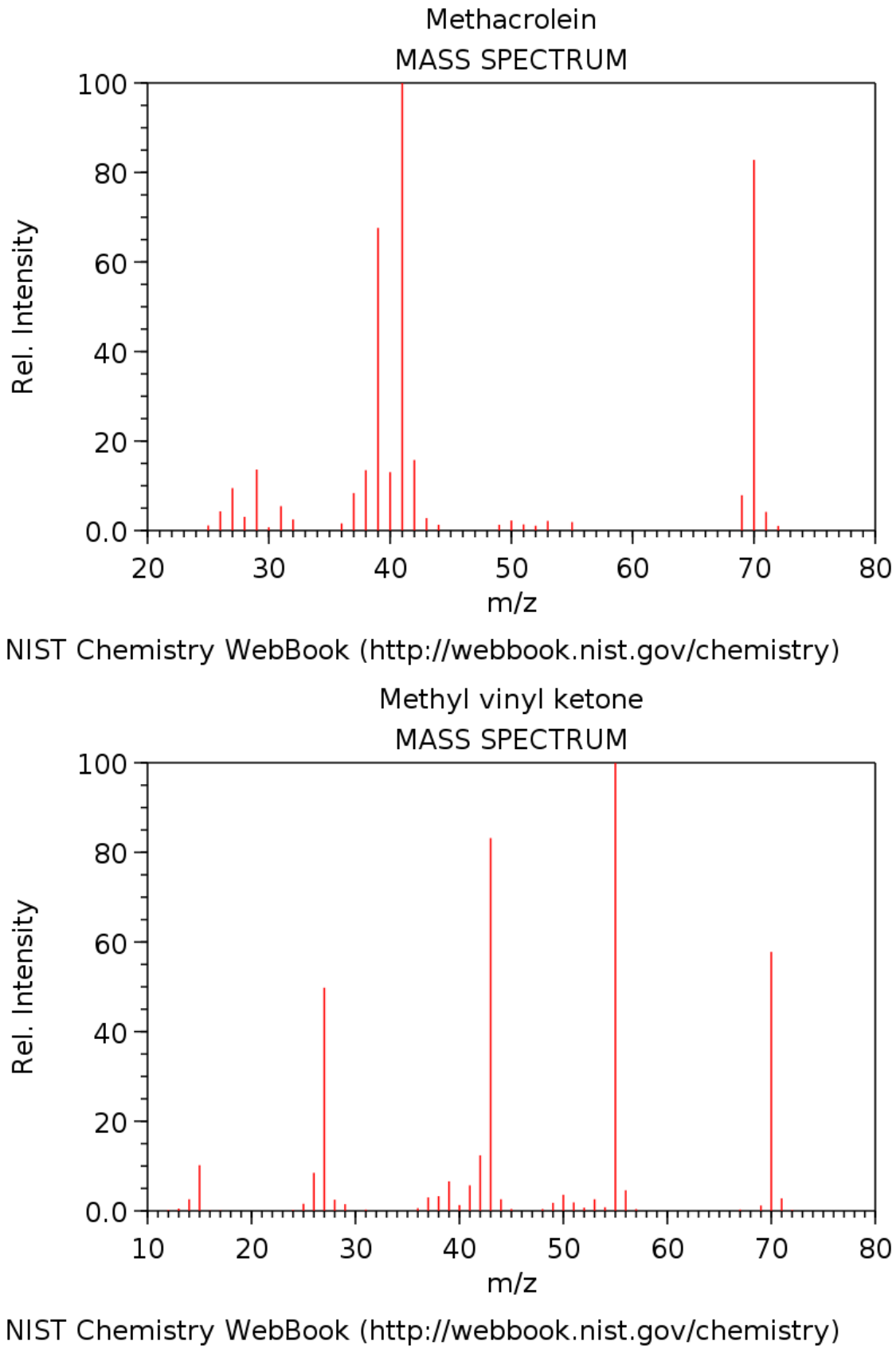

Figure 3.14: The mass spectra of methacrolein (top) and methyl vinyl ketone (bottom). *Source: NIST Web book.*

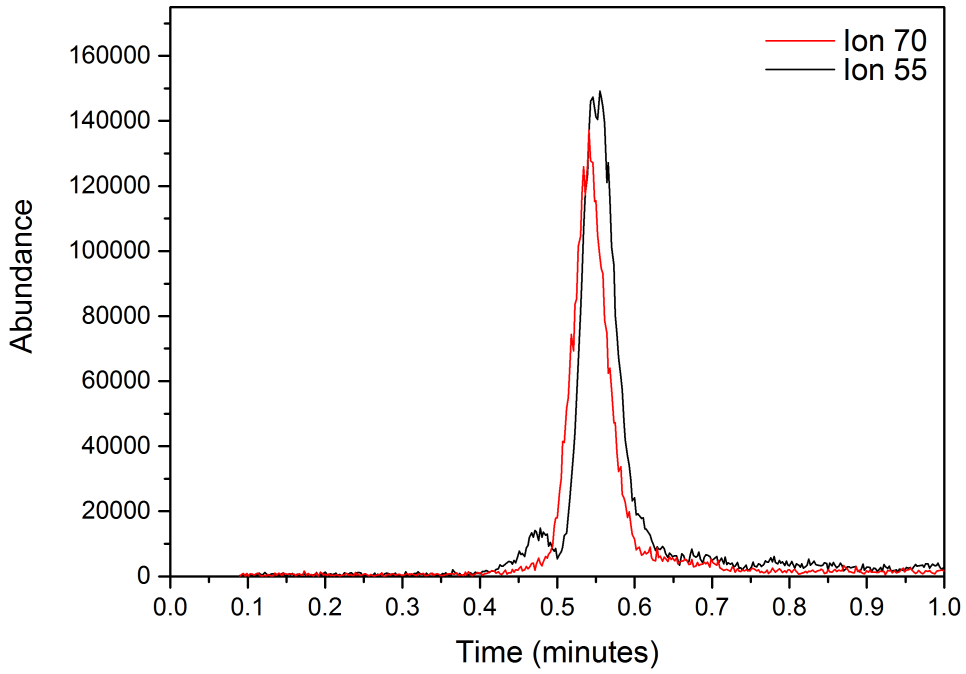

Figure 3.15: Typical extracted ion chromatogram from the SAMBBA campaign, showing MVK and MACR. Both compounds display ions 70, whilst only MVK produces an ion at m/z 55. The image shows the two compounds almost exactly coeluting.

Initially, the area under the ion 55 peak was integrated, and attributed to MVK. However, after a comparison with literature values for combined MVK and MACR measurements, the figures given by this style of analysis were deemed to be highly inaccurate (**?**Greenberg and Guenther (1999); Crutzen et al. (2000); Kuhn et al. (2007) etc.)

GEOS-Chem is a global chemical transport model, with this work using version 9-02 (www.geos-chem.org). The model was run at 4 ° x 5 ° spatial resolution. The model is forced by assimilated meteorological and surface fields (GEOS-5) from NASA's Global Modelling and Assimilation Office. The model chemistry includes O_x, HO_x, NO_x, BrO_x and VOC chemistry as described in Mao et al. (2013), as are the emissions. Model simulations were run for 2 years (1st July 2005 - 1st July 2007) at first with the first year used as a spin up and the diagnostics performed on the second year. VOC concentration profiles were used from the model grid box that covers the region of Manaus (coordinates 3.1 ° S, 60.02 ° W). Firstly, isoprene was compared to the GEOS-Chem output for the grid box containing Porto Velho. This is shown in Figure 3.16.

When the model output is compared to the observations, it would appear that the model accurately predicts the isoprene mixing ratio for this region, at this time of year. This again, increases the amount of confidence in the GC/MS data. However, when the model was run for MVK and MACR, the comparison was very poor. Figure 3.17 shows the vertical profiles of MVK and MACR, with Figure 3.19 showing the model output.

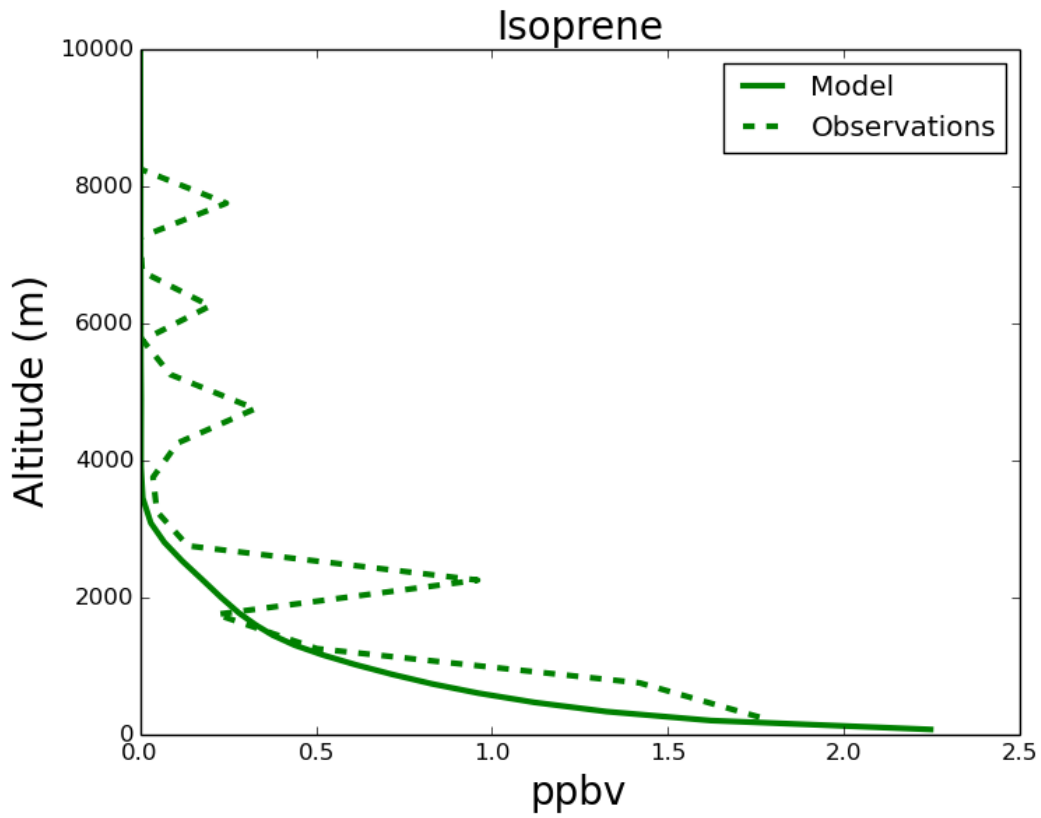

Figure 3.16: A comparison between the vertical profiles from the measurements (dashed line) and the model output (solid line). The model predicts the emission, and subsequent removal from the atmosphere over the altitudes analysed well. It is important to note that the model predicts that no isoprene crosses the top of the boundary layer.

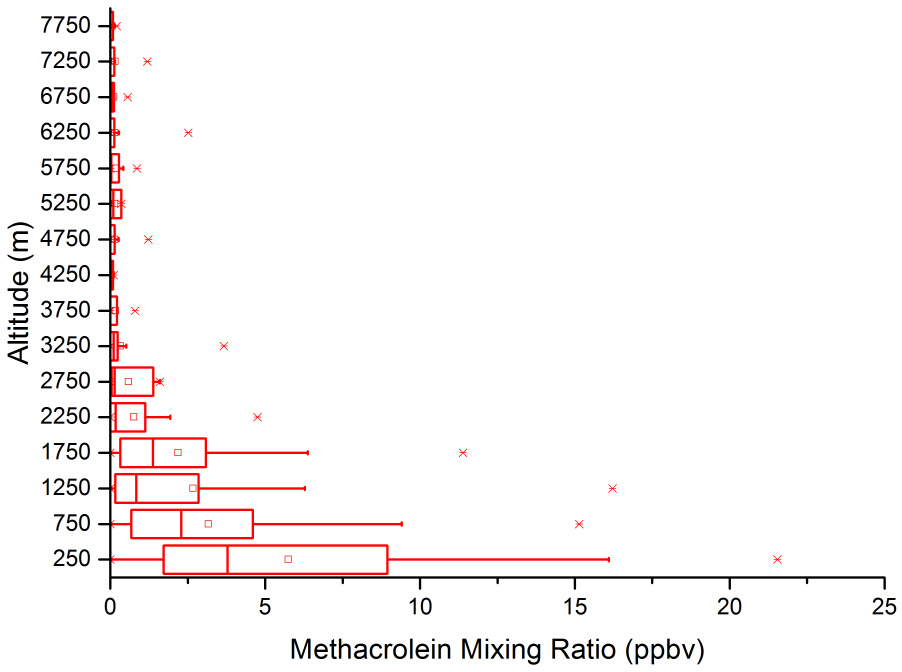

Figure 3.17: Vertical profile of methacrolein, as measured by the *in situ* GC/MS during the SAMBBA campaign.

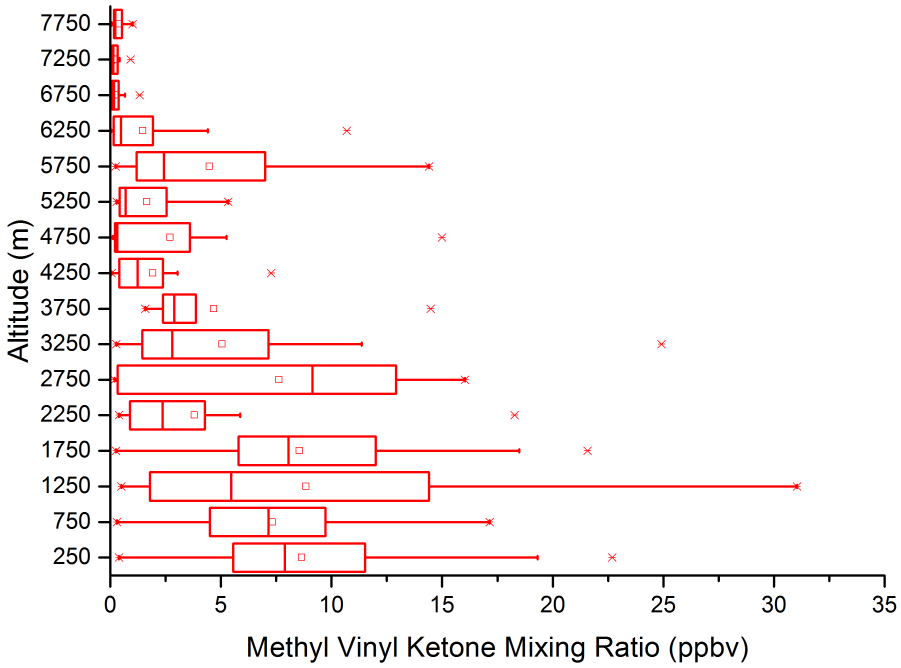

Figure 3.18: Vertical profile of methyl vinyl ketone, as measured by the *in situ* GC/MS during the SAMBBA campaign.

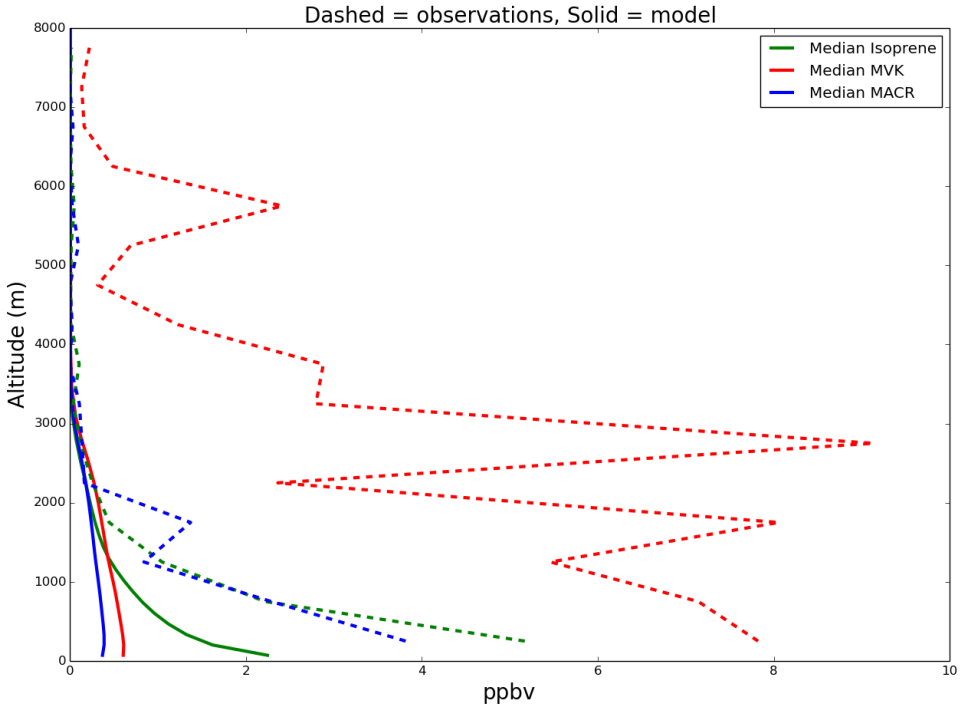

Figure 3.19: Plot of model output (solid line) compared to measurements (dashed line). The model captures isoprene and MACR well, but the comparison for MVK is very poor

The MVK vertical profile was produced by integrating ion 55. The ratio of ion 55:70 for MVK was then used to determine the contribution of MACR to ion 70. However, when compared to literature, the combined PTR-MS measurements and the GEOS-Chem model output, it was clear that the *in situ* GC/MS was misreporting the MVK values, possibly due to other VOC ion interferences, particularly at the start of the chromatogram. Both these compounds elute in ˜35 seconds, meaning very little time interacting with the stationary phase, with many other light VOCs also eluting early in the chromatogram. However, with the recent modifications outlined in chapter 2, should the study be repeated, the instrument should be able to perform well, and speciate the two compounds. This is mainly due to the introduction of the Stirling cooler cold trap and the CO_2 cold on column systems, meaning 'cleaner,' more reproducible data. The results are shown in Figure 3.20. The figure shows the EIC of the two major ions, showing that the instrument is now capable of giving speciated MVK/MACR measurements.

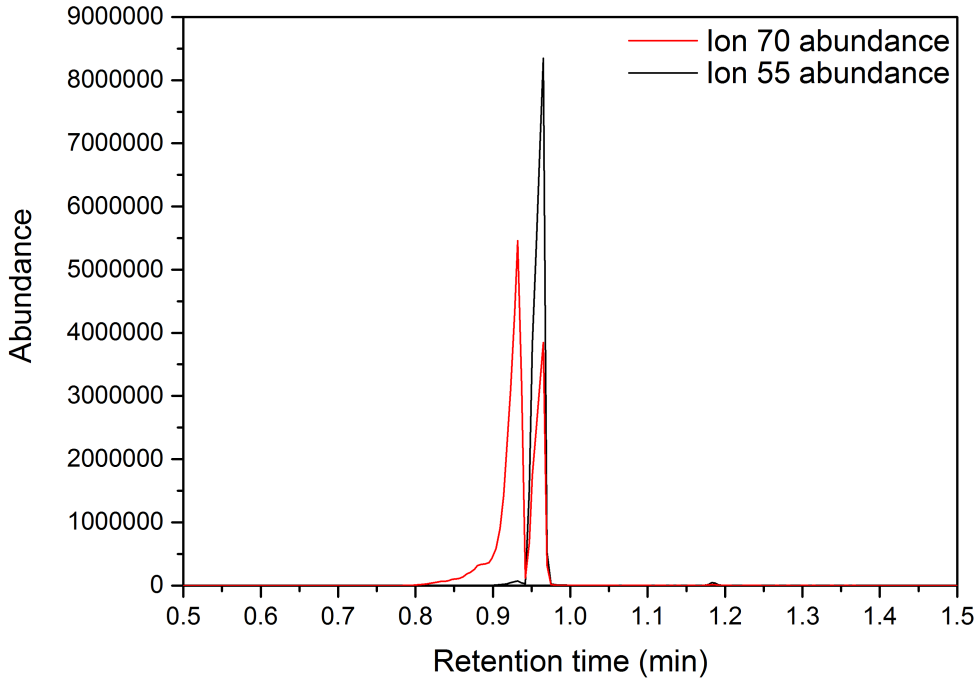

Figure 3.20: EIC of ions 70 and 55, representing Methyl Vinyl Ketone (red- ion 70) and Methacrolein (black- ion 55). After the modifications made to the GC/MS, the two compounds now elute with a resolution factor of 1.8, meaning that they are effectively baseline resolved.

Overall, the instrument was capable of measuring isoprene and MACR, but due to coelution of unknowns, it could not accurately measure MVK. Based on the available data,

even the MACR data cannot be trusted. Therefore, although attempts were made to make speciated measurements of these two compounds, the instrument would have benefitted from more pre-campaign calibrations, which were not done due to time constraints.

3.1.5 CO:VOC Ratios

Several studies have previously investigated the ratio between CO and VOCs in biomass burning plumes, primarily from forest fires. Three of these such studies are summarised here and compared to the ratios that have been calculated by this study. In 2011, a study by Simpson et al. was conducted around 'fresh' Canadian smoke plumes. They analysed approximately 65 compounds within these smoke plumes, using WAS and analysed by GC coupled to ECD, FID and MS. They also measured CO, CO_2, methane and NO_x using *in situ* techniques. They calculated the CO:VOC ratio of a subset of these compounds, in different plumes, and took an average of the ratios. Additionaly, Lewis et al. (2013) conducted a similar study with more aged forest fire plumes, again in Northern Canada, with calculated CO:VOC emission ratios. Finally, Evtyugina et al measured emissions from combustion in Central Portugal, with a subset of compounds analysed, and the CO:VOC ratios published. Using the WAS data, xy plots of CO and a range of VOCs were plotted and analysed for the best fit line. The gradient indicates the CO:VOC ratio. Figure **??** shows three tracers, benzene toluene and ethene, and their relationship to CO over the entire campaign.

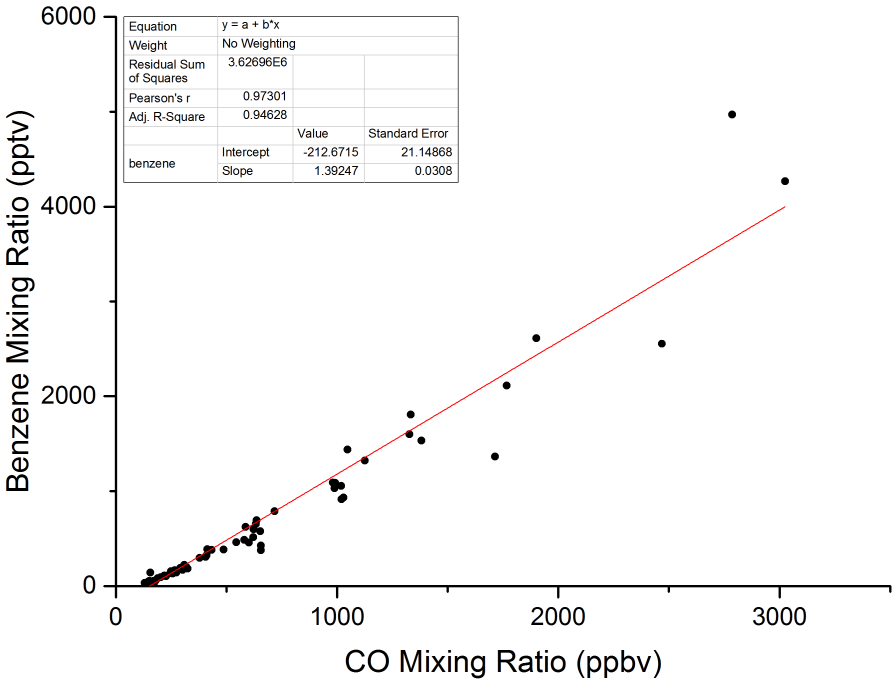

Figure 3.21: CO vs benzene, showing a reasonable agreement data ($R^2 = 0.95$.) The gradient of the slope shows the ratio between the two compounds (1.39 ± 0.03

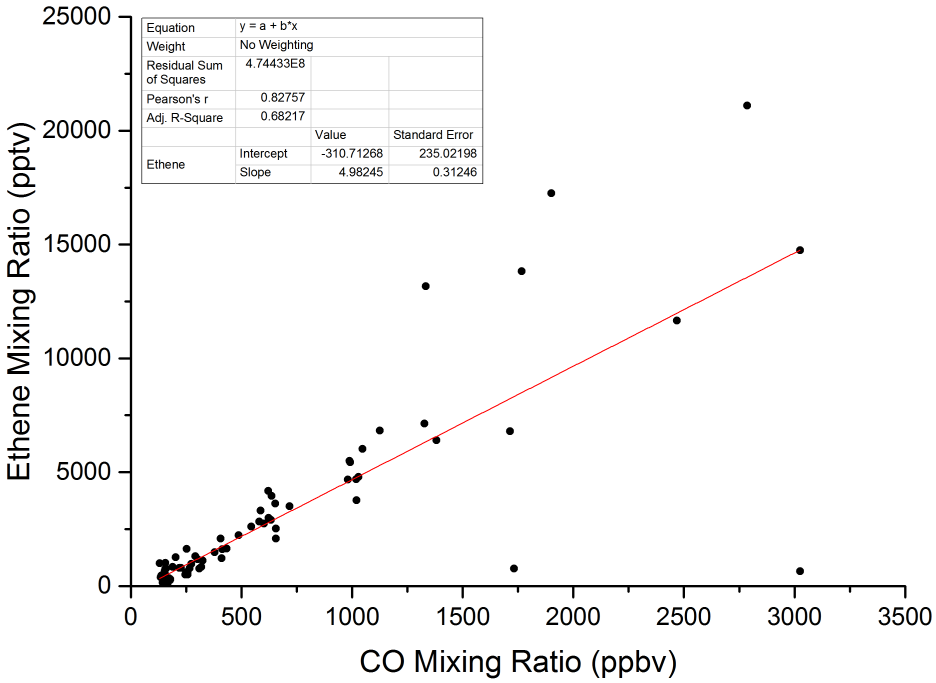

Figure 3.22: CO vs ethene, showing a reasonable agreement data ($R^2 = 0.68$.) The gradient of the slope shows the ratio between the two compounds (4.98 ± 0.31

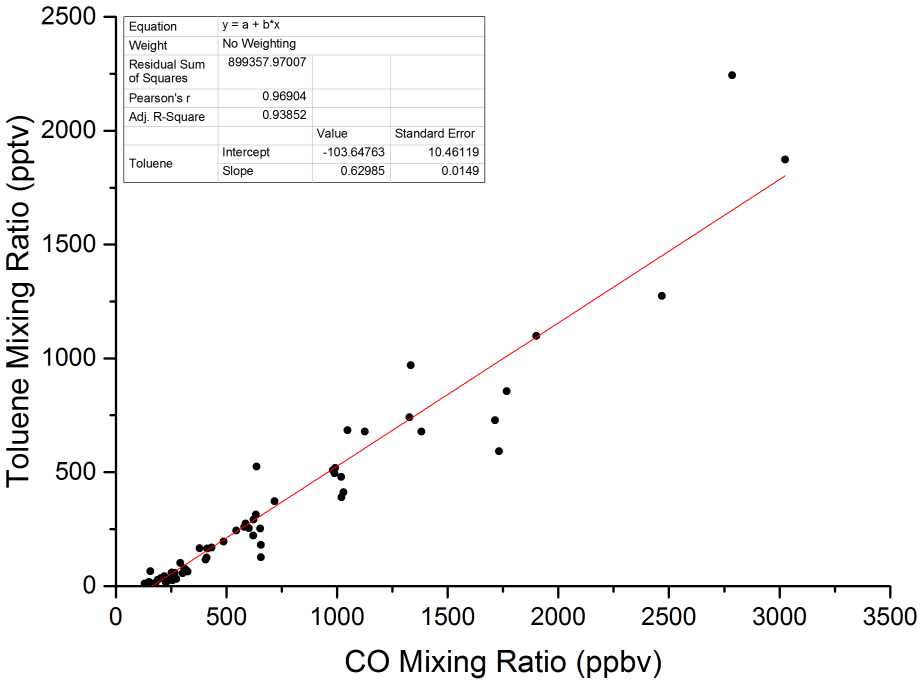

Figure 3.23: CO vs toluene, showing a reasonable agreement data ($R^2 = 0.94$.) The gradient of the slope shows the ratio between the two compounds (0.63 ± 0.015

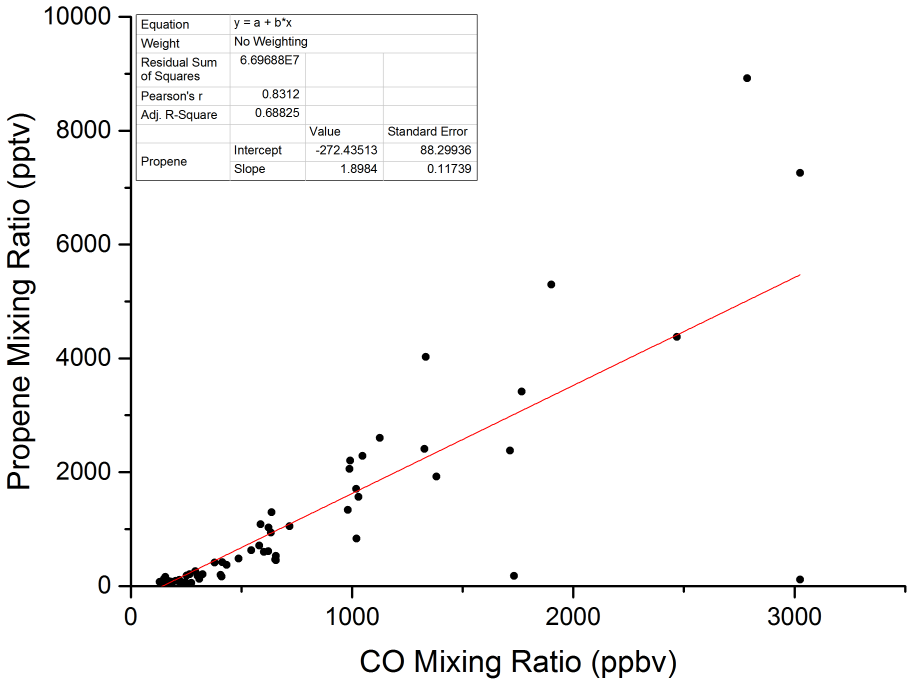

Figure 3.24: CO vs propene, showing a reasonable agreement data ($R^2 = 0.69$.) The gradient of the slope shows the ratio between the two compounds (1.89 ± 0.12

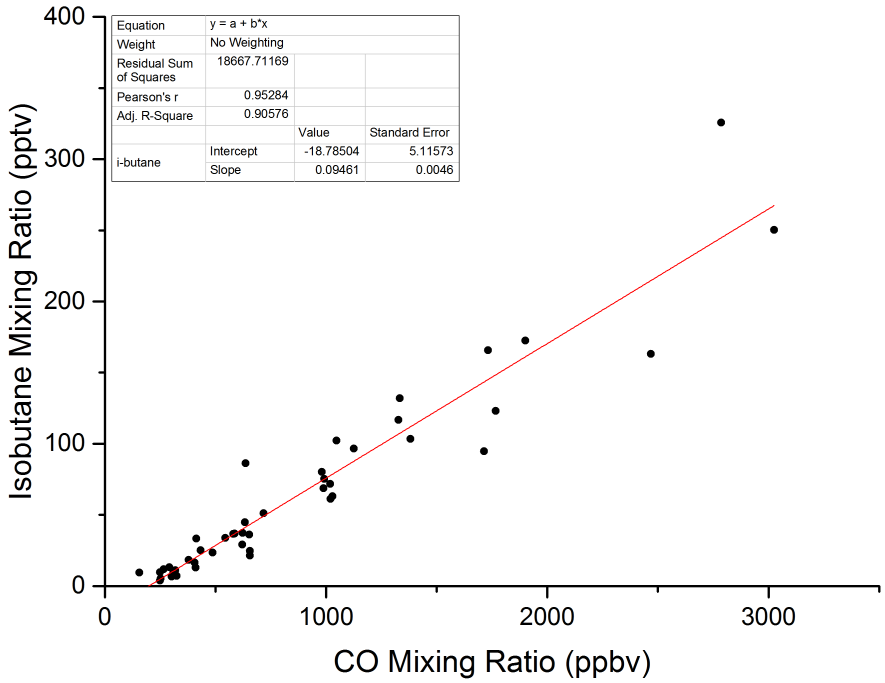

Figure 3.25: CO vs isobutene, showing a reasonable agreement data ($R^2 = 0.9$.) The gradient of the slope shows the ratio between the two compounds (0.095 ± 0.0046

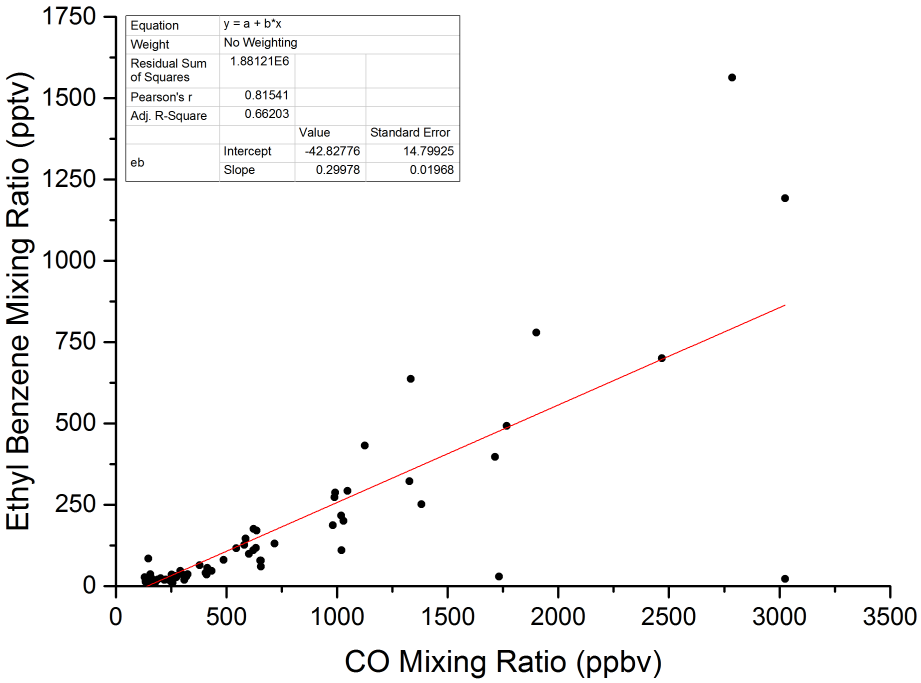

Figure 3.26: CO vs ethylbenzene, showing a reasonable agreement data ($R^2 = 0.66$.) The gradient of the slope shows the ratio between the two compounds (0.3 ± 0.02)

There has been some discussion regarding CO emission ratios according to different forest types, leading to the assumption that different species of trees and plants will emit different ratios of compounds. Additionally, proximity to the sources, as well as the oxidative capacity in the particular regions are relevent. In Lewis et al. (2013) and Simpson et al (2011), they reported CO:VOC ratios for a number of different species, both species from biogenic sources and from biomass burning sources. The comparison with this study is highlighted in Table 3.2.

Table 3.2 shows the comparison between this study and three previous studies for these compounds. Generally, the ratios agree well, with some small discrepancies. These discrepanices are could be down to a range of factors. Perhaps most relevant is the distance to the fire the measurements were made. Additionally, factors such as the heat of the fire, the species of tree and the meteorology could all also play a part. The good agreement of these measurements to previous literature studies shows the success and adds credence to the measurements. The stand out measurements are those made by Evtyugina et al, (2013). However, their study was measuring wildfires in Portugal, and involved only ground based measurements (1.5 m elevation). Samples were collected at a distance of 10 - 200 m downwind of the fires, which is much closer than any measurements made by aircraft. This could explain the lower ratios seen in this study, when compared to the other three.

Table 3.2: The CO:VOC ratios as calculated from this study, and compared to those given by 3 previous studies by Lewis et al. (2013), Simpson et al. (2011) and Evytugina et al. (2013)

Species	CO:VOC Ratio (this study)	CO:VOC Ratio (Lewis et al., 2013)	CO:VOC Ratio (Simpson et al., 2011)	CO:VOC Ratio (Evtyugina et al., 2013)
Ethene	4.98	6.97	7.88	*N/A*
Toluene	0.63	0.69	0.853	0.02
Benzene	1.39	1.4	2.11	*N/A*
Propene	1.9	1.19	2.55	*N/A*
iso-Butane	0.095	0.07	0.4	*N/A*
Ethyl Benzene	0.3	0.1	0.078	0.002

3.1.6 Conclusions

The purpose of this chapter was to determine the vertical profiles of both biomass burning, and biogenic tracers, namely, CO, benzene and isoprene over the Amazon. The amount by which each compound is constrained to the boundary layer largely depends on the compounds OH dependent lifetime. Carbon monoxide released from forest fires have a relatively long OH dependent lifetime of 2 months. Therefore the vertical profile shows that crossing the boundary layer provides little restriction. This means that CO enters the free troposphere in large quantities, and can be transported long distances. However, the source of the compound also has an impact on it's vertical transportation. Being released in forest fires, the rate of vertical transport is higher than for pristine forest. Benzene follows a similar trend, with large amounts detected at the surface, above the fires. Benzene also has an atmospheric lifetime greater than that of the rate of vertical transport out of the boundary layer, albeit shorter than that of CO. This means that benzene can also detrain into the free troposphere. Isoprene on the other hand has a very short atmospheric lifetime of only half an hour, meaning that almost all of it has reacted to form other species prior to moving into the free troposphere. Therefore isoprene is entirely constrained to the boundary layer.

Attempts were also made to try and quantify the oxidation products of isoprene-MVK and MACR, but after comparisons with other instruments, and the GEOS-Chem chemical transport model, it was clear that the instrument could not fully speciate the two compounds, with calibration issues and a co-elution with other VOCs. However, after the modifications made to the instrument over the course of the project, it is now possible to make speciated MVK and MACR measurements, should the opportunity arise again.

Finally, plots to determine emission ratios based on CO emissions were analysed and compared to previous studies investigating CO:VOC ratios above fire sources. Whilst the CO:benzene ratio matched previously reported figures, other burning products varied from published sources, indicating that tree and foliage type affects these compounds.

Chapter 4

Coordinated Airborne Studies in the Tropics (CAST) Project

4.1 Coordinated Airborne Studies in the Tropics (CAST) Project

This chapter will discuss the results from the *in situ* GC/MS system and the WAS system acquired during the CAST campaign.

4.1.1 Introduction

4.1.1.1 Overview

The CAST campaign took place in January and February of 2014. The FAAM BAe-146 aircraft was deployed in Guam, in the Western Tropical Pacific. The region is shown in Figure 4.1.

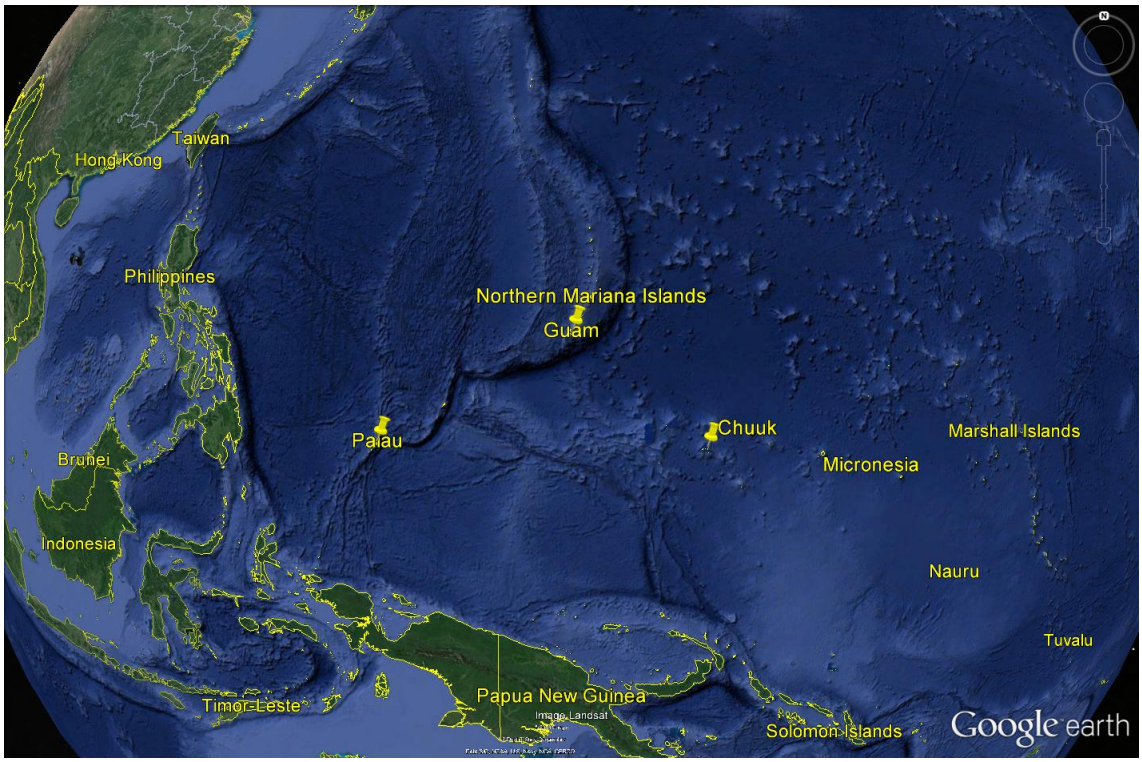

Figure 4.1: Google Earth image of the three islands used as bases during the campaign- Chuuk, Palau and Guam

The science objective for the campaign was to understand vertical and horizontal long-range transport of biogenic compounds from the Pacific warm pool. In order to understand the transport and chemistry, the campaign was carried out in conjunction with the NCAR Gulf Stream V (GV) aircraft and the NASA Global Hawk UAV (GH). All platforms contained a payload of science instruments that were able to analyse and quantify similar compounds. More details on the GV and GH aircraft can be found in section 4.1.2.1. The

BAe-146 science payload is shown later.

Using the three aircraft, measurements were made from the ocean surface, up to 20 km. The different aircraft were capable of flying at different altitudes, ensuring the full profile was covered. The FAAM aircraft made measurements from the ocean surface to 8 km, with the GV operating in the free troposphere and the GH operating in and around the tropical tropopause layer. The FAAM aircraft flew 25 flights in January and February 2014. Almost all flying was located within the marine boundary layer, with flights over open ocean, and around small atolls.

4.1.1.2 Motivations for this Study

Halogenated Very Short Lived Substances (VSLS) are a significant source of reactive halogens to the lower stratosphere (Carpenter et al. (2014); Hossaini et al. (2015)). These compounds enter the atmosphere from the oceans, migrating across the sea surface microlayer. The sea surface microlayer is the top 1 mm of the sea surface, and is the location for all sea-atmosphere exchange of compounds. Large changes in chemical and physical properties take place in the sea surface microlayer when compared to the rest of oceanic layers (Zhang et al., 2003; Carpenter and Nightingale, 2015). Dissolved compounds can come out of solution and enter the atmosphere through this microlayer. Brominated compounds such as bromoform and dibromomethane are produced by a wide variety of oceanic organisms such as seaweed, plankton and macro algae (Chance et al. (2009); Carpenter and Liss (2000); Leblanc et al. (2006); Carpenter et al. (2005)). These compounds are highly important for stratospheric ozone depletion, and can reach the stratosphere through large convective currents like those seen in the western tropical Pacific. Subsequent photolysis of these compounds results in BrO_x, a reactive radical species which contributes to catalytic ozone depletion (Hughes et al. (2009)).

Sea surface temperatures in this region are among the highest on the planet. This leads to increased activity across the sea surface microlayer, meaning more dissolved gases can enter the atmosphere. Many different halocarbon compounds are released from sea weed beds and, due to the warm temperatures, can move into the atmosphere (Carpenter and Liss (2000)). The role of the CAST project was to understand how these compounds can move through the tropical troposphere and enter the stratosphere. These halocarbons, once they enter the stratosphere, can catalytically destroy ozone (Read et al. (2008); Platt and Hönninger (2003); Prather and Watson (1990)).

The Pacific warm pool is a major source of atmospheric halocarbons, due to increased biological activity. Certain seaweed species such as kelp and micro- and macro algae have been observed to release chloro- and bromocarbons. (Carpenter and Liss (2000); Hughes et al. (2009); Leblanc et al. (2006))

The formation of ozone in the stratosphere is shown in the Chapman cycle, shown in Equations 4.1 to 4.4. Equations 4.1 and 4.2 show the formation of ozone (Chapman (1930)). Light of wavelength <242 nm atomizes the molecular oxygen. This is followed by the reaction of these with molecular oxygen, along with a medium, M, which serves to remove excess energy. Equations 4.3 and 4.4 show the destruction of ozone with light and monatomic oxygen respectively.

Halogen-assisted ozone destruction is shown in Equations 4.6 to 4.8, where X is any halogen. It is important to note that X is recycled in the process, causing the process to be catalytic. Many ozone molecules can be destroyed by a single halogen atom. The species, M, is an inert molecule, used to remove excess reaction energy. This is usually nitrogen, as it is the most dominant gas. O• represents an oxygen radical.

$$O_2 + hv \rightarrow 2O \tag{4.1}$$

$$O_2 + hv + M \rightarrow O_3 + M \tag{4.2}$$

$$O_3 + hv \rightarrow O + O_2 \tag{4.3}$$

$$O_3 + O \rightarrow 2O_2 \tag{4.4}$$

$$NET : 3O_2 \rightarrow 2O_3 \tag{4.5}$$

$$X + O_3 \rightarrow XO + O_2 \tag{4.6}$$

$$XO + O\bullet \rightarrow X + O_2 \tag{4.7}$$

$$O_3 + O\bullet \rightarrow 2O_2 \tag{4.8}$$

Globally, the ocean surface forms the primary source of atmospheric organic bromine emissions. A significant proportion of this exists as organic bromine. However, in the presence of sunlight, or the reaction with the OH radical, the bromine can be released, and enter into the catalytic cycles shown above. Alternatively, the inorganic species can be removed from the atmosphere by wet deposition. Bromocarbons exist as both long lived species, with chemical lifetimes in the order of years, whilst some are classified as

very short lived species (VSLS) which have chemical lifetimes of < 6 months (Laube et al. (2008)). Specifically, CH_2Br_2 and $CHBr_3$ contribute some 15-40 % towards stratospheric bromine (via tropical transport processes, described below) , with $CHBr_3$ the largest individual source of organic bromine to the atmosphere (via macro algae) (Carpenter and Liss, 2000). CH_2Br_2 and $CHBr_3$ have average atmospheric lifetimes of 120 days and 25 days respectively. Oceanic emissions, particularly of bromoform, peak around equatorial regions in both the Pacific and Atlantic (1-3 ppt(parts per trillion)), with coastal emssions (1-10 ppt) as well as upwellings (10-17 ppt) contributing significantly. This is in contrast with gyres where emissions are low (0.2-0.8 ppt) (Ziska et al., 2013). Dibromomethane mixing ratios can be significantly lower than bromoform emissions, particularly in coastal regions, but can reach greater altitudes, due to its longer atmospheric lifetime.

The tropical tropopause layer is a region of the atmosphere, located between the troposphere and the stratosphere. At the equator, the TTL has a lower boundary at ˜14 km, and extends up to ˜18.5 km (or between 150-70 hPa). Horizontally, it extends out to +/- 30°, thinning further away from the equator. The TTL shares properties of both the stratosphere and troposphere (Fueglistaler et al., 2009). Weather systems have a large impact on the structure of the TTL, with deep convection often reaching 10-15 km. Additionally, temperature and wind can also impact on it, affecting depth, structure and horizontal size. It can act as a gateway into the stratosphere for tropospheric tracers such as water vapour and very short lived species (VSLS). Ozone production (from photolysis of oxygen) varies within the TTL, yielding $\sim$ 0.1 ppbv/d at the bottom, to $\sim$ 2.4 ppbv/day at the top (Dessler et al. (2008)). The TTL functions as the main route for troposphere/stratosphere interactions. Figure 4.2 shows a schematic of the TTL, indicating transfer processes throughout the lower atmosphere.

Due to the deep convection present in the Pacific warm pool, halogenated compounds released from the ocean surface, can be rapidly transported through the free troposphere and into the TTL. This biogenic contribution towards stratospheric ozone destruction must be fully understood if we are to try and quantify anthropogenic climate change. However, at present, large uncertainties exist in our knowledge of the emissions and transport of these compounds, represented by an uncertainty in future stratospheric ozone depletion. Oceanic dibromomethane and bromoform are the main sources of organic bromine to the free troposphere. These compounds can have a direct effect on stratospheric ozone, after transport through the TTL (von Glasow et al. (2004), Yang et al. (2005)).

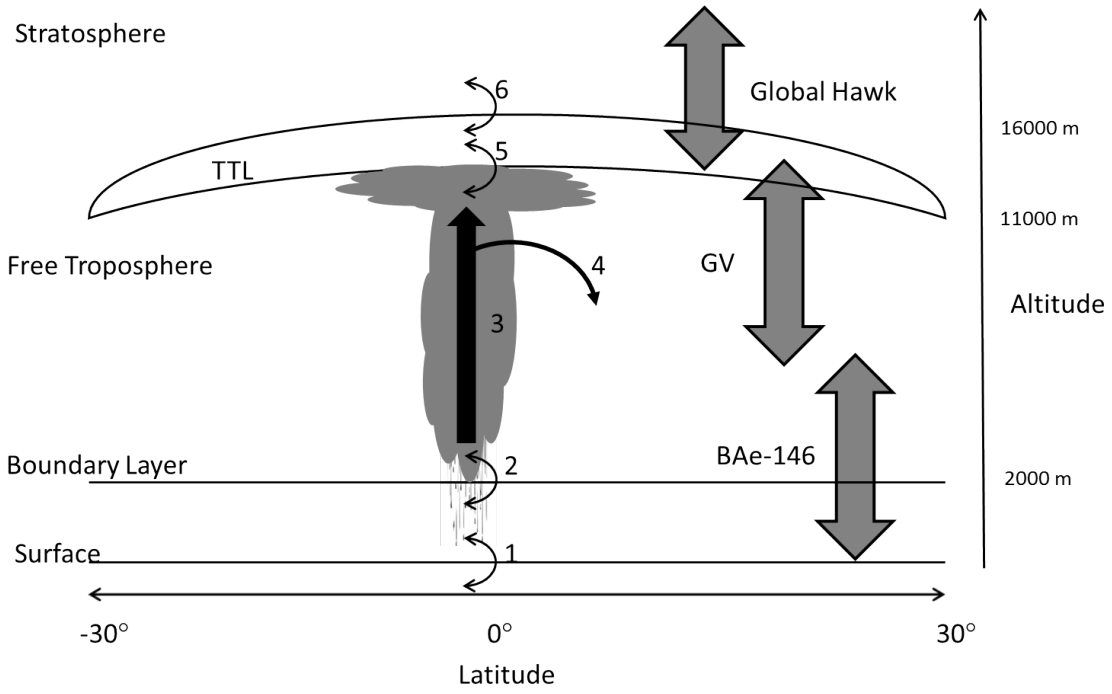

Figure 4.2: A schematic of the Tropical Tropopause layer, demonstrating weather systems involved in transportation of VSLS: 1) Interactions between the air an sea surface, releasing compounds into the atmosphere; 2) Entrainment of compounds across the boundary layer, into large cumulonimbus clouds; 3) Rapid vertical transport within the cloud; 4) Detrainment of air masses out of the cloud into the free troposphere; 5) Movement of VSLS into the TTL, with O3 into the free troposphere; 6)TTL-Stratosphere interactions. Additionally, the altitude ranges of each aircraft are shown (see section 4.1.2)

During the campaign, the FAAM aircraft was used to measure airborne chemical species from the surface to 8 km. As part of the payload (described in 4.1.2.2), two instruments measuring organic halogen compounds (henceforth referred to as halocarbons) were deployed. The in situ GC/MS discussed in Chapter 2 was fitted, taking 5 minute averaged data, with the Whole Air sampling (WAS) system taking samples as often as necessary in flight. The WAS canisters were subsequently analysed, usually within 72 hours of collection, by TD-GC/MS. This chapter will discuss the results from these two systems.

4.1.2 Experimental

4.1.2.1 Flight Planning

FAAM BAe-146

The campaign was organized and implemented by a consortium of international universities and organisations, notably the University of York, University of Cambridge, University

of Manchester, University of Edinburgh, University of Miami and (National Oceanic and Atmospheric Administration) NOAA. The FAAM aircraft was based at the A. B. Won Pat International Airport, Guam. During the campaign, 25 flights were made (Figure 4.3). In order to extend the range of the aircraft and enable sampling over a large cross section of the Western Tropical Pacific region, overnight stops were planned at Roman Tmetuchl International Airport, Republic of Palau and Chuuk International Airport, FSM. This enabled the aircraft to fly south of the equator to measure the outflow from oceanic upwellings. Flights were planned in conjunction with the NCAR GV and NASA GH aircraft. Of the 25 flights, a total of 5 flights were undertaken with either the GV or GH operating in the immediate area. A single flight was dedicated to analysing inflow/outflow from the Chuuk atoll, to determine island influences on the wider area. Two flights were conducted to the East of Guam on the same day to determine diurnal effects. The flight track of the FAAM aircraft is shown in Figure 4.3.

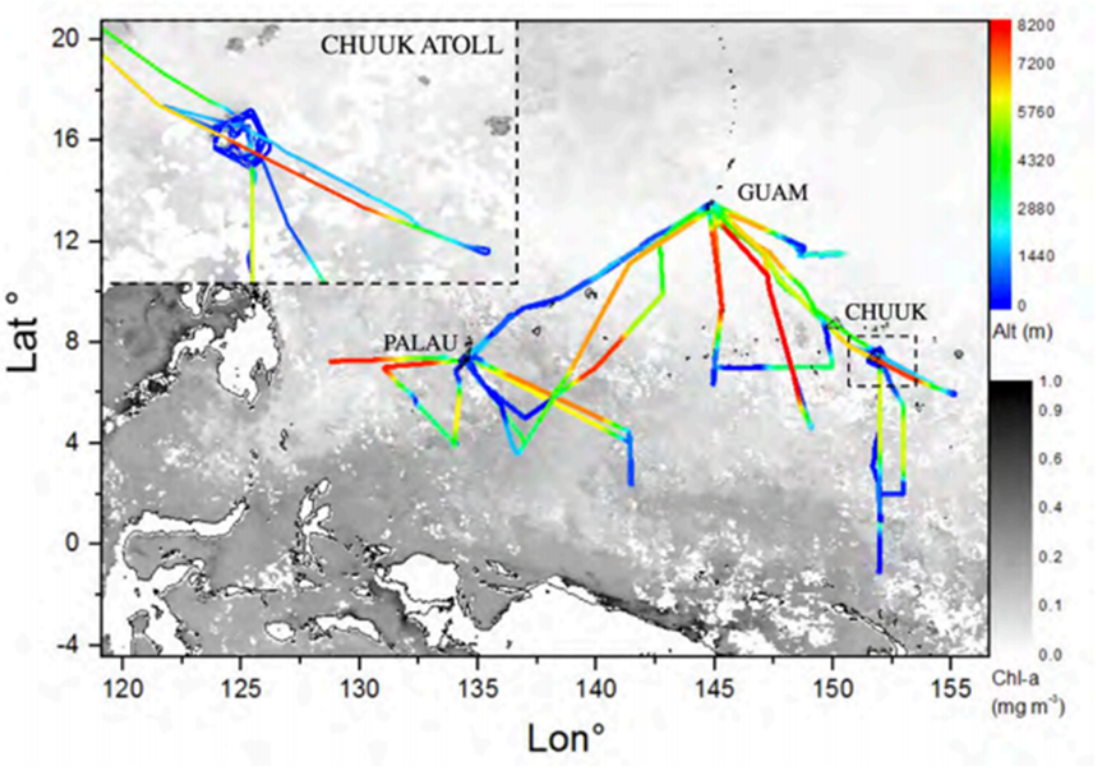

Figure 4.3: FAAM aircraft track plot during the CAST campaign. The track plot is coloured by altitude, with the sea surface coloured by chlorophyll, as this is a suitable proxy of biological activity.

Measurements were taken from 30 meters above sea level (with occasional dips down to 15 meters) up to 8000 meters, so as to overlap with the GV aircraft in the level above. Stacked legs at various different altitudes were also flown in order to produce a vertical

profile of compounds emitted from the sea surface.

NCAR HIAPER Gulfstream GV

Similarly, the GV aircraft was based at the A.B.Won Pat International Airport. The GV has a much larger range than the FAAM aircraft, and can remain airborne for >8 hours. For the purposes of VSLS measurements, the GV was equipped with systems roughly equivalent to both the WAS and *in situ* GC/MS, namely Advanced Whole Air Sampler (AWAS) and Trace Organic Gas Analyser (TOGA) respectively (Salawitch et al. (2014); Apel (2003)). The TOGA is a GC/MS system mounted in the cabin. Samples are drawn in to the instrument, dried, and preconcentrated onto a trap, using liquid nitrogen. Following preconcentration, analytes are transferred to the GC column, employing the use of a liquid nitrogen cryofocusing trap. Analytes are then separated and detected by mass spectrometry. The TOGA has a total cycle time of 2 minutes. The system was calibrated using two NOAA standards: SX-3515 and SX-3562. Cross calibrations were performed between the WAS, AWAS and TOGA, with a further cross calibration carried out between the WAS and GC/MS.

4.1.2.2 Science Payload

The FAAM aircraft was fitted with a range of different chemistry instruments, in addition to an aerosol probe and positional data. Core data such as position, altitude, aircraft time, temperature and other aircraft parameters were logged centrally on the aircraft networks. A brief description of each of the chemistry instruments is given below:

NO was measured using a chemiluminescence technique. A second channel measured NO_2 using a second channel, which employed the use of 395 nm light to convert the NO_2 into NO. The mixing ratio of NO_2 was calculated as a function of total NO_x and NO. The instrument was calibrated in flight when out of the boundary layer to ensure stable low concentrations, then spiking in a standard of known NO mixing ratios. More details on the instrument are described in Allan et al. (2014).

Ozone measurements were taken using a commercially available UV absorption photometer (Thermo Fischer). Calibrations were carried out using an NPL standard (NPL, UK).

CO was measured using a commercially available UV fluorescence photometer as described in Gerbig et al. (1999). Calibrations were carried out using a NOAA traceable

standard approximately every 45 minutes in flight.

CO_2 and CH_4 were measured using a Fast Greenhouse Gas Analyser employing a cavity-enhanced IR absorption spectrometer (Los Gatos Research Ltd., USA). A full description of the instrument can be found in O'Shea et al. (2013). The instrument was calibrated in flight using World Meteorological Organization (WMO) traceable standards, in addition to providing targets at atmospheric concentrations.

A Chemical Ionisation Mass Spectrometer (CIMS) was also included in the payload to measure inorganic halogen species. The instrument used CH_3I to ionise compounds, before analysis by quadrupole mass spectrometry. Simultaneous measurements of BrO, BrCl, Br_2 and HOBr were made and averaged over 30 seconds. The instrument is fully described in Le Breton et al. (2012).

Prior to each flight, a full complement (64) of evacuated WAS bottles were fitted. These were manually filled in flight, either at intervals along a flight leg, or when an instrument reported unusual readings. Each bottle was pressurised using a double headed metal bellows pump for 20 seconds to $\sim$ 3 bar, although the precise pressure varied with altitude. The bottles were subsequently analysed (usually within 72 hours of filling) by both TD-GC/MS and TD-GC/FID. The GC/MS was used to analyse a range of organic halocarbons, with the GC/FID analysing hydrocarbons in the range of $C_2 \rightarrow C_7$.

The *in situ* GC/MS was also fitted onto the aircraft prior to the detachment. As described in Chapter 2, the instrument employed the use of a counter current Nafion dryer to remove water from the sample. Samples were collected by passing 1 L of air over one of two Tenax traps, cooled to 0 °C at a flow rate of 200 mL/min. The traps were subsequently desorbed at 230 °C, onto a 10 m RTX 502 column. Analysis and detection was carried out by quadrupole Mass Spectrometry, which was set up for selected ion monitoring (SIM). Due to a variance in retention time, a single SIM window was set up. For full details of the instrument set up, see Chapter 2. A total of 573 air samples were analysed during the campaign. Filters were applied to remove blanks, calibrations, part samples, double injections, any water issues discussed above and any other anomalous data. Figure 4.4 shows the average locations of the GC/MS sample locations, based on the midtime of sample collection.

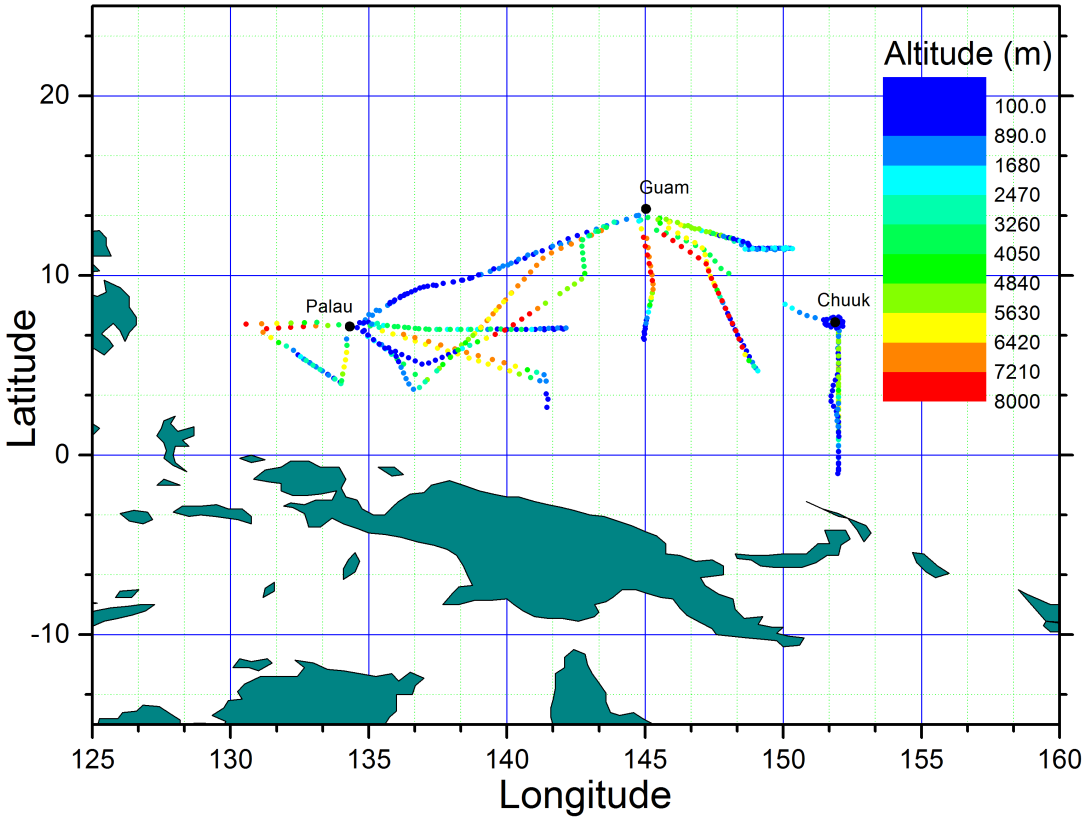

Figure 4.4: Average locations of in situ GC/MS samples over the entire CAST campaign, coloured by altitude.

Table 4.1: Caption

Species / parameter	**Method / Instrument details**	**Averaging time**	**Precision/ accuracy**	**Affiliation, Reference**
Physics / Positional				
Position, wind (U,V,W)	INS, GPS, Turbulence Probe , RadAlt	1s	0.01 P/Ps	FAAM, Petersen and Renfrew (2009)
Humidity (Dew Point, Temperature)	General Eastern Hygrometer	1s	0.5 - 3 K (pressure dependent)	FAAM, Ström et al. (1994)
Temperature	Rosemount Sensor, Aerospace Ltd	1s	0.3K	FAAM
Cloud Microphysics	CDP	1s		FAAM, Rosenberg et al. (2012)
Chemistry				
CO	UV resonance fluorescence, Aerolaser 5002	1s	1 ppbv	FAAM, Gerbig et al. (1999)
O_3	UV absorption, TECO 49C	1s	1 ppbv	FAAM, Wilson and Birks (2006)
CO_2, CH_4	CEAS, Los Gatos, USA	1s	0.5 ppmv and 2.5 ppbv respectively	FAAM, UoM, O'Shea et al. (2013)
NO, NO_2	Chemiluminescence with photolytic conversion for NO2, Air Quality Design Inc	10s	5 pptv and 15 pptv respectively	FAAM, UoY, Pike et al. (2010)
Subset of Halocarbons	WAS (analysed by GC/MS)	30s (Fill time)	Species Dependent	UoY, Andrews et al (2013; 2016)
VOCs	WAS (analysed by GC/FID)	30s (Fill time)	Species Dependent	UoY, Hopkins et al. (2003)
Subset of Halocarbons	in situ GC/MS	5 min	Species Dependent	UoY, Andrews et al. (2016)
Inorganic bromine	CIMS	30s	Species Dependent	UoM, Le Breton et al. (2012)
IO	BBCEAS			UoC (Kennedy et al. (2001)

4.1.2.3 Mid-campaign Modifications

At the start of the campaign, the instrument employed the use of the Peltier chiller to freeze water out of the sample. However, due to high temperatures and humidity in the region, it was quickly noticed that the device was not going to be sufficient for operating in the Western Tropical Pacific. On inspection, liquid water was found within the sample lines, and was making its way into the mass spectrometer. The instrument was recording pressure fluctuations to water blocking the transfer line/column, and the ionization filament was observed to be flickering, indicating large amounts of water entering the mass spectrometer. It was at this point that the instrument was stopped, baked out for ˜ 12 hours (over 3 days) and the Peltier device was switched out in favour of the counter current Nafion dryer (as explained in Chapter 2).

Further problems arose during the campaign with the metal bellows pump. During flight B823 (only the second flight of the campaign), high levels of limonene were detected in the sample. This was associated to a cleaning product used in the aircraft toilet, implying a leak in the tubing, causing the pump to preferentially pull on the cabin air, as the cabin was pressurised.

The pump used to pressurise the WAS canisters was used instead, as the two pumps were the same model, giving similar output flows. With the WAS control rack located towards the fore of the aircraft, and the canisters located in the rear hold, the sample line passed next to the GC/MS rack. Therefore, the flow was split between the GC/MS and the WAS canisters. The pneumatic pressure relief valve was adjusted to give 2.5 bar to the GC/MS, whilst the WAS fill pressure was monitored to ensure a full sample was taken.

4.1.3 Discussion

4.1.3.1 Calibrations and Comparisons with other aircraft

A series of compunds were scanned for including bromodichloromethane, chlorodibromomethane, chloroiodomethane, iodomethane and di-iodomethane. Of all the compounds scanned for, only four were consistently above detection limits: dichloromethane, chloroform, dibromomethane and bromoform. The statistics of these are shown in Table 4.2

Various transport models include bromocarbons $CHBr_3$ and CH_2Br_2, primarily driven by oceanic emissions (Liang et al., 2010; Ordóñez et al., 2012; Ziska et al., 2013). However, due to few, and scattered measurements of the Western Pacific region, this leads to the

Table 4.2: Minimum, maximum, average and standard deviation of 4 key halocarbons measured by the *GC/MS*

	Dichloromethane	Chloroform	Dibromomethane	Bromoform
MIN	0.050	0.014	0.010	0.006
MAX	152.066	33.948	3.430	4.187
AVERAGE	42.114	7.598	0.837	0.639
STDEV	19.027	4.350	0.298	0.385
%STDEV	45.180	57.255	35.539	60.222

models being poorly constrained, leading to large model uncertainties. Therefore, in order to provide accurate measurements, and reduce uncertainty between platforms, a robust intercalibration needed to be performed. This is reported in Andrews et al. (2016) in which I made a significant contribution. The four instruments (*in situ* GC/MS, WAS, AWAS and TOGA) were all calibrated using the same two traceable standards: SX-3515 and SX-3562.

GC/MS calibrations were carried out either pre- or post-flight. For two-sector flights, an additional calibration was carried out during the intermediate refueling time. The calibration gas used was a NOAA standard, containing a subset of halocarbons (SX-3515). For the purpose of comparisons with instruments on the other aircraft, this standard was analysed on all related instruments (i.e Trace Organic Gas Analyser (TOGA) and Advanced Whole Air Sampler (AWAS)). Due to differences in flight capabilities, a wing-tip to wing-tip comparison could not be made, so alternatively, all calibration standards were shared between all instruments. An intercalibration was performed against the instrument used to analyse the WAS canisters using SX-3562. It is important of note that the NASA Global Hawk did not sample at the altitudes of the BAe-146, so only the FAAM aircraft collected data at low altitudes.

The intercalibration itself was very simple. Each calibration standard was run several times on each instrument. The *in situ* GC/MS wasn't calibrated directly from the cylinder due to difficulties of carrying the cylinder onto the aircraft. Instead, a 2 L silco can of the same specification (same valves, same coating, different size) of the WAS canisters was filled to 40 psig. The can was connected to the instruments sample port and sampled at least 6 times prior to every flight. Figures 4.8 and 4.6 show extracted ion chromatograms from a calibration sample and a real air sample. Additionally, the spatial variation of bromoform and dibromomethane as measured by the *in situ* GC/MS are shown in Figure

4.7.

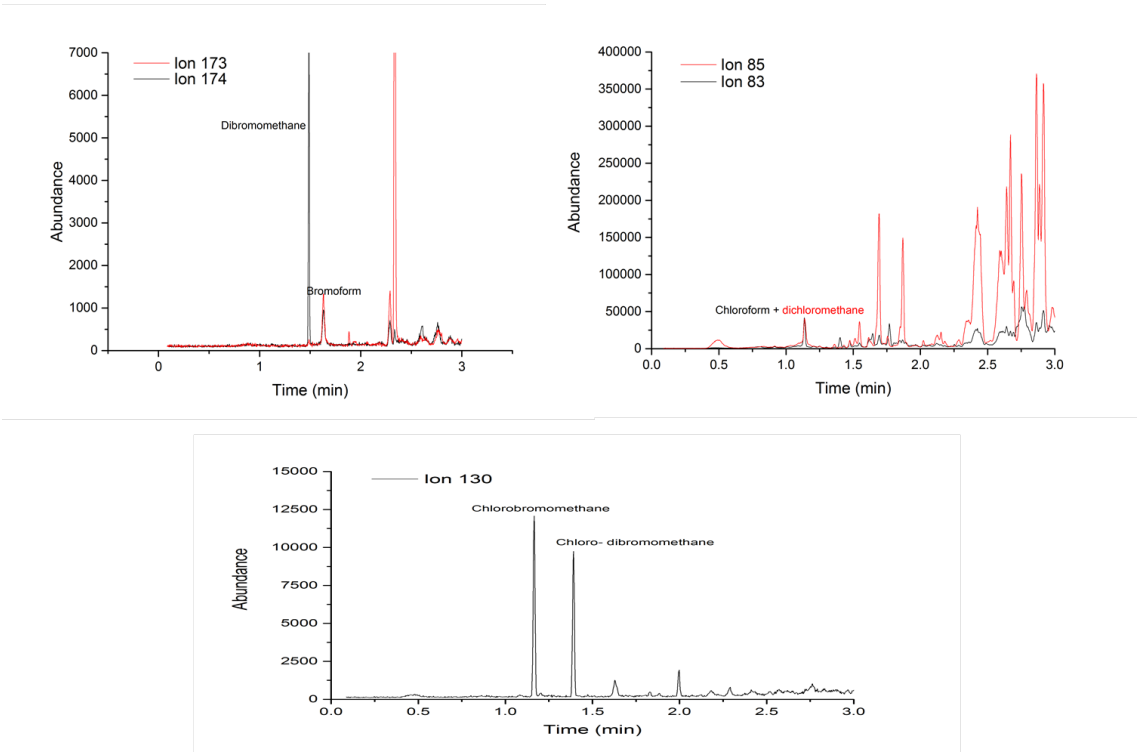

Figure 4.5: Extracted ion chromatogram showing a calibration sample from the CAST campaign. This shows 6 of the halcarbons analysed during this study: chloroform, dichloromethane, bromoform, dibromomethane, chloro-bromomethane and chlorodibromomethane. All compounds are baseline resolved and generally show a good peak shape.

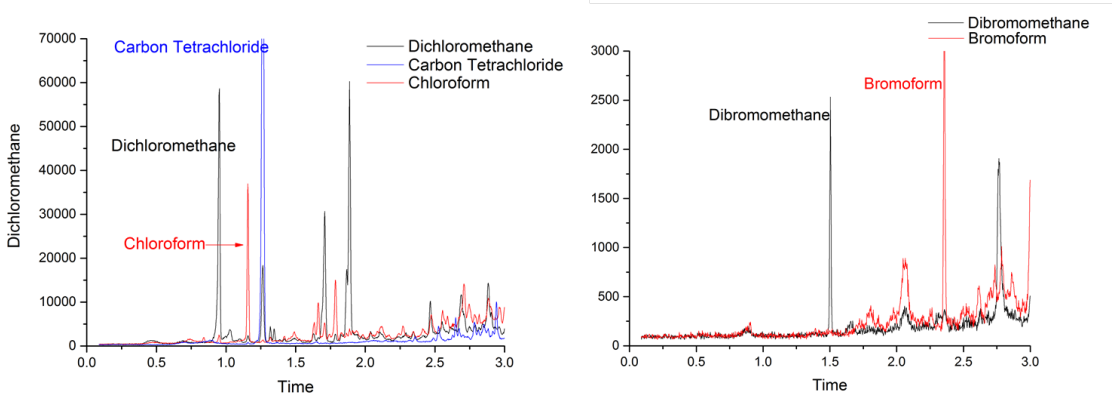

Figure 4.6: Extracted ion chromatogram showing a typical real air sample from the CAST campaign.

The values reported by each instrument broadly agreed, with the average % relative standard deviation (RSD) for all instruments and all analytes was < 10 % for standard SX-3515, with a slightly higher value of ≈ 13 % for SX-3562, due to slight discrepancies in $CHBR_3$. As the objective of the campaign was to determine vertical transport of

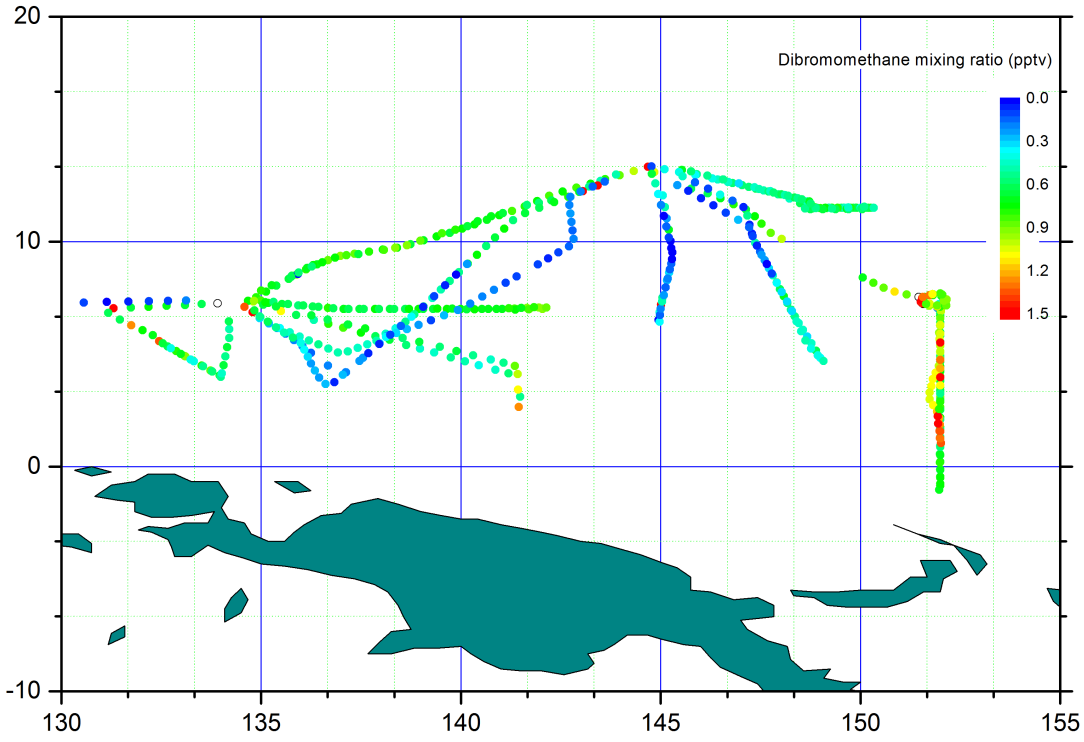

Figure 4.7: Trackplot of the FAAM BAe-146 averaged over the *in situ* GC/MS sample times, and coloured by bromoform, showing the spatial variability. It is important to note that these measurements were taken between 0 and 3000 m.

halocarbons, therefore, the best way of comparing platforms is as vertical profiles. Data from both York instruments (GC/MS and WAS) was analysed and plotted.

First to consider is $CHCl_3$, which is predominantly biogenic, emitted mainly from the ocean (Laturnus et al., 2002). The % RSD for each of the instruments was 12%, 16%, 15% and 25% for the WAS, *in situ* GC/MS, AWAS and TOGA respectively. A comparison of the means yields a % RSD of 7%, showing a good agreement between the platforms, considering the different locations and sample time and days.

A preliminary analysis of the data showed a good agreement between the GC/MS and the AWAS and TOGA. However, there appeared to be a consistent offset between higher volatility compounds with the WAS analysed data. For example, the offset to the WAS data when compared to the other platforms was 19% (+/-1%) for CH_2Br_2. This can potentially be attributed to high humidity in the tropics, and water accumulating in the long WAS sample lines, despite efforts to flush the system prior, and during, each flight. This did not affect other instruments as the GC/MS, TOGA and AWAS all take

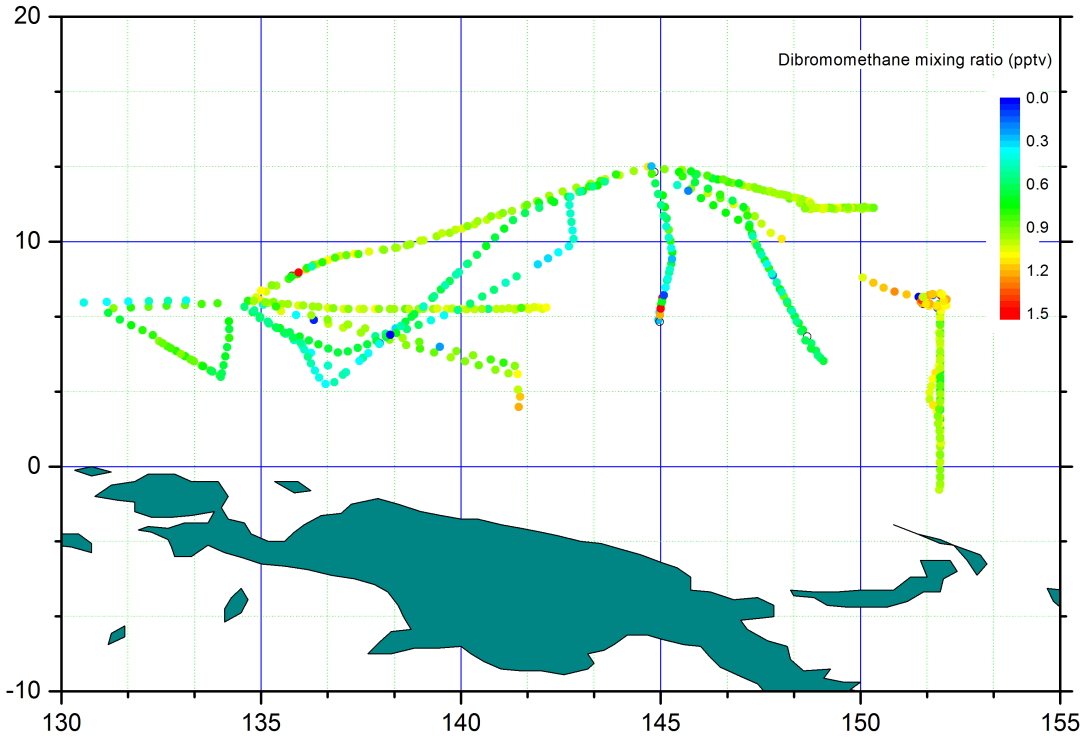

Figure 4.8: Trackplot of the FAAM BAe-146 averaged over the *in situ* GC/MS sample times, and coloured by dibromomethane, showing the spatial variability. It is important to note that these measurements were taken between 0 and 3000 m.

samples directly from dedicated inlets in window blanks. The upshot of this was a species-dependent offset in the WAS data. In order to quantify the offset, a comparison of $CHCl_3$ was made, as it has a longer atmospheric lifetime than other species measured during the campaign (150 days, (Carpenter et al., 2014)). Additionally, it has a relatively higher atmospheric mixing ratio of ˜ 10 pptv. The comparison of all four platforms is shown in Figure 4.10.

The offset can be seen, particularly at lower altitudes, whilst the other three platforms show a good agreement. As the WAS and *in situ* GC/MS were sampling concurrently, a direct comparison can be made, and a calculation of the offset could be made. The offset was quantified and adjustments to the data were made, bringing it in-line with the other platforms. After this was taken into account, the WAS and GC/MS data were compared. Specific analytes were chosen based on the ability of the *in situ* GC/MS to detect and quantify species. Choro- and bromocarbons showed enough reproducibility during calibrations to be given enough confidence in the results. The vertical profiles of 4

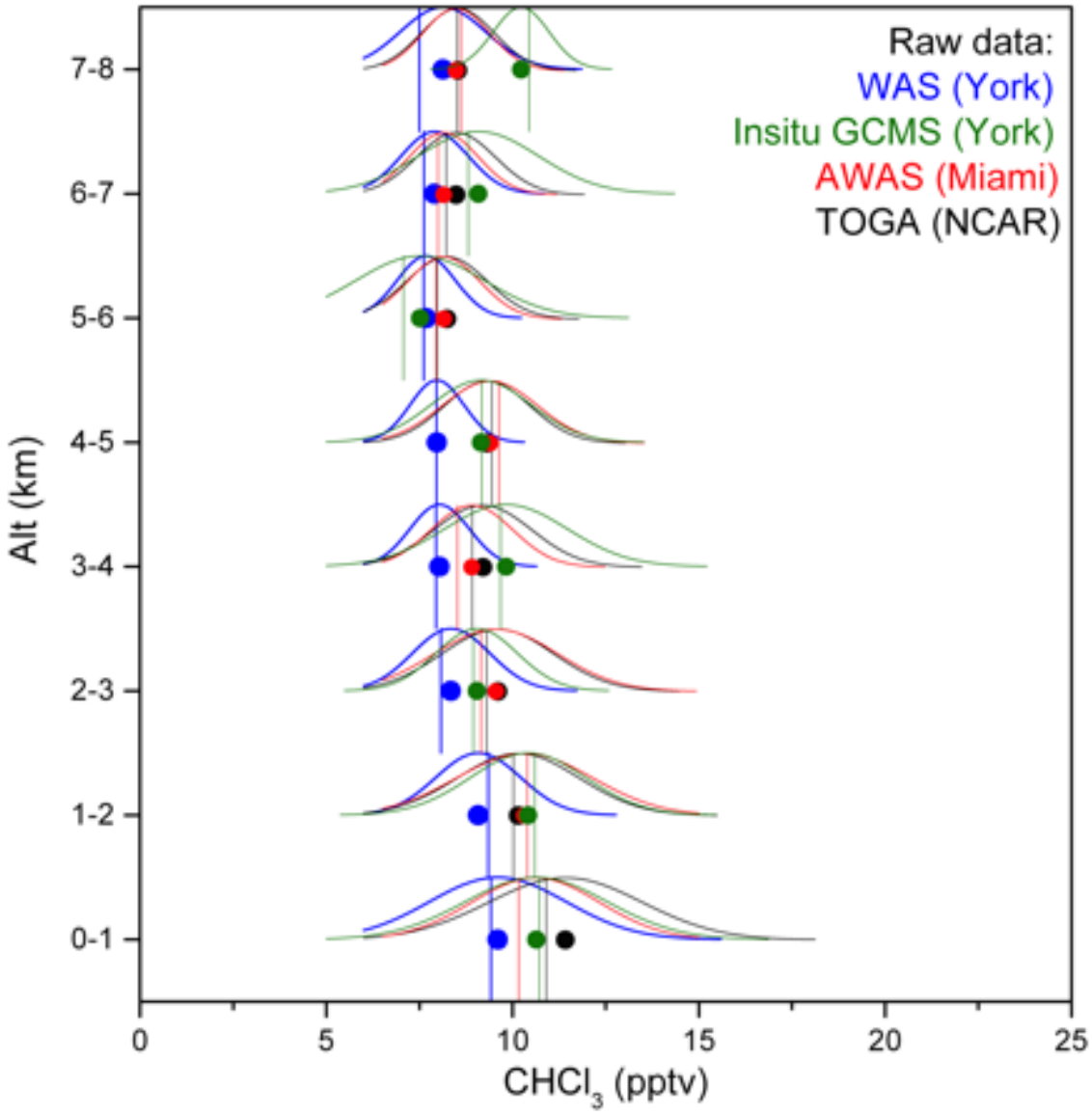

Figure 4.9: A comparison of the vertical profiles of a relatively long-lived species from all platforms, averaged into 1000 m bins. The circles and vertical lines represent the mean and medians respectively, with the curve representing the distribution. The systematic offset in the WAS data can be seen, particularly at the lower an mid altitudes. (Andrews et al., 2016)

analytes are shown in Figure 4.10.

Figure 4.10 shows the adjusted WAS data compares favourably with the GC/MS data, despite the GC/MS having a large spread. This can be attributed to the use of fast chromatography, in order to improve spatial distribution, and the very low mixing ratios of analytes. However, the means and medians agree well with the adjusted WAS data set, despite different sampling techniques.

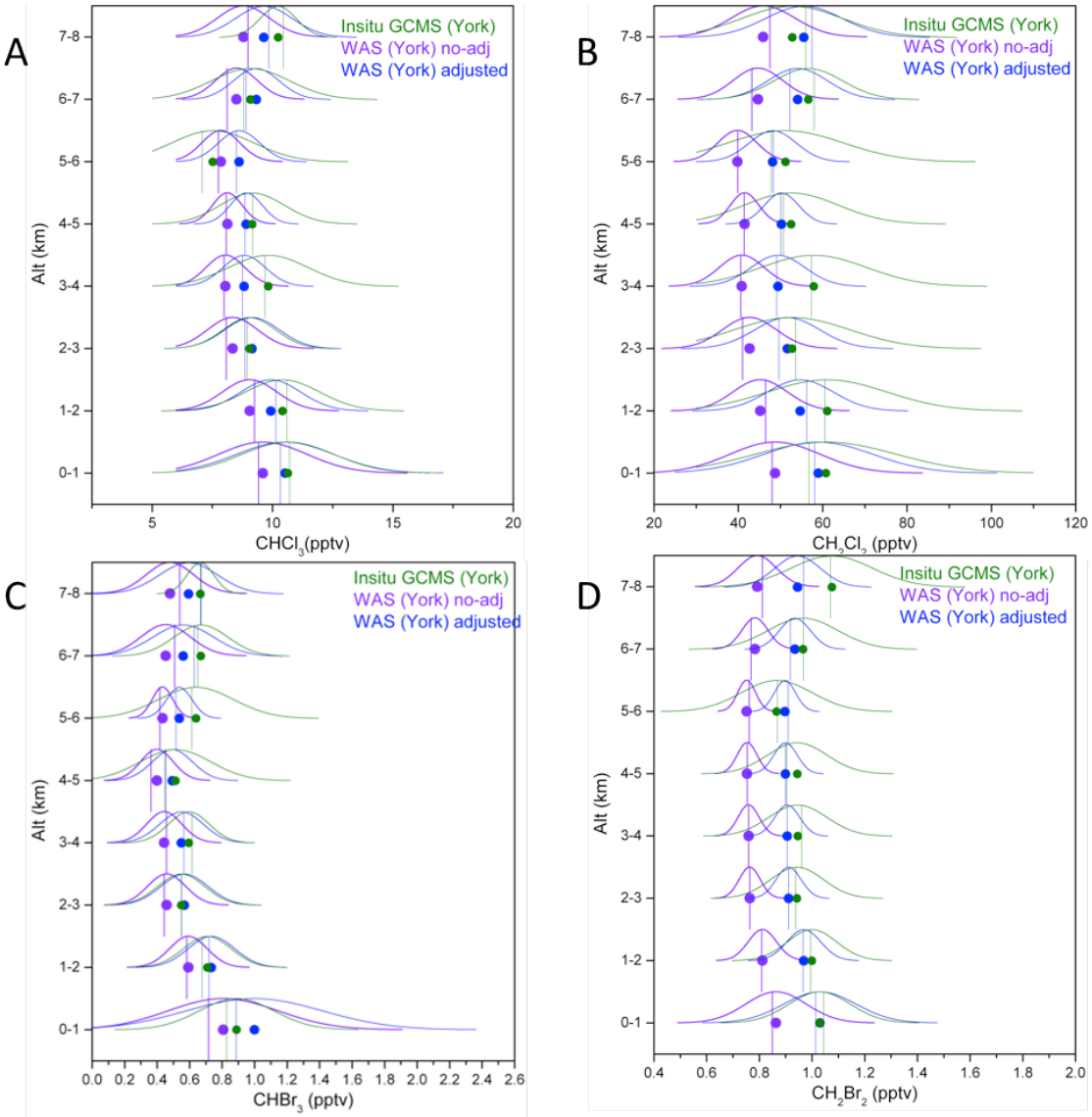

Figure 4.10: Comparisons of vertical profiles of A: Chloroform, B: Dichloromethane, B: Bromoform and C: Dibromomethane measured by both the York *in situ* GC/MS and the WAS system. Data has been binned into 1000 m altitude bins, with the circles and vertical lines representing the mean and medians of the data, represented by a normal distribution curve.

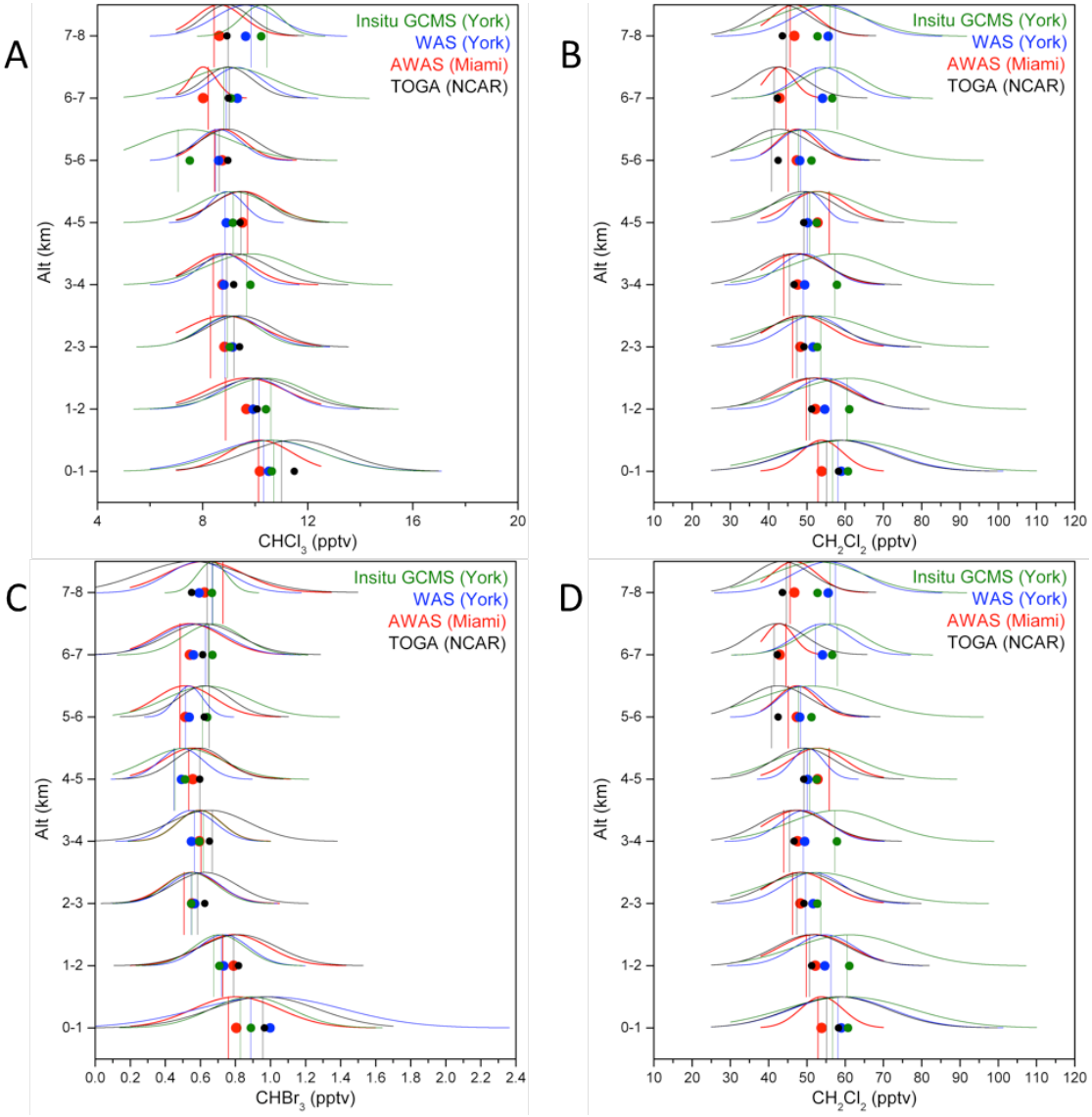

Figure 4.11: Vertical profiles showing a comparison of all platforms for 4 compounds: A) chloroform, B) dichloromethane, C) bromoform and D) dibromomethane (Andrews et al., 2016).

An analysis of the data shows a very good agreement between the 4 platforms, when considering that the measurements were separated spatially and temporally, and using different sampling and analysis methods. The 0-1 km bin shows a large spread across all platforms, but principally the WAS and *in situ* GC/MS. This is most likely due to the significant amount of FAAM aircraft flying hours dedicated to low flying in and around atolls in and around Chuuk and Palau. The highest enhancements were seen during the downwind leg of a circle of the Chuuk atolls and at low levels over the ocean in the South West portion of the flights. These flights were conducted at 100-500 ft above the ocean, giving the high mixing ratios shown. One flight in particular, B838, involved orbits of the Chuuk atolls at three different altitudes, to determine in flow and outflow from the islands. Additionally, contributions from the atolls can be quantified and incorporated into global models. The results from the GC/MS from flight B838 are shown in Figure 4.12.

The spatial plot shows an enhancement in bromoform on the Western legs of the orbits. This is confirmed by the wind rose, which indicates a strongly predominant Easterly wind direction. Flights such as this can account for the large spread in the data for the instruments on board the FAAM aircraft.

Overall, this analysis, which is explained in more detail in Andrews et al. (2016), shows that the GC/MS data has a good agreement with other instruments, despite issues with humidity and sample pressures as described in section 4.1.2.3.

In addition to the agreement seen by the 4 instrument platforms, the data also agrees favourably with literature values. For instance, a study by Fuhlbrugge et al (2016), who conducted a ship based experiment in the Western Pacific region, analysing airborne halocarbons. Their analysis showed agreements in both the absolute measurements, and the CH_2Br_2:$CHBr_3$ ratios at the surface. More historical references also broadly agree with the data presented here, with papers by Atlas et al (1993), Blake et al (2001) and Moore et al (1996), all reporting similar values for measurements taken close to, or at, the ocean surface of between 0.1 and 5 pptv for $CHBr_3$, and 0.5 and 2 pptv for CH_2Br_2. This is within close agreement with measurements taken across this campaign, at a variety of altitudes and locations.

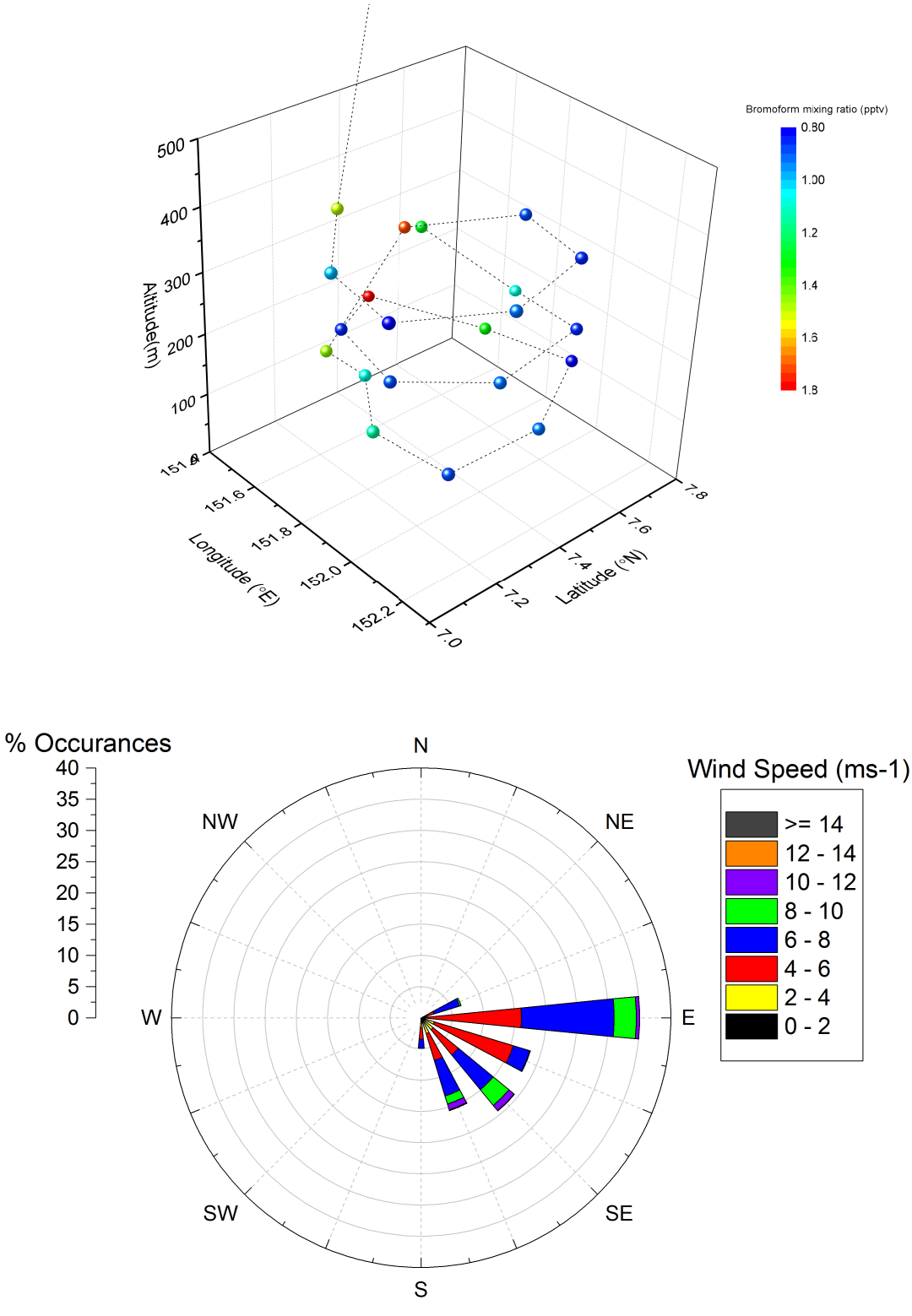

Figure 4.12: An analysis of flight B838, circling the Chuuk atoll. The spatial plot (top) shows the average locations of the GC/MS sampling, coloured by bromoform mixing ratio. The wind rose (bottom) shows a strongly predominant Easterly wind, meaning that relatively high levels of bromoform were seen on the West side of the atoll.

4.1.3.2 Back Trajectories

Combined vertical profies of the two most abundant bromocarbons, dibromomethane and bromoform, were plotted for all platform. These were then coloured by ozone, in an attempt to characterise the profile. These are shown in Figure 4.13.

Areas with high amounts of ozone generally coincide with low bromocarbon mixing rations, with the region at ˜ 5 km representing convective outflow and the region above 17 km representing the tropopause/lower stratosphere. However, the region at ˜6- 8 km could represent differing air masses intersecting the flight paths. In order to investigate this further, the GC/MS data was plotted separately from the other platforms to determine the cause of the high ozone/low bromocarbon mixing ratios at ˜6- 8 km. These profiles are shown in Figure 4.14.

In the profiles, ozone mixing ratios are < 40 ppb below 3000 m. Above 3000 m, ozone mixing ratios begin to increase, whilst above 6000 m, the profile splits into two different branches. The regimes are defined by either low bromocarbon mixing ratio, with a high ozone mixing ratio, or vice versa. These two regimes are indicated by the inset graph in Figure 4.14. A further analysis into the underlying cause involved running the Hysplit model to determine the origin of these air masses. The results of this anaysis is shown in Figure 4.15.

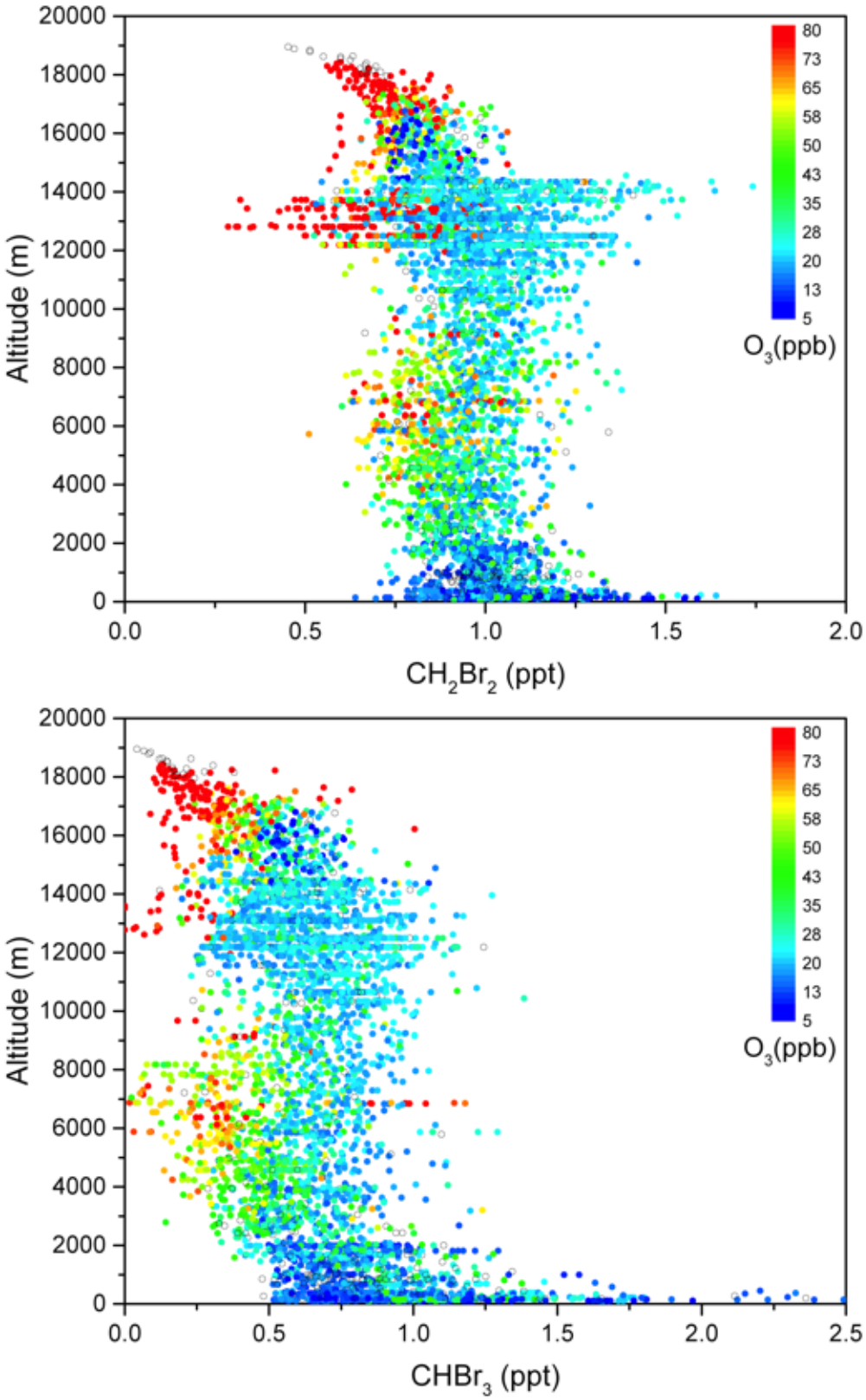

Figure 4.13: Vertical profiles of CH_2Br_2 (top) and $CHBr_3$ (bottom) as measured by all platforms and coloured by ozone. Empty circles indicate where no ozone data was available.

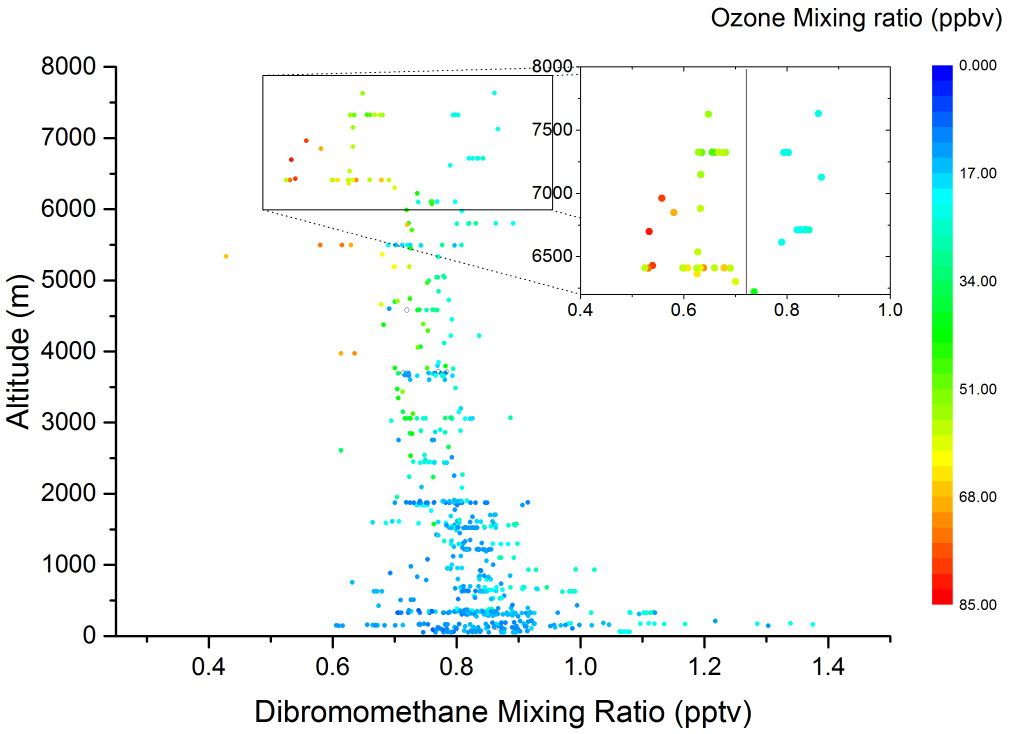

alt o3.png alt o3.png

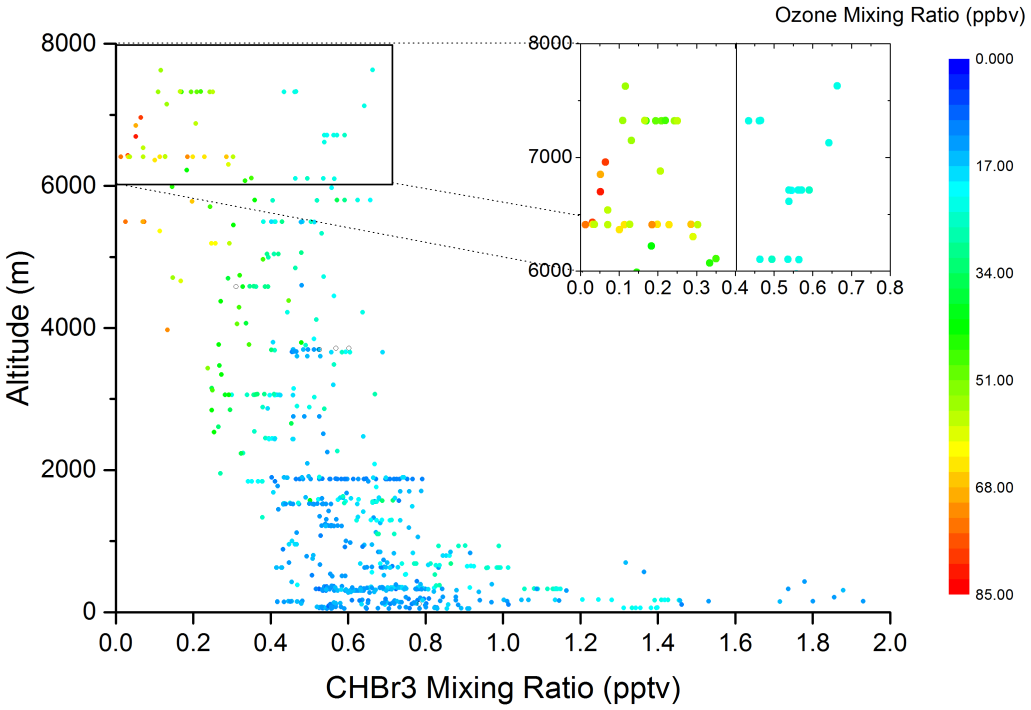

Figure 4.14: Vertical profiles of CH_2Br_2 (top) and $CHBr_3$ (bottom) as measured by the *in situ* GC/MS, coloured by ozone. Open circles indicate where no ozone data was available. Inset in both graphs is an enlarged image of the top 2 km of data. Two different regimes can clearly be seen, spearated by the vertical line.

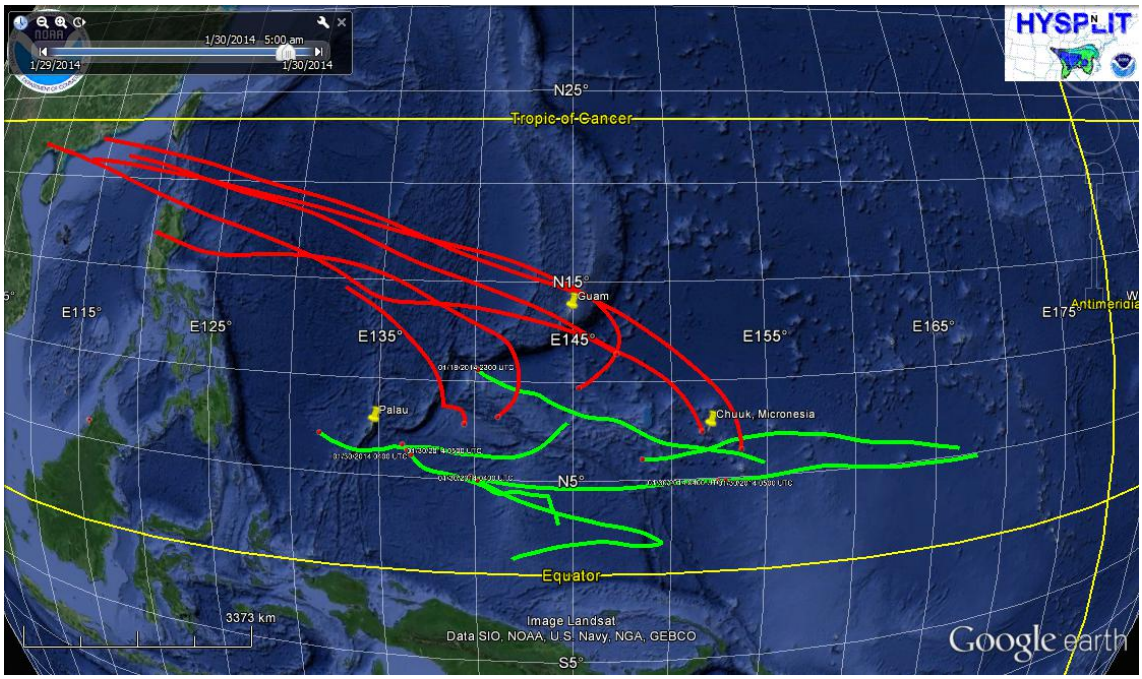

Figure 4.15: A Google Earth plot showing the 72 hour back trajectories of the 6 highest, and 7 lowest ozone mixing ratios measured above 6000 m. The red tracks show the trajectories that corresponded to high ozone, low bromocarbon mixing ratios, with the green tracks showing the trajectories that correspond to low ozone, high bromoform mixing ratios. The locations of the 3 airports used during the campaign are also labelled for reference.

It is important to note that all the measurements were taken between 6000 and 8000 m. As can be seen, where an air mass with high ozone mixing ratios is encountered, the back trajectories show that, over the 72 hours the model was run for, the air mass passed over South East Asia, before moving East over the analysis region. Conversely, air masses with low ozone mixing ratios, shown in green, passed over the open Pacific ocean for the time the model was run for. For the air masses that passed over South East Asia, it can be determined whether the air masses originated from the surface, and being influenced by anthropogenic emissions, or whether it originated in the stratosphere and carried high ozone levels down into the troposphere. The altitude plots of the back trajectories can be seen in Figure 4.16.

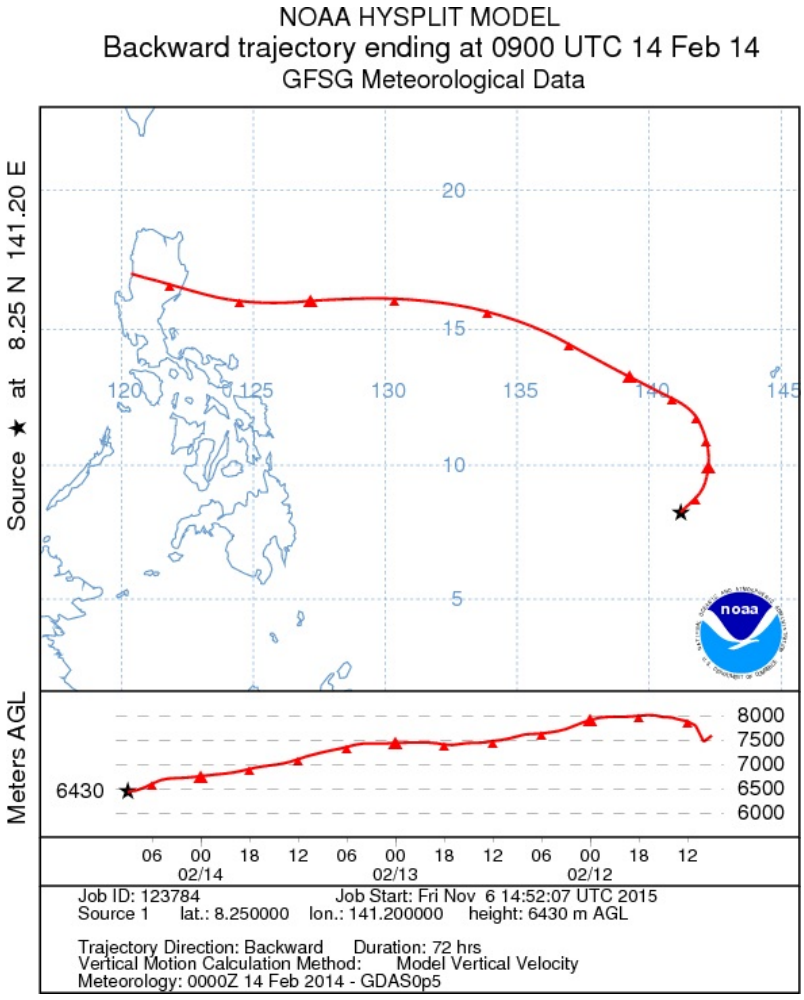

The high ozone events were detected in the mid-troposphere, which does not account for the high levels of ozone observed. Whilst past studies may have concluded some stratospheric influence, the data collected doesn't neccessarily agree with this conclusion The origins of these air masses are likely to have originated at ground level over East Asia,

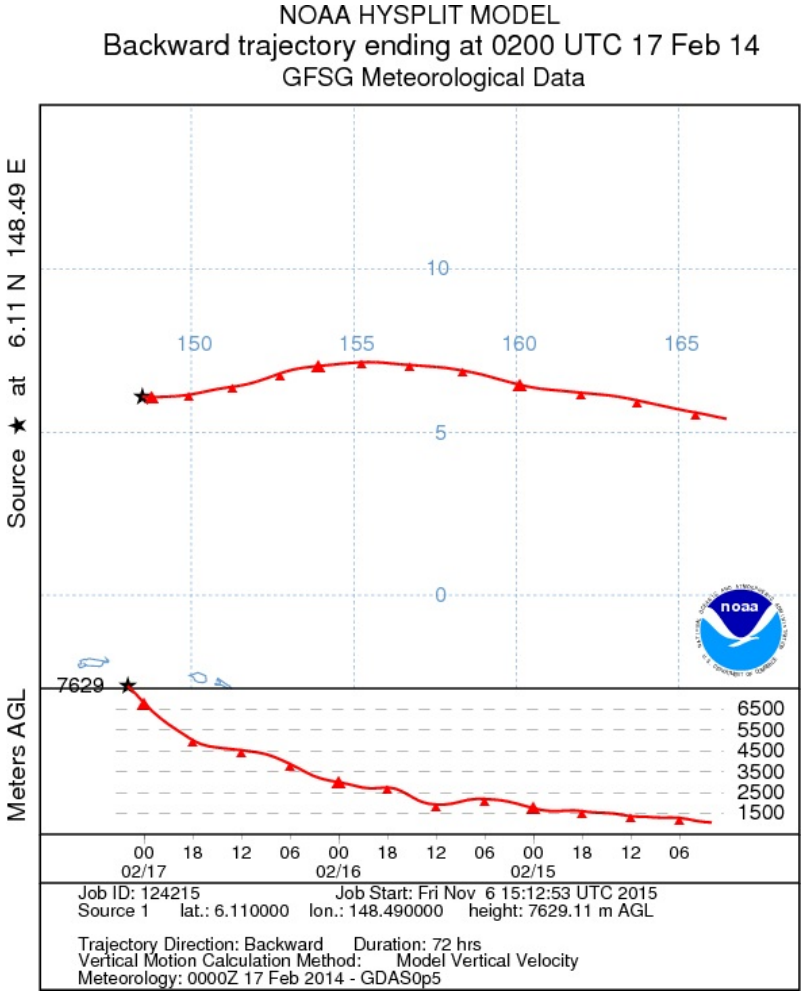

Figure 4.16: Typical 72 hour Hysplit back trajectories from when high ozone, low bromocarbons were measured (top), and low ozone, high bromocarbons were measured (bottom). The high ozone back trajectory shows the air mass originating in the mid- to upper- troposphere, whilst the low ozone trajectory shows the air mass originating from the surface.

around the China coast. Anderson et al. (2016) explains this phenomenon during the CAST/CONTRAST campaign, using High Ozone Low Water (HOLW) as the signifiers. They found that the high ozone was likely to have originated within the tropical troposphere, and concluded that it was heavily influenced by emissions from Eastern China and South East Asia. The air parcels had then risen up into the atmosphere, where water vapour had condensed out, before being moved out over the tropical Pacific, to the position of the measurement through fast, large scale descent of the air parcel. Satellites data showed the presence of forest fires in South East Asia, providing the dominant source of high ozone When taking into account this study, the same set of results apply. The high ozone in these air parcels have catalytically destroyed any bromocarbons, whilst recycling the ozone.

As ozone has a high influence on radiative forcing, the influence of these events can have an effect on the radiative forcing of the Tropical Western Pacific climate, to an extent that was previously underestimated (Stevenson et al., 2013) (Shindell, 2009). With the emission of ozone into the tropical tropopause more efforts will have to be focused on reducing emissions in the tropics, rather than the current legislation, which generally focuses on the extra-tropics (Anderson et al., 2016).

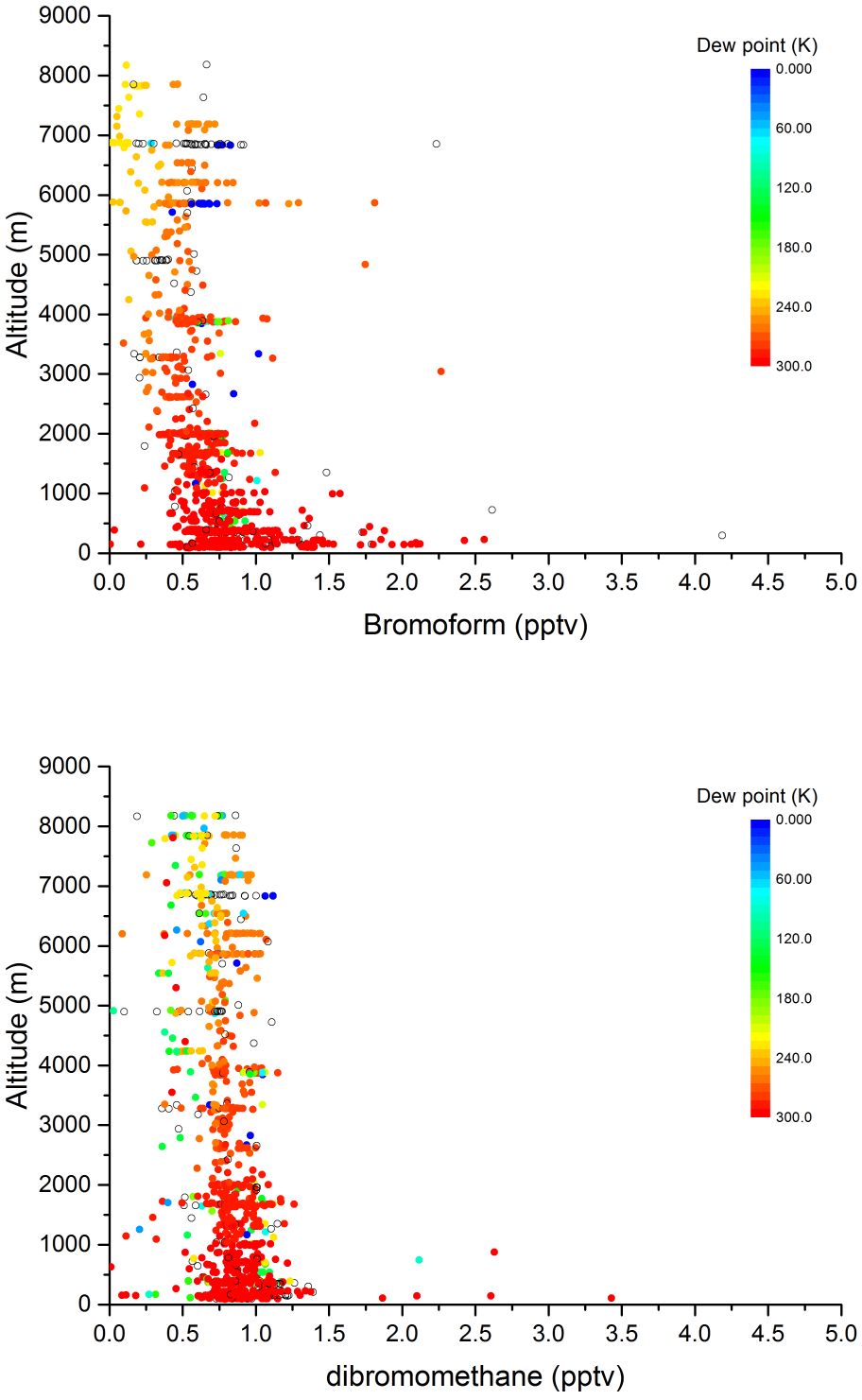

Figure 4.17: Plots of $CHBr_3$ and CH_2Br_2 against altitude, coloured by dew points, as measured by the *in situ* GC/MS and WAS systems. The blue points on the graph correspond to the high ozone, low bromocarbon measurements, indicating stratospheric influence.

A final method of determining the age of an air mass is to look at the ratio between CH_2Br_2 and $CHBr_3$. The higher the $CHBr_3$:CH_2Br_2 ratio, the fresher the emissions. The comparison is shown in Figure 4.18. The plot is coloured by ozone and at very low bromocarbon mixing ratios, the ozone is highest. This indicates that the emissions to these air masses occurred on timescales similar the the atmospheric lifetimes of CH_2Br_2 and $CHBr_3$ (120 and 25 days respectively. Although few of these measurements exist in, a change in the slope of the graph can be seen at these low mixing ratios, again, indicating an older air mass.

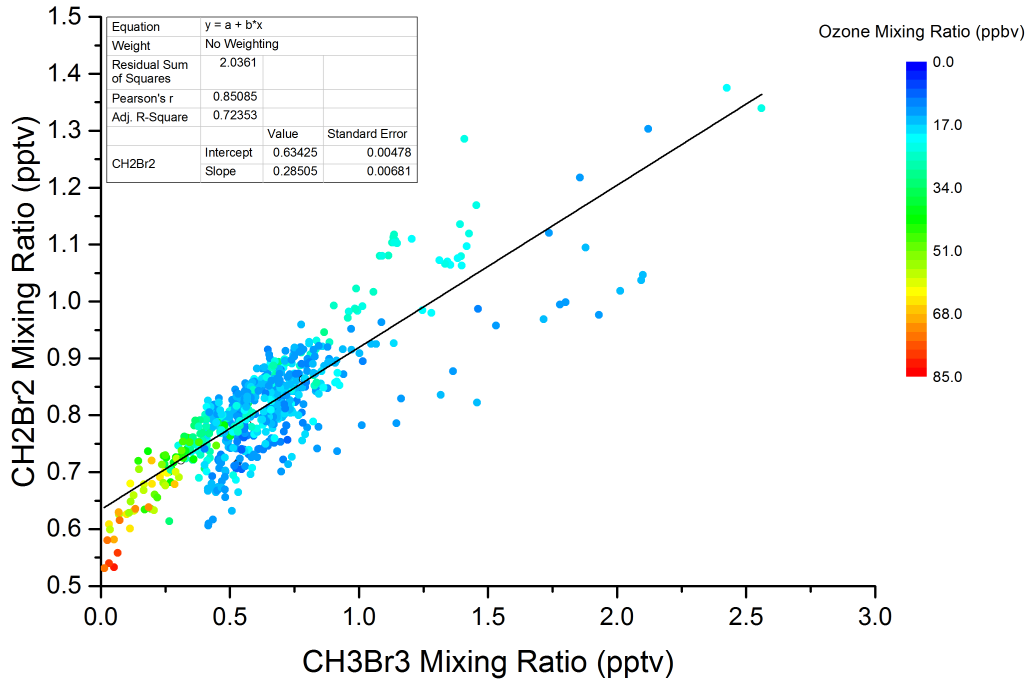

Figure 4.18: A plot of bromoform against dibromomethane as measured by the *in situ*. The bromocarbons show a good correlation with an R^2 value of 0.72. Additionally, the data is coloured by ozone, showing high levels of ozone, coinciding with low bromocarbon mixing ratios.

4.1.4 Conclusions

During the course of the CAST campaign, which took place in the western tropical Pacific in January and February 2014, 3 aircraft were deployed to the region to determine vertical profiles of VSLS. A total of 4 instrument platforms were used, taking measurements using both online and offline methods, and all were cross calibrated. These instruments included two from the University of York: the *in situ* GC/MS and the WAS system. The data

reported in this chapter initially shows a good agreement between three instruments, with a systematic offset on the WAS system, thought to be caused by high levels of humidity in the gas lines whilst sampling. After this offset was taken into account, the data was compared and agreed very closely, considering the fact that measurements were taken on different days, and in different geographical locations.

Additionally, the vertical profiles of the GC/MS and WAS systems were analysed, with high and low ozone mixing ratio samples investigated. Back trajectories for the high ozone events at ˜6000 m were ran and compared to the corresponding low ozone events. The back trajectories show for the high ozone events, the air masses originated from below the TTL over eastern China, and have anomalously low dew points. This is consistent from entrainment down from the TTL. Conversely, the low ozone events correspond to higher bromocarbon mixing ratios, and back trajectories show the air masses originated from the surface.

This chapter also demonstrates the performance of the *in situ* GC/MS, when compared to other instruments, whose data has been used repeatedly in peer-reviewed journal articles.

Chapter 5

Investigations into North Sea Oil and Gas Fields

5.1 Investigations into North Sea Oil and Gas Fields

This chapter will discuss data collected during Summer 2015, when the FAAM research aircraft was deployed to the North Sea in order to determine the background composition around Oil and Gas rigs. A total of 5 flights were carried out from Cranfield Airport, Cranfield University, Bedfordshire, UK.

5.1.1 Introduction

Fossil fuel extraction, and leaks associated with it, is a major source of VOCs released into the atmosphere. Over recent decades, coal extraction has largely given way to oil and gas for many reasons. Natural gas provides a quarter of energy used in the USA, and up to 47 % in the UK (U.S. Energy Administration, 2012). In the USA, it has been estimated that of this natural gas, almost half is coming from shale and tight sand sources (Gilman et al., 2013). Since 2005, extraction of gas using horizontal drilling and hydraulic fracking has increased, causing concern over fugitive emissions of VOCs close to urban population densities.

Natural gas contains between 60-90 % methane (Lyons and Plisga, 2005). The remaining portion depends on the individual reservoir. This includes a range of NMHCs, including alkanes, alkenes, aromatics and non hydrocarbon gases such as sulphur compounds and water. Often, separation of fractions is done at the well site, close to the well head. Whilst this is advantageous from a transport point of view, each individual piece of equipment is a potential leak site for the more volatile fractions. These leakages are usually not well defined or constrained, potentially leading to large amounts of fugitive emissions. Several studies have been carried out on emissions, emission rates, and the effect of these gases in the local atmosphere (Gilman et al., 2013; Edwards et al., 2014; Warneke et al., 2014; **?**, etc).

Many of these studies focus on fracking regions in the US, coupling fugitive emissions with high winter ozone events. For example, Edwards et al. (2014) studies the effect of a large fracking operation in the Uintah Basin, near Horsepool, Utah. Due to a temperature inversion lasting over a week, a compressed boundary layer led to leaking gas from the well heads build up to ˜ 1 ppmv total VOCs. These extremely high levels, mixed with low amounts of NO_x lead to ozone peaking at > 120 ppbv. Isopleths simulating the atmosphere in the basin show that the VOC/NO_x ratio was almost at peak efficiency with regards to ozone production.

Several incidents have occurred around offshore oil and gas rigs. On 20th April 2010 the Deepwater Horizon Rig (coordinates: 28.7381N, -88.3658E) began to spill oil out into the Caribbean sea. This spill followed a fatal methane explosion on the platform, and caused the rig to sink a couple of days later. Estimates for the amount of oil released stand at 779 million liters (or 4.9 million barrels) (Daly et al., 2016), with 9.5 million liters of chemical dispersant added after in an attempt to clean up the spill (Kujawinski et al., 2011). Following the oil spill on the ocean floor, vast quantities of oil reached the sea surface, where a significant fraction of the more volatile hydrocarbon mass started to evaporate into the atmosphere (Ryerson et al., 2011). In addition, surface oil slicks were set alight in order to remove it, but introducing another source of VOCs into the atmosphere. Several studies have investigated the impact on the atmosphere, most notably a paper by Ryerson et al. (2011), which discusses the data gathered from a series of research flights over the spill area. They reported elevated levels of compounds over the area, and calculated an evaporation rate of 258,000 kg/day of hydrocarbon evaporation from the fresh oil slicks., with C_6 to C_{11} aromatics contributing 45,000 kg/day. A significantly larger proportion of cycloalkanes was also found downwind of the oil spill, whilst concentrations of these compounds are relatively low in urban air (Yuan et al., 2014; Ryerson et al., 2012)

The North Sea is home to one of the largest concentrations of Oil and Gas rigs in the world. There are some 127 operational installations, with a further 21 listed as non-operational located within UK waters. Figure 5.1 shows the distribution of these rigs across the North Sea.

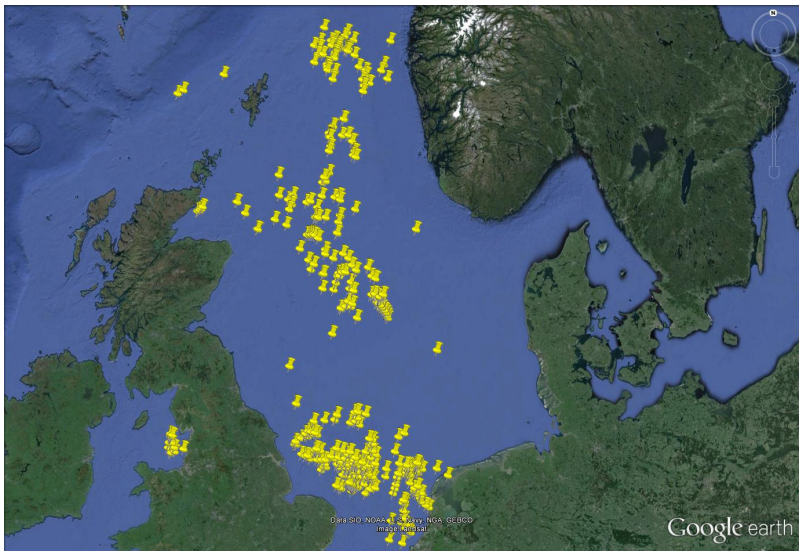

Figure 5.1: Location of rigs in the North Sea. Note the large clusters off the coasts of East Anglia and Aberdeen.

Methane and non-methane hydrocarbons can be released during the drilling, extraction, and transporting processes. In addition, hydrocarbons have the potential to evaporate into the air from sea surface pollution, such as oil slicks. Releases such as these can pose major environmental issues, as well as the loss of revenue due to the escaped fuel. Small individual leaks are unlikely to yield significant environmental harm, however, more data is needed in the area to help distinguish between significant and insignificant leaks and the cumulative impacts.It has been estimated that small leaks can amount to ˜4 % of the total gas extracted from a well. Further to this, emissions from routine operations are legislated by national and international agreements. However, given the remoteness of the operations there is little evidence for actual real-world emission, the variability of emissions between individual rigs, normal operation leaks or during one-off or uncontrolled leaks

On 25th March 2012, gas rig 22/30c-G4, in the Elgin-Franklin gas field sprung a leak at the well head. The FAAM research aircraft was mobilised to survey the area on 5 separate days. Flights focused on the composition of the leak, as well as it's footprint. To this end, flight legs were positioned perpendicular to the prevailing wind at a variety of distances and heights from the rig (Mobbs et al., 2012, *manuscript in preparation*). This allowed the plume to be mapped, as well as determining the changing chemical composition as the plume moved further from the source. Additionally, flight legs were conducted upwind of the rig, in an attempt to characterise the background. During this event, the leak rate was estimated using methane as the primary tracer. The study concluded that the methane flow rate a few days after the leak was sprung was ˜1 kg s^{-}1, dropping to < 0.5 kg s^{-}1 after around 6 weeks. Additionally, a close relationship between methane and C4 hydrocarbons was observed. However, larger hydrocarbons ($> C_2$) showed no correlation with methane mixing ratios. The study suggested that larger hydrocarbons were deposited straight onto the sea surface, creating a seawater sheen.

At the time, however, absolute enhancement factors were not able to be given, due to a lack of background concentration information.

In case of future leaks or fires, a series of survey flights were planned, in order to determine concentrations of chemical tracers, both downwind of current, functioning rigs, and in the surrounding air. In combination, providing context for typical enhancements in emissions that would be expected under normal operational conditions and against which future unintentional leaks could be evaluated for their significance.

5.1.2 Experimental

A total of six flights were conducted during May, June and July of 2015. The first 4 flights were conducted over the North Sea, to the north of East Anglia. These flights all assumed the same flight plan, with little to no deviation from the planned route. The track of flight B907, representative of the first 4 flights, is shown in Figure 5.2. The tracks are coloured by altitude, as measured using the aircraft radar altimeter. Flights were planned so as to survey the region in a variety of wind conditions (between an average of 4 - 9 ms^{-1}), and at a variety of altitudes, to determine the vertical extent of plumes released from active rigs. Cross wind legs were flown at altitudes of 500 ft (˜150 m) and 1000 ft (˜300 m), with a short leg above the boundary layer for instrument calibrations.

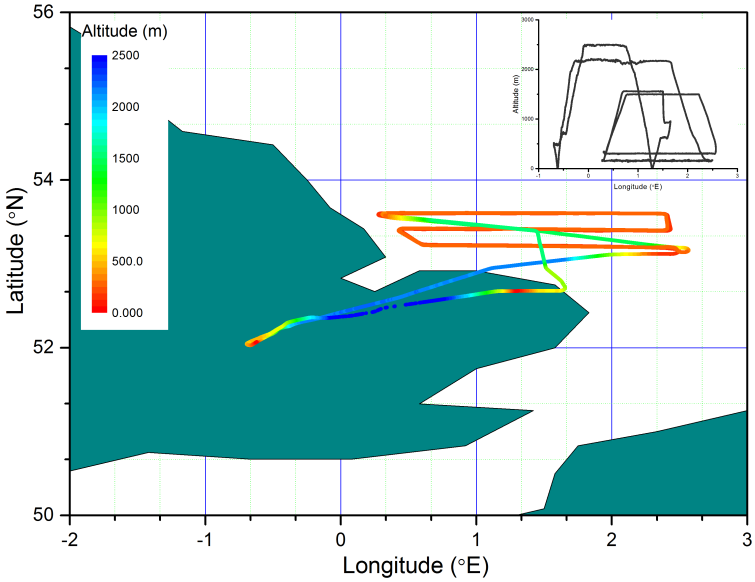

Figure 5.2: Track of flight B907, coloured by altitude. Flights B908, B910 and B912 also followed a very similar track. Inset is a plot of longitude v altitude, showing the different levels that were surveyed.

The last two flights were conducted further north, surveying the gas fields off the coast of Aberdeen. Both flights were based around the Forties collection of rigs (location: 57.716667 N, 1.016667 E). The first of these two was a survey, in which the flight plan was followed, in order to determine background conditions. The flight track for this flight is shown in Figure 5.3. The location of the collection of rigs is indicated in the figure, along with a plot of longitude against altitude, showing the different survey altitudes. The track plot is coloured by altitude, taken from the aircraft radar altimeter. The radar altimeter is accurate at low altitudes, however, stops recording at altitudes over 2500 m, hence the gaps in the track plot. The flight was planned in order to determine background conditions

downwind of the rigs. On the date of the flight, winds were from a Northerly direction, causing the flight legs to be conducted to the south, at three different altitudes.

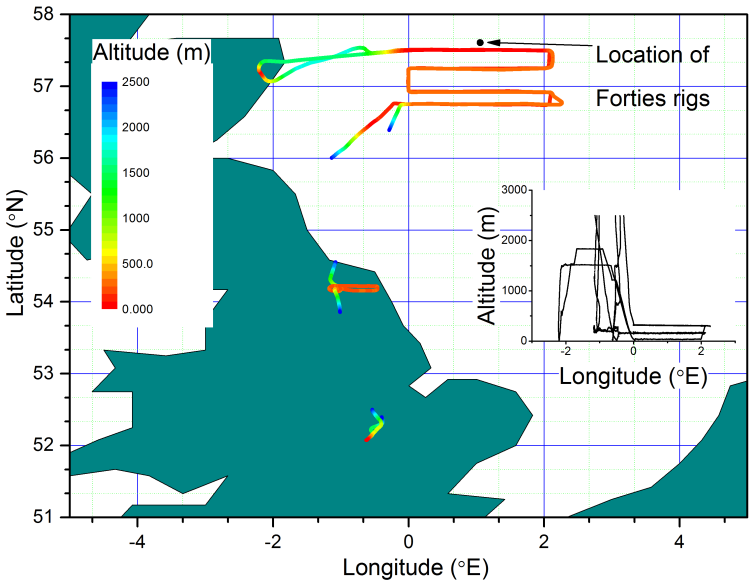

Figure 5.3: Track of flight B913 during the Oil and Gas campaign coloured by altitude as measured by the radar altimeter. The purpose of this flight was to survey the region surrounding the Forties collection of rigs. Inset is a plot of longitude against altitude, showing the various flight levels surveyed.

The last flight was undertaken to gather data relating to plumes being emitted from a specified set of rigs. The Forties collection of rigs were chosen . Figure 5.4 shows the track of the aircraft taken, with a close up of the plume-chasing inset. Again, the track is coloured by altitude as measured using the aircraft radar altimeter. The northern and southern locations were chosen due to high concentrations of active rigs in the regions.

The FAAM research aircraft was equipped to measure NO_x, O_3, SO_2, CO, CH_4, CO_2 and a series of physical and positional parameters. Details and references of other instruments can be found in Table 5.1.

For more details on the instrumentation and techniques, see Chapter 2, or follow the references given. Trace VOCs were also measured using the *in situ* GC/MS and the WAS system, which was in turn, analysed by GC/FID within 72 hours.

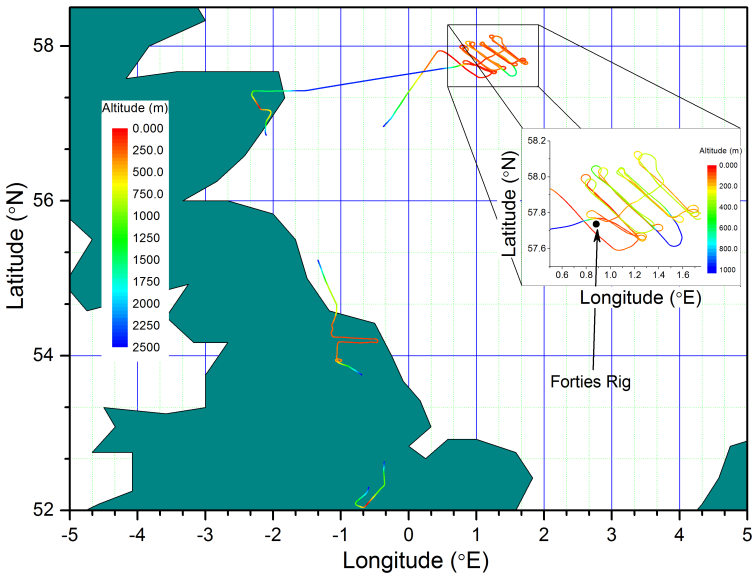

Figure 5.4: Track of flight B918 during the Oil and Gas campaign. A series of legs at a variety of altitudes were conducted at 5 different distances from the rig in order to determine the location, size and shape of the plume. Inset is a close up of the plume chasing sector of the flight, with the approximate location of the rigs indicated

Table 5.1: Details of instruments fitted to the FAAM BAe-146 during the Oil and Gas flying campaign in Summer 2015. See references for more details.

Species / parameter	Method / Instrument details	Averaging time	Precision/ accuracy	Affiliation, Reference
Physics / Positional				
Position, wind (U,V,W)	INS, GPS, Turbulence Probe , RadAlt	1s	0.01 P/Ps	FAAM, Petersen and Renfrew (2009)
Humidity (Dew Point, Temperature)	General Eastern Hygrometer	1s	0.5 - 3 K (pressure dependent)	FAAM, Ström et al. (1994)
Temperature	Rosemount Sensor, Aerospace Ltd	1s	0.3K	FAAM
Cloud Microphysics	CDP	1s		FAAM, Rosenberg et al. (2012)
Chemistry				
CO	UV resonance fluorescence, Aerolaser 5002	1s	1 ppbv	FAAM, Gerbig et al. (1999)
O_3	UV absorption, TECO 49C	1s	1 ppbv	FAAM, Wilson and Birks (2006)
CO_2, CH_4	CEAS, Los Gatos, USA	1s	0.5 ppmv and 2.5 ppbv respectively	FAAM, UoM, O'Shea et al. (2013)
NO, NO_2	Chemiluminescence with photolytic conversion for NO2, Air Quality Design Inc	10s	5 pptv and 15 pptv respectively	FAAM, UoY, Pike et al. (2010)
NMHCs (C_1-C_7)	Whole Air Sampling with analysis by GC/FID	30s (Fill time)	Species Dependent	UoY, Hopkins et al. (2003)

5.1.3 Results

5.1.3.1 Survey Flights

As shown in Figure 5.2, survey flights were conducted north of East Anglia. The flight track took the aircraft past several collections of rigs, but no deviation was made to target specific groups. This was done to ensure full background conditions were measured, including occasionally intersecting a plume.

5.1.3.2 Southern Sector Flights

For each flight, two legs were conducted at 500 and 1000 ft. For B907, wind speeds of ˜ 4 metres per second with an average direction of 330 were recorded (averaged over the two legs). The tracks of the 500 ft and 1000 ft legs are shown in Figures 5.5 and 5.6, coloured by NO. Additionally, the average locations of each GC/MS samples are shown, coloured by benzene. The NO_x instrument carried out zero calibrations in flight, approximately every 6 minutes (although this can be paused if neccessary) leading to the gaps present in the data.

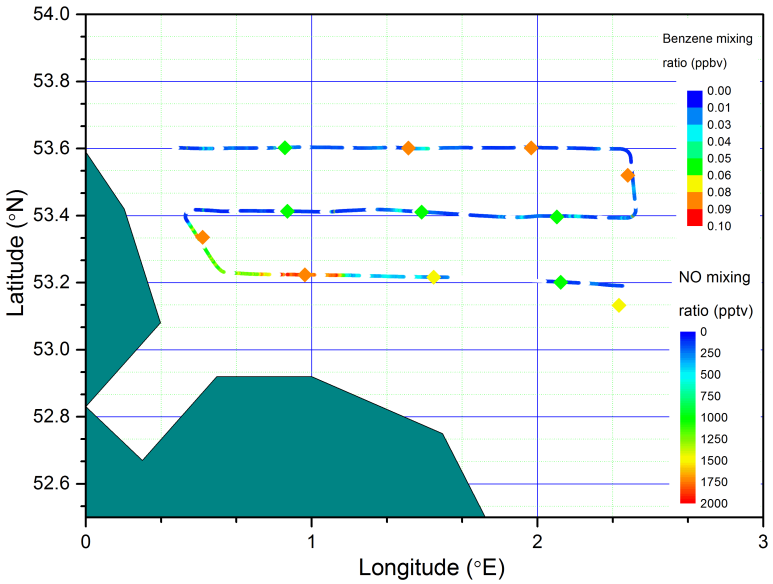

Figure 5.5: Track plot of the 500 ft leg from Flight B907, coloured by NO. The diamonds represent the average sampling location of the GC/MS, coloured by benzene. The gaps in the flight track represent times when the NO_x instrument was carrying out a zero calibration.

The NO plot shows a few isolated plumes, particularly on the Northern most leg, with these plumes generally not exceeding ˜500 pptv. A large increase can be seen in the south western corner, closest to the coast. This is most likely to be emissions from the coast, as

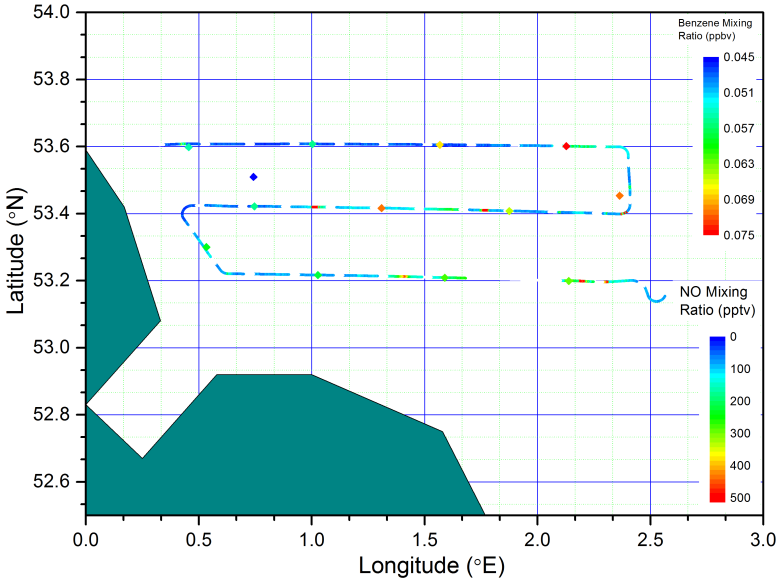

Figure 5.6: Track plot of the 1000 ft leg from Flight B907. See Figure 5.5 for more details.

the wind direction suggests the air had passed over East Anglia.

The diamonds represent the average position of a GC/MS sample, coloured by benzene. It is important to note that the scale on which the benzene is plotted on ranges from 0 to 100 pptv. Concentrations were very low over the area, meaning that very little in terms of trends or links to other pollutants could be identified.

Another finding from this flight was that peaks in NO_x and methane did not always coincide with each other. Some peaks contained just NO_x, whilst others contained just methane. This is demonstrated in Figure 5.7, which shows the 500 ft leg, and Figure 5.8, which shows the 1000 ft leg. Several large NO_x peaks, separate to the couple of methane peaks can be seen.

B908, B910 and B912 followed the same track as B907, and with similar wind speeds (˜4-8 ms¯1), with wind direction being either Northerly or Southerly. Similar trends in the chemical tracers were also observed for NO_x, methane, CO, benzene and toluene.

Due to the sampling time of the *in situ* GC/MS, it wasn't possible to measure emissions from individual rigs. Given a sampling time of 5 minutes, and an extremely narrow peak (as shown by Figure 5.9), samples were too diluted in the thermal desorption system to determine any enhancement in compounds. For these reasons, coupled with the very low concentrations of benzene and toluene in the region as a whole, enhancement factors could not be determined for individual, or even collections of rigs using this method.

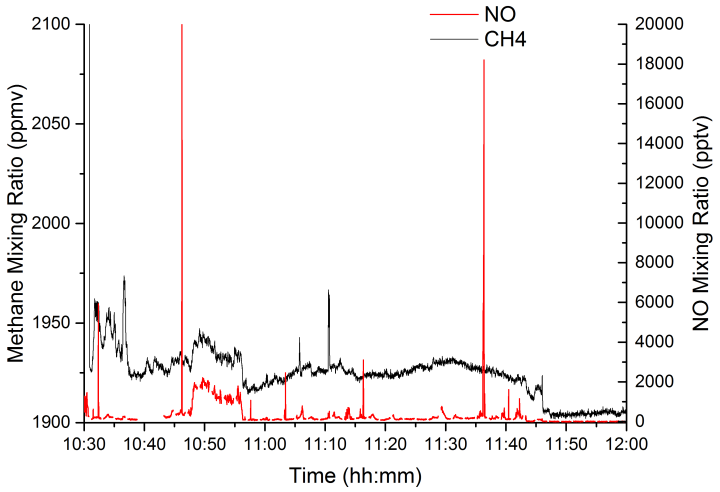

Figure 5.7: Time series of methane and NO during the 500 ft leg of flight B907. Some rigs emit NO, others emit methane.

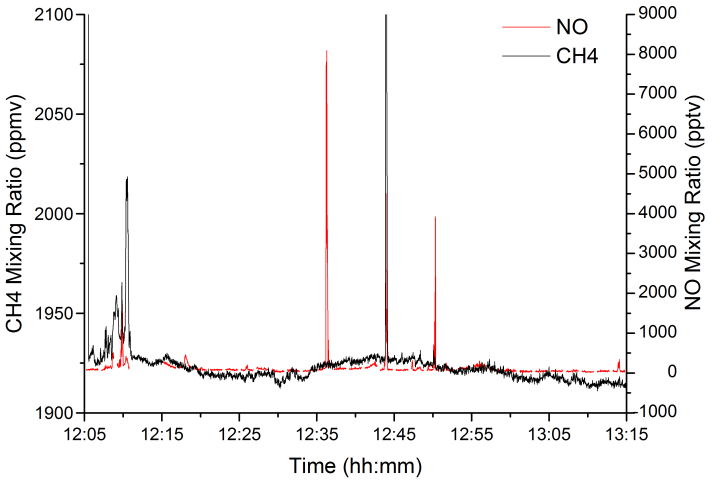

Figure 5.8: Time series of methane and NO during the 1000 ft leg of flight B907.

5.1.3.3 B913

B913 involved runs at 500 and 1000 ft, making it consistent with the southern sector flights. The legs were conducted cross winds, with the average wind direction over the legs being 335, and wind speeds of 8 metres per second.

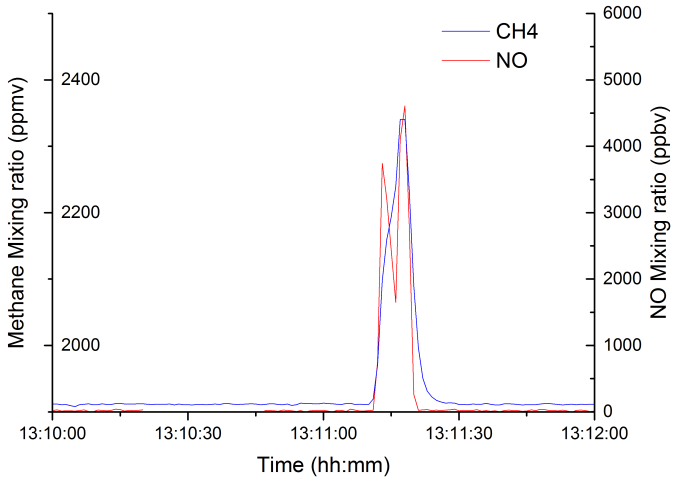

Figure 5.9: Time series of methane and NO, during flight B908, showing a peak in both data sets. The peak lasts < 30 seconds, meaning it cannot be distinguished using the *in situ* GC/MS.

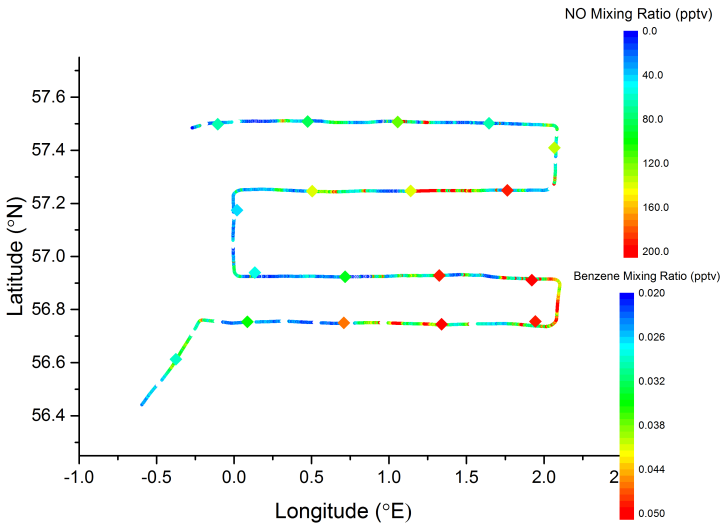

Figure 5.10: Trackplot of flight B913 at 500 ft, coloured by NO. The diamonds represent the average location of the GC/MS measurement, coloured by benzene.

5.1.3.4 B918

5.1.4 Discussion

The separation of the methane and NO_x plumes indicate different sources for the two tracers. The methane plume can be attributed to leaks within the pipelines, from the reservoir up to the rig, and then during storage. However, the NO_x plumes can be attributed to the activity of ships and generators located on the rigs. The largest source of VOC emissions is likely to be gas leakage around the pipelines and possible flaring of excess gas.

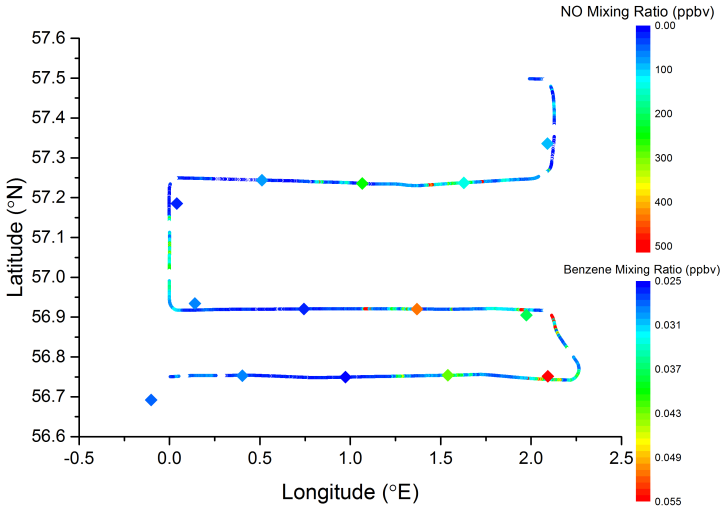

Figure 5.11: Trackplot of flight B913 at 1000 ft, coloured as in Figure 5.10

The data was analysed for spikes in the methane data. Then, each of the spikes were measured for duration and height. Figure 5.12 shows a histogram of the duration of spikes in the methane data. Most plumes lasted less than 20 seconds, meaning it was more difficult to determine increases in VOCs using the *in situ* GC/MS. Additionally, it was also difficult to completely characterise a plume using the WAS system, as a degree of chance was required when filling in order to fill a bottle entirely during a single plume.

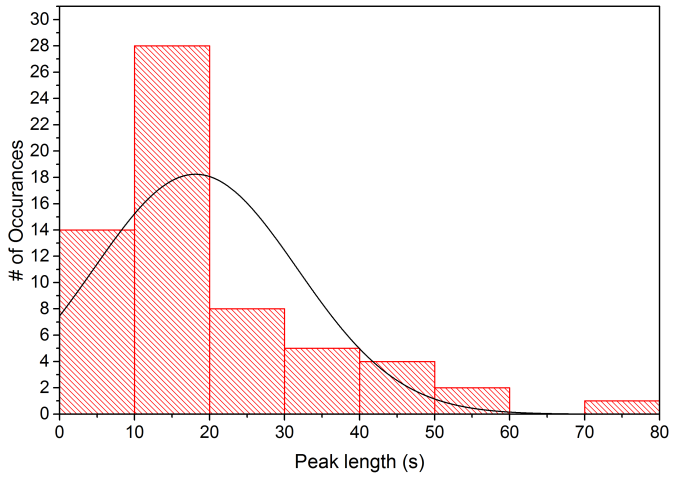

Figure 5.12: A histogram of the length of spikes in the methane data taken from all six flights of the Oil and Gas campaign. The majority of spikes in the data lasted less than 20 seconds.

It was then necessary to start to constrain the GC/MS 5 minute sample time to take into account the short nature of the individual plumes. As Figure 5.12 shows, the majority

of plumes were measured at < 20 seconds in duration.

Figure 5.13 shows the time series for the 500 ft leg of flight B912. The tracers marked on it are 1 Hz methane measurements, benzene as measured by the GC/MS and methane, averaged over the GC/MS sampling times. Once averaged, even the methane trace cannot distinguish the plumes.

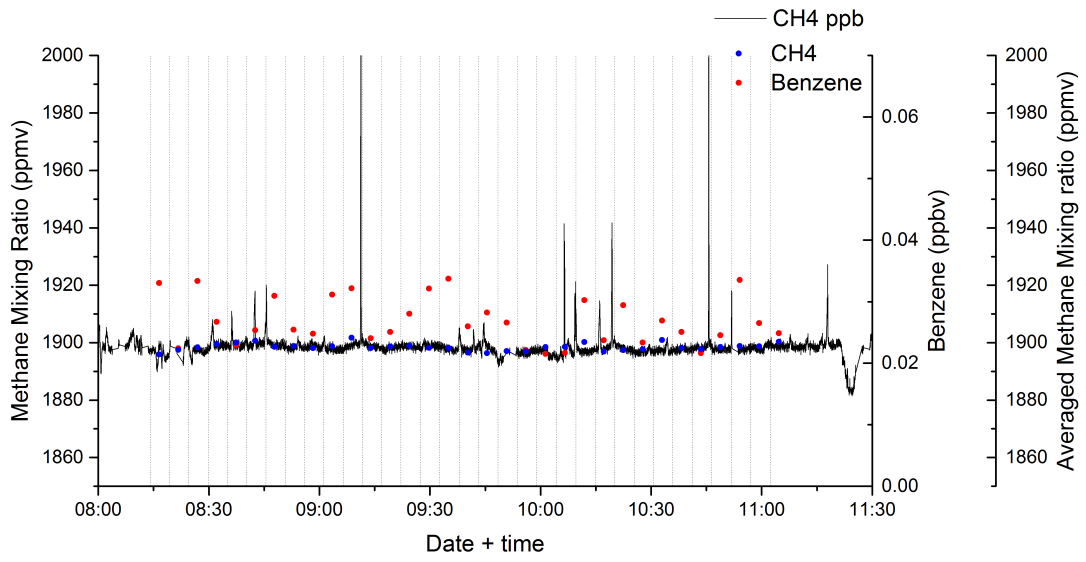

Figure 5.13: Time series of the 500 ft leg of flight B912. The black line represents the 1 Hz methane measurements, the vertical lines represent the start and end times of the GC/MS measurements. The blue and red dots represent methane averaged over the GC/MS sample times and the benzene measurements respectively.

Therefore, an alternative approach was attempted. Instead of attempting to directly calculate an enhancement in benzene, it was assumed that any increase in benzene mixing ratio is the direct result of intersecting a plume. The plume width and height was determined using the methane measurements. This is demonstrated in Figures 5.14 and 5.15. Therefore, the mixing ratio of benzene in this peak is 0.02565 ppbv (25.7 pptv) (0.05241-0.02676).

This can then be converted into a release rate. If, for instance, the benzene enhancement is 25.7 over 5 minutes, this can used to determine the amount in the 20 second long plume, as above. If the enhancement over 5 minutes is 25.7, then the enhancement over 20 seconds must be 25.7 x 15 (300 seconds / 20 seconds = 15). Therefore the benzene enhancement is calculated for this plume as 385.5 pptv.

This analysis was carried out on 20 separate methane plumes. However, of these 20, there was no enhancement in benzene. The lack of benzene can be attributed to the wide variety of rigs occupying the regions. Some of the rigs were either non-operational, or

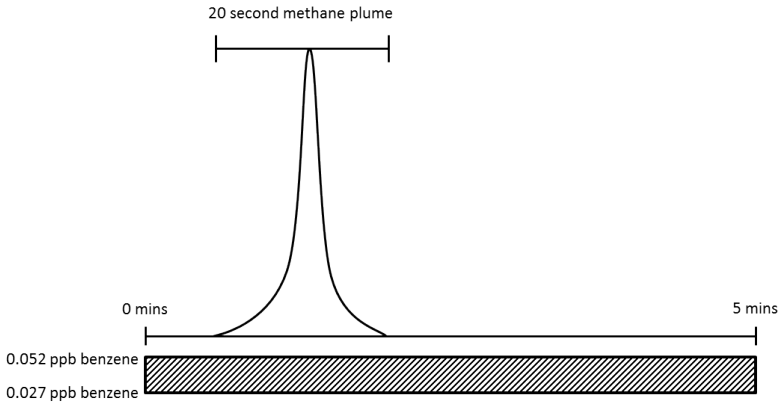

Figure 5.14: Schematic to determine the benzene mixing ratio within a plume. The background mixing ratio can be subtracted from the sample taken that intersects a plume. It is assumed that the entire benzene enhancement has the same source as the methane. The schematic shows a methane peak lasting 20 seconds, and a GC/MS sample time lasting 5 minutes.

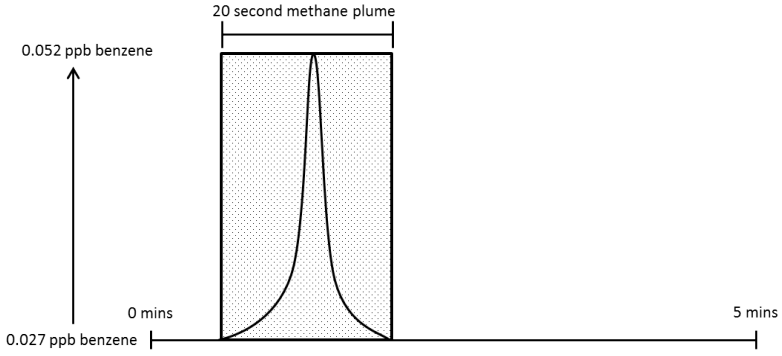

Figure 5.15: Schematic of the second step in determining the benzene mixing ratio within a plume. The difference between the background and the enhanced measurement can be associated to the 20 second methane plume.

used to store gas before being transported to the mainland. Therefore the plumes that did contain benzene can be associated with rigs that were actively involved in the extraction process, therefore using energy from generators. A summary of these plumes is given in Table 5.2. It is important to note that some samples bisected more than one methane plume. On occurences such as these, the width of the peaks were summed, in order to calculate the amount of benzene. Multiple peaks could then be differentiated between, based on their respective peak areas, however, this assumes that the methane:benzene ratio is consistent for all plumes. Due to the many variety of rigs, this assumption cannot necessarily be assumed to be true, but it is a simplification used here.

The diversity of measurements also demonstrates the differing amounts of emissions from individual rigs. Additionally, some of the plumes intersected were also the product of ship emissions, which were servicing the rigs.

Table 5.2: Table of the enhancement of benzene in plumes. The benzene enhancement is calculated by subtracting the background from samples containing a plume. The enhancement factor is the result of dividing the 300 second GC sample time by the plume width.

Plume Number	Benzene Enhancement	Methane Plume Length (s)	Enhancement Factor	Benzene in Plume (ppbv)	Benzene in Plume (pptv)
1	0.02624	100	3	0.07872	79
2	0.00184	15	20	0.0368	37
3	0.00779	20	15	0.11685	117
4	0.30486	40	7.5	2.28645	2286
5	0.01507	40	7.5	0.113	113
6	0.0063	15	20	0.1326	133
7	0.03187	40	7.5	0.24	240
8	0.02762	20	15	0.414	414
9	0.02067	20	15	0.31	310
10	0.12011	50	6	0.72	720

There are errors with such calculations. Firstly an assumption must be made that the only enhancement in benzene stems from the plume. Secondly, an assumption must be made that the response of the instrument is entirely linear, even at these low values. As calibrations have been performed at a variety of mixing ratios (see chapter 2), this is a reasonable assumption to make. Finally, the calculations are performed assuming the benzene measured is spread evenly across the plume, when it must be assumed to follow a Gaussian distribution, as the methane peak does. Calculations could be conducted to determine the shape and size of the benzene peak, based on the methane peak. However, because of the assumptions already made, such a process would be time consuming and be a further source of errors.

Even within the plume, there are still relatively low concentrations of benzene estimated using this method. The estimations given here wouldn't be above the annual EC Air quality limit value for benzene. Therefore, it can be concluded that the rigs are a significant source of largely un-reported NO_x and CH_4, but due to the constraints of using GC/MS, it is not possible to assert whether or not they form a significant source of VOCs. The figues quoted here cannot be taken seriously, due to the large sources of errors. However, we can use the data gathered to invesitgate the 'background' mixing ratios of

compounds, and also make a comparison to some early measurements taken during the ACCACIA campaign.

5.1.5 Comparison with Background Levels over the Arctic

Further flights were conducted around Svalbard, during February and March 2013. The primary scientific impulse for conducting these flights was to gather information on Arctic spring vortices and Aerosol Cloud Coupling and Climate Interactions in the Arctic (ACCACIA), which is beyond the scope of this thesis. The *in situ* GC/MS was mounted on board the FAAM aircraft with the principle task of detecting dimethyl sulfide (DMS) which has been demonstrated act as a cloud condensation nucleus (CCN) (Charlson et al., 1987), and released from phytoplankton activity. However, DMS was consistently below the instrument limit of detection (LOD) of 200 ppt. This is thought to be due to the flights to be conducted too early in the year, so the biology of the Arctic Ocean was still inactive, leading to diminished biogenic emissions. Two anthropogenic tracers were also analysed and quantified during ACCACIA- benzene and toluene. The flight tracks for the ACCACIA are shown in Figure 5.16. The flights were made between Kiruna, Sweden, and Longyearbyen, Svalbard.

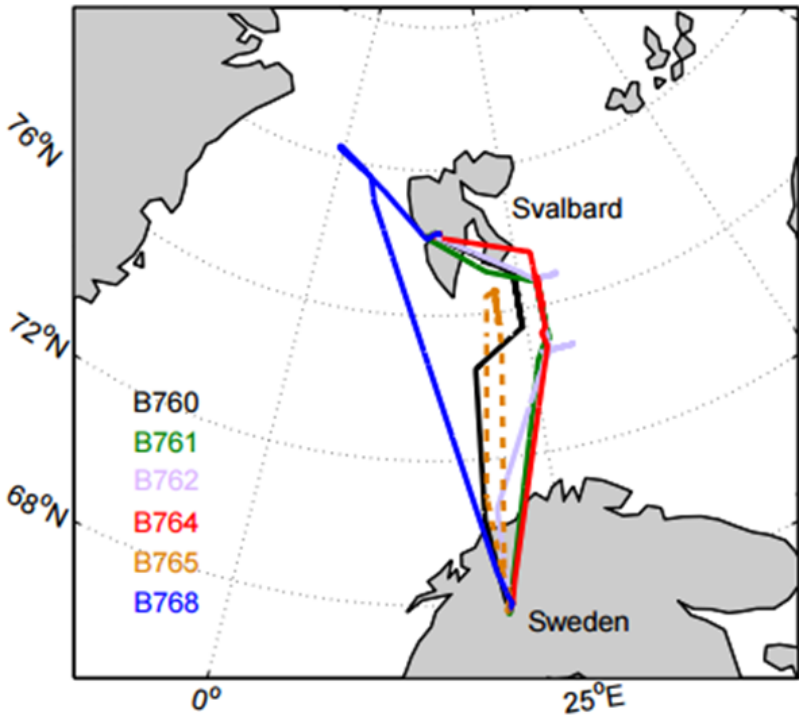

Figure 5.16: Track plot of the flights made by the FAAM BAe-146 during the ACCACIA campaign (Image ref: (Young et al., 2016)

As these two compounds were also analysed during the Oil and Gas campaign, comparisons between the'background' mixing ratios of these anthropogenic tracers in the Arctic Ocean and North Sea can now be made. The relative operating areas of ACCACIA and Oil and Gas are shown in Figure 5.17

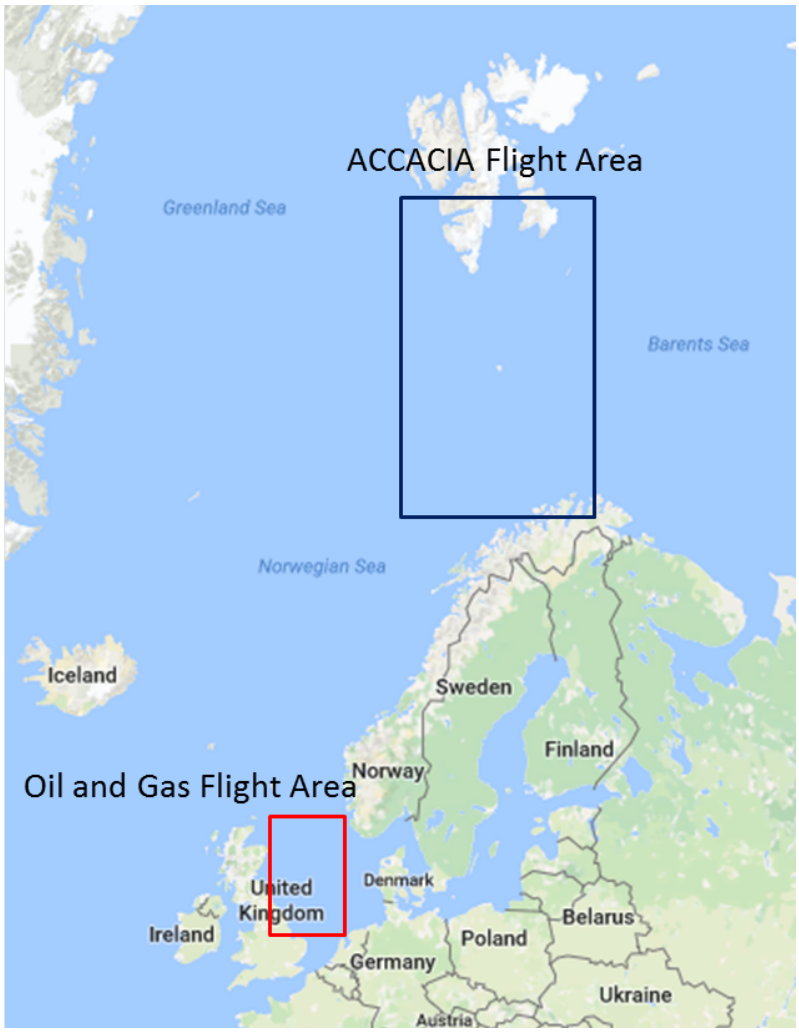

Figure 5.17: Operating areas of the ACCACIA and Oil and Gas Campaigns

Data from the two campaigns were worked up using carbon tetrachloride as the internal standard. For ACCACIA, the instrument was set up to run in full scan mode, but, due to the objectives of the campaign, was only calibrated to measure DMS, BTEX and monoterpenes. Again, the monoterpenes were continually below LOD (approximately 20 ppt). Therefore, the best compounds to be comparedare benzene and toluene. Box and whisker plots of these compounds from both campaigns are shown in Figure 5.18.

Figure 5.18 shows how benzene and toluene mixing ratios differ between the between the North Sea and the European Arctic ocean. The statistics for these plots are shown

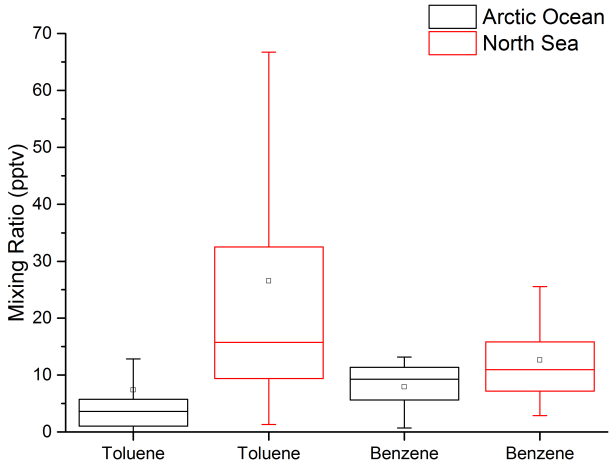

Figure 5.18: Benzene and Toluene comparison

in Table 5.3. It should be noted that the scale of the plots as been altered to show the spread of data, and the maximum values have not been shown (but are still included in the data).

Table 5.3: Statistics of the box and whisker plots showing the spread of benzene and toluene mixing ratios from ACCACIA and Oil and Gas Campaigns

Campaign	Compound	Mean	Standard Deviation
ACCACIA	Toluene	7.4	13.6
	Benzene	7.92	4.17
Oil and Gas	Toluene	26.5	33.4
	Benzene	12.6	7.8

The data clearly shows higher mixing ratios for both compounds in the North Sea than in the Arctic Ocean. Toluene in particular shows a much higher enhancement, with benzene having only a slight enhancement. The ratios between these two compounds tell a different story for the two regions. The North Sea data shows a greater toluene:benzene ratio (2.1), which is consistent with fresher emissions, possibly due to outflow from the UK/Europe, depending on wind direction. However, the data from the Arctic Ocean shows a much lower toluene:benzene ratio (0.93). This is much more indicative of older emissions, possibly from North America, which have travelled large distances.

Additionally, there is a large spread on the toluene data from the North Sea. This is likely due to the measurement of different air masses, some of which contain fresh emis-

sions, some of which contain more processed emissions. As some flights were conducted with a Northerly wind direction, it is possible that measurements were also made of air that had more recently spent time in the Arctic Polar vortex. However, as the North Sea mean is still higher than the 95th percentile from Arctic Ocean, these instances were not particularly common.

An assumption that needs to be made is that the toluene:benzene ratio was the same upon emission for both areas. This is a fairly good assumption, as, for both regions, the main source of these gases is transport and energy generation, whether from cars or diesel powered ski-doos. This kind of analysis is also not concerned with unique emission sources, but rather the overall emission ratios. It should be noted that, this far from sources, all these mixing ratios are extremely low.

5.1.6 Conclusions

During the summer of 2015, a series of flights were conducted around the North Sea oil and gas rigs, in an attempt to characterise ambient conditions in the area. These flights were conducted in two locations - off the North East coast of East Anglia, and off the East coast of Aberdeen. The first four flights off East Anglia were survey flights to determine background conditions, and to intersect plumes coming from rigs. The last two flights were an analysis of a group of rigs collectively termed 'Forties'. Initially, background conditions in the region were measured, followed by a 'plume chasing' flight, in which the emissions from these rigs were measured at a variety of distances and altitudes. Analysis of the data found a large difference between different types of rigs. Some rigs, mainly those active, or with a human presence showed peaks in methane and NO_x, whilst others only emitted methane or NO_x, depending on the level of activities. As the plume lengths were particularly narrow, the GC/MS was unable to determine enhancements in absolute mixing ratios, due to the amount of dilution in each sample. Instead, an assumption was made that any increase in benzene was solely due to benzene contained in the methane plume. Therefore the amount of benzene could be estimated using the width of the methane peak. This analysis was completed on a range of peaks, which showed very different benzene plume mixing ratios. This is indicative of the wide variety of activities on each rig. Whilst this can be extremely difficult to analyse, the baseline measurements both in and out of plumes can assist in the diagnosis of issues, should further leaks, or uncontrolled flaring should occur. Even in plumes, concentrations were low for VOCs, however, CH_4 and NO_x are potentially higher than are reported in inventories.

Additionally, the background data collected from the North Sea flights were compared to boundary layer data collected during the Arctic Ocean flights. This showed that whilst there were more varied air masses, the North Sea mixing ratios of benzene and toluene were higher than in the Arctic Ocean. The ratio of toluene to benzene showed that air masses in the North Sea contained fresher emissions than those in the Arctic.

Chapter 6

Conclusions

6.1 Conclusions

This project was undertaken to further develop and improve the measurements made by the University of York *in situ* airborne GC/MS. Additionally, the instrument was also fitted to the FAAM BAe-146 Atmospheric Research Aircraft, to measure airborne VOCs and halocarbons. Explained in this thesis is an account of development work done on the instrument, and an analysis of data from three campaigns.

A series of modifications were designed and carried out to improve instrument performance. Firstly, the water removal system was redesigned, due to the original Nafion membrane interferring negatively with the sample passing through. The system was altered to a cold finger powered by a series of Peltier plates, designed to freeze water out of the sample. This system performed well in the laboratory, and during ACCACIA campaign, which took place in Nothern Sweden and Svalbard. However, this setup was not ideal in more humid climates, such as the Amazon, or the Western Pacific. To solve this, a more robust system was designed and implemented. This took the form of a Stirling chiller, which was used to chill a glass cold finger down to -30 ° C. It was kept at this temperautre using a PID controller and a thermocouple, which proved efficient at freezing out water in a wide variety of conditions.

A CO_2 system was implemented to freeze the head of the column. This had the effect of re-trapping compounds as they entered the column, and then desorbing in a single band. Therefore, peak shape was vastly improved, witht the peak width being greatly reduced. Because of this, the split injection could then be changed to splitless, as peaks that were coeluting, came out in two (or more) distinct peaks. As a result, the sensitivity of the instrument increased by a factor of the split flow (i.e. going from a split ratio of 10:1 to 1:1 increased sensitivity by 10x).

Further modifications made included setting triggers on the GC, and controlling Arduino board to increase run-to-run reproducibility, and the addition of a back pressure controller. This was an essential modification, was changing air and cabin pressure were previously affecting the system. The addition of the BPC regulated the sample pressure, as it was calibrated to an absolute pressure.

The overall objective was to improve the measurements made by the instrument by regulating and controlling each sample, to improve reproducibility. By the end of this project, the instrument was capable of performing at the same level as other similar instruments in the field, such as the NOAA TOGA instrument. This had to be conducted

in a highly specialised environment, with safety concerns being paramount. Whilst further modifications could be carried out, due to time, money and safety restrictions, the developments made here are suitable for the instrument to be taken back into the field, and reliable measurements made.

Chapter 3 focussed on the analysis of results from the South American Biomass Burning Analysis (SAMBBA) campaign. Whilst instrument performance was non-optimal for all compounds, benzene, and isoprene data were able to be extracted from it. Vertical profiles of both compounds, along with CO were produced and analysed. These vertical profiles showed the extent to which compounds could move from the surface to the top of the boundary layer, and undergo entrainment into the free troposphere. With long atmospheric lifetimes, both CO and benzene were able to escape regions of intense biomass burning, entering the free troposphere and undergoing long range trasnport. Isoprene, however, with a much shorter atmospheric lifetime is generally constrained to the boundary layer. Additionally, a comparison with literature values reported in Lewis et al. (2013), Evtyugina et al (2013) ttand Simpson et al (2011) on CO:VOC ratios was also performed. It was found that of the species reported, the ratios agree well, with some small discrepancies. The differences between the ratios could be attributed to a range of factors: distance from fire to measurement location, heat of the fire, species of tree and meteorological conditions.

Chapter 4 investigates the data collected during the Coordinated Airborne Studies in the Tropics (CAST) campaign. Firstly, a large-scale comparison was carried out between 4 different platforms, all of which were set up to measure halocarbons. A systematic offset was found between the WAS system and the other three platforms, which was attributed to the presence of liquid water in the sample stream. After correcting for this, all four platforms showed a very good agreement, lending confidence to the measurements taken by the GC/MS. Vertical profiles of the GC/MS measurements were produced which showed two different air masses were encountered at an altitude of 6000 m. When back trajectory analyses were conducted, it became apparent that the two air masses had followed different trajectories. This led to the 'splitting' of the profile at this altitude and, when coloured by ozone, this reinforced this. Samples containing high ozone and low bromocarbons had migrated down from just below the tropical tropopause layer, carrying emissions released over Eastern Asia, whilst being processed in the transport from location of source to the locus of the measurement. Conversely, samples containing low ozone and high

bromocarbons had spent long periods of time over open ocean at low altitudes.

Chapter 5 investigates the data collected during flights that took place over the North Sea Oil and Gas fields. These flights took place over two different regions, in order to determine background conditions over a large area. As plumes were extremely narrow compared to the GC sample time (20 seconds), the GC was unable to directly measure mixing ratios in the plume. Therefore, an assumption was made that any increase in mixing ratios was solely due to plumes, as identified by the methane plot. Calculations were then performed on a range of peaks to establish the mixing ratio of benzene if the whole sample had been taken in the plume by scaling the enhancement by the ratio of the plume width to the 5 minute GC sample time. The wide variety of emission ratios calculated show that each rig can have a different plume type, based on differing activities on each rig. A comparison between background levels of benzene and toluene in the North Sea and the Arctic Ocean was also conducted, showing different air masses and different levels of atmospheric processing.

6.1.1 Further work and Final Thoughts

By the end of this project, the instrument is now ready to be deployed to the field. All constituent parts of the instrument have been more rigorously tested than previously, and the instrument can now be deployed to a wide variety of environments, without the need for any further changes. An exception to this would be to change GC and MS parameters to be more sensitive to a particular species, or family of species, depending on a particular projects objective.

Additionally, further laboratory work could be carried out to improve and characterise losses to the walls of the sample path, although all lines are now heated, which should minimise this loss. Finally, additional development could be carried out on the volume of sample collected, by increasing the flow across the traps.

Finally, the overall message of this project is as a proof of concept for the instrument. It can be extremely advantageous to be able to use an *in situ* GC/MS for VOC sampling, rather than using the WAS system. The GC/MS is not limited in the same way to a specific number of samples, and can sample continously over a flight. Additionally, for field campaigns in remote regions, where it is not possible to set up a laboratory for analysing the WAS canisters, the GC recquires on minimal ground support, in the shape of spare cylinders of helium, CO_2 and calibrations. Therefore power requirements, and the

infrastructure of a region are not neccessarily required. The fact that this instrument can now perform in a variety of environments, can produce data that compares well with other systems, and requires minimal ground requirements shows the success of this project.

Appendix A

Appendix A: Arduino Code

The following is the code uploaded to the Arduino Leonardo microcontroller used to control processes in the Flow Control Box as highlighted in Chapter 2.

```
//CO2 trap automatic control. Jamie Minaeian & Stephen Andrews 2013/14

//define constants and variables
//Leonardo board pin selections:
int manualswitch = 4;
int systemactivate = 7;
int CO2relay = 2;
int TriggerA = 8;
int TriggerB = 9;
int GCtrig = 11;
int LED = 13;
int TrapHeaterRelay = 6;
const int lineheater = 3;
const int Dtolsample = 12;
const int Dtolinject = 5;

//heating
int heaterpower = 50;
int heatervalue = heaterpower*2.55;

//timing
long currenttime = 0;
long switchreadtime = 100;
long previousswitchreadtime = 0;
long triggerreadtime = 100;
long previoustriggerreadtime = 0;
long Acount = 0;
long Bcount = 0;
long triggertime = 0;
long CO2ontime = 60000;   //time that CO2 is switched on for in ms
long trapheattime = 10000;  //time that trap heater is switched on for
```

```
long trapheatstarttime = 0;
long heater_CO2_overlaptime = 5000;
long heater_CO2_overlap = 0;
long valveactuatedtime = 10000;

//logic
boolean systemactivated = false;
boolean running = false;
int switchcount = 0;
int switchoffcount = 0;
int activationcount = 0;
int deactivationcount = 0;
int trigAvalue = HIGH;
int trigBvalue = HIGH;
int GCsignal = HIGH;
boolean trapheating = false;

void setup()// This code will only run once, after each powerup
or reset of the board
{
  //initialise serial comm with laptop @ 9600 bps
  Serial.begin(9600);

  //define pins as inputs or outputs
  pinMode(manualswitch, INPUT);
  pinMode(systemactivate, INPUT);
  pinMode(CO2relay, OUTPUT);
  pinMode(TriggerA, INPUT);
  pinMode(TriggerB, INPUT);
  pinMode(LED, OUTPUT);
  pinMode(GCtrig, INPUT);
  pinMode(Dtolsample, OUTPUT);
  pinMode(Dtolinject, OUTPUT);
```

```
  //Line Heating
  pinMode(lineheater, OUTPUT);
  digitalWrite(lineheater, heatervalue);

  //pull IO pins low
  digitalWrite(manualswitch, LOW);
  digitalWrite(systemactivate, HIGH);
  digitalWrite(CO2relay, LOW);
  digitalWrite(TriggerA, HIGH);
  digitalWrite(TriggerB, HIGH);
  digitalWrite(GCtrig, HIGH);
  digitalWrite(Dtolsample, HIGH);
  digitalWrite(Dtolinject, HIGH);
}

void loop() // This code will loops consecutively
{
 currenttime = millis(); //read the time in ms since the program started

  // set the speed at which the switch is read to stop spikes
  if (currenttime - previousswitchreadtime > switchreadtime){
    previousswitchreadtime = currenttime;

    //read pins connected to the switches
    int manualswitchstate = digitalRead(manualswitch);
    int systemactivationstate = digitalRead(systemactivate);

    //perform actions from switch inputs

    //manual switch CO2 on/off
 if (systemactivationstate == LOW){
    digitalWrite(Dtolsample, HIGH);
```

```
   digitalWrite(Dtolinject, HIGH);
  //Serial.println(" valve on manual ");

   if (manualswitchstate == HIGH) {
      switchcount = switchcount +1;
     if (switchcount == 1) {digitalWrite(CO2relay, HIGH);
    digitalWrite(LED, HIGH);
    Serial.print(currenttime);
     Serial.println(" CO2 MANUALLY ACTIVATED!");}}
   else {digitalWrite(CO2relay, LOW);
       digitalWrite(LED, LOW);
       switchcount = 0 ;}

    if (manualswitchstate == LOW) {
         switchoffcount = switchoffcount +1;
      if (switchoffcount == 1) {Serial.print(currenttime);
          Serial.println(" CO2 manually switched off");}}
   else {switchoffcount = 0;}
}

   //activate/deactivate automatic CO2 switching
   if (systemactivationstate == HIGH) {
        activationcount = activationcount +1;
     if (activationcount == 1){systemactivated = true;
         Serial.print(currenttime);
         Serial.println(" AUTO CO2 SYSTEM ACTIVATED");}}
   else {systemactivated = false;
         activationcount = 0;}

      if (systemactivationstate == LOW) {
         deactivationcount = deactivationcount +1;
      if (deactivationcount == 1) {Serial.print(currenttime);
          Serial.println(" AUTO CO2 SYSTEM DEACTIVATED");}}
```

```
    else {deactivationcount = 0;}
  }

//read values of the triggers from TD unit
if (currenttime - previoustriggerreadtime > triggerreadtime){
    previoustriggerreadtime = currenttime;
 trigAvalue = digitalRead(TriggerA);
 trigBvalue = digitalRead(TriggerB);
 GCsignal = digitalRead(GCtrig);
 //Serial.println(GCsignal);
}
//turn CO2 on if system activated and triggered but only do it once per sample
if ((systemactivated == true) && (trigAvalue == LOW))  {

      Acount = Acount +1;

          if ((Acount ==1) && (running == false)){
              if ((trigAvalue == LOW) && (Acount == 1) && (running == false))
              {
                Serial.println("TRAP B about to fire,
                CO2 switched on, DTol injd!"); }

          triggertime = millis();
          digitalWrite(CO2relay, HIGH);
          digitalWrite(Dtolinject, LOW);
          running = true;
          }
}
else {Acount = 0;}

if ((systemactivated == true) && (trigBvalue == LOW)) {

      Bcount = Bcount +1;
```

```
          if ((Bcount ==1) && (running == false)){

              if ((trigBvalue == LOW) && (Bcount == 1) && (running == false))
              {
                Serial.println("TRAP A about to fire,
                CO2 switched on, Dtol injd!"); }

          triggertime = millis();
          digitalWrite(CO2relay, HIGH);
          digitalWrite(Dtolinject, LOW);
          running = true;
          }
}
else {Bcount = 0;}

  if ((running == true) && (currenttime - triggertime > CO2ontime)){
  digitalWrite(CO2relay, LOW);
  digitalWrite(Dtolinject, HIGH);
  digitalWrite(Dtolsample, LOW);
  Serial.println("CO2 timed out, Dtol sampling");
  running = false;
  }
  if ((running == true) && (GCsignal == LOW)){
  digitalWrite(TrapHeaterRelay, HIGH);
  digitalWrite(Dtolinject, HIGH);
  digitalWrite(Dtolsample, LOW);
  Serial.println("GC turned on Trap Heat, Dtol sampling");
  trapheating = true;
  trapheatstarttime = millis();
  heater_CO2_overlap = millis();
  running = false;

  }
```

```
  //this next if statement turns off CO2 a set time after heating trap
  if ((trapheating == true) && (currenttime - heater_CO2_overlaptime
  > heater_CO2_overlap)){
    digitalWrite(CO2relay, LOW);
    Serial.println("GC turned off CO2");
  }
  if ((trapheating == true) && (currenttime - trapheatstarttime
  > trapheattime)){
    digitalWrite(TrapHeaterRelay, LOW);
    trapheating = false;
    Serial.println("Trap heating off");
  }

}
```

Appendix B

Aircraft Standard Operating Procedures

Outlined here is the Standard Operating Procedure (SOP) for the Aircraft GC/MS.

Table B.1: The Standard operating procedure used to operate the GC/MS on a flight

#	PHASE	ACTION	DETAIL
	PRE-FLIGHT SET-UP		
1	Switch on power to the rack	Push-in ALL the breakers on the side service point	4 aft facing (GCMS rack) and 3 fore facing (Pump tray)
2	Switch on Vacuum pump	Toggle marked switch on Orange box on pump tray	After the pump has heated up for 5 mins, open black tap to reveal red band
3	Switch on power to the rack	Push the 'Main' Switch on the Power Distribution box	
4	Turn on Helium cylinder	Turn tap on helium cylinder and set outlet pressure is set to ∼37-40 psi	
5	Turn on GC	Push 'GC' breaker on Power Distribution box	GC will boot up and eventually read 'Waiting for Ready'
6	Turn on MS	Push 'MS' breaker on Power Distribution box	MS will boot up and read 'Pump down'
		Wait for the MS to read 'Pump down', then press the 'Menu' button until 'MS parameters' shows.	
		Then press the item button until 'Turbo pump speed' appears.	Monitor pump speed. It should take ∼5 mins to get to 100%. If not, there is a problem in the system.

7	Turn on Laptop	Push the 'Laptop' breaker on Power Distribution Box Open the laptop and press the power button; after it boots up, no password is required	
8	Open GC/MS software	After the Turbo pump speed is at 100%, open up the software labelled 'Jenny' in the upper right corner of the desktop	Click 'Apply/Yes' to all MS parameter questions
9	Turn on TD Unit	Push the 'TD' breaker on Power Distribution Hub Open 'TD' software on right of desktop Press the black button on the front of the TD	Top light on TD will turn on, appearing red The firmware will start to download The bottom light will turn on, red and the firmware will start to download. This may take 5 mins
10	Start cycling the Traps	In the TD software, enter the following parameters: Purge time: 1.5 mins Sample time: 0.5 mins Trap Low temp: 50 Trap High Temp: 230 Ensure trap split is checked Click 'View', 'Options', and 'Ports'. Change GC ready signal from 'Closed' To 'Open' Turn blue tap on outboard side of helium cylinder to open Close the dialog box and click the 'Play' button	 The valves will click and the TD will start to alternatively heat each trap

11	Set the GC Temperature	In the GC software, Click on the 'Parameters' Button and navigate to the 'Oven' tab. Change the 'Starting' and 'End' Temps to 200C. Click 'Apply' and close the dialogue box	
12	Turn on UPS	Push the 'UPS' breaker on Power Distribution Hub Press and hold the 'On/Off' button on the UPS until it beeps	
		Move the toggle switch on Power Distribution Hub from 'Main' to 'UPS'	This protects the MS from a power outage (more common than you might think)
13	Change cold finger	Remove all screws from Flow Control box and pull out to reveal white casing. Remove white insulation and stainless steel. Remove stainless steel nuts attached to glass tubing.	
		Change out coldfinger, replace all fittings and place screws in flow control box	Push box back in and screw in place
14	Turn on Flow Control box	Push 'Flow Control' breaker on Power Distribution box	
		Turn 'Sterling Cooler' toggle switch to 'on'	Stirling cooler will take ∼20 mins to get to ∼-30C, may take longer if extremely hot.
		Turn 'Automatic CO2' toggle switch to 'On'	

15	Change CO2 cylinders	Replace any empty CO2 cylinders by loosening screws on the top of the bracket. Open CO2 cylinder	Use size 11 socket with extension
16	Set up system for the flight	In the GC software, click on 'Sequence', then 'edit sequence'. In the data file box navigate to .Cmsdchem.data.1 then select the campaigns folder In one of these folders create a new folder and name it the same as the flight number	
		Order the sequence so that the sample type and sample name match up to what will be run.	Note: I usually set it up to run 20 blanks, as this can always be changed later.
		Type	Name
		if blank: blank.0.no flow blank	blank_###
		if std: std.1.1L std	std_waclexp5_00#
		if sample: air.1.1L air	air_00#
		Close the dialogue box and then start the sequence by clicking 'Sequence', 'Position and Run' Click 'Begin Spequence' then click 'No' when 'Process Keywords' box comes up	

17	Prepare TD for flight	Change parameters to the following Purge time: 0.5 Sample time: 5 mins Trap low temp: 0 Trap high temp: 230 Ensure trap split is unchecked Click 'View', 'Options', and 'Ports'. Change GC ready signal from 'Open' To 'Closed' Close the dialog box and click the 'Play' button	
18	Calibration Procedure	On the rear of the Flow Control Box, disconnect the stainless steel tubing leading to the sample pump labelled 'SAMPLE IN' Connect the Calibration cylinder Set the output pressure to ∼1.5 bar To begin the calibrations, keeping an eye on the cycle of the TDU, when a new sample begins (valves click), open the tap marked 'SAMPLE' on the front of the Flow Control Box Run at least 6 calibration analyses. Close tap on front of Flow Control Box marked 'SAMPLE' Disconnect cylinder from tubing, and reattach sample line Remove cylinder from aircraft	The same line can be used if necessary, just disconnect the tubing at the union about half way down Any higher and the BPC will start to vent Remember to rename the GC sequence as and when necessary

	IN-FLIGHT PROCEDURES		
1	Turn on sample pump	ASAP after take off, turn on sample pump toggle switch On the flow control box, open tap labelled 'Sample'	
2	check for faults on GCMS	go to GCMS software and check there are no error messages check that the run number is counting up the run-time clock should either be counting up or report that it is "waiting for GC ready"	Remember to rename samples in GC sequence builder
3	Check for faults on TD	go to TD software and check for error messages	
4	Turn off sample pump	Just before landing, turn sample pump off and close tap on front of flow control box labelled 'SAMPLE'	
	POST-FLIGHT PROCEDURES		
1	Stop sequence	Click 'Pause' in the GC software	The next instrument will complete its run and stop; no need to save sequence
2	Stop TD software	Press the 'stop' button	

3	Turn off flow control box	Toggle the Automatic CO2 and Sterling Cooler switches to 'off' Switch off the flow control box Push the Flow control breaker	
4	Turn off the TD	Close the TD software, press the black button on the front of the TD, then push the TD breaker on the power distribution box	
5	Shut down GCMS	Turn blue tap on outboard side of helium cylinder to off In the software, click 'Tune and vacuum', 'vacuum' then 'Vent' DO NOT TURN OFF UNTIL TURBO PUMP SPEED IS <50% Close the software Press the GC and MS breakers on the Power Distribution box	Vent cycle will start
6	Turn off vacuum pump	Close black tap firmly, then switch 'VACUUM' toggle switch on orange box on pump tray	
7	Turn off helium cylinder	Close tap and turn regulator pressure down to 0	
8	Turn off UPS and rack	Press and hold on/off button on UPS Turn off all breakers	

Abbreviations

ACCACIA Aerosol-Cloud Coupling and Climate Interactions in the Arctic

ARA Atmospheric Research Aircraft

AWAS Advanced Whole Air Sampler

BAS British Antarctic Survey

BORTAS BOReal forest fires on Tropospheric oxidants using Aircraft and Satellites

BPC Back Pressure Controller

CAD Computer Aided Design

CAST Coordinated Airborne Studies in the Tropics

CFC Cloro- Fluoro Carbon

CIMS Chemical Ionisation Mass Spectrometry

D-toluene Deuterated Toluene

EIC Extracted ion chromatogram

EM Electron Multiplier

EPC Electronic Pressure Controller

eV Electron Volts

FAAM Facility for Airborne Atmospheric Measurements

FID Flame Ionisation Detection

FPSC Free Piston Stirling Engine

FT Free Troposphere

GAW Global Atmospheric Watch

GC/MS Gas Chromatography/Mass Spectrometer

GC Gas Chromatography

GIN GPS-aided Inertial Navigation System

HETP Height Equivalent of Theoretical Plates

INS Inertial Navigation System

LAQN London Air Quality Network

MACR Methacrolein

MS Mass Spectrometry

MVK Methyl vinyl ketone

NAEI National Atmospheric Emissions Inventory

NCAS National Center for Atmospheric Science

NCD Nitrogen Chemiluminescence Detector

NERC Natural Environment Research Council

NMHC Non-Methane Hydrocarbons

NMOC Non-Methane Organic Compounds

NPL National Physics Laboratory

OVOC Oxygenated Volatile Organic Compound

PBL Plantary Boundary Layer

PDB Power Distribution Box

PID Proportional Integral Derivative

PID Photoionisation Detector

ppb (v) parts per billion (by volume)

ppm (v) parts per million (by volume)

ppq (v) parts per quadrillion (by volume)

ppt (v) parts per trillion (by volume)

psi Pounds per square inch

psig Pounds per square inch gauge

PTFE Polytetrafluoroethylene

PTR-MS Proton Transfer Reaction Mass Spectrometry

RSD Relative Standard Deviation

SAMBBA South American Biomass Burning Analysis

SIM Selected Ion Monitoring

SOP Standard Operating Procedure

TDU Thermal Desorption Unit

TOF Time of Flight

TOGA Trace Organic Gas Analyser

TTL Tropical Tropopause Layer

UoY University of York

UPS Uninterrupted Power Supply

UV Ultraviolet

VOC Volatile Organic Compounds

VSLS Very Short Lived Substances

WAS Whole Air Sampling

WMO World Meterological Organisation

References

U.S. Energy Information Administration. Annual Energy Outlook 2012. Technical Report September, 2012. URL http://www.eia.gov/forecasts/aeo/pdf/0383(2012).pdf.

J. D. Allan, W. T. Morgan, E. Darbyshire, M. J. Flynn, P. I. Williams, D. E. Oram, P. Artaxo, J. Brito, J. D. Lee, and H. Coe. Airborne observations of IEPOX-derived isoprene SOA in the Amazon during SAMBBA. *Atmospheric Chemistry and Physics*, 14(20):11393–11407, 2014. ISSN 1680-7324. doi: 10.5194/acp-14-11393-2014. URL http://www.atmos-chem-phys.net/14/11393/2014/.

Daniel C. Anderson, Julie M. Nicely, Ross J. Salawitch, Timothy P. Canty, Russell R. Dickerson, Thomas F. Hanisco, Glenn M. Wolfe, Eric C. Apel, Elliot Atlas, Thomas Bannan, Stephane Bauguitte, Nicola J. Blake, James F. Bresch, Teresa L. Campos, Lucy J. Carpenter, Mark D. Cohen, Mathew Evans, Rafael P. Fernandez, Brian H. Kahn, Douglas E. Kinnison, Samuel R. Hall, Neil R.P. P Harris, Rebecca S. Hornbrook, Jean-Francois Lamarque, Michael Le Breton, James D. Lee, Carl Percival, Leonhard Pfister, R. Bradley Pierce, Daniel D. Riemer, Alfonso Saiz-Lopez, Barbara J.B. B Stunder, Anne M. Thompson, Kirk Ullmann, Adam Vaughan, and Andrew J. Weinheimer. A pervasive role for biomass burning in tropical high ozone/low water structures. In *Nature communications* Anderson et al. (2016), page 10267.

M. O. Andreae. Atmospheric Aerosols: Biogeochemical Sources and Role in Atmospheric Chemistry. *Science*, 276(5315):1052–1058, may 1997. ISSN 00368075. doi: 10.1126/science.276.5315.1052. URL http://www.sciencemag.org/cgi/doi/10.1126/science.276.5315.1052.

MO Andreae and P Merlet. Emission of trace gases and aerosols from biomass burning. *Global biogeochemical cycles*, 2001. URL

http://scholar.google.com/scholar?hl=en&btnG=Search&q=intitle:Emission+of+trace+gases+and+aerosols+from+biomass+burning#0.

S. J. Andrews, S. C. Hackenberg, and L. J. Carpenter. Technical Note: A fully automated purge and trap GC-MS system for quantification of volatile organic compound (VOC) fluxes between the ocean and atmosphere. *Ocean Science*, 11(2):313–321, 2015. ISSN 1812-0792. doi: 10.5194/os-11-313-2015. URL http://www.ocean-sci.net/11/313/2015/.

Stephen J. Andrews, Lucy J. Carpenter, Eric C. Apel, Elliot Atlas, Valeria Donets, James F. Hopkins, Rebecca S. Hornbrook, Alastair C. Lewis, Richard T. Lidster, Richard Lueb, Jamie Minaeian, Maria Navarro, Shalini Punjabi, Daniel Riemer, and Susan Schauffler. A comparison of very short-lived halocarbon (VSLS) and DMS aircraft measurements in the Tropical West Pacific from CAST, ATTREX and CONTRAST. *Atmospheric Measurement Techniques Discussions*, (April):1–23, 2016. ISSN 1867-8610. doi: 10.5194/amt-2016-94. URL http://www.atmos-meas-tech-discuss.net/amt-2016-94/.

E. C. Apel. A fast-GC/MS system to measure C2 to C4 carbonyls and methanol aboard aircraft. *Journal of Geophysical Research*, 108(D20), 2003. ISSN 0148-0227. doi: 10.1029/2002JD003199.

E. Aruffo, F. Biancofiore, P. Di Carlo, M. Busilacchio, M. Verdecchia, B. Tomassetti, C. Dari-Salisburgo, F. Giammaria, S. Bauguitte, J. Lee, S. Moller, J. Hopkins, S. Punjabi, S. Andrews, A. C. Lewis, P. I. Palmer, E. Hyer, M. Le Breton, and C. Percival. Impact of biomass burning emission on total peroxy nitrates: fire plume identification during the bortas campaign. In *Atmospheric Measurement Techniques Discussions* Aruffo et al. (2016), pages 1–28. doi: 10.5194/amt-2016-45. URL http://www.atmos-meas-tech-discuss.net/amt-2016-45/.

R Atkinson. Atmospheric chemistry of VOCs and NOx. *Atmospheric Environment*, 34 (12-14):2063–2101, 2000. ISSN 13522310. doi: 10.1016/S1352-2310(99)00460-4. URL http://linkinghub.elsevier.com/retrieve/pii/S1352231099004604.

Roger Atkinson and Janet Arey. Atmospheric degradation of volatile organic compounds. *Chemical reviews*, 103(12):4605–38, dec 2003. ISSN 0009-2665. doi: 10.1021/cr0206420. URL http://www.ncbi.nlm.nih.gov/pubmed/14664626.

Barbara Barletta, Simone Meinardi, Isobel J Simpson, Haider a Khwaja, Donald R Blake, and F.Sherwood Rowland. Mixing ratios of volatile organic compounds (VOCs) in the atmosphere of Karachi, Pakistan. *Atmospheric Environment*, 36(21): 3429–3443, jul 2002. ISSN 13522310. doi: 10.1016/S1352-2310(02)00302-3. URL http://linkinghub.elsevier.com/retrieve/pii/S1352231002003023.

E V Browell, G L Gregory, R C Harriss, and V W J H Kirchhoff. Tropospheric Ozone and Aerosol Distributions Across the Amazon Basin. *J. Geophys. Res.*, 93 (MARCH):1431–1451, 1988. ISSN 0148-0227. doi: 10.1029/JD093iD02p01431. URL http://dx.doi.org/10.1029/JD093iD02p01431.

R H Brown and C J Purnell. Collection and analysis of trace organic vapour pollutants in ambient atmospheres; The performance of a TENAX-GC adsorbent tube. *Journal of Chromatography*, 178:79–90, 1979.

L. J. Carpenter and P. S. Liss. On temperate sources of bromoform and other reactive organic bromine gases. *Journal of Geophysical Research*, 105 (D16):20539, 2000. ISSN 0148-0227. doi: 10.1029/2000JD900242. URL http://doi.wiley.com/10.1029/2000JD900242.

L J Carpenter, S Reimann, J B Burkholder, C Clerbaux, B D Hall, R Hossaini, J C Laube, S A Yvon-Lewis, D R Blake, M Dorf, G S Dutton, P J Fraser, L Froidevaux, F Hendrick, J Hu, A Jones, P B Krummel, L J M Kuijpers, M J Kurylo, Q Liang, E Mahieu, J Mühle, S O\textquoterightDoherty, K Ohnishi, V L Orkin, K Pfeilsticker, M Rigby, I J Simpson, Y Yokouchi, A Engel, and S A Montzka. *Update on Ozone-Depleting Substances (ODSs) and Other Gases of Interest to the Montreal Protocol (Chapter 1)*. Global Ozone Research and Monitoring Project-Report No. 55, World Meteorological Organization, Geneva, Switzerland, 2014.

Lucy J. Carpenter and Philip D. Nightingale. Chemistry and Release of Gases from the Surface Ocean. *Chemical Reviews*, 115(10):4015–4034, 2015. ISSN 15206890. doi: 10.1021/cr5007123.

Lucy J Carpenter, James R Hopkins, Charlotte E Jones, Alastair C Lewis, Rajendran Parthipan, David J Wevill, Laurier Poissant, Martin Pilote, and Philippe Constant. Abiotic source of reactive organic halogens in the sub-arctic atmosphere? *Envi-*

ronmental science & technology, 39(22):8812–6, nov 2005. ISSN 0013-936X. URL http://www.ncbi.nlm.nih.gov/pubmed/16323781.

Rosie Chance, Alex R. Baker, Frithjof C. Kupper, Claire Hughes, Bernard Kloareg, and Gill Malin. Release and transformations of inorganic iodine by marine macroalgae. *Estuarine, Coastal and Shelf Science*, 82(3):406–414, 2009. ISSN 02727714. doi: 10.1016/j.ecss.2009.02.004.

S. Chapman. XXXV. On ozone and atomic oxygen in the upper atmosphere. *The London, Edinburgh, and Dublin Philosophical Magazine and Journal of Science*, 10(64):369–383, 1930. ISSN 1941-5982. doi: 10.1080/14786443009461588. URL http://www.tandfonline.com/doi/abs/10.1080/14786443009461588.

Robert J. Charlson, James E. Lovelock, M. Andreae, and Stephen G. Warren. Oceanic phytoplankton, atmospheric sulphur, cloud albedo and climate. *Nature*, 326, 1987.

Paul J. Crutzen. The influence of nitrogen oxides on the atmospheric ozone content. *Quarterly Journal of the Royal Meteorological Society*, 96:320–325, 1970. ISSN 00359009. doi: 10.1002/qj.49709640815.

PJ Crutzen and AC Delany. Tropospheric chemical composition measurements in Brazil during the dry season. *... Atmospheric Chemistry*, 2:233–256, 1985. URL http://link.springer.com/article/10.1007/BF00051075.

PJ Crutzen, LE Heidt, and JP Krasnec. Biomass burning as a source of atmospheric gases CO, H2, N2O, NO, CH3Cl and COS. *Nature*, 1979. URL http://adsabs.harvard.edu/abs/1979Natur.282..253C.

PJ Crutzen, J Williams, and U Pöschl. High spatial and temporal resolution measurements of primary organics and their oxidation products over the tropical forests of Surinam. *Atmospheric ...*, 34:1161–1165, 2000. URL http://www.sciencedirect.com/science/article/pii/S1352231099004823.

Gabriel da Silva, Claire Graham, and Zhe-Fei Wang. Unimolecular beta-hydroxyperoxy radical decomposition with OH recycling in the photochemical oxidation of isoprene. *Environmental science & technology*, 44(1):250–6, jan 2010. ISSN 0013-936X. doi: 10.1021/es900924d. URL http://www.ncbi.nlm.nih.gov/pubmed/19943615.

Kendra L. Daly, Uta Passow, Jeffrey Chanton, and David Hollander. Assessing the impacts of oil-associated marine snow formation and sedimentation during and after the Deepwater Horizon oil spill. *Anthropocene*, 2016. ISSN 22133054. doi: 10.1016/j.ancene.2016.01.006. URL http://linkinghub.elsevier.com/retrieve/pii/S2213305416300066.

KR Darnall and AC Lloyd. Reactivity scale for atmospheric hydrocarbons based on reaction with hydroxyl radical. *Environmental Science & ...*, 1976. URL http://pubs.acs.org/doi/abs/10.1021/es60118a008.

a. E. Dessler, Z. Zhang, and P. Yang. Water-vapor climate feedback inferred from climate fluctuations, 20032008. *Geophysical Research Letters*, 35 (20):10–13, oct 2008. ISSN 0094-8276. doi: 10.1029/2008GL035333. URL http://www.agu.org/pubs/crossref/2008/2008GL035333.shtml.

Peter M Edwards, Steven S Brown, James M Roberts, Ravan Ahmadov, Robert M Banta, A Joost, Robert A Field, James H Flynn, Jessica B Gilman, Martin Graus, Detlev Helmig, Abigail Koss, William P Dube, Andrew O Langford, Barry L Lefer, Brian M Lerner, Rui Li, Shao-meng Li, Stuart A Mckeen, Shane M Murphy, David D Parrish, Christoph J Senff, Jeffrey Soltis, Jochen Stutz, Colm Sweeney, Chelsea R Thompson, Michael K Trainer, Catalina Tsai, Patrick R Veres, Rebecca A Washenfelder, Carsten Warneke, Robert J Wild, Cora J Young, Bin Yuan, and Robert Zamora. High winter ozone pollution from carbonyl photolysis in an oil and gas basin. *Nature*, 514:351, 2014. doi: 10.1038/nature13767.

US EPA. Guideline on Data Handling Conventions for the 8-Hour Ozone Naaqs. 1998.

J. C. Farman, B. G. Gardiner, and J. D. Shanklin. Large losses of total ozone in Antarctica reveal seasonal ClOx/NOx interaction. *Nature*, 315(6016):207–210, 1985. ISSN 0028-0836. doi: 10.1038/315207a0.

Fred Fehsenfeld, Jack Calvert, Ray Fall, and Paul Goldan. Emissions of volatile organic compounds from vegetation and the implications for atmospheric chemistry. *Global Biogeochemical*, 6(4):389–430, 1992. URL http://www.agu.org/pubs/crossref/1992.../92GB02125.shtml.

S Fueglistaler, a E Dessler, T J Dunkerton, I Folkins, Q Fu, and P W Ote.

Tropical tropopause layer. *Geophys., 47, RG1004*, doi(2008):101029/, 2009. doi: 10.1029/2008RG000267.1.INTRODUCTION.

Christoph Gerbig, Sandra Schmitgen, Dieter Kley, Andreas Volz-Thomas, Ken Dewey, and Dieter Haaks. An improved fast-response vacuum-UV resonance fluorescence CO instrument. *Journal of Geophysical Research*, 104(D1):1699, 1999. ISSN 0148-0227. doi: 10.1029/1998JD100031. URL http://doi.wiley.com/10.1029/1998JD100031.

J B Gilman, B M Lerner, W C Kuster, and J A De Gouw. Source Signature of Volatile Organic Compounds from Oil and Natural Gas Operations in Northeastern Colorado. *Environmental science & technology*, 47:1297–1305, 2013.

Bim Graham. Water-soluble organic compounds in biomass burning aerosols over Amazonia1. Characterization by NMR and GC-MS. *Journal of Geophysical Research*, 107(D20), 2002. ISSN 0148-0227. doi: 10.1029/2001JD000336. URL http://www.agu.org/pubs/crossref/2002/2001JD000336.shtml.

JP Greenberg and A Guenther. Tethered balloon measurements of biogenic VOCs in the atmospheric boundary layer. *Atmospheric ...*, 33:855–867, 1999. URL http://www.sciencedirect.com/science/article/pii/S1352231098003021.

Gerald L Gregory, Edward V Browell, and Linda S Warren. Boundary layer ozone: An airborne survey above the Amazon Basin. *Journal of Geophysical Research: Atmospheres*, 93(D2):1452–1468, 1988. ISSN 0148-0227. doi: 10.1029/JD093iD02p01452. URL http://dx.doi.org/10.1029/JD093iD02p01452\nhttp://onlinelibrary.wiley.com/doi/10.1029/JD093iD02p01452/abstract\n http://onlinelibrary.wiley.com/store/10.1029/asset/jgrd887.pdf?v=1&t=hmc6yajb&s=d90eed046ddc7894ad219a5963c7b2ec45c462b0.

Alex Guenther, CN Hewitt, and D Erickson. A global model of natural volatile organic compound emissions. *Journal of geophysical ...*, 100(94):8873–8892, 1995. URL http://www.agu.org/pubs/crossref/1995/94JD02950.shtml.

Alex B. Guenther, Patrick R. Zimmerman, Peter C. Harley, Russell K. Monson, and Ray Fall. Isoprene and monoterpene emission rate variability: Model evaluations and sensitivity analyses. *Journal of Geophysical Research*, 98(D7):12609, 1993. ISSN 0148-0227. doi: 10.1029/93JD00527. URL http://doi.wiley.com/10.1029/93JD00527.

C. L. Heald, A. H. Goldstein, J. D. Allan, a. C. Aiken, E. Apel, E. L. Atlas, a. K. Baker, T. S. Bates, a. J. Beyersdorf, D. R. Blake, T. Campos, H. Coe, J. D. Crounse, P. F. DeCarlo, J. a. de Gouw, E. J. Dunlea, F. M. Flocke, A. Fried, P. Goldan, R. J. Griffin, S. C. Herndon, J. S. Holloway, R. Holzinger, J. L. Jimenez, W. Junkermann, W. C. Kuster, a. C. Lewis, S. Meinardi, D. B. Millet, T. Onasch, A. Polidori, P. K. Quinn, D. D. Riemer, J. M. Roberts, D. Salcedo, B. Sive, a. L. Swanson, R. Talbot, C. Warneke, R. J. Weber, P. Weibring, P. O. Wennberg, D. R. Worsnop, a. E. Wittig, R. Zhang, J. Zheng, and W. Zheng. Total observed organic carbon (TOOC) in the atmosphere: a synthesis of North American observations. (March 2006):2007–2025, 2008. ISSN 1680-7324. doi: 10.5194/acpd-7-17825-2007. URL `http://eprints.whiterose.ac.uk/48735/`.

C N Hewitt, S Hayward, and A Tani. The application of proton transfer reaction-mass spectrometry (ptr-ms) to the monitoring and analysis of volatile organic compounds in the atmosphere. In *Journal of environmental monitoring : JEM* Hewitt et al. (2003), pages 1–7. doi: 10.1039/b204712h.

J R Hopkins, A C Lewis, and K A Read. A two-column method for long-term monitoring of non-methane hydrocarbons (NMHCs) and oxygenated volatile organic compounds (oVOCs). *J Environ Monit*, 5(1):8–13, 2003. ISSN 14640325. doi: 10.1039/b202798d. URL `http://www.ncbi.nlm.nih.gov/entrez/query.fcgi?cmd=Retrieve&db=PubMed&dopt=Citation&list_uids=12619750`.

R Hossaini, M P Chipperfield, S A Montzka, A Rap, S Dhomse, and W Feng. Efficiency of short-lived halogens at influencing climate through depletion of stratospheric ozone. *Nature Geoscience*, 8(February):186–190, 2015. ISSN 1752-0894. doi: 10.1038/NGEO2363.

Claire Hughes, Adele L Chuck, Helen Rossetti, Paul J Mann, Suzanne M Turner, Andrew Clarke, Rosie Chance, and Peter S Liss. Seasonal cycle of seawater bromoform and dibromomethane concentrations in a coastal bay on the western Antarctic Peninsula. *Global Biogeochemical Cycles*, 23(2):1–13, 2009. ISSN 08866236. doi: 10.1029/2008GB003268. URL `http://www.agu.org/journals/ABS/2009/2008GB003268.shtml`.

Charlotte E. Jones, Karen E. Hornsby, Roberto Sommariva, Rachel M. Dunk, Roland von Glasow, Gordon McFiggans, and Lucy J. Carpenter. Quantifying the contribution of marine organic gases to atmospheric iodine. *Geophysical Research Let-*

ters, 37(18), sep 2010. ISSN 0094-8276. doi: 10.1029/2010GL043990. URL http://www.agu.org/pubs/crossref/2010/2010GL043990.shtml.

N. B. Jones, K. Riedel, W. Allan, S. Wood, P. I. Palmer, K. Chance, and J. Notholt. Long-term tropospheric formaldehyde concentrations deduced from ground-based fourier transform solar infrared measurements. *Atmospheric Chemistry and Physics*, 9:7131–7142, 2009. ISSN 1680-7375. doi: 10.5194/acpd-7-14543-2007.

J Kesselmeier, U Kuhn, a Wolf, M.O Andreae, P Ciccioli, E Brancaleoni, M Frattoni, a Guenther, J Greenberg, P De Castro Vasconcellos, Telles de Oliva, T Tavares, and P Artaxo. Atmospheric volatile organic compounds (VOC) at a remote tropical forest site in central Amazonia. *Atmospheric Environment*, 34(24):4063–4072, jan 2000. ISSN 13522310. doi: 10.1016/S1352-2310(00)00186-2. URL http://linkinghub.elsevier.com/retrieve/pii/S1352231000001862.

U. Kuhn, M. O. Andreae, C. Ammann, a. C. Araújo, E. Brancaleoni, P. Ciccioli, T. Dindorf, M. Frattoni, L. V. Gatti, L. Ganzeveld, B. Kruijt, J. Lelieveld, J. Lloyd, F. X. Meixner, a. D. Nobre, U. Pöschl, C. Spirig, P. Stefani, a. Thielmann, R. Valentini, and J. Kesselmeier. Isoprene and monoterpene fluxes from Central Amazonian rainforest inferred from tower-based and airborne measurements, and implications on the atmospheric chemistry and the local carbon budget. *Atmospheric Chemistry and Physics Discussions*, 7(1):641–708, jan 2007. ISSN 1680-7375. doi: 10.5194/acpd-7-641-2007. URL http://www.atmos-chem-phys-discuss.net/7/641/2007/.

Elizabeth B. Kujawinski, Melissa C. Kido Soule, David L. Valentine, Angela K. Boysen, Krista Longnecker, and Molly C. Redmond. Fate of dispersants associated with the Deepwater Horizon oil spill. *Environmental Science and Technology*, 45(4):1298–1306, 2011. ISSN 0013936X. doi: 10.1021/es103838p.

Frank Laturnus, Kim F. Haselmann, Thomas Borch, and Christian Grøn. Terrestrial natural sources of trichloromethane (chloroform, chcl3) – an overview. *Biogeochemistry*, 60(2):121–139, 2002. ISSN 1573-515X. doi: 10.1023/A:1019887505651. URL http://dx.doi.org/10.1023/A:1019887505651.

J. C. Laube, a. Engel, H. Bönisch, T. Möbius, D. R. Worton, W. T. Sturges, K. Grunow, and U. Schmidt. Contribution of very short-lived organic substances to stratospheric chlorine and bromine in the tropics – a case study. *Atmospheric Chemistry and*

Physics Discussions, 8(3):8491–8515, 2008. ISSN 1680-7375. doi: 10.5194/acpd-8-8491-2008.

M. Le Breton, M. R. McGillen, J. B. A. Muller, A. Bacak, D. E. Shallcross, P. Xiao, L. G. Huey, D. Tanner, H. Coe, and C. J. Percival. Airborne observations of formic acid using a chemical ionization mass spectrometer. *Atmospheric Measurement Techniques*, 5(12):3029–3039, 2012. ISSN 1867-8548. doi: 10.5194/amt-5-3029-2012. URL `http://www.atmos-meas-tech.net/5/3029/2012/amt-5-3029-2012.html`.

M. Le Breton, A. Bacak, J. B. A. Muller, S. J. O'Shea, P. Xiao, M. N. R. Ashfold, M. C. Cooke, R. Batt, D. E. Shallcross, D. E. Oram, G. Forster, S. J.-B. Bauguitte, P. I. Palmer, M. Parrington, A. C. Lewis, J. D. Lee, and C. J. Percival. Airborne hydrogen cyanide measurements using a chemical ionisation mass spectrometer for the plume identification of biomass burning forest fires. In *Atmospheric Chemistry and Physics* Le Breton et al. (2013), pages 9217–9232. doi: 10.5194/acp-13-9217-2013.

Catherine Leblanc, Carole Colin, Audrey Cosse, Ludovic Delage, Stéphane La Barre, Pascal Morin, Bruno Fiévet, Claire Voiseux, Yves Ambroise, Elodie Verhaeghe, David Amouroux, Olivier Donard, Emmanuel Tessier, and Philippe Potin. Iodine transfers inthecoastal marine environment: thekey role ofbrown algae andoftheirvanadium-dependent haloperoxidases. *Biochimie*, 88(11):1773–1785, 2006. ISSN 03009084. doi: 10.1016/j.biochi.2006.09.001.

Jos Lelieveld and Frank J. Dentener. What controls tropospheric ozone? *Journal of Geophysical Research*, 105(D3):3531, 2000. ISSN 0148-0227. doi: 10.1029/1999JD901011.

A. C. Lewis, M. J. Evans, J. R. Hopkins, S. Punjabi, K. A. Read, R. M. Purvis, S. J. Andrews, S. J. Moller, L. J. Carpenter, J. D. Lee, A. R. Rickard, P. I. Palmer, and M. Parrington. The influence of biomass burning on the global distribution of selected non-methane organic compounds. *Atmospheric Chemistry and Physics*, 13(2):851–867, 2013. ISSN 16807316. doi: 10.5194/acp-13-851-2013.

Q. Liang, R. S. Stolarski, S. R. Kawa, J. E. Nielsen, A. R. Douglass, J. M. Rodriguez, D. R. Blake, E. L. Atlas, and L. E. Ott. Finding the Missing Stratospheric Bry: A Global Modeling Study of CHBr3 and CH2Br2. *Atmospheric Chemistry and Physics Discussions*, 10:2269–2286, 2010. ISSN 1680-7324. doi: 10.5194/acp-10-2269-2010. URL `http://hdl.handle.net/2060/20110014292`.

D. J. Luecken, W. T. Hutzell, M. L. Strum, and G. A. Pouliot. Regional sources of atmospheric formaldehyde and acetaldehyde, and implications for atmospheric modeling. *Atmospheric Environment*, 47(2):477–490, 2012. ISSN 13522310. doi: 10.1016/j.atmosenv.2011.10.005. URL http://dx.doi.org/10.1016/j.atmosenv.2011.10.005.

W. C Lyons and G. J Plisga. *Standard Handbook of Petroleum and Natural Gas Engineering*. Elsevier, 2nd edition, 2005. ISBN 0750677856.

Glesni MacLeod and Jennifer M. Ames. Comparative assessment of the artefact background on thermal desorption of tenax GC and tenax TA. *Journal of Chromatography A*, 355:393–398, jan 1986. ISSN 00219673. doi: 10.1016/S0021-9673(01)97343-1. URL http://linkinghub.elsevier.com/retrieve/pii/S0021967301973431.

Jingqiu Mao, Fabien Paulot, Daniel J. Jacob, Ronald C. Cohen, John D. Crounse, Paul O. Wennberg, Christoph A. Keller, Rynda C. Hudman, Michael P. Barkley, and Larry W. Horowitz. Ozone and organic nitrates over the eastern United States: Sensitivity to isoprene chemistry. *Journal of Geophysical Research Atmospheres*, 118(19):11256–11268, 2013. ISSN 21698996. doi: 10.1002/jgrd.50817.

UK Markes. TT24/7 Operating Manual. 44(0), 2006.

Stephen Mobbs, Stéphane Bauguitte, Axel Wellpott, Ralph Burton, James Lee, Alastair Lewis, and Shalini Punjabi. Monitoring of the Elgin Rig Leak using the FAAM Atmospheric Research Aircraft. Technical Report December, 2012.

Paul S Monks. Gas-phase radical chemistry in the troposphere. *Chemical Society reviews*, 34(5):376–395, 2005. ISSN 0306-0012. doi: 10.1039/b307982c.

SA Montzka, JH Butler, and RC Myers. Decline in the tropospheric abundance of halogen from halocarbons: Implications for stratospheric ozone depletion. *Science*, 1996. URL http://www.osti.gov/energycitations/product.biblio.jsp?osti_id=263039.

C. Ordóñez, J. F. Lamarque, S. Tilmes, D. E. Kinnison, E. L. Atlas, D. R. Blake, G. Sousa Santos, G. Brasseur, and A. Saiz-Lopez. Bromine and iodine chemistry in a global chemistry-climate model: Description and evaluation of very short-lived oceanic sources. *Atmospheric Chemistry and Physics*, 12(3):1423–1447, 2012. ISSN 16807316. doi: 10.5194/acp-12-1423-2012.

S J O'Shea, S J.-B. Bauguitte, M W Gallagher, D Lowry, and C J Percival. Development of a cavity-enhanced absorption spectrometer for airborne measurements of CH_{4} and CO_{2}. *Atmospheric Measurement Techniques*, 6 (5):1095–1109, 2013. ISSN 1867-8548. doi: 10.5194/amt-6-1095-2013. URL http://www.atmos-meas-tech.net/6/1095/2013/.

L. L. Pan, E. L. Atlas, R. J. Salawitch, S. B. Honomichl, J. F. Bresch, W. J. Randel, E. C. Apel, R. S. Hornbrook, A. J. Weinheimer, D. C. Anderson, S. J. Andrews, S. Baidar, S. P. Beaton, T. L. Campos, L. J. Carpenter, D. Chen, B. Dix, V. Donets, S. R. Hall, T. F. Hanisco, C. R. Homeyer, L. G. Huey, J. B. Jensen, L. Kaser, D. E. Kinnison, T. K. Koenig, J-F Lamarque, C. Liu, J. Luo, Z. J. Luo, D. D. Montzka, J. M. Nicely, R. B. Pierce, D. D. Riemer, T. Robinson, P. Romashkin, A. Saiz-Lopez, S. Schauffler, O. Shieh, M. H. Stell, K. Ullmann, G. Vaughan, R. Volkamer, and G. Wolfe. The Convective Transport of Active Species in the Tropics (CONTRAST) Experiment. *Bulletin of the American Meteorological Society*, page 160309141232001, 2016. ISSN 0003-0007. doi: 10.1175/BAMS-D-14-00272.1. URL http://journals.ametsoc.org/doi/abs/10.1175/BAMS-D-14-00272.1.

G. N. Petersen and Ian Renfrew. Aircraft-based observations of air-sea fluxes over Denmark Strait and the Irminger Sea during high wind speed conditions. *Quarterly Journal of the Royal . . .*, 135(October):2030–2045, 2009. ISSN 00359009. doi: 10.1002/qj. URL http://onlinelibrary.wiley.com/doi/10.1002/qj.71/abstract.

V. V. Petrenko, P. Martinerie, P. Novelli, D. M. Etheridge, I. Levin, Z. Wang, T. Blunier, J. Chappellaz, J. Kaiser, P. Lang, L. P. Steele, S. Hammer, J. Mak, R. L. Langenfelds, J. Schwander, J. P. Severinghaus, E. Witrant, G. Petron, M. O. Battle, G. Forster, W. T. Sturges, J. F. Lamarque, K. Steffen, and J. W C White. A 60 yr record of atmospheric carbon monoxide reconstructed from Greenland firn air. *Atmospheric Chemistry and Physics*, 13(15):7567–7585, 2013. ISSN 16807316. doi: 10.5194/acp-13-7567-2013.

R. C. Pike, J. D. Lee, P. J. Young, G. D. Carver, X. Yang, N. Warwick, S. Moller, P. Misztal, B. Langford, D. Stewart, C. E. Reeves, C. N. Hewitt, and J. A. Pyle. NOx and O3 above a tropical rainforest: An analysis with a global and box model. *Atmospheric Chemistry and Physics*, 10(21):10607–10620, 2010. ISSN 16807316. doi: 10.5194/acp-10-10607-2010.

U. Platt and G. Hönninger. The role of halogen species in the troposphere. *Chemosphere*, 52(2):325–338, 2003. ISSN 00456535. doi: 10.1016/S0045-6535(03)00216-9.

Michael J. Prather and Robert T Watson. Stratospheric ozone delpetion and future levels of atmospheric chlorine and bromine. *Nature*, 344:729–734, 1990.

R. A. Rasmussen and M. A. K. Khalil. Atmospheric benzene and toluene, 1983. ISSN 0094-8276.

Katie a Read, Anoop S Mahajan, Lucy J Carpenter, Mathew J Evans, Bruno V E Faria, Dwayne E Heard, James R Hopkins, James D Lee, Sarah J Moller, Alastair C Lewis, Luis Mendes, James B McQuaid, Hilke Oetjen, Alfonso Saiz-Lopez, Michael J Pilling, and John M C Plane. Extensive halogen-mediated ozone destruction over the tropical Atlantic Ocean. *Nature*, 453(7199):1232–5, jun 2008. ISSN 1476-4687. doi: 10.1038/nature07035. URL `http://www.ncbi.nlm.nih.gov/pubmed/18580948`.

Alejandra Ribes, Guillem Carrera, Eva Gallego, Xavier Roca, M a José Berenguer, and Xavier Guardino. Development and validation of a method for air-quality and nuisance odors monitoring of volatile organic compounds using multi-sorbent adsorption and gas chromatography/mass spectrometry thermal desorption system. *Journal of chromatography. A*, 1140(1-2):44–55, jan 2007. ISSN 0021-9673. doi: 10.1016/j.chroma.2006.11.062. URL `http://www.ncbi.nlm.nih.gov/pubmed/17187810`.

P. D. Rosenberg, A. R. Dean, P. I. Williams, J. R. Dorsey, A. Minikin, M. A. Pickering, and A. Petzold. Particle sizing calibration with refractive index correction for light scattering optical particle counters and impacts upon PCASP and CDP data collected during the Fennec campaign. *Atmospheric Measurement Techniques*, 5(5):1147–1163, 2012. ISSN 18671381. doi: 10.5194/amt-5-1147-2012.

T. B. Ryerson, K. C. Aikin, W. M. Angevine, E. L. Atlas, D. R. Blake, C. A. Brock, F. C. Fehsenfeld, R. S. Gao, J. A. De Gouw, D. W. Fahey, J. S. Holloway, D. A. Lack, R. A. Lueb, S. Meinardi, A. M. Middlebrook, D. M. Murphy, J. A. Neuman, J. B. Nowak, D. D. Parrish, J. Peischl, A. E. Perring, I. B. Pollack, A. R. Ravishankara, J. M. Roberts, J. P. Schwarz, J. R. Spackman, H. Stark, C. Warneke, and L. A. Watts. Atmospheric emissions from the deepwater Horizon spill constrain air-water partitioning,

hydrocarbon fate, and leak rate. *Geophysical Research Letters*, 38(7):6–11, 2011. ISSN 00948276. doi: 10.1029/2011GL046726.

T. B. Ryerson, R. Camilli, J. D. Kessler, E. B. Kujawinski, C. M. Reddy, D. L. Valentine, E. Atlas, D. R. Blake, J. de Gouw, S. Meinardi, D. D. Parrish, J. Peischl, J. S. Seewald, and C. Warneke. Chemical data quantify Deepwater Horizon hydrocarbon flow rate and environmental distribution. *Proceedings of the National Academy of Sciences*, 109(50): 20246–20253, 2012. ISSN 0027-8424. doi: 10.1073/pnas.1110564109.

R.˜J. Salawitch, J.˜M. Nicely, D.˜C. Anderson, E.˜L. Atlas, S Schauffler, V Donets, R Lueb, M.˜A. Navarro, E.˜C. Apel, N.˜J. Blake, A.˜J. Hills, R.˜S. Hornbrook, D.˜D. Riemer, D Chen, L.˜G. Huey, D Tanner, R.˜M. Volkamer, T.˜K. Koenig, S Baidar, B.˜K. Dix, A.˜J. Weinheimer, G.˜M. Wolfe Jr., T.˜F. Hanisco, S.˜R. Hall, K Ullmann, R Fernandez, A Saiz-Lopez, D.˜E. Kinnison, and J.˜F. Lamarque. Stratospheric Injection of Bromine from Very Short Lived (VSL) Sources Inferred from CONTRAST. *AGU Fall Meeting Abstracts*, dec 2014.

R. Seco, J. Peñuelas, I. Filella, J. Llusià, R. Molowny-Horas, S. Schallhart, a. Metzger, M. Müller, and a. Hansel. Contrasting winter and summer VOC mixing ratios at a forest site in the Western Mediterranean Basin: the effect of local biogenic emissions. *Atmospheric Chemistry and Physics*, 11(24):13161–13179, dec 2011. ISSN 1680-7324. doi: 10.5194/acp-11-13161-2011. URL `http://www.atmos-chem-phys.net/11/13161/2011/`.

Greg Shindell, Drew Faluvegi. Climate response to regional radiative forcing during the twentieth century. *Nature Geoscience*, 2(4):294–300, 2009. URL `http://dx.doi.org/10.1038/ngeo473`.

K. Sindelarova, C. Granier, I. Bouarar, A. Guenther, S. Tilmes, T. Stavrakou, J.-F. Müller, U. Kuhn, P. Stefani, and W. Knorr. Global data set of biogenic voc emissions calculated by the megan model over the last 30 years. In *Atmospheric Chemistry and Physics* Sindelarova et al. (2014), pages 9317–9341. doi: 10.5194/acp-14-9317-2014.

Susan Solomon, Diane J Ivy, Doug Kinnison, Michael J Mills, Ryan R Neely Iii, and Anja Schmidt. Emergence of healing in the Antarctic ozone layer. *Science*, 353:269–274, 2016.

D. S. Stevenson, P. J. Young, V. Naik, J.-F. Lamarque, D. T. Shindell, A. Voulgarakis, R. B. Skeie, S. B. Dalsoren, G. Myhre, T. K. Berntsen, G. A. Folberth, S. T.

Rumbold, W. J. Collins, I. A. MacKenzie, R. M. Doherty, G. Zeng, T. P. C. van Noije, A. Strunk, D. Bergmann, P. Cameron-Smith, D. A. Plummer, S. A. Strode, L. Horowitz, Y. H. Lee, S. Szopa, K. Sudo, T. Nagashima, B. Josse, I. Cionni, M. Righi, V. Eyring, A. Conley, K. W. Bowman, O. Wild, and A. Archibald. Tropospheric ozone changes, radiative forcing and attribution to emissions in the atmospheric chemistry and climate model intercomparison project (accmip). In *Atmospheric Chemistry and Physics* Stevenson et al. (2013), pages 3063–3085. doi: 10.5194/acp-13-3063-2013. URL `http://www.atmos-chem-phys.net/13/3063/2013/`.

J Ström, R Busen, M Quante, B Guillemet, P. R. A. Brown, and J Heintzenberg. Pre-EUCREX Intercomparison of Airborne Humidity Measuring Instruments. *Journal of Atmospheric and Oceanic Technology*, 11:1392, 1994.

D. Taraborrelli, M. G. Lawrence, J. N. Crowley, T. J. Dillon, S. Gromov, C. B. M. Groß, L. Vereecken, and J. Lelieveld. Hydroxyl radical buffered by isoprene oxidation over tropical forests. *Nature Geoscience*, 5(3):190–193, feb 2012. ISSN 1752-0894. doi: 10.1038/ngeo1405. URL `http://www.nature.com/doifinder/10.1038/ngeo1405`.

R. von Glasow, R. von Kuhlmann, M. G. Lawrence, U. Platt, and P. J. Crutzen. Impact of reactive bromine chemistry in the troposphere. *Atmospheric Chemistry and Physics Discussions*, 4(4):4877–4913, 2004. ISSN 1680-7324. doi: 10.5194/acpd-4-4877-2004.

Zhendi Wang, Merv Fingas, and Gary Sergy. Chemical characterization of crude oil residues from an Arctic beach by GC/MS and GC/FID. *Environmental science & technology*, 29(10):2622–2631, 1995. URL `http://pubs.acs.org/doi/abs/10.1021/es00010a025`.

C Warneke, R Holzinger, and A Hansel. Isoprene and its oxidation products methyl vinyl ketone, methacrolein, and isoprene related peroxides measured online over the tropical rain forest of Surinam in March 1998. *Journal of Atmospheric . . .*, pages 167–185, 2001. URL `http://link.springer.com/article/10.1023/A:1006326802432`.

C; Warneke, F Geiger, P. M. Edwards, W Dube, G Petron, J Kofler, A Zahn, S.S Brown, M Graus, J.B Gilman, B. M. Lerner, J Peischl, T. B Ryerson, J. de Gouw, and J. M. Roberts. Volatile organic compound emissions from the oil and natural gas industry in the Uintah Basin , Utah : oil and gas well pad emissions compared to ambient

air composition. *Atmospheric Chemistry and Physics*, (x):10977–10988, 2014. doi: 10.5194/acp-14-10977-2014.

J Jason West, Steven J Smith, Raquel A Silva, Vaishali Naik, Yuqiang Zhang, Zachariah Adelman, Meridith M Fry, Susan Anenberg, Larry W Horowitz, and Jean-Francois Lamarque. Co-benefits of global greenhouse gas mitigation for future air quality and human health. In *Nature climate change* West et al. (2013), pages 885–889. doi: 10.1038/NCLIMATE2009. URL `http://dx.doi.org/10.1038/nclimate2009`.

Kevin L. Wilson and John W. Birks. Mechanism and elimination of a water vapor interference in the measurement of ozone by UV absorbance. *Environmental Science and Technology*, 40(20):6361–6367, 2006. ISSN 0013936X. doi: 10.1021/es052590c.

P. H. Wine and A. R. Ravishankara. Kinetics of O(1D) interactions with the atmospheric gases N2, N2O, H2O, H2, CO2, and O3. *Chemical Physics Letters*, 77(1):103–109, 1981. ISSN 00092614. doi: 10.1016/0009-2614(81)85609-6.

D J Wuebbles and K Hayhoe. Atmospheric methane and global change. *Earth-Science Reviews*, 57(3-4):177–210, 2002. ISSN 0012-8252. doi: 10.1016/S0012-8252(01)00062-9. URL `ISI:000176314100001\nc:/reference/1541.pdf`.

Xin Yang, Richard A. Cox, Nicola J. Warwick, John A. Pyle, Glenn D. Carver, Fiona M. O'Connor, and Nick H. Savage. Tropospheric bromine chemistry and its impacts on ozone: A model study. *Journal of Geophysical Research*, 110 (D23):D23311, 2005. ISSN 0148-0227. doi: 10.1029/2005JD006244. URL `http://doi.wiley.com/10.1029/2005JD006244`.

N Yassaa and J Williams. Analysis of enantiomeric and non-enantiomeric monoterpenes in plant emissions using portable dynamic air sampling/solid-phase microextraction (PDAS-SPME) and chiral gas chromatography/mass spectrometry. *Atmospheric Environment*, 39(27):4875–4884, sep 2005. ISSN 13522310. doi: 10.1016/j.atmosenv.2005.04.034. URL `http://linkinghub.elsevier.com/retrieve/pii/S1352231005004218`.

G. Young, H. Jones, E. Darbyshire, K. Baustian, J. B. McQuaid, K. Bower, P. Connolly, M. W. Gallagher, and T. Choularton. Size-segregated cocomposition analysis of aerosol pparticle collected in the european arctic during the accacia campaign. *Atmospheric Chemistry and Physics*, 16:4063–4079, 2016.

Bin Yuan, Carsten Warneke, Min Shao, and Joost A. De Gouw. Interpretation of volatile organic compound measurements by proton-transfer-reaction mass spectrometry over the deepwater horizon oil spill. *International Journal of Mass Spectrometry*, 358(1):43–48, 2014. ISSN 13873806. doi: 10.1016/j.ijms.2013.11.006. URL http://dx.doi.org/10.1016/j.ijms.2013.11.006.

Zhengbin Zhang, Liansheng Liu, Chunying Liu, and Weijun Cai. Studies on the sea surface microlayer: II. The layer of sudden change of physical and chemical properties. *Journal of Colloid and Interface Science*, 264(1):148–159, 2003. ISSN 00219797. doi: 10.1016/S0021-9797(03)00390-4.

Lei Zhu, Daniel J. Jacob, Patrick S. Kim, Jenny A. Fisher, Karen Yu, Katherine R. Travis, Loretta J. Mickley, Robert M. Yantosca, Melissa P. Sulprizio, Isabelle De Smedt, Gonzalo Gonzalez Abad, Kelly Chance, Can Li, Richard Ferrare, Alan Fried, Johnathan W. Hair, Thomsa F. Hanisco, Dirk Richter, Amy Jo Scarino, James Walega, Petter Weibring, and Glenn M. Wolfe. Observing atmospheric formaldehyde (HCHO) from space: validation and intercomparison of six retrievals from four satellites (OMI, GOME2A, GOME2B, OMPS) with SEAC⁴RS aircraft observations over the Southeast US. *Atmospheric Chemistry and Physics Discussions*, (March):1–24, 2016. ISSN 1680-7375. doi: 10.5194/acp-2016-162. URL http://www.atmos-chem-phys-discuss.net/acp-2016-162/.

F. Ziska, B. Quack, K. Abrahamsson, S. D. Archer, E. Atlas, T. Bell, J. H. Butler, L. J. Carpenter, C. E. Jones, N. R P Harris, H. Hepach, K. G. Heumann, C. Hughes, J. Kuss, K. Krüger, P. Liss, R. M. Moore, A. Orlikowska, S. Raimund, C. E. Reeves, W. Reifenhäuser, A. D. Robinson, C. Schall, T. Tanhua, S. Tegtmeier, S. Turner, L. Wang, D. Wallace, J. Williams, H. Yamamoto, S. Yvon-Lewis, and Y. Yokouchi. Global sea-to-air flux climatology for bromoform, dibromomethane and methyl iodide. *Atmospheric Chemistry and Physics*, 13(17):8915–8934, 2013. ISSN 16807316. doi: 10.5194/acp-13-8915-2013.